Convolution, Rotation, and Data Fusion with Orthogonal Expansions

by

Kristopher L. Reynolds

A dissertation submitted to The Johns Hopkins University in conformity with the requirements for the degree of Doctor of Philosophy.

Baltimore, Maryland

August, 2018

© Kristopher L. Reynolds 2018

All rights reserved

Abstract

This dissertation investigates certain special function classes, namely Hermite and Bessel functions, and uncovers some useful properties relating multiplication, convolution, rotation, and coordinate conversion. These mathematical operations are performed on the underlying basis functions and are thus continuous in nature, lending itself to higher accuracy and computational speed. Some integral transformations involving these special functions (e.g. Abel transform, $3h$ integrals, $3J$ integrals) possess recurrence relations, and so given a finite set of analytic starting conditions, higher order forms of these integrals can be obtained quickly. It will be shown how these integrals and the aforementioned special function properties are used in engineering applications including data fusion, deconvolution, continuum normal mode analysis, cryo-electron microscopy (cryo-EM) and small angle X-ray scattering (SAXS).

ABSTRACT

Advisor: Professor Gregory S. Chirikjian

Dissertation Committee:

Professor Gregory S. Chirikjian, Mechanical Engineering, JHU

Professor Bernard Shiffman, Department of Mathematrics, JHU

Assistant Professor Marin Kobilarov, Mechanical Engineering, JHU

Acknowledgments

First and foremost, I would like to thank my advisor Professor Gregory Chirikjian. He has taught me so much in the ways of research and how to carry myself professionally. His attitude towards research is inspiring, and I hope I can adopt that mindset and carry it with me into my professional career. I would also like to thank my defense committee members Professor Bernard Shiffman and Professor Marin Kobilarov for their flexibility and helpful feedback. I also want to thank the Robot and Protein Kinematics (RPK) lab, both current and former members, with a special thanks to my friend Dr. Joshua Davis. His Ph.D. timeline coincided with mine, and so we both got to enjoy all aspects of the program simultaneously. Good luck in your career, Josh. I also want to thank Professor Wooram Park for his feedback on topics involving Hermite functions and Dr. Jin Seob Kim for his help with Bessel function integrals. Thank you Matthew Sheckells, Subhransu Mishra, and Gowtham Garimella. I enjoyed our technical discussions, and appreciated your suggestions.

ACKNOWLEDGMENTS

I would next like to thank my family, including my mother for giving me the opportunity to follow my dream of becoming an engineer, and my mother-in-law for her continuous encouragement and support throughout my studies. Finally, I would like to thank my wonderful wife Aubrey for all of the sacrifices she made so that I could complete my Ph.D. Without you sweetheart, none of this would be possible. I love you.

Dedication

This dissertation is dedicated to my daughter, Kyrie.

Contents

List of Figures

Part I

Introduction

Chapter 1

Introduction and Organization

1.1 Introduction

Function approximation is a classic technique in engineering applications, where some finite set of data $\bar{f}$ is fit to an expansion, something like

$$\bar{f} \approx \sum_i \hat{f}_i \phi_i(x).$$

Sometimes the basis functions have a key purpose, such as a Fourier series and its use in decomposing a periodic single into sines and cosines. The coefficients that make up this series are the Fourier transform, and are used to analyze a discrete signal versus frequency, a useful tool in fields such as sonar, radar, etc. Sines and cosines are not the only complete orthogonal basis. For square-integrable functions $f \in \mathcal{L}^2(\mathbb{R})$,

one could also approximate a function $f(x)$ with say a Hermite function basis $h_n(x)$, or for functions $f(r)$ with nonnegative arguments r, a radial basis such as Laguerre functions $L_n^k(x)$ or Bessel functions $J_m(r)$ is appropriate.

Once data has been transformed into an orthogonal expansion, some very special properties are acquired, depending on the underlying basis functions. For a Hermite function basis, expansions of this form can be multiplied together, converted between coordinate systems, convolved, rotated, and/or projected, just to name a few. Bessel function expansions have a multiplicative property, in that the coefficients of the product of two Bessel function expansions can be recast as a sum of coefficients from the original two expansions. This technique implicitly solves the data fusion problem in radial, polar and planar rigid body coordinates. The same fusion technique is also available for d-dimensional Hermite expansions that span $\mathbb{R}^d$ in Cartesian coordinates. These fusion solutions are made possible with the aid of what are to be called $3X$ integrals (i.e. the integral of the product of three orthogonal functions), which can be computed recursively.

The aforementioned properties and $3X$ integrals will be used to solve various engineering problems in signal and image processing that use discrete and finite sets of data.

1.2 Organization

This dissertation is organized into three main parts. The first part is an introduction, comprised of two chapters (including this one) that provides background for upcoming concepts and derivations. The second part has three additional chapters, and derives properties of Hermite expansions as well as recurrence relations for $3h$ integrals (Hermite) and $3J$ integrals (Bessel). The final part of this dissertation is application-based, with chapters that focus on coordinate interconversion, data fusion, Cryo-electron microscopy (cryo-EM) and Small Angle X-ray Scattering (SAXS), and select topics further involving Hermite functions and expansions thereof. A concluding chapter summarizes everything and provides a few possible future research avenues.

Chapter 2

Mathematical Background

This chapter presents the necessary mathematical background required for a clear understanding of derivations throughout this dissertation. There are two main sections, namely special functions and Lie groups. The special functions presented include Hermite, Bessel, and Laguerre functions. The two Lie groups used in this thesis are $SO(N)$ and $SE(N)$, which are the rotation and Euclidean groups respectively.

2.1 Special Functions

The notion of a "special" function is one that appears as a solution to differential equations or integrals. One could also conjecture that properties of orthogonality and completeness are also indeed special. This section reviews three special function classes, namely Hermite, Bessel, and Laguerre functions.

2.1.1 Hermite Functions

Hermite polynomials $H_n(x)$ are defined in terms of Rodrigues' formula [1]

$$H_n(x) \doteq (-1)^n e^{x^2} \frac{d^n}{dx^n}(e^{-x^2}), \tag{2.1}$$

and are solutions to the differential equation

$$y'' - 2xy' + 2ny = 0.$$

They have the orthogonality condition

$$\int_{-\infty}^{\infty} H_m(x) H_n(x) e^{-x^2} dx = 2^n n! \sqrt{\pi} \delta_{m,n}, \tag{2.2}$$

where δ_{mn} is the Kronecker delta function. The first several Hermite Polynomials are

$$H_0(x) = 1,$$

$$H_1(x) = 2x,$$

$$H_2(x) = 4x^2 - 2,$$

and

$$H_3(x) = 8x^3 - 12x.$$

In general, $H_n(-x) = (-1)^n H_n(x)$. These polynomials have the corresponding orthogonality condition

$$\int_{-\infty}^{\infty} H_n(x) H_m(x) w(x) dx = 2^n n! \sqrt{\pi} \delta_{m,n}, \tag{2.3}$$

where $w(x) = e^{-x^2}$ is a weighting function. Hermite functions are defined by the equation

$$h_n(x) \doteq c_n H_n(x) e^{-x^2/2}, \tag{2.4}$$

where $c_n = \frac{1}{2^{n/2}\sqrt{n!\sqrt{\pi}}}$ is a normalizing coefficient. These Hermite functions satisfy the orthonormality condition

$$\int_{-\infty}^{\infty} h_n(x) h_m(x) dx = \delta_{mn}. \tag{2.5}$$

Since Hermite functions form a complete orthornomal basis for the set of square-integrable functions $f \in \mathcal{L}^2(\mathbb{R})$, these functions can be expressed with the infinite series

$$f(x) = \sum_{k=0}^{\infty} \hat{f}_k h_k(x), \tag{2.6}$$

where

$$\hat{f}_k = \int_{-\infty}^{\infty} f(x) h_k(x) dx. \tag{2.7}$$

This series expansion can be truncated at some band limit N as

$$\tilde{f}(x) = \sum_{k=0}^{N} \hat{f}_k h_k(x), \tag{2.8}$$

where N is a very large integer that implies $\tilde{f}(x) \approx f(x)$. These expansions will be referred to throughout this dissertation as a Hermite expansion and/or a Hermite series. Hermite functions can also be used as a basis to expand a 2D function $f(x, y) \in \mathcal{L}^2(\mathbb{R}^2)$ according to the series

$$\tilde{f}(x, y) = \sum_{m=0}^{N_1} \sum_{n=0}^{N_2} \hat{f}_{m,n} h_m(x) h_n(y), \tag{2.9}$$

where

$$\hat{f}_{m,n} = \int_{-\infty}^{\infty} \int_{-\infty}^{\infty} f(x, y) h_m(x) h_n(y) dx dy. \tag{2.10}$$

Similarly, a 3D function $f(x, y, z) \in \mathcal{L}^2(\mathbb{R}^3)$ can be expanded as

$$\tilde{f}(x, y, z) = \sum_{m=0}^{N_1} \sum_{n=0}^{N_2} \sum_{k=0}^{N_3} \hat{f}_{m,n,k} h_m(x) h_n(y) h_k(z), \tag{2.11}$$

where it is not necessarily the case that N_i are all equal. In fact, a special kind of bandlimit is explored later in which these are not equal, and this enables special properties under rotation and coordinate conversion. The coefficients of this 3D

expansion are obtained as

$$\hat{f}_{m,n,k} = \int_{-\infty}^{\infty}\int_{-\infty}^{\infty}\int_{-\infty}^{\infty} f(x,y,z)h_m(x)h_n(y)h_k(z)dxdydz. \tag{2.12}$$

More generally, functions $f(x_1, x_2, \cdots, x_N)$ can be expanded as

$$\tilde{f}(x_1, x_2, \cdots, x_N) = \sum_{n_1,n_2,\cdots,n_N} \hat{f}_{n_1,n_2,\cdots,n_N} h_{n_1}(x_1)h_{n_2}(x_2)\cdots h_{n_N}(x_N), \tag{2.13}$$

where

$$\hat{f}_{n_1,n_2,\cdots,n_N} = \int_{\mathbb{R}^N} f(x_1, x_2, \cdots, x_N)h_{n_1}(x_1)h_{n_2}(x_2)\cdots h_{n_N}(x_N)dx_1dx_2\cdots dx_N. \tag{2.14}$$

Hermite polynomials have the recurrence relations

$$H_n'(x) = 2nH_{n-1}(x), \tag{2.15}$$

and

$$H_{n+1}(x) = 2xH_n(x) - 2nH_{n-1}(x). \tag{2.16}$$

If the Hermite polynomials of interest are scaled as $H_n(ax)$, then the corresponding recurrence relations become

$$H_n'(ax) = 2anH_{n-1}(ax), \tag{2.17}$$

and

$$H_{n+1}(ax) = 2axH_n(ax) - 2nH_{n-1}(ax), \tag{2.18}$$

or equivalently

$$H_n(ax) = \frac{H_{n+1}(ax)}{2ax} + \frac{nH_{n-1}(ax)}{ax}. \tag{2.19}$$

Similarly, Hermite functions have the recurrence relation

$$h_n(x) = \frac{1}{x\sqrt{2}}\left[\sqrt{n}h_{n-1}(x) + \sqrt{n+1}h_{n+1}(x)\right]. \tag{2.20}$$

Now, consider $h_n'(x)$, which when carrying out this derivative with respect to x gives

$$\begin{aligned}
h_n'(x) &= \frac{d}{dx}[h_n(x)] \\
&= \frac{d}{dx}[\frac{1}{2^{n/2}\sqrt{n!\sqrt{\pi}}}H_n(x)e^{-x^2/2}] \\
&= \frac{1}{2^{n/2}\sqrt{n!\sqrt{\pi}}}H_n'(x)e^{-x^2/2} - x\frac{1}{2^{n/2}\sqrt{n!\sqrt{\pi}}}H_n(x)e^{-x^2/2} \\
&= \frac{1}{2^{n/2}\sqrt{n!\sqrt{\pi}}}2nH_{n-1}(x)e^{-x^2/2} - xh_n(x) \\
&= (\frac{2^{-1/2}}{2^{-1/2}})2n\frac{1}{2^{n/2}\sqrt{n(n-1)!\sqrt{\pi}}}H_{n-1}(x)e^{-x^2/2} - xh_n(x) \\
&= n\frac{2^{1-1/2}}{\sqrt{n}}\frac{1}{2^{\frac{n-1}{2}}\sqrt{(n-1)!\sqrt{\pi}}}H_{n-1}(x)e^{-x^2/2} - xh_n(x) \\
&= \sqrt{2n}h_{n-1}(x) - xh_n(x).
\end{aligned} \tag{2.21}$$

In this derivation, a recurrence relation for Hermite coefficients was created as

$$2nc_n = \sqrt{2n}c_{n-1}. \tag{2.22}$$

After inserting equation (2.20), this recurrence relation becomes

$$h_n'(x) = \frac{\sqrt{n}}{\sqrt{2}}h_{n-1}(x) - \frac{\sqrt{n+1}}{\sqrt{2}}h_{n+1}(x). \tag{2.23}$$

Scaled Hermite functions have the similar recurrence relations

$$h_n(ax) = \frac{1}{ax\sqrt{2}}\left[\sqrt{n}h_{n-1}(ax) + \sqrt{n+1}h_{n+1}(ax)\right], \tag{2.24}$$

and

$$\begin{aligned} h_n'(ax) &= 2anc_nH_{n-1}(ax)e^{-a^2x^2/2} - a^2xc_nH_n(ax)e^{-a^2x^2/2} \\ &= a\sqrt{2n}h_{n-1}(ax) - a^2xh_n(ax). \\ &= a\frac{\sqrt{n}}{\sqrt{2}}h_{n-1}(ax) - a\frac{\sqrt{n+1}}{\sqrt{2}}h_{n+1}(ax). \end{aligned} \tag{2.25}$$

Another useful property is that Hermite functions are eigenfunctions of the Fourier transform. In other words, the Fourier transform of a Hermite function is itself a scaled Hermite function [2]. More specifically

$$\mathcal{F}[h_n](\omega) = \int_{-\infty}^{\infty} h_n(x)e^{-i\omega x}dx = (-i)^n\sqrt{2\pi}h_n(\omega). \tag{2.26}$$

This also true for the inverse Fourier transform of a Hermite function

$$\mathcal{F}^{-1}[h_n](x) = \int_{-\infty}^{\infty} h_n(w)e^{iwx}dw = i^n\sqrt{2\pi}h_n(x). \tag{2.27}$$

The next subsection will review Bessel functions and relevant properties.

2.1.2 Bessel Functions

Bessel functions are solutions to the differential equation

$$y'' + (d-1)\frac{y'}{x} + \left(\lambda - \frac{m^2}{x^2}\right)y = 0.$$

when $d = 2$, and for each m, there is a solution rendered by setting $\lambda = 1$ given by the function [3]

$$J_m(x) \doteq \frac{x^m}{2^m}\sum_{n=0}^{\infty}\frac{(-1)^n}{2^{2n}n!(m+n)!}x^{2n}. \tag{2.28}$$

This is referred to as a Bessel function of the first kind (of order m). Bessel functions also have the integral representation

$$J_m(x) = \frac{1}{2\pi}\int_0^{2\pi} cos(m\theta - x\sin\theta)d\theta. \tag{2.29}$$

The property

$$J_{-m}(x) = (-1)^m J_m(x), \tag{2.30}$$

allows for Bessel functions of negative integer orders to be computed. Bessel functions have the following relations

$$J'_m(x) = \frac{1}{2}\left[J_{m-1}(x) - J_{m+1}(x)\right], \tag{2.31}$$

$$(x^m J_m(x))' = x^m J_{m-1}(x), \tag{2.32}$$

and

$$J_m(x) = \frac{x}{2m}\left[J_{m-1}(x) + J_{m+1}(x)\right]. \tag{2.33}$$

The orthogonality conditions

$$\int_0^\infty J_m(px)J_m(qx)xdx = \frac{1}{p}\delta(p-q), \tag{2.34}$$

and

$$\int_0^\infty J_m(px)J_m(qx)xdx = \frac{1}{p}\delta(p-q), \tag{2.35}$$

allow for functions to be expanded with the Hankel and inverse Hankel transforms

$$\hat{f}_m(p) = \int_0^\infty f(x)J_m(px)xdx, \tag{2.36}$$

and

$$f(x) = \int_0^\infty \hat{f}_m(p)J_m(px)pdp. \tag{2.37}$$

2.1.3 Laguerre Polynomials

The Laguerre polynomials can be defined according to Rodrgiues' formula

$$L_n^k(x) \doteq \frac{e^x x^{-k}}{n!} \frac{d^n}{dx^n}(e^{-x} x^{n+k}), \tag{2.38}$$

and have the orthogonality condition

$$\int_0^\infty L_m^k(x) L_n^k(x) w(x) dx = \frac{(n+k)!}{n!} \delta_{m,n}, \tag{2.39}$$

where $w(x) = x^k e^{-x}$ is the necessary weighting function. By defining the first few Laguerre polynomials

$$L_0^k(x) = 1,$$

$$L_1^k(x) = -x + k + 1,$$

$$L_2^k(x) = x^2/2 - (k+2)x + (k+1)(k+2)/2,$$

higher order polynomials can be generated using the recurrence relations

$$(n+1) L_{n+1}^k(x) = (2n + 1 + k - x) L_n^k(x) - (n+k) L_{n-1}^k(x), \tag{2.40}$$

$$L_{n+1}^k(x) = L_{n+1}^{k-1}(x) + L_n^k(x), \tag{2.41}$$

and

$$(n+1)L_{n+1}^{k}(x) = (n+1+k)L_{n}^{k}(x) - xL_{n}^{k+1}(x). \tag{2.42}$$

The Laguerre polynomials can be combined with a Fourier series to span functions in polar coordinates as

$$\tilde{f}^{p}(\rho,\phi) = \sum_{m=0}^{N}\sum_{n=-m}^{m} \check{f}_{m,n}\chi_{m,n}^{*}(\rho,\phi), \tag{2.43}$$

where

$$\chi_{m,n}(\rho,\phi) = (-1)^{(m-|n|)/2}\sqrt{\frac{[(m-|n|)/2]!}{\pi\,[(m+|n|)/2]!}}\rho^{|n|}L_{(m-|n|)/2}^{|n|}(\rho^2)e^{-\rho^2/2}e^{-in\phi}, \tag{2.44}$$

are the corresponding basis functions. The coefficients under the square root assumes $m\pm|n|$ is even, otherwise the argument is zero. The function $\chi_{m,n}(\rho,\phi)$ can be separated as

$$\chi_{m,n}(\rho,\phi) = \mathcal{Y}_{m,n}(\rho)Z_{n}(\phi), \tag{2.45}$$

where

$$\mathcal{Y}_{m,n}(\rho) = (-1)^{(m-|n|)/2}\sqrt{\frac{2\,[(m-|n|)/2]!}{[(m+|n|)/2]!}}\rho^{|n|}L_{(m-|n|)/2}^{|n|}(\rho^2)e^{-\rho^2/2}, \tag{2.46}$$

and

$$Z_{n}(\phi) = \frac{1}{\sqrt{2\pi}}e^{-in\phi}. \tag{2.47}$$

The Laguerre-Fourier coefficients are

$$\check{f}_{m,n} = \int_0^{2\pi} \int_0^{\infty} f^p(\rho, \phi) \chi_{m,n}(\rho, \phi) \rho d\rho d\phi. \tag{2.48}$$

The next section will present key definitions for the Lie groups $SO(N)$ and $SE(N)$.

2.2 Lie Groups

This section defines the Lie groups $SO(N)$ and $SE(N)$ for various parameterizations and shows how to integrate on these groups. Also articulated is how to expand a Lie group-valued function with a Fourier series.

2.2.1 The Rotation Group $SO(N)$

The rotation group $SO(N)$ is defined as [4]

$$SO(N) \doteq R \in \mathbb{R}^{N \times N} | RR^T = I_N, \det(R) = +1,$$

and is also called the special orthogonal group. The orthogonality property RR^T is sufficient to deduce that $R^T R = I_N$ (i.e. an $N \times N$ identity matrix). One parameterization of rotations $R \in SO(3)$ is with Euler angles. Consider rotations about the

x, y, and z axes by angles α, β, and γ

$$R_x(\alpha) = \begin{pmatrix} 1 & 0 & 0 \\ 0 & \cos\alpha & -sin(\alpha) \\ 0 & \sin\alpha & \cos\alpha \end{pmatrix}, \tag{2.49}$$

$$R_y(\beta) = \begin{pmatrix} \cos\beta & 0 & \sin\beta \\ 0 & 1 & 0 \\ -\sin\beta & 0 & \cos\beta \end{pmatrix}, \tag{2.50}$$

and

$$R_z(\gamma) = \begin{pmatrix} \cos\gamma & -\sin\gamma & 0 \\ \sin\gamma & \cos\gamma & 0 \\ 0 & 0 & 1 \end{pmatrix}. \tag{2.51}$$

Other rotations can be composed by stringing together the above rotations about principle axes. For example, a "zxz" parameterization looks like

$$\begin{aligned} R_{zxz}(\alpha,\beta,\gamma) &= R_z\alpha)R_x(\beta)R_z(\gamma) \\ &= \begin{pmatrix} c\alpha c\gamma - s\alpha c\beta s\gamma & -c\alpha s\gamma - s\alpha c\beta c\gamma & s\alpha s\beta \\ s\alpha c\gamma + c\alpha c\beta s\gamma & -s\alpha s\gamma + c\alpha c\beta c\gamma & -c\alpha s\beta \\ s\beta s\gamma & s\beta c\gamma & c\beta \end{pmatrix}. \end{aligned} \tag{2.52}$$

The shorthand notation $c(\,) = \cos(\,)$ and $s(\,) = \sin(\,)$ was used above. There are also xyz and zyz compositions for example. Alternatively, the axis-angle representation can be used, where corresponding rotations are of the form

$$R(\mathbf{v}) = \exp(\hat{\mathbf{v}}) = I_3 + \frac{\sin||\mathbf{v}||}{||\mathbf{v}||}\hat{\mathbf{v}} + \frac{(1-\cos||\mathbf{v}||)}{||\mathbf{v}||^2}\hat{\mathbf{v}}^2. \tag{2.53}$$

Equation (2.53) is also known as Rodrigues' rotation formula, and

$$\hat{\mathbf{v}}^T = -\hat{\mathbf{v}},$$

is a 3×3 skew-symmetric matrix. The hat operator$\hat{}$: $\mathbb{R}^3 \to so(3)$ for a vector $\mathbf{v} \in \mathbb{R}^3$. and a skew-symmetric matrix $\hat{\mathbf{v}} \in so(3)$. The space $so(3)$ is called the Lie algebra of $SO(3)$. For more on Lie algebras, the reader is referred to [4] and [5]. The matrix logarithm for $SO(3)$ has the closed-form expression

$$\hat{\mathbf{v}} = \log(R) = \begin{cases} \frac{\theta}{2\sin\theta}\left(R - R^T\right), \ \theta \neq 0 \text{ and } \theta \in [0,\pi) \\ \hat{\mathbf{0}}, \ \theta = 0 \end{cases}, \tag{2.54}$$

where

$$\theta = \cos^{-1}\left(\frac{\text{trace}(R)-1}{2}\right).$$

At $\theta = \pi$, the matrix logarithmic map is not unique.

Integrating a function $f(R)$ over $SO(3)$ looks like

$$\int_{SO(3)} f(R)dR = \int_{\mathbf{q}} f(R(\mathbf{q}))w(\mathbf{q})d\mathbf{q}, \tag{2.55}$$

where $\mathbf{q}$ is the parameterization of elements $R \in SO(3)$. The function

$$w(\mathbf{q}) = c \cdot |\mathcal{J}(\mathbf{q})|,$$

is a weighting function with normalization constant c. This weighting function is sometimes referred to as a Haar measure [6]. The variable $\mathcal{J}(\mathbf{q})$ is a Jacobian matrix, parameterized by local coordinates $\mathbf{q}$. For Euler angles, integration over $SO(3)$ follows

$$\int_{SO(3)} f(R)dR = \frac{1}{8\pi^2} \int_{\alpha=0}^{2\pi} \int_{\beta=0}^{\pi} \int_{\gamma=0}^{2\pi} f(R(\alpha, \beta, \gamma)) \sin\beta d\alpha d\beta d\gamma, \tag{2.56}$$

and integrating functions with the axis-angle parameterization is structured as

$$\int_{SO(3)} f(R)dR = c \cdot \int_{||\mathbf{v}||<\pi} f(R(\mathbf{v}))|\mathcal{J}(\mathbf{v})|d\mathbf{v}. \tag{2.57}$$

Integration on Lie groups will be used in this thesis to compute the coefficients of Fourier series expansions on $SO(3)$ and $SE(2)$. The Fourier inversion formula for Lie

groups is defined generally as

$$f(g) \doteq \int_{\lambda \in \hat{G}} \text{trace}[\hat{f}(\lambda) U(g, \lambda)] d(\lambda), \tag{2.58}$$

with coefficients according to

$$\hat{f}(\lambda) = \int_G f(g) \overline{U(g, \lambda)} dg. \tag{2.59}$$

The function $U(g, \lambda)$ is called an irreducible unitary representation matrix (IUR), and each λ is an element of the dual of the corresponding Lie group G, which is denoted as $\hat{G}$. In particular, the Fourier inversion formula for $SO(3)$ becomes the infinite summation

$$\begin{aligned} f(R) &= \sum_{l=0}^{\infty} (2l+1) \text{trace}[\hat{f}(l) U(R, l)] \\ &= \sum_{l=0}^{\infty} (2l+1) \sum_{m,n=-l}^{l} \hat{f}^l_{m,n} U_{n,m}(R, l), \end{aligned} \tag{2.60}$$

with

$$\begin{aligned} \hat{f}^l_{m,n} &= \int_{SO(3)} f(R) \overline{U_{n,m}(R, l)} dR \\ &= \int_{SO(3)} f(R) U_{m,n}(R^{-1}, l) dR \\ &= \int_{SO(3)} f(R) U_{m,n}(R^T, l) dR. \end{aligned} \tag{2.61}$$

Note the indices m and n, and their order in the inversion formula compared to their order in the Fourier coefficients. The inversion formula can be truncated at some band limit in order to approximate a rotation-valued function $f(R)$. Elements of the

IURs (using the Euler-angle parameterization) are

$$\begin{aligned} U_{m,n}(R,l) &= U_{m,n}(R(\alpha,\beta,\gamma),l) \\ &= D^l_{m,n}(\alpha,\beta,\gamma) \\ &= e^{-im\alpha} d^l_{m,n}(\cos\beta) e^{-in\gamma}. \end{aligned} \tag{2.62}$$

The function $d^l_{m,n}(\cos\beta)$ can be calculated by solving the integral

$$\begin{aligned} d^l_{m,n}(\cos\beta) = \frac{i^{m-n}}{2\pi}\left[\frac{(l-m)!(l+m)!}{(l-n)!(l+n)!}\right]^{\frac{1}{2}} \int_0^{2\pi} \left(\cos\frac{\beta}{2}e^{i\phi/2} + i\sin\frac{\beta}{2}e^{-i\phi/2}\right)^{l-n} \\ \times \left(\cos\frac{\beta}{2}e^{-i\phi/2} + i\sin\frac{\beta}{2}e^{i\phi/2}\right)^{l+n} e^{im\phi} d\phi, \end{aligned} \tag{2.63}$$

and is called a generalized associated Legendre function. The functions $D^l_{m,n}(\alpha,\beta,\gamma)$ and $d^l_{m,n}(\cos\beta)$ are also referred to as Wigner-D an Wigner-d functions respectively [7]. The Haar measure for Euler angle parameterized rotations is

$$dR = \frac{1}{8\pi^2}\sin\beta d\alpha d\beta d\gamma.$$

All together, the Fourier coefficients for $SO(3)$ are

$$\hat{f}^l_{m,n} = \frac{1}{8\pi^2}\int_0^{2\pi}\int_0^{\pi}\int_0^{2\pi} f(R(\alpha,\beta,\gamma))\overline{D^l_{n,m}(\alpha,\beta,\gamma)}\sin\beta d\alpha d\beta d\gamma. \tag{2.64}$$

The next subsection defines Lie group $SE(N)$ and how to perform integration over this group.

2.2.2 The Euclidean Motion Group $SE(N)$

The (special) Euclidean group, $SE(N)$ has elements $g \in SE(N)$ that are rigid body matrices of the form

$$g = \begin{pmatrix} R & t \\ 0^T & 1 \end{pmatrix},$$

where $R \in SO(N)$ is a rotation and $t \in \mathbb{R}^N$ is a translation. This dissertation will focus on the planar Euclidean motion group, which is for $N = 2$. Using coordinates $\mathbf{q} = [x, y, \theta]$, elements $g \in SE(2)$ are parameterized using the matrix

$$g(x, y, \theta) = \begin{pmatrix} \cos\theta & -\sin\theta & x \\ \sin\theta & \cos\theta & y \\ 0 & 0 & 1 \end{pmatrix},$$

or equivalently

$$g(\rho, \phi, \theta) = \begin{pmatrix} \cos\theta & -\sin\theta & r\cos\phi \\ \sin\theta & \cos\theta & r\sin\phi \\ 0 & 0 & 1 \end{pmatrix},$$

with the relationship $(x, y) = (r\cos\phi, r\sin\phi)$. The Fourier inversion formula for $SE(2)$ is defined by

$$f(g) = \sum_{m,n\in\mathbb{Z}} \int_0^\infty \hat{f}_{m,n}(p) U_{n,m}(g, p) p dp, \tag{2.65}$$

with coefficients

$$\begin{aligned}\hat{f}_{m,n}(p) &= \int_{SE(2)} f(g)\overline{U_{n,m}(g,p)}dg. \\ &= \int_{SE(2)} f(g)U_{m,n}(g^{-1},p)dg\end{aligned} \tag{2.66}$$

Notice that the inversion formula for $SE(2)$ is continuous, whereas for $SO(3)$ the inversion formula was an infinite summation. This due to the fact that $SO(3)$ is a "compact" Lie group, whereas $SE(2)$ is not (see [5] for further articulation). Notwithstanding, the inversion formula for $SE(2)$ can be approximated using the summation

$$\begin{aligned}f(g) &= \sum_{m,n\in\mathbb{Z}} \int_0^\infty \hat{f}_{m,n}(p)U_{n,m}(g,p)pdp \\ &\approx \sum_{l=0}^{N-1} \sum_{m,n\in\mathbb{Z}} \hat{f}_{m,n}(p_l)U_{n,m}(g,p_l)p_l\Delta p.\end{aligned} \tag{2.67}$$

The freequency parameter p has ben discretized and now contains N points

$$\mathbf{p} = \begin{bmatrix} p_0 & p_1 & \cdots & p_{N-1} \end{bmatrix}.$$

The Fourier transform on $SE(2)$ for the l^{th} point of p is

$$\hat{f}_{m,n}(p_l) = \int_{SE(2)} f(g)U_{m,n}(g^{-1},p_l)dg. \tag{2.68}$$

The main difference between the inversion formula for $SO(3)$ and $SE(2)$ is that $SO(3)$ only requires indices $l \in \mathbb{Z}$, whereas $SE(2)$ requires the additional frequency parameter $p \in \mathbb{R}$. Notwithstanding, IURS for $SO(3)$ and $SE(2)$ are both size $(2l +$

1) $\times$ $(2l+1)$. IURS on $SE(2)$ can be parameterized with exponential and Bessel functions

$$U_{m,n}(g(r,\phi,\theta),p) = i^{n-m}e^{-i[n\theta+(m-n)\phi]}J_{n-m}(pr). \tag{2.69}$$

Conjugation follows

$$\begin{aligned} U_{m,n}(g^{-1}(r,\phi,\theta),p) &= U^{-1}_{m,n}(g(r,\phi,\theta),p) \\ &= \overline{U_{n,m}(g(r,\phi,\theta),p)} \\ &= i^{n-m}e^{+i[m\theta+(n-m)\phi]}J_{m-n}(pr). \end{aligned} \tag{2.70}$$

This assumes that elements $g \in SE(2)$ are parameterized as

$$g(r,\phi,\theta) = \begin{pmatrix} \cos\theta & -\sin\theta & r\cos\phi \\ \sin\theta & \cos\theta & r\sin\phi \\ 0 & 0 & 1 \end{pmatrix}.$$

Finally, the Fourier coefficients for $SE(2)$ are given by the integral

$$\begin{aligned} \hat{f}_{m,n}(p_l) &= \int_{SE(2)} f(g)U_{m,n}(g^{-1},p_l)dg \\ &= \int_0^{2\pi}\int_0^{2\pi}\int_0^{\infty} f(g(r,\phi,\theta))i^{n-m}e^{+i[m\theta+(n-m)\phi]}J_{m-n}(p_l r)rdrd\phi d\theta. \end{aligned} \tag{2.71}$$

Part II

Orthogonal Functions: Properties and Recurrence Relations

Chapter 3

Properties of Hermite Expansions

3.1 Introduction

This chapter derives properties of Hermite-function expansions under scaling, multiplication, convolution, projection, rotation, and coordinate conversion. The majority of the derivations in this chapter serve as building blocks for engineering applications in later chapters of this dissertation. Some of the upcoming derivations are extensions to 3D from 2D, motivating further applications.

The structure of the rest of this chapter is as follows. Section 3.2 discusses scaling of Hermite function expansions, where an optimal scale factor (in the least-squares sense) can be chosen. Section 3.3 shows how the product of two Hermite functions can be recast as a Hermite expansion whose bandlimit is the product of Hermite function

orders. Similarly, it will be shown that the product of two Hermite expansions is also a Hermite expansion. Section 3.4 is a simple extension of this notion to convolution, showing that the convolution of two Hermite-function expansions is itself another Hermite expansion. Section 3.5 illustrates how projecting a multi-dimensional Hermite expansion can be done in closed-form, and Section 3.6 extends a lossless property of Hermite expansions under rotation from 2D to 3D. Section 3.7 repurposes the rotation property as a means of coordinate conversion in 2D and 3D. Section 3.8 summarizes the chapter and provides a little insight into upcoming application chapters.

3.2 Scaling Hermite Expansions

Recall that Hermite functions form a complete orthonormal basis for square-integrable functions with the orthogonality condition

$$\int_{-\infty}^{\infty} h_m(x)h_n(x)dx = \delta_{m,n}.$$

This orthogonality equation can be scaled as

$$\int_{-\infty}^{\infty} h_m(ax)h_n(ax)dx = a\delta_{m,n},$$

for some $a \in \mathbb{R}_{>0}$. For a fixed band limit N, there is an optimal $a = a(N)$ that will minimize the normalized least-squared error (to be defined soon) between a function

and its corresponding Hermite function series approximation

$$\tilde{f}(x) = \sum_{k=0}^{N} \hat{f}_k h_k(ax), \tag{3.1}$$

where

$$\hat{f}_k = a \int_{-\infty}^{\infty} f(x) h_k(ax) dx. \tag{3.2}$$

To illustrate this, an example characteristic function

$$\chi(x) = \begin{cases} 1, -2 \leq x \leq 2 \\ \\ 0, \text{otherwise} \end{cases},$$

is approximated with a Hermite expansion for values $a = \frac{1}{s}$, where s ranges from 0.1 to 2. The normalized least-squares error (NLSE) between the true function $\chi(x)$ and an estimate $\tilde{\chi}(x)$

$$NLSE(\tilde{\chi}, \chi) = \frac{\sum_i (\tilde{\chi}(x_i) - \chi(x_i))^2}{\sum_i \chi^2(x_i)} \times 100,$$

is plotted versus s and is depicted in Figure 3.1, which also shows a comparison of the fit to $\chi(x)$ for an unscaled series and a scaled series with the optimal s value.

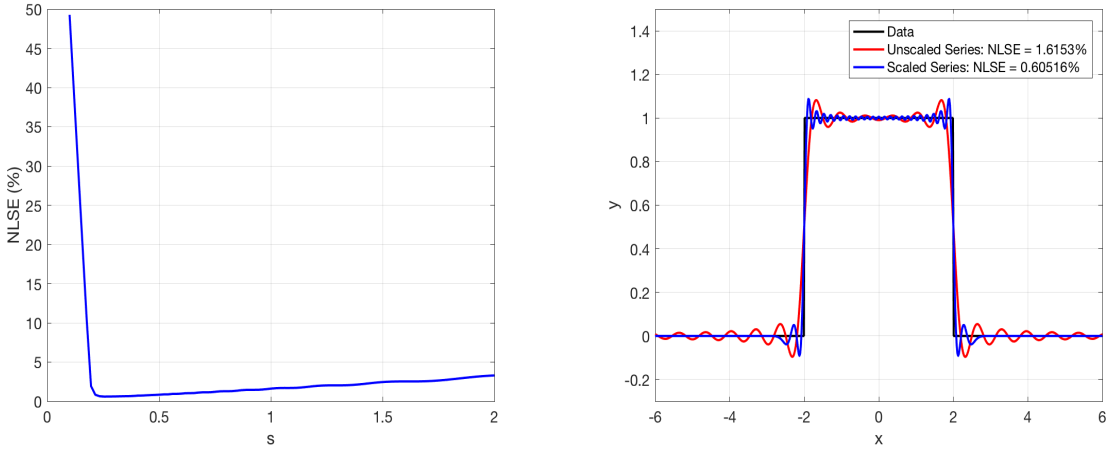

NLSE vs. s Hermite Series Expansions for $N = 100$

Figure 3.1: Scaled 1D Hermite Expansion Example

The next section describes how the product of two Hermite expansions can be represented as another Hermite-function expansion.

3.3 Products of Hermite Expansions

If one wanted to represent the product of two Hermite function expansions in terms of a single Hermite series, so called 3h integrals of the following form are required:

$$\begin{pmatrix} m & n & k \\ a & b & c \end{pmatrix}_h \doteq \int_{-\infty}^{\infty} h_m(ax) h_n(bx) h_k(cx) dx. \tag{3.3}$$

These 3h integrals have a closed-form solution. Moreover, they can be computed recursively (see Chapter 4). The product of two Hermite functions can be expanded

as

$$h_m(ax)h_n(bx) = c \cdot \sum_{k=0}^{\infty} \begin{pmatrix} m & n & k \\ a & b & c \end{pmatrix}_h h_k(cx), \tag{3.4}$$

and truncating this series expansion at a some large integer N will adequately approximate this function product. However, there is an alternative way to express the product of two Hermite functions as a new series with an exact band limit of $m+n$. Consider representing the product of $h_m(ax)$ and $h_n(bx)$ as

$$h_m(ax)h_n(bx) = c_m c_n H_m(ax)H_n(bx)e^{-(a+b)x^2/2}, \tag{3.5}$$

where $c_n = \frac{1}{2^{n/2}\sqrt{n!\sqrt{\pi}}}$ are the Hermite coefficients. Since $H_m(ax)$ and $H_n(bx)$ are polynomials, their product is the finite series

$$H_m(ax)H_n(bx) = \sum_{k=0}^{m+n} \alpha_{m,n}^k H_k(x), \tag{3.6}$$

with coefficients α_{mn}^k according to the integral

$$\alpha_{m,n}^k = \frac{1}{2^k k!\sqrt{\pi}} \int_{-\infty}^{\infty} H_m(ax)H_n(bx)H_k(x)w(x)dx. \tag{3.7}$$

Recall $w(x)$ is the weighting function for Hermite polynomials, ensuring orthogonality and completeness (see Chapter 2). Similarly, $H_m(ax)H_n(bx)$ can be expressed with a

scaled basis

$$H_m(ax)H_n(bx) = \sum_{k=0}^{m+n} \beta_{m,n}^k H_k(cx), \tag{3.8}$$

where

$$\beta_{m,n}^k = c \cdot \frac{1}{2^k k! \sqrt{\pi}} \int_{-\infty}^{\infty} H_m(ax)H_n(bx)H_k(cx)w(cx)dx, \tag{3.9}$$

for $c \in \mathbb{R}$. If $c = \sqrt{a^2 + b^2}$, then the product of two Hermite functions $h_m(ax)h_n(bx)$ can be recast as the new Hermite series

$$\begin{aligned} h_m(ax)h_n(bx) &= c_m c_n \sum_{k=0}^{m+n} \beta_{mn}^k H_k(x\sqrt{a^2+b^2}) e^{-(a^2+b^2)x^2/2} \\ &= c_m c_n \sum_{k=0}^{m+n} \beta_{mn}^k \frac{h_k(x\sqrt{a^2+b^2})}{c_k}. \end{aligned} \tag{3.10}$$

The coefficient $\beta_{m,n}^k$ relates to the 3h integral

$$\begin{pmatrix} m & n & k \\ a & b & \sqrt{a^2+b^2} \end{pmatrix}_h,$$

as

$$\begin{aligned}
\beta_{m,n}^{k} &= \frac{\sqrt{a^2+b^2}}{2^k k!\sqrt{\pi}} \int_{-\infty}^{\infty} H_m(ax) H_n(bx) H_k(x\sqrt{a^2+b^2}) w(x\sqrt{a^2+b^2}) dx \\
&= \frac{\sqrt{a^2+b^2}}{2^k k!\sqrt{\pi}} \int_{-\infty}^{\infty} H_m(ax) H_n(bx) H_k(x\sqrt{a^2+b^2}) e^{-(a^2+b^2)x^2} dx \\
&= \frac{\sqrt{a^2+b^2}}{2^k k!\sqrt{\pi}} \int_{-\infty}^{\infty} H_m(ax) e^{-(ax)^2/2} H_n(bx) e^{-(bx)^2/2} H_k(x\sqrt{a^2+b^2}) e^{-(x\sqrt{a^2+b^2})^2/2} dx \\
&= \frac{\sqrt{a^2+b^2}}{2^k k!\sqrt{\pi}} \int_{-\infty}^{\infty} \frac{h_m(ax)}{c_m} \frac{h_n(bx)}{c_n} \frac{h_k(x\sqrt{a^2+b^2})}{c_k} dx \\
&= \frac{\sqrt{a^2+b^2}}{2^k k!\sqrt{\pi}} \frac{1}{c_m c_n c_k} \begin{pmatrix} m & n & k \\ a & b & \sqrt{a^2+b^2} \end{pmatrix}_h .
\end{aligned} \tag{3.11}$$

With some reshaping, the final form for the product of two Hermite functions as a series with band limit $m+n$ (in terms of 3h integrals) is

$$h_m(ax) h_n(bx) = \sqrt{a^2+b^2} \sum_{k=0}^{m+n} \eta_k \begin{pmatrix} m & n & k \\ a & b & \sqrt{a^2+b^2} \end{pmatrix}_h h_k(x\sqrt{a^2+b^2}), \tag{3.12}$$

where $\eta_k = \frac{1}{c_k^2 2^k k!\sqrt{\pi}}$. The product of two Hermite expansions

$$\tilde{f}(x) = \sum_{m=0}^{M} \hat{f}_m h_m(ax),$$

and

$$\tilde{g}(x) = \sum_{n=0}^{N} \hat{g}_n h_n(bx),$$

can also be represented as a new Hermite expansion using equation (3.12) as

$$\begin{aligned}\tilde{q}(x) &= \tilde{f}(x)\tilde{g}(x) \\ &= \sqrt{a^2+b^2}\sum_{m=0}^{M}\sum_{n=0}^{N}\hat{f}_m\hat{g}_n\sum_{k=0}^{m+n}\eta_k \begin{pmatrix} m & n & k \\ a & b & \sqrt{a^2+b^2} \end{pmatrix}_h h_k(x\sqrt{a^2+b^2}).\end{aligned} \tag{3.13}$$

An example of the "fusion" (i.e. product) of two Hermite expansions is illustrated in Figure 3.2. The test function is

$$d(x;\mu,\sigma) = \sin(2x)e^{-(x-\mu)^2/\sigma^2},$$

giving the two distributions $f(x) = d(x; 0.2, 1)$ and $g(x) = d(x; 0.4, 2)$, with $q(x) = f(x)g(x)$. The variable x is sampled from -10 to 10 with 5000 samples. The band limits for $\tilde{f}(x)$ and $\tilde{g}(x)$ are $M = 25$ and $N = 35$ respectively, with corresponding scale factors $a = 1.2$ and $b = 1.5$. The NLSE

$$NLSE(\tilde{q}, q) = \sum_i \frac{\left(\tilde{q}(x_i) - q(x_i)\right)^2}{q(x_i)^2} \times 100,$$

is $3.2878e-07$.

A natural extension of representing the product of two Hermite expansions is to convolution, which is the topic of the next section.

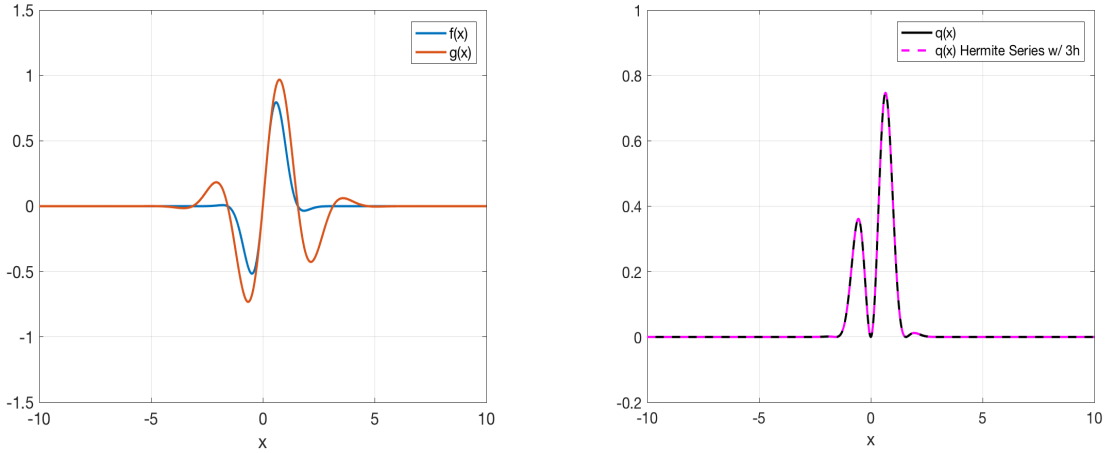

$f(x)$ and $g(x)$ $q(x)$ and $\tilde{q}(x)$ with 3h Integrals

Figure 3.2: Product of Two Scaled Hermite Expansions Example

3.4 Convolution of Hermite Expansions

The convolution of two Hermite functions over the real line is defined by the equation

$$h_m(ax) * h_n(bx) \doteq \int_{-\infty}^{\infty} h_m(a\sigma)\, h_n(b(x-\sigma))\, d\sigma, \tag{3.14}$$

and can be equivalently represented with Fourier transforms as

$$h_m(ax) * h_n(bx) = \mathcal{F}^{-1}\left[\mathcal{F}\left[h_n(ax)\right]\mathcal{F}\left[h_n(bx)\right]\right]. \tag{3.15}$$

Invoking the eigenfunction property of Hermite functions with scaling gives

$$\begin{aligned}\mathcal{F}\left[(h_m(ax) * h_n(bx))\right] &= \mathcal{F}[h_m(ax)]\mathcal{F}[h_n(bx)] \\ &= \left[\frac{1}{a}(-i)^m\sqrt{2\pi}h_m(\omega/a)\right]\left[\frac{1}{b}(-i)^n\sqrt{2\pi}h_n(\omega/b)\right] \\ &= \frac{1}{ab}2\pi(-i)^{m+n}h_m(\omega/a)h_n(\omega/b) \\ &= s_a s_b 2\pi(-i)^{m+n}h_m(s_a\omega)h_n(s_b\omega).\end{aligned} \tag{3.16}$$

Without loss of generality, we can insert the representation of $h_m(s_a\omega)h_n(s_b\omega)$ as a Hermite series according to equation (3.12) as

$$\begin{aligned}\mathcal{F}\left[(h_m(ax) * h_n(bx))\right] &= s_a s_b 2\pi(-i)^{m+n}\sqrt{s_a^2+s_b^2} \\ &\sum_{k=0}^{m+n}\eta_k \begin{pmatrix} m & n & k \\ s_a & s_b & \sqrt{s_a^2+s_b^2}\end{pmatrix}_h h_k\left(\omega\sqrt{s_a^2+s_b^2}\right).\end{aligned} \tag{3.17}$$

Letting $s_c = \sqrt{s_a^2+s_b^2}$, the inverse Fourier transform of $h_k(s_c\omega)$ again leverages the eigenfunction property, with some scaling as

$$\mathcal{F}^{-1}[h_k(r\omega)] = \int_{-\infty}^{\infty} h_k(s_c\omega)e^{i\omega x}d\omega = \frac{1}{s_c}i^k\sqrt{2\pi}h_k(x/s_c). \tag{3.18}$$

All together, the convolution of two Hermite functions is

$$h_m(ax) * h_n(bx) = s_a s_b \sqrt{2\pi}(-i)^{m+n} \sum_{k=0}^{m+n} i^k \eta_k \begin{pmatrix} m & n & k \\ s_a & s_b & \sqrt{s_a^2 + s_b^2} \end{pmatrix}_h h_k\left(x/\sqrt{s_a^2 + s_b^2}\right). \tag{3.19}$$

Note that the resulting expansion was divided by 2π giving $\sqrt{2\pi} = \frac{2\pi^{3/2}}{2\pi}$ instead of $2\pi^{3/2}$. If two functions are again represented as two separate Hermite expansions $\tilde{f}(x)$ and $\tilde{g}(x)$, then the convolution of these two Hermite function expansions is

$$\begin{aligned} \tilde{q}(x) = \tilde{f}(x) * \tilde{g}(x) &= \sum_{m=0}^{M} \sum_{n=0}^{N} \hat{f}_m \hat{g}_n h_m(ax) * h_n(bx) \\ &= s_a s_b 2\pi^{\frac{3}{2}} \sum_{m=0}^{M} \sum_{n=0}^{N} \hat{f}_m \hat{g}_n (-i)^{m+n} \\ &\sum_{k=0}^{m+n} i^k \eta_k \begin{pmatrix} m & n & k \\ s_a & s_b & \sqrt{s_a^2 + s_b^2} \end{pmatrix}_h h_k\left(x/\sqrt{s_a^2 + s_b^2}\right). \end{aligned} \tag{3.20}$$

The notion of convolution can be easily extended to 2D and 3D due to separation of variables. The same can be said for fusion of 2D and 3D Hermite expansions. As another illustration, the functions from Figure 3.2 are used again, only this time the convolution $\tilde{q}(x) = \tilde{f}(x) * \tilde{g}(x)$ is illustrated with 3h integrals. This is depicted in Figure 3.3.

The self-convolution (i.e. auto-correlation) of $\tilde{f}(x)$ can also be computed with 3h

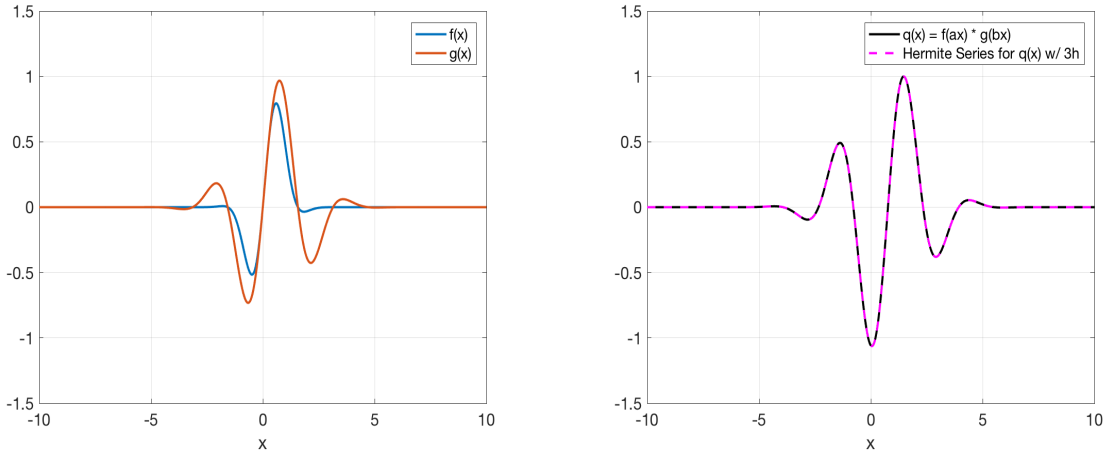

$f(x)$ and $g(x)$ $q(x)$ and $\tilde{q}(x)$ with 3h Integrals

Figure 3.3: Convolution of Two Scaled Hermite Expansions Example

integrals by replacing $\tilde{g}(x)$ with $\tilde{f}(-x)$ as

$$\begin{aligned}\tilde{f}(x) * \tilde{f}(-x) &= \sum_{m=0}^{M}\sum_{n=0}^{M} \hat{f}_m \hat{f}_n h_m(ax) * h_n(-ax) \\ &= \sqrt{2\pi}\sum_{m=0}^{M}\sum_{n=0}^{M} \hat{f}_m \hat{f}_n (-i)^{m+n}(-1)^n \\ &\sum_{k=0}^{m+n} i^k \eta_k \begin{pmatrix} m & n & k \\ s_a & s_a & \sqrt{s_a^2+s_a^2} \end{pmatrix}_h h_k\left(x/\sqrt{s_a^2+s_a^2}\right).\end{aligned} \tag{3.21}$$

This uses the property $h_n(-ax) = (-1)^n h_n(ax)$.

The next section describes how Hermite expansions in either 2D or 3D can be marginalized by integrating the Hermite functions along one of the available dimensions. This integration is effectively parallel-beam projection, and it is caveated that there are of course other models of projection (e.g. fan-beam) [8]. However these are not what the integration of Hermite functions seeks to model.

3.5 Projection with Hermite Expansions

A 2D function $f(x, y)$ can be projected by integrating over the y direction as

$$p(x) = \int_{-\infty}^{\infty} f(x, y)dy. \tag{3.22}$$

When combining this equation with a Hermite series, the result is

$$\begin{aligned} \tilde{p}(x) &= \int_{-\infty}^{\infty} \tilde{f}(x, y)dy \\ &= \int_{-\infty}^{\infty} \sum_{m=0}^{N_1} \sum_{n=0}^{N_2} \hat{f}_{mn} h_m(x) h_n(y)dy \\ &= \sum_{m=0}^{N_1} \sum_{n=0}^{N_2} \hat{f}_{mn} h_m(x)\nu_n. \end{aligned} \tag{3.23}$$

The integral

$$\nu_n = \int_{-\infty}^{\infty} h_n(t)dt, \tag{3.24}$$

can be called a Hermite projection coefficient. This projection notion extends naturally to 3D as

$$\tilde{p}(x, y) = \sum_{m=0}^{N_1} \sum_{n=0}^{N_2} \sum_{k=0}^{N_3} \hat{f}_{m,n,k} h_m(x) h_n(y)\nu_k. \tag{3.25}$$

Recall that Hermite functions can be scaled, thus a scaled projection coefficient $\nu_n(a)$ can be defined as

$$\nu_n(a) = \int_{-\infty}^{\infty} h_n(at)dt. \tag{3.26}$$

The simple recurrence relation

$$\nu_n = \frac{\sqrt{n-1}}{\sqrt{n}}\nu_{n-2}, \tag{3.27}$$

was derived in [9], and holds for scaling as

$$\nu_n(a) = \frac{\sqrt{n-1}}{\sqrt{n}}\nu_{n-2}(a). \tag{3.28}$$

The starting condition for these recurrence relations is

$$\nu_0(a) = \int_{-\infty}^{\infty} exp(-(ax)^2/2)dx = \frac{1}{a}\sqrt{2\sqrt{\pi}}.$$

Odd coefficients equal zero due to the effect of integrating an odd function over a symmetric domain. In the field of tomography, 1D projections can be represented as [10]

$$p^{\theta}(x) \approx \tilde{p}^{\theta}(x) = \sum_{m=0}^{N_1}\sum_{n=0}^{N_2} \hat{f}^{\theta}_{m,n} h_m(x)\nu_n, \tag{3.29}$$

and similarly for 2D projections of 3D densities as

$$p^{\theta,\phi}(x,y) \approx \tilde{p}^{\theta,\phi}(x,y) = \sum_{m=0}^{N_1}\sum_{n=0}^{N_2}\sum_{k=0}^{N_3} \hat{f}^{\theta,\phi}_{m,n,k} h_m(x)h_n(y)\nu_k. \tag{3.30}$$

For 1D projections, θ is a projection angle along a parallel beam, and for 2D projections θ and ϕ are the elevation and azimuth angles respectively. It will be shown in

the following section how Hermite expansions can be rotated by applying a lossless transformation to the corresponding coefficients in a way that preserves the band limits.

3.6 Rotation of Hermite Expansions

Since Hermite functions form an orthonormal basis for $\mathcal{L}^2(\mathbb{R})$, and hence products of Hermite functions in x and y form an orthonormal basis for $\mathcal{L}^2(\mathbb{R}^2)$, it is clear that any square-integrable function and a rotated version thereof both can be expanded in a Hermite-function series. The same is true for a translated version. What is perhaps less obvious is that when a special kind of bandlimit is imposed, this bandlimit is preserved under arbitrary rotations. No such bandlimit preservation is possible for translations of Hermite-function expansions.

A well known approach for rotating a discrete 2D function utilizes Fast Fourier Transforms (FFTs) combined with shear transformations [11], and has been further investigated in related work [12], [13]. Moreover, concepts have been extended to 3D in [14–16]. However, in [17] it was shown that using Hermite functions, and properties relating Hermite coefficients $\hat{f}_{m,n}$ to rotated ones $\hat{f}^{\theta}_{m,n}$ gives a more accurate result than the shear transformation/FFT-based method. This section will illustrate how a 2D expansion is rotated, and then will extend this concept to 3D Hermite expansions.

3.6.1 Rotation of 2D Hermite Expansions

The 2D Hermite expansion of a function $f(x, y)$ can be written with the special band limits

$$f(x,y) \approx \tilde{f}(x,y) = \sum_{m=0}^{N} \sum_{n=0}^{N-m} \hat{f}_{m,n} h_m(x) h_n(y), \tag{3.31}$$

where

$$\hat{f}_{n,m-n} = \int_{-\infty}^{\infty} \int_{-\infty}^{\infty} f(x,y) h_n(x) h_{m-n}(y) dx dy, \tag{3.32}$$

are the Hermite series coefficients. These coefficients can be computed numerically using a rectangular integration method, provided the function of interest is well-behaved and decays sufficiently before the limits of integration. Equivalently

$$f(x,y) = \sum_{m=0}^{N} \sum_{n=0}^{m} \hat{f}_{n,m-n} h_n(x) h_{m-n}(y), \tag{3.33}$$

is also a bandlimit-preserved expansion under rotation. In general, when a function $f(\mathbf{x}) = f(x, y)$ is rotated, the rotation operator R^θ is applied inversely under the function as

$$R^\theta \left[f(\mathbf{x}) \right] = f(R^T(\theta)\mathbf{x}) = f(x\cos\theta + y\sin\theta, -x\sin\theta + y\cos\theta).$$

The property

$$\begin{aligned} R^\theta \left[h_n(x)h_{m-n}(y)\right] &= h_n(x\cos\theta + y\sin\theta)h_{m-n}(-x\sin\theta + y\cos\theta) \\ &= \sum_{q=0}^{m} S_{q,n}^m(\theta)h_q(x)h_{m-q}(y), \end{aligned} \tag{3.34}$$

can be applied to equation (3.31) as

$$\begin{aligned} f^\theta(x,y) = R^\theta\left[f(x,y)\right] &= R^\theta\left[\sum_{m=0}^{N}\sum_{n=0}^{N-m}\hat{f}_{m,n}h_m(x)h_n(y)\right] \\ &= R^\theta\left[\sum_{m=0}^{N}\sum_{n=0}^{m}\hat{f}_{n,m-n}h_n(x)h_{m-n}(y)\right] \\ &= \sum_{m=0}^{N}\sum_{n=0}^{m}\hat{f}_{n,m-n}R^\theta\left[h_n(x)h_{m-n}(y)\right] \\ &= \sum_{m=0}^{N}\sum_{n=0}^{m}\hat{f}_{n,m-n}\sum_{q=0}^{m}S_{q,n}^m(\theta)h_q(x)h_{m-q}(y) \\ &= \sum_{m=0}^{N}\sum_{n=0}^{m}\sum_{q=0}^{m}\hat{f}_{n,m-n}S_{q,n}^m(\theta)h_q(x)h_{m-q}(y) \\ &= \sum_{m=0}^{N}\sum_{q=0}^{m}\sum_{n=0}^{m}\hat{f}_{n,m-n}S_{q,n}^m(\theta)h_q(x)h_{m-q}(y) \\ &= \sum_{m=0}^{N}\sum_{q=0}^{m}\hat{f}_{q,m-q}^\theta h_q(x)h_{m-q}(y) \\ &= \sum_{m=0}^{N}\sum_{q=0}^{N-m}\hat{f}_{m,q}^\theta h_m(x)h_q(y). \end{aligned} \tag{3.35}$$

It is easy to see that the original Hermite series coefficients map linearly to rotated ones as

$$\hat{f}_{q,m-q}^\theta = \sum_{n=0}^{m} S_{q,n}^m(\theta)\hat{f}_{n,m-n}. \tag{3.36}$$

Moreover, the bandlimit of the rotated Hermite series is the same as the unrotated series. Equation (3.36) can be represented in matrix-vector form as

$$\mathbf{f}_m^{\theta} = S^m(\theta)\mathbf{f}_m, \tag{3.37}$$

where

$$\mathbf{f}_m = \begin{bmatrix} \hat{f}_{0,m} & \hat{f}_{1,m-1} & \cdots & \hat{f}_{m,0} \end{bmatrix}, \tag{3.38}$$

and

$$\mathbf{f}_m^{\theta} = \begin{bmatrix} \hat{f}_{0,m}^{\theta} & \hat{f}_{1,m-1}^{\theta} & \cdots & \hat{f}_{m,0}^{\theta} \end{bmatrix}, \tag{3.39}$$

for $m = 0, 1, \cdots, N$. The matrix $S^m(\theta) \in \mathbb{R}^{(m+1)\times(m+1)}$, is an orthogonal matrix comprised of steering coefficients that has the recurrence equations

$$\begin{pmatrix} S_{q+1,n}^{m+1}(\theta) \\ S_{q,n}^{m+1}(\theta) \end{pmatrix} = \begin{pmatrix} \frac{1}{\sqrt{q+1}} & 0 \\ 0 & \frac{1}{\sqrt{m-q+1}} \end{pmatrix} \begin{pmatrix} \cos\theta & -\sin\theta \\ \sin\theta & \cos\theta \end{pmatrix} \begin{pmatrix} \sqrt{n} S_{q,n-1}^{m+1}(\theta) \\ \sqrt{m-n+1} S_{q,n}^{m}(\theta) \end{pmatrix}, \tag{3.40}$$

and

$$\begin{pmatrix} S_{q,n+1}^{m+1}(\theta) \\ S_{q,n}^{m+1}(\theta) \end{pmatrix} = \begin{pmatrix} \frac{1}{\sqrt{n+1}} & 0 \\ 0 & \frac{1}{\sqrt{m-n+1}} \end{pmatrix} \begin{pmatrix} \cos\theta & \sin\theta \\ -\sin\theta & \cos\theta \end{pmatrix} \begin{pmatrix} \sqrt{q} S_{q-1,n}^{m+1}(\theta) \\ \sqrt{m-q+1} S_{q,n}^{m}(\theta) \end{pmatrix}. \tag{3.41}$$

Another useful property that was proved in [9] is that

$$S^{m'}_{q',n'}(\theta) = P^{l}_{m,n}(\cos 2\theta), \tag{3.42}$$

where $P^{l}_{m,n}(\cos 2\theta)$ is a generalized associated Legendre function. The indices relate as

$$\begin{pmatrix} m' \\ q' \\ n' \end{pmatrix} = \begin{bmatrix} 0 & 0 & 2 \\ 1 & 0 & 1 \\ 0 & 1 & 1 \end{bmatrix} \begin{pmatrix} m \\ n \\ l \end{pmatrix}.$$

The first three S matrices are explicitly

$$S^{0}(\theta) = 1, \tag{3.43}$$

$$S^{1}(\theta) = \begin{pmatrix} \cos\theta & \sin\theta \\ -\sin\theta & \cos\theta \end{pmatrix}, \tag{3.44}$$

and

$$S^{2}(\theta) = \begin{pmatrix} \cos^2\theta & \sqrt{2}\cos\theta\sin\theta & \sin^2\theta \\ -\sqrt{2}\cos\theta\sin\theta & \cos^2\theta - \sin^2\theta & \sqrt{2}\cos\theta\sin\theta \\ \sin^2\theta & -\sqrt{2}\cos\theta\sin\theta & \cos^2\theta \end{pmatrix}. \tag{3.45}$$

These three matrices are sufficient starting conditions to generate any higher order $S^m(\theta)$ provided that the corners of $S^m(\theta)$ are filled in with the closed-form equations

$$S^m_{0,0}(\theta) = S^m_{m,m}(\theta) = [\cos\theta]^m, \tag{3.46}$$

$$S^m_{m,0}(\theta) = [-\sin\theta]^m, \tag{3.47}$$

and

$$S^m_{0,m}(\theta) = [\sin\theta]^m. \tag{3.48}$$

Applying these four corner cases ensures completeness. A second way to compute $S^m(\theta)$ is via the matrix exponential. As it was proven in [17], $S^m(\theta)$ is a unitary matrix. Moreover, it is the matrix exponential of a sparse skew-symmetric matrix Ω^m, where

$$\Omega^m_{n,q} = \sqrt{n}\sqrt{m-n+1}\delta_{q,n-1} - \sqrt{n+1}\sqrt{m-n}\delta_{q,n+1}. \tag{3.49}$$

More concretely

$$S^m(\theta) = exp(\theta\Omega^m). \tag{3.50}$$

There is an additional way to represent $S^m(\theta)$. This is with direct matrix multiplication (denoted by $\cdot$) as

$$S^m(\theta) = E \cdot \left(S^m(\frac{\pi}{4})\right)^T \cdot G(\theta) \cdot \left(S^m(\frac{\pi}{4})\right) \cdot E^*, \tag{3.51}$$

where

$$E = \text{diag}\left(\begin{bmatrix} i^0 & i^1 & \dots & i^m \end{bmatrix}\right), \tag{3.52}$$

and

$$G(\theta) = \text{diag}\left(\begin{bmatrix} e^{im\theta} & e^{i(m-2)\theta} & \dots & e^{-im\theta} \end{bmatrix}\right). \tag{3.53}$$

This form will be very useful when computing integrals involving these steering coefficients. The underlying Hermite expansion basis functions did not have any scaling like $h_m(ax)$ or $h_n(by)$, although the property

$$h_n(ax\cos\theta + by\sin\theta)h_{n-m}(-ax\sin\theta + by\cos\theta) = \sum_{q=0}^{m} S_{q,n}^{m}(\theta)h_q(ax)h_{m-q}(by), \tag{3.54}$$

is true for any $a, b \in \mathbb{R}_{>0}$. Thus expansions with scaling are also band limit invariant under rotation. Figure 3.4 shows an example of how a 2D Gaussian can be rotated with the aforementioned Hermite expansion rotation method. The bandlimit for the example is $N = 50$.

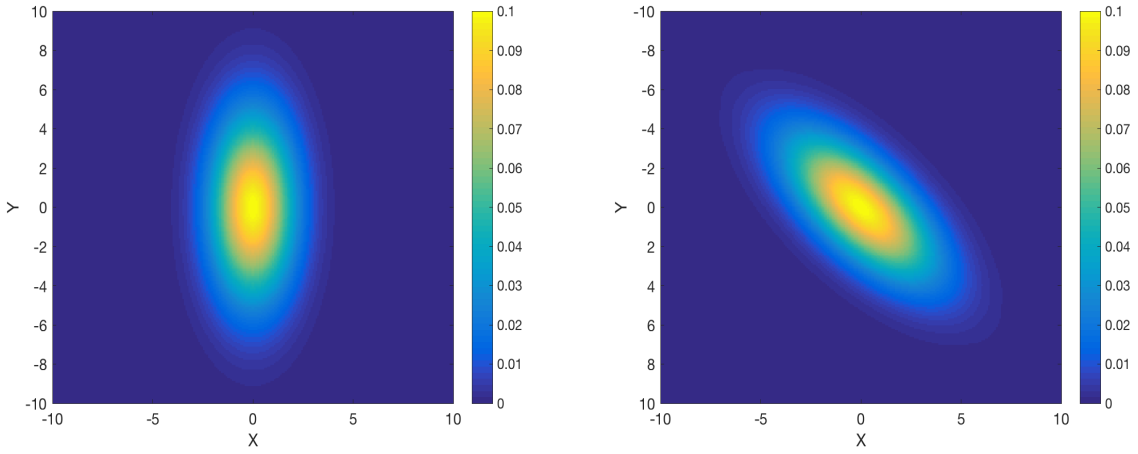

Unrotated Gaussian Rotated Gaussian about z by $\frac{\pi}{4}$

Figure 3.4: 2D Hermite Expansion Rotation Example

Next, it will be shown how a 3D Hermite function expansion can be rotated in a way that also preserves the band limits.

3.6.2 Rotation of 3D Hermite Expansions

This section builds upon the principles of band limit invariance under rotation, extending the discussion to 3D. Some of these techniques were guided by Dr. Wooram Park, a professor at the University of Texas at Dallas with some of his unpublished notes. Consider the rotation invariant 3D Hermite expansion of $f(\mathbf{x}) = f(x, y, z)$ with special band limits

$$f(x,y,z) = \sum_{m=0}^{N} \sum_{n=0}^{N-m} \sum_{k=0}^{N-m-n} \hat{f}_{m,n,k} h_m(x) h_n(y) h_k(z), \tag{3.55}$$

or equivalently

$$f(x,y,z) = \sum_{m=0}^{N} \sum_{n=0}^{m} \sum_{k=0}^{n} \hat{f}_{k,n-k,m-n} h_k(x) h_{n-k}(y) h_{m-n}(z). \tag{3.56}$$

It will be shown how rotations about either the x, y, or z axes can be applied to these 3D Hermite expansions by using the techniques presented for 2D Hermite expansions. First, the bandlimit-invariance principle (under rotation) for z-axis rotations will be derived.

3.6.2.1 Rotating Hermite Expansions about the z-Axis

Applying the rotation operator R_z^α to $f(x,y,z)$ about the z-axis gives

$$\begin{aligned}
f^\alpha(x,y,z) = R_z^\alpha[f(x,y,z)] &= R_z^\alpha\left[\sum_{m=0}^{N}\sum_{n=0}^{N-m}\sum_{k=0}^{N-m-n}\hat{f}_{m,n,k}h_m(x)h_n(y)h_k(z)\right] \\
&= R_z^\alpha\left[\sum_{k=0}^{N}\sum_{m=0}^{N-k}\sum_{n=0}^{N-k-m}\hat{f}_{m,n,k}h_m(x)h_n(y)h_k(z)\right] \\
&= R_z^\alpha\left[\sum_{k=0}^{N}\sum_{m=0}^{N_k}\sum_{n=0}^{N_k-m}\hat{f}_{m,n,k}h_m(x)h_n(y)h_k(z)\right] \\
&= \sum_{k=0}^{N}R_z^\alpha\left[\sum_{m=0}^{N_k}\sum_{n=0}^{m}\hat{f}_{n,m-n,k}h_n(x)h_{m-n}(y)h_k(z)\right] \\
&= \sum_{k=0}^{N}\sum_{m=0}^{N_k}\sum_{n=0}^{m}\hat{f}_{n,m-n,k}\left[\sum_{d=0}^{m}S_{d,n}^m(\alpha)h_d(x)h_{m-d}(y)\right]h_k(z) \\
&= \sum_{k=0}^{N}\sum_{m=0}^{N_k}\sum_{d=0}^{m}\sum_{n=0}^{m}\left[\hat{f}_{n,m-n,k}S_{d,n}^m(\alpha)h_d(x)h_{m-d}(y)\right]h_k(z) \\
&= \sum_{k=0}^{N}\sum_{m=0}^{N_k}\sum_{d=0}^{m}\hat{f}_{d,m-d,k}^\alpha h_d(x)h_{m-d}(y)h_k(z). \\
&= \sum_{k=0}^{N}\sum_{m=0}^{N_k}\sum_{d=0}^{N_k-m}\hat{f}_{m,d,k}^\alpha h_m(x)h_d(y)h_k(z). \\
&= \sum_{k=0}^{N}\sum_{m=0}^{N-k}\sum_{d=0}^{N-k-m}\hat{f}_{m,d,k}^\alpha h_m(x)h_d(y)h_k(z). \\
&= \sum_{m=0}^{N}\sum_{d=0}^{N-m}\sum_{k=0}^{N-m-d}\hat{f}_{m,d,k}^\alpha h_m(x)h_d(y)h_k(z).
\end{aligned} \tag{3.57}$$

Similarly, the rotated coefficients of this 3D Hermite series map linearly to the original 3D Hermite series coefficients as

$$\hat{f}^{\alpha}_{d,m-d,k} = \sum_{n=0}^{m} S^{m}_{d,n}(\alpha)\hat{f}_{n,m-n,k}. \tag{3.58}$$

Equation (3.58) can be represented in matrix-vector form as

$$\mathbf{f}^{\alpha}_{m,k} = S^{m}(\alpha)\mathbf{f}_{m,k}, \tag{3.59}$$

where

$$\mathbf{f}_{m,k} = \begin{bmatrix} \hat{f}_{0,m,k} & \hat{f}_{1,m-1,k} & \cdots & \hat{f}_{m,0,k} \end{bmatrix}, \tag{3.60}$$

and

$$\mathbf{f}^{\alpha}_{m,k} = \begin{bmatrix} \hat{f}^{\alpha}_{0,m,k} & \hat{f}^{\alpha}_{1,m-1,k} & \cdots & \hat{f}^{\alpha}_{m,0,k} \end{bmatrix}, \tag{3.61}$$

for $m = 0, 1, \cdots, N_k$ and $k = 0, 1, \cdots, N$. Figure 3.5 shows an example of a 3D Gaussian being rotated about z by $\frac{\pi}{4}$ using Hermite functions expansions. The subplots are marginalizations over x, y, and z.

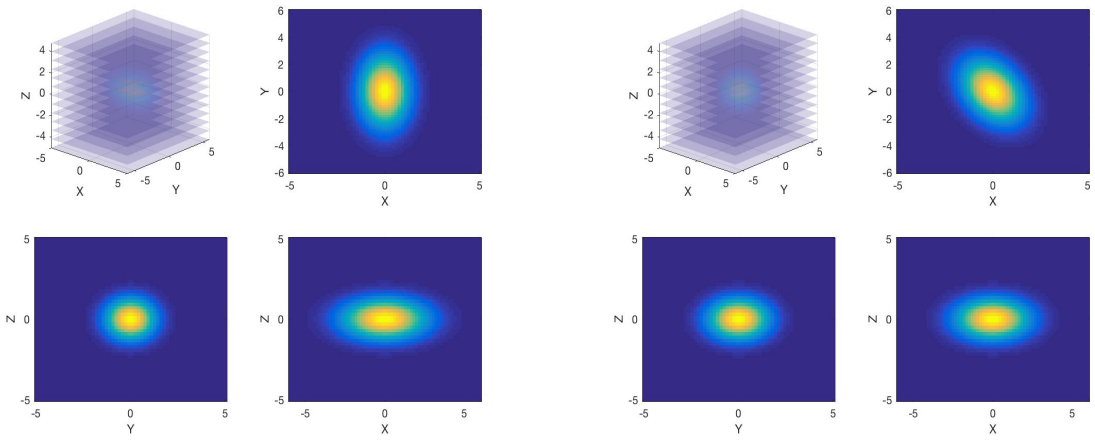

Unrotated Gaussian Rotated Gaussian about z by $\frac{\pi}{4}$

Figure 3.5: Example of Rotated Hermite Series about z-axis

The zero-mean Gaussian has the covariance matrix

$$\Sigma = \begin{bmatrix} 2 & 0 & 0 \\ 0 & 1 & 0 \\ 0 & 0 & \frac{2}{3} \end{bmatrix},$$

and the bandlimit of the corresponding Hermite expansion is $N = 25$. Next, it will be shown how a Hermite series can be rotated about the x-axis.

3.6.2.2 Rotating Hermite Expansions about the x-Axis

Applying the rotation operator R_x^β to $f(x,y,z)$ about the x-axis gives

$$\begin{aligned}
f^\beta(x,y,z) = R_x^\beta[f(x,y,z)] &= R_x^\beta\left[\sum_{m=0}^{N}\sum_{n=0}^{N-m}\sum_{k=0}^{N-m-n}\hat{f}_{m,n,k}h_m(x)h_n(y)h_k(z)\right] \\
&= \sum_{m=0}^{N} R_x^\beta\left[\sum_{n=0}^{N-m}\sum_{k=0}^{N-m-n}\hat{f}_{m,n,k}h_m(x)h_n(y)h_k(z)\right] \\
&= \sum_{m=0}^{N} R_x^\beta\left[\sum_{n=0}^{N_m}\sum_{k=0}^{N_m-n}\hat{f}_{m,n,k}h_n(y)h_k(z)\right]h_m(x) \\
&= \sum_{m=0}^{N} R_x^\beta\left[\sum_{n=0}^{N_m}\sum_{k=0}^{n}\hat{f}_{m,k,n-k}h_k(y)h_{n-k}(z)\right]h_m(x) \\
&= \sum_{m=0}^{N}\sum_{n=0}^{N_m}\sum_{k=0}^{n}\sum_{d=0}^{n}\hat{f}_{m,k,n-k}S_{d,k}^n(\beta)h_d(y)h_{n-d}(z)h_m(x) \\
&= \sum_{m=0}^{N}\sum_{n=0}^{N_m}\sum_{d=0}^{n}\left[\sum_{k=0}^{n}\hat{f}_{m,k,n-k}S_{d,k}^n(\beta)\right]h_d(y)h_{n-d}(z)h_m(x) \\
&= \sum_{m=0}^{N}\sum_{n=0}^{N_m}\sum_{d=0}^{n}\hat{f}_{m,d,n-d}^\beta h_m(x)h_d(y)h_{n-d}(z) \\
&= \sum_{m=0}^{N}\sum_{n=0}^{N_m}\sum_{d=0}^{N_m-n}\hat{f}_{m,n,d}^\beta h_m(x)h_n(y)h_d(z) \\
&= \sum_{m=0}^{N}\sum_{n=0}^{N-m}\sum_{d=0}^{N-m-n}\hat{f}_{m,n,d}^\beta h_m(x)h_n(y)h_d(z).
\end{aligned} \tag{3.62}$$

The rotated coefficients of this 3D Hermite series map linearly to the original 3D Hermite series coefficients as

$$\hat{f}_{m,d,n-d}^\beta = \sum_{k=0}^{n} S_{d,k}^n(\beta)\hat{f}_{m,k,n-k}. \tag{3.63}$$

Equation (3.63) can be represented in matrix-vector form as

$$\mathbf{f}^{\beta}_{m,n} = S^{n}(\beta)\mathbf{f}_{m,n}, \tag{3.64}$$

where

$$\mathbf{f}_{m,n} = \begin{bmatrix} \hat{f}_{m,0,n} & \hat{f}_{m,1,n-1} & \cdots & \hat{f}_{m,n,0} \end{bmatrix}, \tag{3.65}$$

and

$$\mathbf{f}^{\beta}_{m,n} = \begin{bmatrix} \hat{f}^{\beta}_{m,0,n} & \hat{f}^{\beta}_{m,1,n-1} & \cdots & \hat{f}^{\beta}_{m,n,0} \end{bmatrix}, \tag{3.66}$$

for $m = 0, 1, \cdots, N$ and $n = 0, 1, \cdots, N_m$. Figure 3.6 shows an example of the same 3D Gaussian from before being rotated about x by $\frac{\pi}{4}$ using Hermite functions expansions.

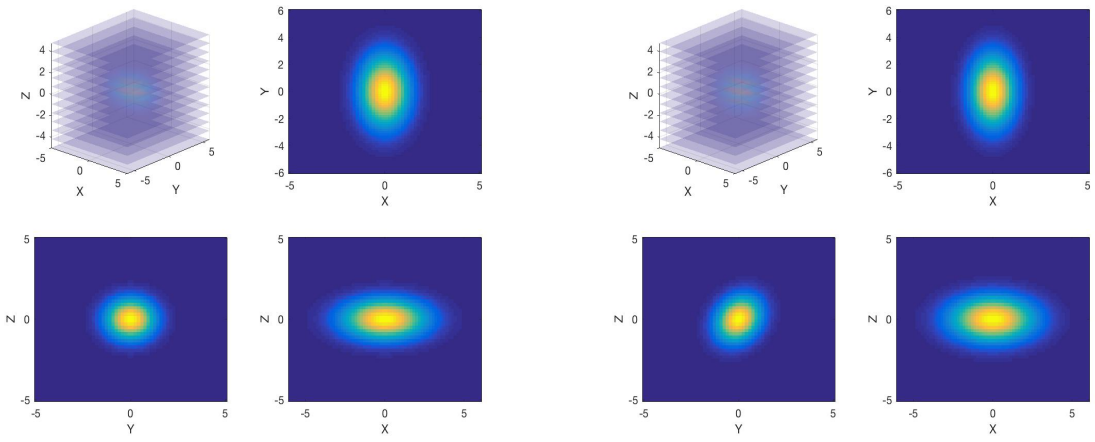

Unrotated Gaussian Rotated Gaussian about x by $\frac{\pi}{4}$

Figure 3.6: Example of Rotated Hermite Series about x-axis

Hermite coefficients can be rotated for any rotation R, by decomposing R as

$$R = R_z(\alpha)R_x(\beta)R_z(\gamma),$$

with Euler angles α, β, and γ, which for this particular composition can be solved for explicitly as

$$\beta = atan2\left[\sqrt{1 - r_{33}^2}, r_{33}\right], \tag{3.67}$$

$$\alpha = atan2\left[\frac{r_{13}}{\sin\beta}, \sqrt{1 - (\frac{r_{13}}{\sin\beta})^2}\ \right], \tag{3.68}$$

and

$$\gamma = atan2\left[\frac{r_{31}}{\sin\beta}, \sqrt{1 - (\frac{r_{31}}{\sin\beta})^2}\ \right], \tag{3.69}$$

provided $\beta \neq 0$. The variables $[r_{ij}]$ correspond to the matrix element in the i^{th} row and j^{th} column of R. A function $f(\mathbf{x}) = f(x, y, z)$ can be rotated as $f(R^T\mathbf{x}) = f(R_z^T(\gamma)R_x^T(\beta)R_z^T(\alpha)\mathbf{x})$ by following the sequence

$$\hat{f}_{m,n,k} \rightarrow \hat{f}^{\gamma}_{m,n,k} \rightarrow \hat{f}^{\beta,\gamma}_{m,n,k} \rightarrow \hat{f}^{\alpha,\beta,\gamma}_{m,n,k}.$$

Note the order of this sequence (i.e. $\gamma \rightarrow \beta \rightarrow \alpha$ and not $\alpha \rightarrow \beta \rightarrow \gamma$). So starting with $\hat{f}_{m,n,k}$, the sequence is to apply equation (3.58), then equation (3.63) to the new coefficients $\hat{f}^{\gamma}_{m,n,k}$, and then equation (3.58) again to the coefficients $\hat{f}^{\beta,\gamma}_{m,n,k}$ to obtain

$\hat{f}^{\alpha,\beta,\gamma}_{m,n,k}$. A rotation about y can be composed as

$$R_y(\theta) = R_z\left(\frac{\pi}{2}\right) R_x\left(\theta\right) R_z^T\left(\frac{\pi}{2}\right). \tag{3.70}$$

Also, new coefficients that result from rotations about z by $\frac{+}{-}\frac{\pi}{2}$ are simply local permutations of the previous coefficients. Equation (3.70) Allows for rotations about the y-axis (and other compositions) without having to derive any additional equations akin to (3.58) or (3.63). As an example, Figure 3.7 shows the same 3D Gaussian being rotated about y by $\frac{\pi}{4}$ using Hermite functions expansions and the above composition rule.

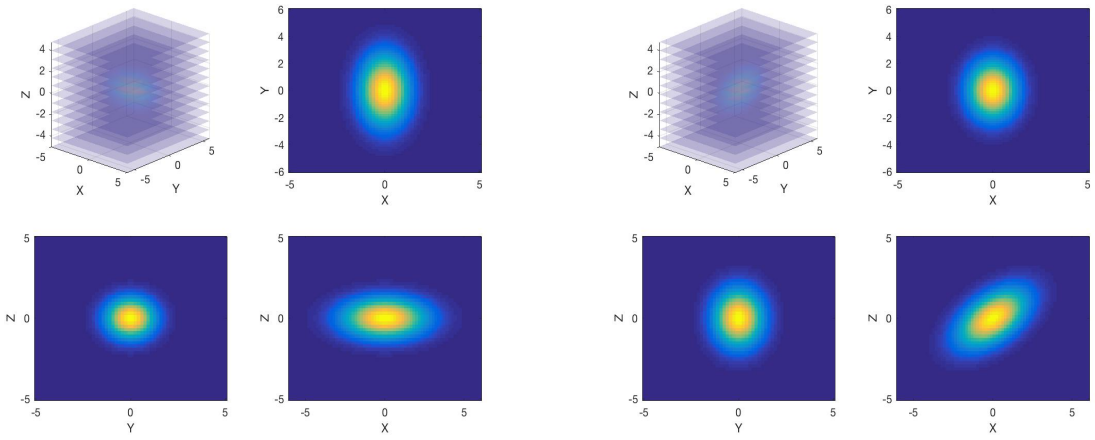

Unrotated Gaussian Rotated Gaussian about y by $\frac{\pi}{4}$

Figure 3.7: Example of Rotated Hermite Series about y-axis

This idea of lossless rotation of Hermite function expansions has applications to data fusion, cryo-electron microscopy (cryo-EM) and SAXS. These applications are articulated in later chapters. More immediate uses are shown in the next section that

deals with coordinate conversion.

3.7 Coordinate Conversion with Hermite Expansions

Rotation of Hermite expansions can be repurposed as a means of coordinate separation. In [18] and [9], the idea of interconversion was presented, where a 2D Hermite expansion could be converted to a Fourier-Laguerre series, and vice versa. This process was deemed lossless, due to a localization property between Fourier-Laguerre and 2D Hermite-function expansions. This section provides an alternative approach when converting from a 2D Hermite series. This one way conversion is also extended to 3D, where a 3D Hermite function expansion is converted to an expansion in spherical coordinates.

Equation (3.34) can be exploited to render a version of the Hermite expansion that has been separated into a product of functions, one for each of the polar variables. In 2D, this is accomplished by setting $x = \rho$, $y = 0$, and $\theta = -\phi$, giving

$$h_n(\rho\cos\phi)h_{m-n}(\rho\sin\phi) = \sum_{q=0}^{m} S_{q,n}^{m}(-\phi)h_q(\rho)h_{m-q}(0). \tag{3.71}$$

The polar variables relate to Cartesian coordinates as

$$(\rho, \phi) = \left(\sqrt{x^2 + y^2}, atan2(y, x) \right).$$

With some manipulation, and by defining $c = n$ and $d = m-n$, the product $h_c(x)h_d(y)$ can be expressed in a similar way as

$$h_c(\rho c\phi)h_d(\rho s\phi) = \sum_{q=0}^{c+d} S_{q,c}^{c+d}(-\phi)h_q(\rho)h_{c+d-q}(0). \tag{3.72}$$

Equations (3.71) and (3.72) show that the product of two Hermite functions (one in x and one in y) can be separated into a sum of ρ-function/ϕ-function products. Corresponding variable-separated Hermite expansions look like

$$\begin{aligned} \tilde{f}(\rho c\phi, \rho s\phi) &= \sum_{c=0}^{N} \sum_{d=0}^{N-c} \hat{f}_{c,d} h_c(\rho c\phi)h_d(\rho s\phi) \\ &= \sum_{c=0}^{N} \sum_{d=0}^{N-c} \hat{f}_{c,d} \sum_{q=0}^{c+d} S_{q,c}^{c+d}(-\phi)h_q(\rho)h_{c+d-q}(0), \end{aligned} \tag{3.73}$$

and

$$\begin{aligned} \tilde{f}(\rho c\phi, \rho s\phi) &= \sum_{m=0}^{N} \sum_{n=0}^{m} \hat{f}_{n,m-n} h_n(\rho c\phi)h_{m-n}(\rho s\phi) \\ &= \sum_{m=0}^{N} \sum_{n=0}^{m} \hat{f}_{n,m-n} \sum_{q=0}^{m} S_{q,n}^{m}(-\phi)h_q(\rho)h_{m-q}(0). \end{aligned} \tag{3.74}$$

This expansion will be called an SH expansion, since it is a sum of products of steering coefficient terms $S_{q,n}^{m}(-\phi)$ and Hermite functions. Next, it will be shown how a 3D

rendition of this SH expansion can be rendered by stringing together two S matrices: one for azimuth (rotation about z) and one for elevation (rotation about x). Consider the rotation $R = R_z(\alpha)R_x(\beta)$. Applying this rotation directly to a 3D Hermite series for a function $f(\mathbf{x}) = f(x, y, z)$ gives

$$\tilde{f}^{\alpha,\beta}(\mathbf{x}) = f(R_x^T(\beta)R_z^T(\alpha)\mathbf{x}) = \sum_{m=0}^{N}\sum_{n=0}^{N-m}\sum_{k=0}^{n}\hat{f}_{m,k,n-k}h_m(x'')h_k(y'')h_{n-k}(z''), \quad (3.75)$$

where

$$\begin{pmatrix} x'' \\ y'' \\ z'' \end{pmatrix} = R_z^T(\alpha)R_x^T(\beta)\begin{pmatrix} x \\ y \\ z \end{pmatrix} = \begin{pmatrix} xc\alpha + ys\alpha \\ zs\beta + yc\alpha c\beta - xc\beta s\alpha \\ zc\beta - yc\alpha s\beta + xs\alpha s\beta \end{pmatrix}. \quad (3.76)$$

Alternatively, the transformation of Hermite coefficients $\hat{f}_{m,n,k}$ for this composition of two rotations would follow

$$\hat{f}_{m,n,k} \rightarrow \hat{f}^{\beta}_{m,n,k} \rightarrow \hat{f}^{\alpha,\beta}_{m,n,k}.$$

Applying equation (3.63) first gives

$$\tilde{f}(R_x^T(\beta)\mathbf{x}) = \sum_{m=0}^{N}\sum_{n=0}^{N-m}\sum_{k=0}^{n}\hat{f}_{m,k,n-k}\sum_{d=0}^{n}S^n_{d,k}(\beta)h_m(x)h_d(y)h_{n-d}(z). \quad (3.77)$$

Similarly, after applying equation (3.63) and then (3.58) to a 3D Hermite series, equation (3.75) can be equivalently represented with steering coefficients stringed

together as

$$\begin{aligned}\tilde{f}(R_x^T(\beta)R_z^T(\alpha)\mathbf{x}) &= \sum_{m=0}^{N}\sum_{n=0}^{N-m}\sum_{k=0}^{n}\hat{f}_{m,k,n-k}h_m(x'')h_k(y'')h_{n-k}(z'') \\ &= \sum_{m=0}^{N}\sum_{n=0}^{N-m}\sum_{k=0}^{n}\hat{f}_{m,k,n-k}\sum_{d=0}^{n}S_{d,k}^{n}(\beta)\sum_{t=0}^{m+d}S_{t,m}^{m+d}(\alpha)h_t(x)h_{m+d-t}(y)h_{n-d}(z).\end{aligned} \tag{3.78}$$

Locally, this means

$$h_m(x'')h_k(y'')h_{n-k}(z'') = \sum_{d=0}^{n}S_{d,k}^{n}(\beta)\sum_{t=0}^{m+d}S_{t,m}^{m+d}(\alpha)h_t(x)h_{m+d-t}(y)h_{n-d}(z), \tag{3.79}$$

or equivalently

$$h_m(x'')h_v(y'')h_w(z'') = \sum_{d=0}^{v+w}S_{d,v}^{v+w}(\beta)\sum_{t=0}^{m+d}S_{t,m}^{m+d}(\alpha)h_t(x)h_{m+d-t}(y)h_{v+w-d}(z), \tag{3.80}$$

where $v = k$ and $w = n - k$. Choosing the coordinates x'',y'', and z'' to be

$$\begin{pmatrix}x''\\ y''\\ z''\end{pmatrix} = R_z^T(-\theta)R_x^T(-\phi)\begin{pmatrix}r\\ 0\\ 0\end{pmatrix} = \begin{pmatrix}rc\theta\\ rs\theta c\phi\\ rs\theta s\phi\end{pmatrix}, \tag{3.81}$$

yields

$$h_m(rc\theta)h_k(rs\theta c\phi)h_{n-k}(rs\theta s\phi) = \sum_{d=0}^{n}S_{d,k}^{n}(-\phi)\sum_{t=0}^{m+d}S_{t,m}^{m+d}(-\theta)h_t(r)h_{m+d-t}(0)h_{n-d}(0), \tag{3.82}$$

or

$$h_m(rc\theta)h_v(rs\theta c\phi)h_w(rs\theta s\phi) = \sum_{d=0}^{v+w} S_{d,v}^{v+w}(-\phi) \sum_{t=0}^{m+d} S_{t,m}^{m+d}(-\theta)h_t(r)h_{m+d-t}(0)h_{v+w-d}(0). \tag{3.83}$$

What is nice about equation (3.83) is that for the left hand side,

$$h_m(rc\theta)h_v(rs\theta c\phi)h_w(rs\theta s\phi) = h_v(rs\theta c\phi)h_w(rs\theta s\phi)h_m(rc\theta).$$

In the derivation, it did not matter that $z'' \neq rc\theta$, which corresponds to a traditional spherical coordinate system with the two additional terms being $x = rs\theta c\phi$ and $y = rs\theta s\phi$. This allows for the 3D Hermite series in spherical coordinates to be partitioned into separate functions as

$$\begin{aligned}\tilde{f}(x,y,z) =& \tilde{f}(rs\theta c\phi, rs\theta s\phi, rc\theta) = \sum_{v=0}^{N}\sum_{w=0}^{N-v}\sum_{m=0}^{N-v-w} \hat{f}_{v,w,m}h_v(rs\theta c\phi)h_w(rs\theta s\phi)h_m(rc\theta) \\ =& \sum_{v=0}^{N}\sum_{w=0}^{N-v}\sum_{m=0}^{N-v-w} \hat{f}_{v,w,m} \sum_{d=0}^{v+w} S_{d,v}^{v+w}(-\phi) \sum_{t=0}^{m+d} S_{t,m}^{m+d}(-\theta)h_t(r)h_{m+d-t}(0)h_{v+w-d}(0).\end{aligned} \tag{3.84}$$

Equation (3.84) will be called an S^2H expansion. This idea of coordinate conversion can be applied to interconversion, computed tomography (CT), and data fusion in polar and spherical coordinates. It is also possible that conversion from d-dimensional Cartesian coordinates to hyper-spherical coordinates could be facilitated with so-called $S^{d-1}H$ expansions. This notion is left to the reader.

3.8 Chapter Summary

The concepts of multiplication, convolution, projection, rotation, and coordinate conversion have been facilitated with Hermite function expansions. These techniques have immediate implications to the topics of grid interconversion, data fusion, and cryo-EM/SAXS data representations, all of which are upcoming chapters in this thesis.

The $3h$ integral was also presented, and clearly has a role in the facilitation of convolutions and fusions of Hermite expansions. We will also see this integral crop up in topics of deconvolution and continuum normal mode analysis.

Chapter 4

Recurrence Relations for $3h$ Integrals

4.1 Introduction

This chapter derives recurrence relations for the integral of the product of three Hermite functions, also known as $3h$ integrals. As mentioned in the previous chapter, $3h$ integrals can be used in analysis involving convolution, fusion, and normal mode decompositions. The focal points of this chapter however are on completeness, starting conditions, and efficient methods to fill an integer block space corresponding to the solutions of these integrals.

The general theme for developing recurrence relations will be to arrive at equations

of the form

$$\begin{bmatrix} \begin{pmatrix} m+1 & n & k \\ a & b & c \end{pmatrix}_h \\ \begin{pmatrix} m & n+1 & k \\ a & b & c \end{pmatrix}_h \\ \begin{pmatrix} m & n & k+1 \\ a & b & c \end{pmatrix}_h \end{bmatrix} = A(m,n,k,a,b,c) \begin{bmatrix} \begin{pmatrix} m-1 & n & k \\ a & b & c \end{pmatrix}_h \\ \begin{pmatrix} m & n-1 & k \\ a & b & c \end{pmatrix}_h \\ \begin{pmatrix} m & n & k-1 \\ a & b & c \end{pmatrix}_h \end{bmatrix}, \tag{4.1}$$

where $A \in \mathbb{R}^{3\times 3}$ and

$$\begin{pmatrix} m' & n' & k' \\ a & b & c \end{pmatrix}_h \doteq \int_{-\infty}^{\infty} h_{m'}(ax) h_{n'}(bx) h_{k'}(cx) dx,$$

is a $3h$ integral. Completeness in this context is the recurrence relation's ability to sufficiently fill an integer space inside $\mathbb{Z}^3_{\geq 0}$ where a point in this space parameterizes the corresponding $3h$ integral's order triplet (m,n,k) . The variables a, b, and c are assumed to be fixed scaling parameters. If one wanted to fill an $L \times L \times L$ size lattice, then the starting conditions required to recursively fill this space are three $L \times L$ square lattices and a "keystone" $3h$ integral

$$\begin{pmatrix} 1 & 1 & 1 \\ a & b & c \end{pmatrix}_h .$$

These square lattices are in mn, nk, and mk coordinates, where m, n, and k are integer values between 0 and $N = L - 1$. 2D versions of the $3h$ integral recurrence relation are of the forms

$$\left[\begin{pmatrix} 0 & n+1 & k \\ a & b & c \end{pmatrix}_h \begin{pmatrix} 0 & n & k+1 \\ a & b & c \end{pmatrix}_h\right] = B(n,k,a,b,c)\left[\begin{pmatrix} 0 & n-1 & k \\ a & b & c \end{pmatrix}_h \begin{pmatrix} 0 & n & k-1 \\ a & b & c \end{pmatrix}_h\right], \tag{4.2}$$

$$\left[\begin{pmatrix} m+1 & 0 & k \\ a & b & c \end{pmatrix}_h \begin{pmatrix} m & 0 & k+1 \\ a & b & c \end{pmatrix}_h\right] = B(m,k,a,b,c)\left[\begin{pmatrix} m-1 & 0 & k \\ a & b & c \end{pmatrix}_h \begin{pmatrix} m & 0 & k-1 \\ a & b & c \end{pmatrix}_h\right], \tag{4.3}$$

or

$$\left[\begin{pmatrix} m+1 & n & 0 \\ a & b & c \end{pmatrix}_h \begin{pmatrix} m & n+1 & 0 \\ a & b & c \end{pmatrix}_h\right] = B(m,n,a,b,c)\left[\begin{pmatrix} m-1 & n & 0 \\ a & b & c \end{pmatrix}_h \begin{pmatrix} m & n-1 & 0 \\ a & b & c \end{pmatrix}_h\right], \tag{4.4}$$

depending on the planes of interest. Completeness for this planar recurrence relation would require two axes (of length L) for each corresponding 2D lattice , with 1D

recurrence relations of the forms

$$\begin{pmatrix} m+1 & 0 & 0 \\ a & b & c \end{pmatrix}_h = \alpha(m,a,b,c) \begin{pmatrix} m-1 & 0 & 0 \\ a & b & c \end{pmatrix}_h , \tag{4.5}$$

$$\begin{pmatrix} 0 & n+1 & 0 \\ a & b & c \end{pmatrix}_h = \alpha(n,a,b,c) \begin{pmatrix} 0 & n-1 & 0 \\ a & b & c \end{pmatrix}_h , \tag{4.6}$$

and

$$\begin{pmatrix} 0 & 0 & k+1 \\ a & b & c \end{pmatrix}_h = \alpha(k,a,b,c) \begin{pmatrix} 0 & 0 & k-1 \\ a & b & c \end{pmatrix}_h . \tag{4.7}$$

These axial recurrence relations require the starting 3h integrals $\begin{pmatrix} 0 & 0 & 0 \\ a & b & c \end{pmatrix}_h$, and either $\begin{pmatrix} 1 & 0 & 0 \\ a & b & c \end{pmatrix}_h$, $\begin{pmatrix} 0 & 1 & 0 \\ a & b & c \end{pmatrix}_h$, or $\begin{pmatrix} 0 & 0 & 1 \\ a & b & c \end{pmatrix}_h$ for the respective m, n, or k axis.

In summary, to fill an integer block space of $3h$ integrals (in the shape of an L-cube), the following steps are to be performed:

1. Generate axes from 1D recurrence relation using starting 3h integrals with equations akin to (4.5), (4.6), and (4.7).

2. Using these axes, generate planes from 2D recurrence relations similar to (4.2), (4.3), and (4.4).

3. Using these planes, fill the entire desired volume using a full 3D recurrence relation like equation (4.1).

The remainder of this chapter is outlined as follows. Section 4.2 will derive the full recurrence relation for $3h$ integrals. Section 4.3 will derive the planar recurrence relation, and Section 4.4 will derive the axial recurrence relation. A propagation description for how the integer block space is filled will be articulated in Section 4.5, followed by some numerical examples in Section 4.6. Section 4.7 will summarize the chapter.

4.2 Recurrence Relations for $3h$ Integrals

The $3h$ and $3H$ integrals are defined as

$$\begin{pmatrix} m & n & k \\ a & b & c \end{pmatrix}_h \doteq c_m c_n c_k \int_{-\infty}^{\infty} e^{\frac{-(a^2+b^2+c^2)x^2}{2}} H_m(ax) H_n(bx) H_k(cx) dx, \tag{4.8}$$

and

$$\begin{pmatrix} m & n & k \\ a & b & c \end{pmatrix}_H \doteq \int_{-\infty}^{\infty} e^{\frac{-(a^2+b^2+c^2)x^2}{2}} H_m(ax) H_n(bx) H_k(cx) dx, \tag{4.9}$$

which map to and from each other via the Hermite coefficients $c_n = \frac{1}{2^{n/2}\sqrt{n!\sqrt{\pi}}}$ since

$$h_n(x) = c_n H_n(x) e^{-x^2/2}.$$

Therefore the focus will be on deriving recurrence relations for 3H integrals, and then scaling them by the coefficients to obtain recurrence relations for 3h integrals. Some shorthand notation $\gamma = a^2 + b^2 + c^2$ will be used in this section. Recall the recurrence relation equations for Hermite polynomials (as defined in Chapter 2)

$$H_n'(ax) = 2anH_{n-1}(ax), \tag{4.10}$$

and

$$H_n(ax) = \frac{H_{n+1}(ax)}{2ax} + \frac{nH_{n-1}(ax)}{ax}. \tag{4.11}$$

The upcoming 3h/3H recurrence relations will utilize these recurrence equations. Consider the expression

$$\begin{aligned} I_{m,n,k}(a,b,c) &= \int_{-\infty}^{\infty} \frac{\partial}{\partial x}\{e^{\frac{-(a^2+b^2+c^2)x^2}{2}} H_m(ax)H_n(bx)H_k(cx)\}dx \\ &= H_m(ax)H_n(bx)H_k(cx)e^{\frac{-\gamma x^2}{2}}\Big|_{-\infty}^{\infty} = 0. \end{aligned} \tag{4.12}$$

Alternatively, carrying out the derivative inside the integral, and inserting equations (4.10) and (4.11) gives

$$\begin{aligned}
I_{m,n,k}(a,b,c) &= \int_{-\infty}^{\infty} \frac{\partial}{\partial x}\{e^{\frac{-\gamma x^2}{2}} H_m(ax)H_n(bx)H_k(cx)\}dx \\
&= \int_{-\infty}^{\infty} -\gamma x e^{\frac{-\gamma x^2}{2}} H_m(ax)H_n(bx)H_k(cx)dx + \\
&\int_{-\infty}^{\infty} e^{\frac{-\gamma x^2}{2}}[H'_m(ax)H_n(bx)H_k(cx) + H_m(ax)H'_n(bx)H_k(cx) \\
&+ H_m(ax)H_n(bx)H'_k(cx)]dx. \\
&= -\frac{\gamma}{2a}\begin{pmatrix} m+1 & n & k \\ a & b & c \end{pmatrix}_H - \frac{\gamma m}{a}\begin{pmatrix} m-1 & n & k \\ a & b & c \end{pmatrix}_H + 2am\begin{pmatrix} m-1 & n & k \\ a & b & c \end{pmatrix}_H \\
&+ 2bn\begin{pmatrix} m & n-1 & k \\ a & b & c \end{pmatrix}_H + 2ck\begin{pmatrix} m & n & k-1 \\ a & b & c \end{pmatrix}_H .
\end{aligned} \tag{4.13}$$

Equating equations (4.13) and (4.12) gives

$$\begin{aligned}
\frac{\gamma}{2a}\begin{pmatrix} m+1 & n & k \\ a & b & c \end{pmatrix}_H &= m(2a - \frac{\gamma}{a})\begin{pmatrix} m-1 & n & k \\ a & b & c \end{pmatrix}_H + 2bn\begin{pmatrix} m & n-1 & k \\ a & b & c \end{pmatrix}_H \\
&+ 2ck\begin{pmatrix} m & n & k-1 \\ a & b & c \end{pmatrix}_H .
\end{aligned} \tag{4.14}$$

If equation (4.11) was used for orders n and k instead of m, the resulting equations would be

$$\frac{\gamma}{2b}\begin{pmatrix} m & n+1 & k \\ a & b & c \end{pmatrix}_H = 2am\begin{pmatrix} m-1 & n & k \\ a & b & c \end{pmatrix}_H + n(2b-\frac{\gamma}{b})\begin{pmatrix} m & n-1 & k \\ a & b & c \end{pmatrix}_H + 2ck\begin{pmatrix} m & n & k-1 \\ a & b & c \end{pmatrix}_H , \tag{4.15}$$

and

$$\frac{\gamma}{2c}\begin{pmatrix} m & n & k+1 \\ a & b & c \end{pmatrix}_H = 2am\begin{pmatrix} m-1 & n & k \\ a & b & c \end{pmatrix}_H + 2bn\begin{pmatrix} m & n-1 & k \\ a & b & c \end{pmatrix}_H + k(2c-\frac{\gamma}{c})\begin{pmatrix} m & n & k-1 \\ a & b & c \end{pmatrix}_H . \tag{4.16}$$

Combing equations (4.14), (4.15), and (4.16) gives the 3D recurrence relation

$$M\begin{bmatrix} \begin{pmatrix} m+1 & n & k \\ a & b & c \end{pmatrix}_H \\ \begin{pmatrix} m & n+1 & k \\ a & b & c \end{pmatrix}_H \\ \begin{pmatrix} m & n & k+1 \\ a & b & c \end{pmatrix}_H \end{bmatrix} = N\begin{bmatrix} \begin{pmatrix} m-1 & n & k \\ a & b & c \end{pmatrix}_H \\ \begin{pmatrix} m & n-1 & k \\ a & b & c \end{pmatrix}_H \\ \begin{pmatrix} m & n & k-1 \\ a & b & c \end{pmatrix}_H \end{bmatrix}, \tag{4.17}$$

where

$$M(a,b,c) = \begin{bmatrix} \frac{\gamma}{2a} & 0 & 0 \\ 0 & \frac{\gamma}{2b} & 0 \\ 0 & 0 & \frac{\gamma}{2c} \end{bmatrix}, \tag{4.18}$$

and

$$N(m,n,k,a,b,c) = \begin{bmatrix} m(2a - \frac{\gamma}{a}) & 2bn & 2ck \\ 2am & n(2b - \frac{\gamma}{b}) & 2ck \\ 2am & 2bn & k(2c - \frac{\gamma}{c}) \end{bmatrix}. \tag{4.19}$$

A solution exists when $\det M = \frac{(a^2+b^2+c^2)^3}{8abc} \neq 0$. The matrix $A_H = M^{-1}N$ is given explicitly as

$$A_H = \frac{1}{\gamma} \begin{bmatrix} 2am(2a - \frac{\gamma}{a}) & 4abn & 4ack \\ 4abm & 2bn(2b - \frac{\gamma}{b}) & 4bck \\ 4acm & 4bcn & 2ck(2c - \frac{\gamma}{c}) \end{bmatrix}. \tag{4.20}$$

With some more shorthand notation

$$\zeta^H_{\pm 1} = \begin{bmatrix} \begin{pmatrix} m \pm 1 & n & k \\ a & b & c \end{pmatrix}_H \\ \begin{pmatrix} m & n \pm 1 & k \\ a & b & c \end{pmatrix}_H \\ \begin{pmatrix} m & n & k \pm 1 \\ a & b & c \end{pmatrix}_H \end{bmatrix},$$

the final recurrence relation for 3H integrals is

$$\zeta^H_{+1} = A_H \zeta^H_{-1}. \tag{4.21}$$

The superscript ^{H} reminds us that this is a recurrence relation for 3H integrals. To obtain a recurrence relation for 3h integrals, the Hermite coefficients will be used. The vectors of 3H integrals $\zeta^H_{\pm 1}$map to vectors of 3h integrals $\zeta^h_{\pm 1}$ as

$$\zeta^h_{\pm 1} = L_{\pm 1} \zeta^H_{\pm 1}, \tag{4.22}$$

where

$$L_{\pm 1} = \begin{bmatrix} c_{m \pm 1} c_n c_k & 0 & 0 \\ 0 & c_m c_{n \pm 1} c_k & 0 \\ 0 & 0 & c_m c_n c_{k \pm 1} \end{bmatrix}. \tag{4.23}$$

The corresponding 3h integrals can be determined after some scaling as

$$\zeta^h_{+1} = A_h \zeta^h_{-1}. \tag{4.24}$$

where

$$\zeta^h_{\pm 1} = \begin{bmatrix} \begin{pmatrix} m \pm 1 & n & k \\ a & b & c \end{pmatrix}_h \\ \begin{pmatrix} m & n \pm 1 & k \\ a & b & c \end{pmatrix}_h \\ \begin{pmatrix} m & n & k \pm 1 \\ a & b & c \end{pmatrix}_h \end{bmatrix},$$

and

$$A_h = L_{+1} A_H (L_{-1})^{-1}. \tag{4.25}$$

As mentioned in the introduction section, this 3D recurrence relation does not stand on its own: It requires a specific set of 2D starting conditions (three planes and a keystone integral) in order to fill a desired integer block space. The next section derives the 2D starting conditions by zeroing out either m, n, or k and applying a similar procedure.

4.3 Planar Recurrence Relations for $3h$ Integrals

This section deals with 3h/3H integrals for the case when either m, n, or k equals zero. Similar to before, the expression

$$I_{m,n}(a,b) = I_{m,n,k=0}(a,b) = \int_{-\infty}^{\infty} \frac{\partial}{\partial x}\{e^{\frac{-(a^2+b^2+c^2)x^2}{2}} H_m(ax)H_n(bx)\}dx = 0, \quad (4.26)$$

will serve as the starting point for the planar recurrence relation derivation. Note that $H_0(t) = 1,\ \forall t \in \mathbb{R}$. Carrying out the partial derivative with respect to x inside the integral, and inserting the recurrence relations according to equations (4.10) and

(4.11) gives

$$\begin{aligned}
I_{m,n}(a,b) &= \int_{-\infty}^{\infty} \frac{\partial}{\partial x}\{e^{\frac{-\gamma x^2}{2}} H_m(ax)H_n(bx)\}dx \\
&= \int_{-\infty}^{\infty} -\gamma x e^{\frac{-\gamma x^2}{2}} H_m(ax)H_n(bx)dx + \int_{-\infty}^{\infty} e^{\frac{-\gamma x^2}{2}}[H'_m(ax)H_n(bx) + H_m(ax)H'_n(bx)]dx. \\
&= \int_{-\infty}^{\infty} -\gamma[\frac{H_{m+1}(ax)}{2a} + \frac{mH_{m-1}(ax)}{a}]H_n(bx)e^{\frac{-\gamma x^2}{2}}dx \cdots \\
&+ \int_{-\infty}^{\infty} e^{\frac{-\gamma x^2}{2}}[2amH_{m-1}(ax)H_n(bx) + 2bnH_m(ax)H_{n-1}(bx)]dx. \\
&= -\frac{\gamma}{2a}\begin{pmatrix} m+1 & n & 0 \\ a & b & c \end{pmatrix}_H - \frac{\gamma m}{a}\begin{pmatrix} m-1 & n & 0 \\ a & b & c \end{pmatrix}_H \cdots \\
&+ 2am\begin{pmatrix} m-1 & n & 0 \\ a & b & c \end{pmatrix}_H + 2bn\begin{pmatrix} m & n-1 & 0 \\ a & b & c \end{pmatrix}_H .
\end{aligned} \tag{4.27}$$

Equating this to zero and rearranging gives

$$\frac{\gamma}{2a}\begin{pmatrix} m+1 & n & 0 \\ a & b & c \end{pmatrix}_H = m(2a - \frac{\gamma}{a})\begin{pmatrix} m-1 & n & 0 \\ a & b & c \end{pmatrix}_H + 2bn\begin{pmatrix} m & n-1 & 0 \\ a & b & c \end{pmatrix}_H . \tag{4.28}$$

If equation (4.11) were used for order n instead of m, a different equation would be yielded, given as

$$\frac{\gamma}{2b}\begin{pmatrix} m & n+1 & 0 \\ a & b & c \end{pmatrix}_H = 2am\begin{pmatrix} m-1 & n & 0 \\ a & b & c \end{pmatrix}_H + n(2b - \frac{\gamma}{b})\begin{pmatrix} m & n-1 & 0 \\ a & b & c \end{pmatrix}_H . \tag{4.29}$$

Combing equations (4.28) and (4.29) gives the 2D recurrence relation

$$M^{(2D)}(a,b)\left[\begin{pmatrix} m+1 & n & 0 \\ a & b & c \end{pmatrix}_H \right] = N^{(2D)}(m,n,a,b)\left[\begin{pmatrix} m-1 & n & 0 \\ a & b & c \end{pmatrix}_H \right], \quad (4.30)$$

where

$$M^{(2D)}(a,b) = \begin{bmatrix} \frac{\gamma}{2a} & 0 \\ 0 & \frac{\gamma}{2b} \end{bmatrix}, \quad (4.31)$$

and

$$N^{(2D)}(m,n,a,b) = \begin{bmatrix} m(2a-\frac{\gamma}{a}) & 2bn \\ 2am & n(2b-\frac{\gamma}{b}) \end{bmatrix}. \quad (4.32)$$

A solution exists when $\det M = \frac{(a^2+b^2+c^2)^2}{4ab} \neq 0$. The matrix $B_H = (M)^{-1}N$ is given by

$$B_H(m,n,a,b) = \frac{1}{\gamma}\begin{bmatrix} 2am(2a-\frac{\gamma}{a}) & 4abn \\ 4abm & 2bn(2b-\frac{\gamma}{b}) \end{bmatrix}. \quad (4.33)$$

again, the shorthand notation

$$\zeta_{\pm 1}^{H,(2D)} = \begin{bmatrix} \begin{pmatrix} m+1 & n & 0 \\ a & b & c \end{pmatrix}_H \\ \begin{pmatrix} m & n+1 & 0 \\ a & b & c \end{pmatrix}_H \end{bmatrix},$$

will be used to express the 2D recurrence relation

$$\zeta_{+1}^{H} = B_H \zeta_{-1}^{H}. \tag{4.34}$$

$$\zeta_{\pm 1}^{h,(2D)} = L_{\pm 1}^{(2D)} \zeta_{\pm 1}^{H,(2D)} \tag{4.35}$$

where the coefficient matrices are now 2×2

$$L_{\pm 1}^{(2D)} = \begin{bmatrix} c_{m\pm 1} c_n & 0 \\ 0 & c_m c_{n\pm 1} \end{bmatrix}. \tag{4.36}$$

Similar to the 3D case, the 3h integrals can be obtained from the 3H integrals after some matrix multiplication and scaling as

$$\zeta_{+1}^{h,(2D)} = B_h \zeta_{-1}^{h,(2D)}, \tag{4.37}$$

where

$$B_h = L_{+1}^{(2D)} B_H (L_{-1}^{(2D)})^{-1}. \tag{4.38}$$

There is an interesting property of 3h/3H integrals in that the columns can be permutated without changing the result of the integral.

$$\zeta_{+/-1}^{h,(2D)} = \left(\begin{pmatrix} m \pm 1 & n & 0 \\ a & b & c \end{pmatrix}_h \right) = \left(\begin{pmatrix} 0 & n & m \pm 1 \\ c & b & a \end{pmatrix}_h \right) = \left(\begin{pmatrix} m \pm 1 & 0 & n \\ b & c & a \end{pmatrix}_h \right). \tag{4.39}$$

Therefore, the recurrence relation for the nk ($m = 0$) and mk ($n = 0$) planes can be rendered by swapping the values of a, b, and c. Moreover, for the $L^{(2D)}$ and B_h matrices and their corresponding arguments m', n', a', b', and c' in equations (4.36) – (4.38), these variables evaluate as the following for each of the three planes

$$(m', n') = \begin{cases} (m, n), \text{ mn plane} \\ (m, k), \text{ mk plane} \\ (n, k), \text{ nk plane} \end{cases},$$

and

$$(a', b', c') = \begin{cases} (a, b, c), \text{ mn plane} \\ (a, c, b), \text{ mk plane} \\ (b, c, a), \text{ nk plane} \end{cases} .$$

The starting conditions for these planar recurrence relations are the m, n and k axes, which is the next topic.

4.4 Axial Recurrence Relations for $3h$ Integrals

For axial recurrence relations, two of the three variables m, n, and k are set to zero. The expression

$$I_k = I_{m=0,n=0,k} \doteq \int_{-\infty}^{\infty} \frac{\partial}{\partial x} \{ e^{\frac{-(a^2+b^2+c^2)x^2}{2}} H_k(cx) \} dx = 0, \tag{4.40}$$

is the starting point, and just like for $I_{m,n,k}$ and $I_{m,n}$, I_k equals zero since the exponential decays to zero as x tends to $+/-\infty$. If the derivative with respect to x is

carried out, then I_k becomes

$$\begin{aligned} I_k &= \int_{-\infty}^{\infty} \frac{\partial}{\partial x}\{e^{\frac{-(a^2+b^2+c^2)x^2}{2}} H_k(cx)\}dx \\ &= \int_{-\infty}^{\infty} -(a^2+b^2+c^2)xe^{\frac{-(a^2+b^2+c^2)x^2}{2}} H_k(cx)dx + \int_{-\infty}^{\infty} e^{\frac{-(a^2+b^2+c^2)x^2}{2}} H_k'(cx)dx. \end{aligned} \tag{4.41}$$

Letting $\gamma = a^2+b^2+c^2$ and inserting equations (2.17) and (2.19) into I_k gives

$$\begin{aligned} I_k &= \int_{-\infty}^{\infty} -\gamma x e^{\frac{-\gamma x^2}{2}} H_k(cx)dx + \int_{-\infty}^{\infty} e^{\frac{-\gamma x^2}{2}} H_k'(cx)dx \\ &= \int_{-\infty}^{\infty} -\gamma x e^{\frac{-\gamma x^2}{2}} [\frac{H_{k+1}(cx)}{2cx} + \frac{kH_{k-1}(cx)}{cx}]dx + \int_{-\infty}^{\infty} e^{\frac{-\gamma x^2}{2}} 2ckH_{k-1}(cx)dx \\ &= -\frac{\gamma}{2c} \begin{pmatrix} 0 & 0 & k+1 \\ a & b & c \end{pmatrix}_H + k(2c - \frac{\gamma}{c}) \begin{pmatrix} 0 & 0 & k-1 \\ a & b & c \end{pmatrix}_H . \end{aligned} \tag{4.42}$$

Rearranging this final expression gives the axial recurrence relation for $m = n = 0$ as

$$\begin{pmatrix} 0 & 0 & k+1 \\ a & b & c \end{pmatrix}_H = \frac{2kc}{\gamma}(2c - \frac{\gamma}{c}) \begin{pmatrix} 0 & 0 & k-1 \\ a & b & c \end{pmatrix}_H . \tag{4.43}$$

This easily links to the axial 3h recurrence equation

$$\begin{pmatrix} 0 & 0 & k+1 \\ a & b & c \end{pmatrix}_h = \frac{c_{k+1}}{c_{k-1}} \frac{2kc}{\gamma}(2c - \frac{\gamma}{c}) \begin{pmatrix} 0 & 0 & k-1 \\ a & b & c \end{pmatrix}_h . \tag{4.44}$$

Similarly, if one wanted to recurse along either the m or n axes, those corresponding axial recurrence relations are

$$\begin{pmatrix} m+1 & 0 & 0 \\ & & \\ a & b & c \end{pmatrix}_h = \frac{c_{m+1}}{c_{m-1}} \frac{2ma}{\gamma} (2a - \frac{\gamma}{a}) \begin{pmatrix} m-1 & 0 & 0 \\ & & \\ a & b & c \end{pmatrix}_h , \tag{4.45}$$

and

$$\begin{pmatrix} 0 & n+1 & 0 \\ & & \\ a & b & c \end{pmatrix}_h = \frac{c_{n+1}}{c_{n-1}} \frac{2nb}{\gamma} (2b - \frac{\gamma}{b}) \begin{pmatrix} 0 & n-1 & 0 \\ & & \\ a & b & c \end{pmatrix}_h . \tag{4.46}$$

This is a similar approach to the planar recurrence relations, in that the variables in equation (4.44) evaluate as

$$(k', c') = \begin{cases} (m, a), \text{ m-axis} \\ \\ (n, b), \text{ n-axis} \\ \\ (k, c), \text{ k-axis} \end{cases} .$$

Since each iteration of the axial recurrence relation hops over one point (i.e. $0 \to 2 \to 4 \cdots$ or $1 \to 3 \to 5 \cdots$), the starting 3h integrals

$$\begin{pmatrix} 0 & 0 & 0 \\ & & \\ a & b & c \end{pmatrix}_h = c_0^3 \frac{\sqrt{2\pi}}{\sqrt{a^2 + b^2 + c^2}},$$

and

$$\begin{pmatrix} 1 & 0 & 0 \\ a & b & c \end{pmatrix}_h = 0,$$

for $a^2 + b^2 + c^2 > 0$ are required for a particular axis. Thus the starting conditions are fully defined for 3h integrals.

Something worth mentioning is that any 3h integral for $\frac{m+n+k}{2} \notin \mathbb{Z}$ is zero. This is because odd functions integrated over a symmetric interval equal zero, and the product of three odd order Hermite functions is itself an odd function. two keystone 3h integrals (a planar and a 3D one) are required for completeness. These integrals are

$$\begin{pmatrix} 1 & 1 & 0 \\ a & b & c \end{pmatrix}_h = c_1^2 c_0 \frac{4\sqrt{2\pi}ab}{(a^2+b^2+c^2)^{(3/2)}},$$

and

$$\begin{pmatrix} 1 & 1 & 1 \\ a & b & c \end{pmatrix}_h = 0.$$

The next section will describe and illustrate how a 3D lattice of 3h integrals gets filled.

4.5 Propagating the $3h$ Integral space

The axial, planar, and 3D recurrence relations (according to equations (4.44), (4.37), and (4.24) respectively) have particular looping structures. The axial recurrence relation is set up in a way that the output from the current iteration serves as the input for the next iteration. Thus two copies of equation (4.44) (one for even Hermite function orders and one for odd) can be applied over and over again to fill out an axis sufficiently by stopping at a specified bandlimit. The axial starting conditions are $(m, n, k) = (1, 0, 0)$ and $(m, n, k) = (0, 0, 0)$ for filling out the m axis, and permutation will allow for the n and k axes to be populated. Figure 4.1 shows an example of how an axis propagates, with the starting conditions (magenta), even indices (blue), and odd indices (red).

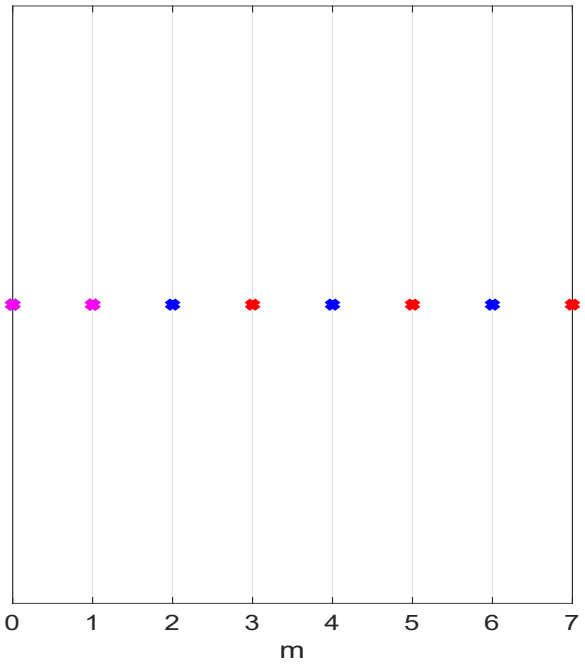

Figure 4.1: Axial Recurrence Relation Propagation Illustration

The 2D and 3D versions do not behave the same way. Consider the planar recurrence relation according to equation (4.37) in (m, n) coordinates with $k = 0$. Starting with the keystone point $(1, 1, 0) = (1, 1)$ as the initial (m, n) index, it is possible to compute the pair $(2, 1)$ and $(1, 2)$ from the pair $(0, 1)$ and $(1, 0)$ since the latter pair is part of the starting set of $3h$ integrals. The next pass considers both $(2, 1)$ and $(1, 2)$ as (m, n). The index $(m, n) = (2, 1)$ queries the points $(m - 1, n) = (1, 1)$ and $(m, n-1) = (2, 0)$ in order to generate $(m+1, n) = (3, 1)$ and $(m, n+1) = (2, 2)$. Then, the index $(m, n) = (1, 2)$ queries the points $(m - 1, n) = (0, 2)$ and $(m, n - 1) = (1, 1)$

in order to generate $(m+1, n) = (2, 2)$ and $(m, n+1) = (1, 3)$. The three points

$$(3, 1),\ (2, 2),\ (1, 3),$$

become the pairs for the next pass, which from these three points, four new points

$$(4, 1),\ (3, 2),\ (2, 3),\ (1, 4),$$

can be generated and so on. Some of the calculations here are redundant, but that is fine: they can simply be skipped or compared for error checking. Figure 4.2 shows the evolution of this space being filled after 7 passes, with the starting points highlighted in magenta.

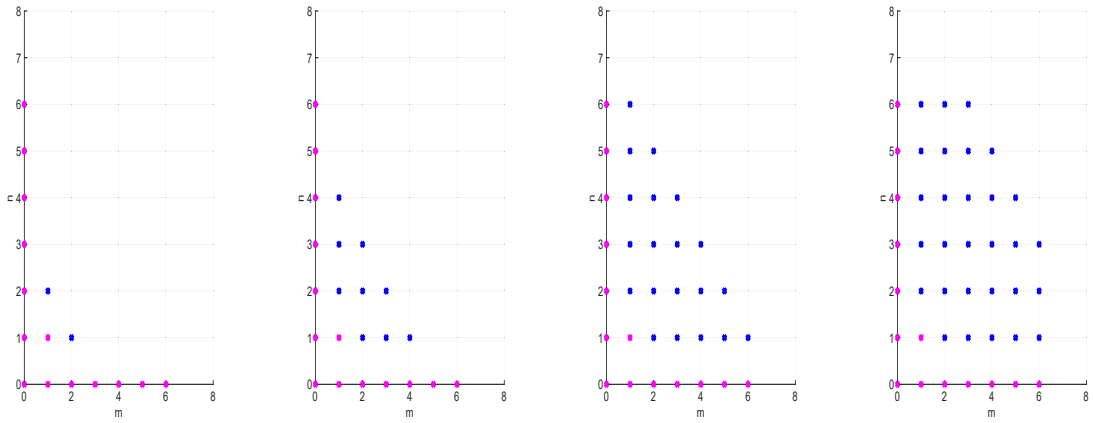

Figure 4.2: Planar Recurrence Relation Propagation Illustration

The loop structure for the full 3D recurrence relation (according to equation

(4.24)) is slightly more complicated. Starting with the keystone point $(m, n, k) = (1, 1, 1)$, a value of 1 is added to either m, n, or k to produce the indices of the next pass. This will give the set

$$(2, 1, 1),\ (1, 2, 1)$$

$$(1, 1, 2).$$

Repeating the process with the above set gives the next set

$$(3, 1, 1),\ (2, 2, 1),\ (1, 3, 1)$$

$$(2, 1, 2),\ (1, 2, 2)$$

$$(1, 1, 3).$$

Generally, each set follows

$$(N, 1, 1),\ (N-1, 2, 1),\ \cdots\ (2, N-1, 1),\ (1, N, 1)$$

$$(N-1, 1, 2),\ (N-2, 2, 2),\ \cdots (2, N-2, 2),\ (1, N, 2)$$

$$\vdots$$

$$(2, 1, N-1),\ (1, 2, N-1)$$

$$(1, 1, N).$$

4.6 Numeric Examples

Consider first an example for filling out an axis. The variables $a = 1$, $b = 1$, and $c = 0.1$ are chosen for the corresponding 3h integrals. The true values for the

3h integrals were computed analytically with a symbolic integration package that is available through Mathematica. Figure 4.3 shows the propagated results for 3h integrals along the k axis, up to $N = 9$. The error metric is absolute difference.

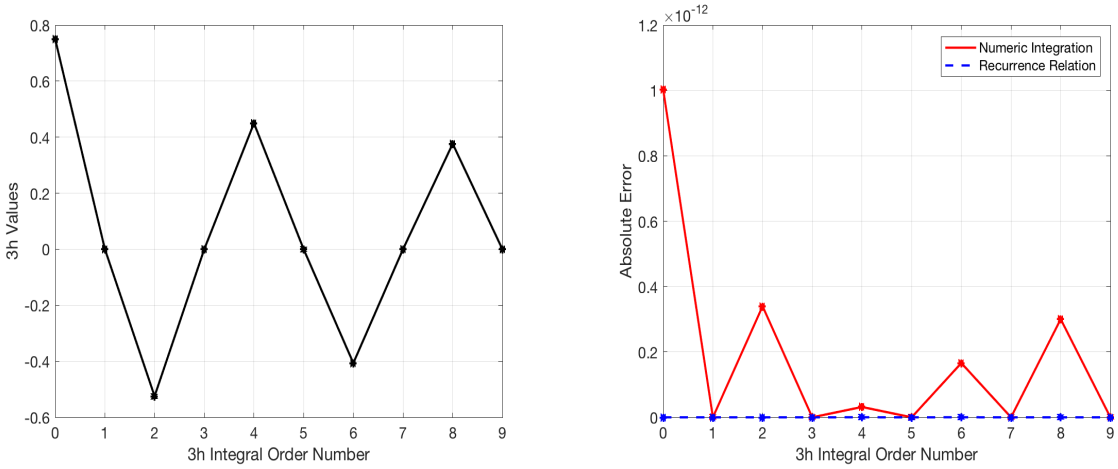

True 3h Values Errors in 3h Estimates

Figure 4.3: Numerical Results for Axial 3h Recurrence Relations

Figure 4.4 shows similar results for filling out an mn plane.

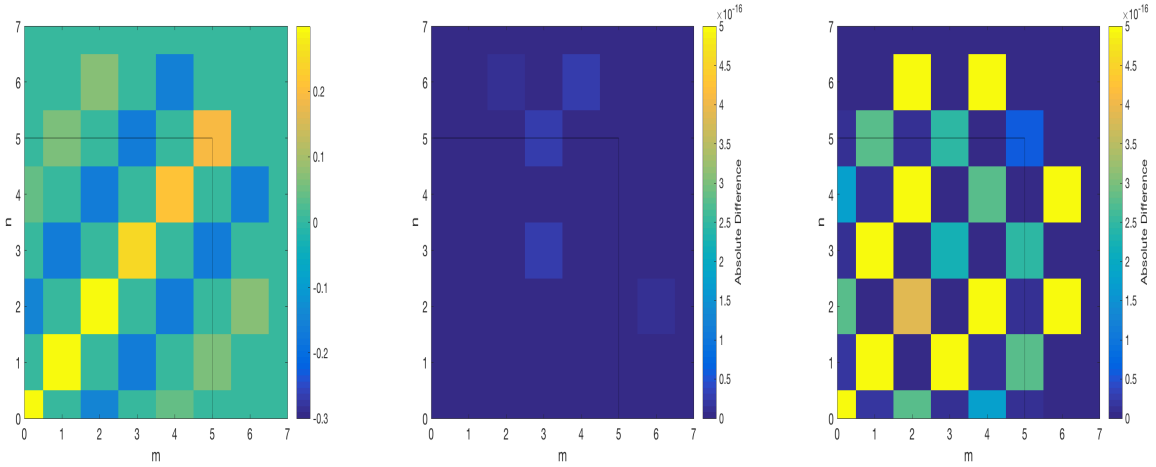

3h Values in mn Plane | Error from Recurrence Relation | Error from Numeric Integration

Figure 4.4: Planar Recurrence Relation Error Plots

Values outside the square are generated as a result of the obscure loop structure, however these terms can be discarded afterwards or just ignored.

Finally, Figure 4.5 shows numerical results using the full 3D recurrence relation. Figures 4.6 and 4.7 show the corresponding error as an absolute difference from numeric integration and recurrsion respectively.

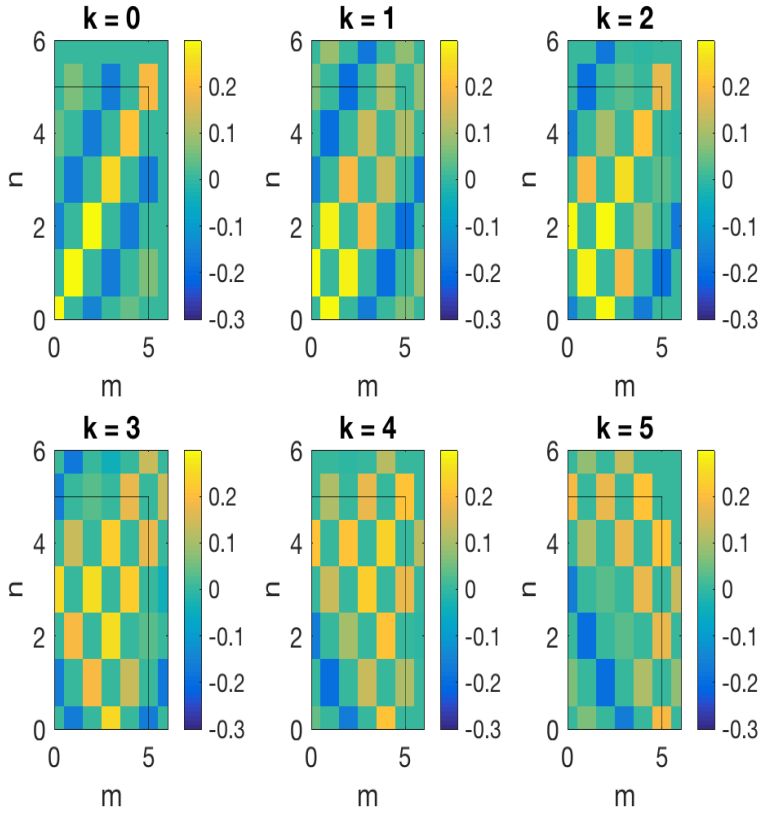

Figure 4.5: 3h Integrals from Recurrence

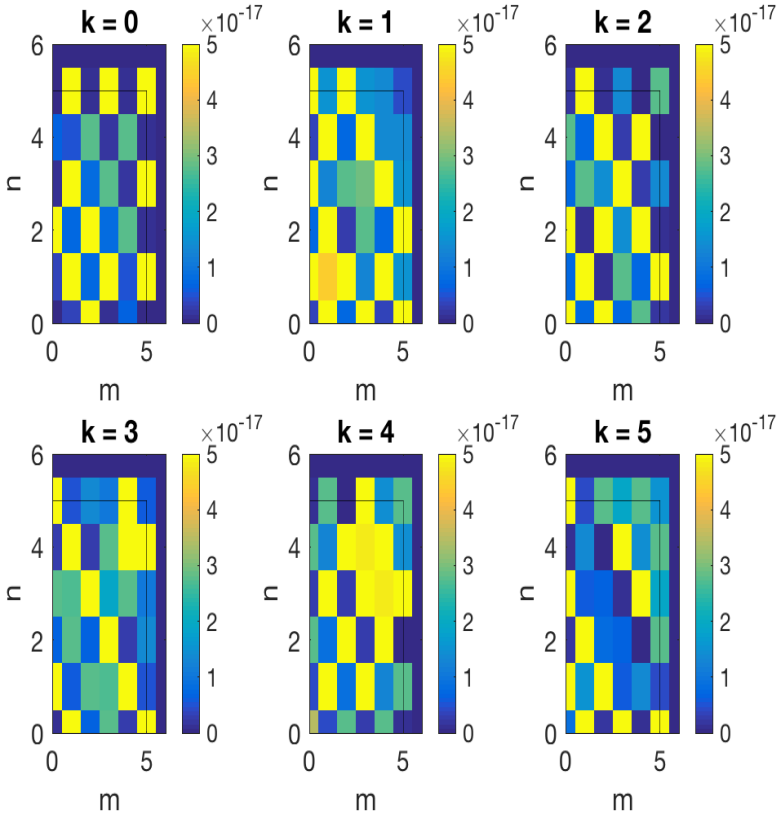

Figure 4.6: Error from Full Numeric Integration

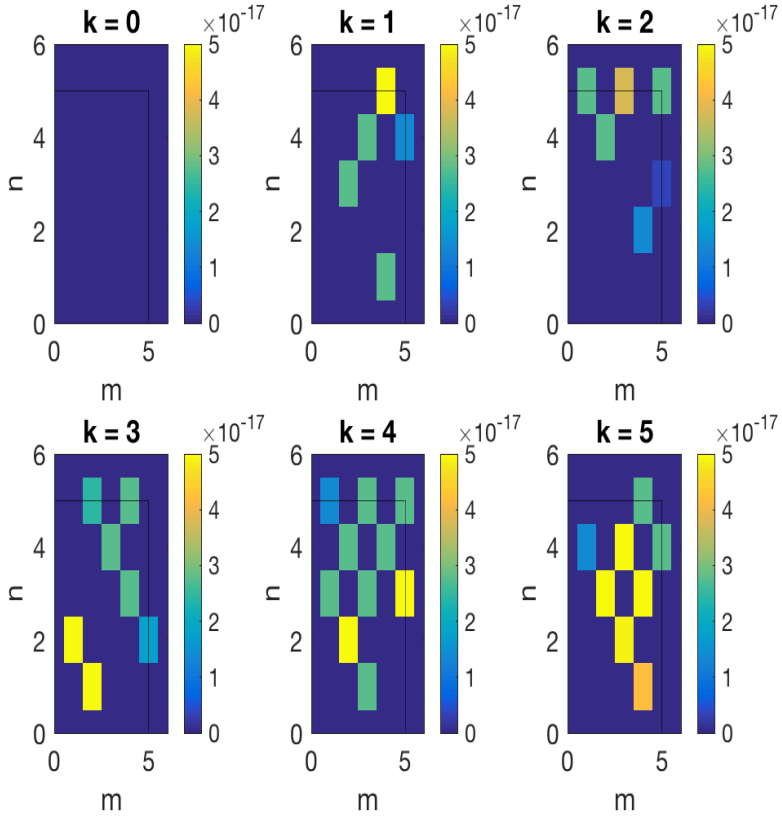

Figure 4.7: Error from Full Recurrence Relation

4.7 Chapter Summary

This chapter derived a complete recurrence relation for the integral of the product of three Hermite functions. These 3h integrals can be used to facilitate data fusion (Chapters 7 & 8), convolution (Chapter 3), representing cryo-EM/SAXS data (Chapter 9), translational deconvolution (Chapter 10), and normal mode analysis (Chapter 10). The accuracy of numerical approximations of 3h integrals is accurate, but results from recursion are better. This is due to analytic starting conditions, which makes

sense intuitively. Given the starting conditions (i.e. three planes and a keystone integral) other $3X$ integrals, where X is the underlying function of interest could be computed recursively. This notion could be applied to say $3L$ (Laguerre) functions for example, which could be used in fusion of expansions involving a radial basis. In fact, the next chapter will focus on recurrence relations for so called $3J$ integrals, namely the integral of the product of three Bessel functions (or the first kind). Numeric approximations for $3J$ integrals are not as accurate as numeric approximations for $3h$ integrals, thus making recurrence relations for $3J$ invaluable.

Chapter 5

Recurrence Relations for $3J$ Integrals

5.1 Introduction

The previous chapter derived recurrence relations for the integral of the product of three Hermite functions. This chapter starts with a recurrence relation for 3J integrals, namely the integral of the product of three Bessel functions (of the first kind) and fills out the derivations with notions of completeness and sufficient starting conditions. This recurrence relation was originally derived in [19], but did not address the starting conditions entirely. Unlike $3h$ integrals, the general analytic solution for $3J$ integrals is not clear [20]. These analytic starting conditions are paramount, for numeric error will accumulate as the recurrence equations are repeatedly applied.

The remainder of this chapter is organized as follows: Section 5.2 restates the full recurrence relation for $3J$ integrals. Section 5.3 derives a planar recurrence relation for $3J$ integrals, which is slightly different than the version from the previous chapter, in that it requires two adjacent planes. Section 5.4 extends the derivation to axial recurrence relations for $3J$ integrals. Section 5.5 articulates the starting conditions, reviewing a technique on how to obtain some of these starting integrals via differentiation. Section 5.6 shows some numeric results, highlighting the sensitivity to numerical errors, and Section 5.7 concludes the chapter with some suggestions for how to obtain the twelve starting $3J$ integrals required to fill out the space.

5.2 Recurrence Relations for $3J$ Integrals

This section is mostly a review, but sets up the approach for deriving planar and axial recurrence relations to follow. The 3J integral is defined as

$$\begin{pmatrix} m & n & l \\ a & b & c \end{pmatrix}_J \doteq \int_0^\infty J_m(ar)J_n(br)J_l(cr)rdr, \tag{5.1}$$

and the following equations will be useful in deriving the proceeding 3J integral recurrence relations

$$J'_m(x) = \frac{1}{2}[J_{m-1}(x) - J_{m+1}(x)], \tag{5.2}$$

$$J_m(x) = \frac{x}{2m}[J_{m-1}(x) + J_{m+1}(x)], \tag{5.3}$$

$$J_{-m}(x) = (-1)^m J_m(x), \tag{5.4}$$

$$(x^m J_m(x))' = x^m J_{m-1}(x), \tag{5.5}$$

and

$$\frac{d}{da}\{(ax)^m J_m(ax)\} = a^m x^{m+1} J_{m-1}(ax). \tag{5.6}$$

Now consider the function $I(m, n, k, a, b, c)$, which is not quite a 3J integral (but close) as

$$I(m, n, k, a, b, c) = \int_0^\infty J_m(ar) J_n(br) J_k(cr) dr. \tag{5.7}$$

This function can be shaped into a sum of 3J integrals by utilizing equation (5.3) as

$$\begin{aligned} I(m, n, k, a, b, c) &= \int_0^\infty J_m(ar) J_n(br) J_k(cr) dr \\ &= \int_0^\infty \frac{ar}{2m} \left[J_{m-1}(ar) + J_{m+1}(ar)\right] J_n(br) J_k(cr) dr \\ &= \frac{a}{2m} \left[\int_0^\infty J_{m-1}(ar) J_n(br) J_k(cr) r dr + \int_0^\infty J_{m+1}(ar) J_n(br) J_k(cr) r dr\right] \\ &= \frac{a}{2m} \left[\begin{pmatrix} m-1 & n & k \\ a & b & c \end{pmatrix}_J + \begin{pmatrix} m+1 & n & k \\ a & b & c \end{pmatrix}_J\right]. \end{aligned} \tag{5.8}$$

A similar expression for $I(m,n,k,a,b,c)$ can be rendered by splitting $J_n(br)$ and $J_k(cr)$ as

$$\begin{aligned} I(m,n,k,a,b,c) &= \int_0^\infty J_m(ar)J_n(br)J_k(cr)dr \\ &= \int_0^\infty \frac{br}{2n} J_m(ar)[J_{n-1}(br)+J_{n+1}(br)]J_k(cr)dr \\ &= \frac{b}{2n}\left[\int_0^\infty J_m(ar)J_{n-1}(br)J_k(cr)rdr + \int_0^\infty J_m(ar)J_{n+1}(br)J_k(cr)rdr\right] \\ &= \frac{b}{2v}\left[\begin{pmatrix} m & n-1 & k \\ a & b & c \end{pmatrix}_J + \begin{pmatrix} m & n+1 & k \\ a & b & c \end{pmatrix}_J\right], \end{aligned} \tag{5.9}$$

and

$$\begin{aligned} I(m,n,k,a,b,c) &= \int_0^\infty J_m(ar)J_n(br)J_k(cr)dr \\ &= \int_0^\infty \frac{cr}{2k} J_m(ar)J_n(br)[J_{k-1}(cr)+J_{k+1}(cr)]dr \\ &= \frac{c}{2k}\left[\int_0^\infty J_m(ar)J_n(br)J_{k-1}(cr)rdr + \int_0^\infty J_m(ar)J_n(br)J_{k+1}(cr)rdr\right] \\ &= \frac{c}{2k}\left[\begin{pmatrix} m & n & k-1 \\ a & b & c \end{pmatrix}_J + \begin{pmatrix} m & n & k+1 \\ a & b & c \end{pmatrix}_J\right]. \end{aligned} \tag{5.10}$$

Alternatively, 3J integrals can arise from manipulating the I-function using integration by parts together with equation (5.2) as

$$
\begin{aligned}
I(m,n,k,a,b,c) &= \int_0^\infty J_m(ar)J_n(br)J_k(cr)dr \\
&= J_m(ar)J_n(br)J_k(cr)r\Big|_0^\infty - \int_0^\infty \frac{\partial}{\partial r}[J_m(ar)J_n(br)J_k(cr)]rdr \\
&= 0 - \int_0^\infty [aJ'_m(ar)J_n(br)J_k(cr) + bJ_m(ar)J'_n(br)J_k(cr) + cJ_m(ar)J_n(br)J'_k(cr)]rdr \\
&= -\int_0^\infty \{\frac{a}{2}[J_{m-1} - J_{m+1}]J_n(br)J_k(cr) + \frac{b}{2}J_m(ar)[J_{n-1}(br) - J_{n+1}(br)]J_k(cr)\cdots \\
&+ \frac{c}{2}J_m(ar)J_n(br)[J_{k-1}(cr) - J_{k+1}(cr)]\}rdr \\
&= -\frac{a}{2}\begin{pmatrix} m-1 & n & k \\ a & b & c \end{pmatrix}_J + \frac{a}{2}\begin{pmatrix} m+1 & n & k \\ a & b & c \end{pmatrix}_J \\
&- \frac{b}{2}\begin{pmatrix} m & n-1 & k \\ a & b & c \end{pmatrix}_J + \frac{b}{2}\begin{pmatrix} m & n+1 & k \\ a & b & c \end{pmatrix}_J \\
&- \frac{c}{2}\begin{pmatrix} m & n & k-1 \\ a & b & c \end{pmatrix}_J + \frac{c}{2}\begin{pmatrix} m & n & k+1 \\ a & b & c \end{pmatrix}_J .
\end{aligned}
\tag{5.11}
$$

Equating (5.8), (5.9), and (5.10) each to equation (5.11) gives three unique equations. Combining these three equations into matrix form gives the final expression

$$M \begin{bmatrix} \begin{pmatrix} m+1 & n & k \\ a & b & c \end{pmatrix}_J \\ \begin{pmatrix} m & n+1 & k \\ a & b & c \end{pmatrix}_J \\ \begin{pmatrix} m & n & k+1 \\ a & b & c \end{pmatrix}_J \end{bmatrix} = N \begin{bmatrix} \begin{pmatrix} m-1 & n & k \\ a & b & c \end{pmatrix}_J \\ \begin{pmatrix} m & n-1 & k \\ a & b & c \end{pmatrix}_J \\ \begin{pmatrix} m & n & k-1 \\ a & b & c \end{pmatrix}_J \end{bmatrix}, \tag{5.12}$$

where

$$M = \begin{bmatrix} \frac{a}{2} - \frac{a}{2m} & \frac{b}{2} & \frac{c}{2} \\ \frac{a}{2} & \frac{b}{2} - \frac{b}{2n} & \frac{c}{2} \\ \frac{a}{2} & \frac{b}{2} & \frac{c}{2} - \frac{c}{2k} \end{bmatrix}, \tag{5.13}$$

and

$$N = \begin{bmatrix} \frac{a}{2} + \frac{a}{2m} & \frac{b}{2} & \frac{c}{2} \\ \frac{a}{2} & \frac{b}{2} + \frac{b}{2n} & \frac{c}{2} \\ \frac{a}{2} & \frac{b}{2} & \frac{c}{2} + \frac{c}{2k} \end{bmatrix}. \tag{5.14}$$

The matrix $D = M^{-1}N$, and M is invertible when

$$|M| = \frac{abc(m+n+k) - abc}{8mnk} \neq 0. \tag{5.15}$$

Explicitly, the matrix elements of D are

$$D_{11} = \frac{m-n-k-1}{m+n+k-1},$$

$$D_{12} = \frac{2bm}{a(m+n+k-1)},$$

$$D_{13} = \frac{2cm}{a(m+n+k-1)},$$

$$D_{21} = \frac{2an}{b(m+n+k-1)},$$

$$D_{22} = -\frac{m-n+k-1}{m+n+k-1},$$

$$D_{23} = \frac{2cn}{b(m+n+k-1)},$$

$$D_{31} = \frac{2ak}{c(m+n+k-1)},$$

$$D_{32} = \frac{2bk}{c(m+n+k-1)},$$

and

$$D_{33} = -\frac{m+n-k-1}{m+n+k-1}.$$

If we let

$$\zeta^J_{\pm 1} = \begin{bmatrix} \begin{pmatrix} m \pm 1 & n & k \\ a & b & c \end{pmatrix}_J \\ \begin{pmatrix} m & n \pm 1 & k \\ a & b & c \end{pmatrix}_J \\ \begin{pmatrix} m & n & k \pm 1 \\ a & b & c \end{pmatrix}_J \end{bmatrix},$$

then the structure for recurrence

$$\zeta^J_{+1} = D\zeta^J_{-1},$$

is the same as from Chapter 4, which was again

$$\zeta^h_{+1} = A_h\zeta^h_{-1}.$$

This means that the starting conditions to fill out an $L \times L \times L$ lattice is again three $L \times L$ planar lattices. Using recurrence equations for Bessel functions, a planar version will be derived next.

5.3 Planar Recurrence Relations for $3J$ Integrals

Consider fixing the m value as either 0, 1, or 2, leading to the shorthand definitions

$$x_{n,k} \doteq \begin{pmatrix} 0 & n & k \\ a & b & c \end{pmatrix}_J , \tag{5.16}$$

$$y_{n,k} \doteq \begin{pmatrix} 1 & n & k \\ a & b & c \end{pmatrix}_J , \tag{5.17}$$

and

$$z_{n,k} \doteq \begin{pmatrix} 2 & n & k \\ a & b & c \end{pmatrix}_J . \tag{5.18}$$

Unlike in Chapter 4 for $3h$ integrals, where one of the three functions was zeroed out, $J_0(ar) \neq 1$, so that approach cannot be used here. A new technique will be used instead. If the variable m is fixed, then the Bessel functions $J_n(br)$ and $J_k(cr)$ can be

split like before as

$$\begin{aligned} g(a,b,c,m=0,n,k) &= \int_0^\infty J_0(ar)J_n(br)J_k(cr)dr \\ &= \int_0^\infty \frac{br}{2n}J_0(ar)\left[J_{n-1}(br)+J_{n+1}(br)\right]J_k(cr)dr \\ &= \frac{b}{2n}\left[\int_0^\infty J_0(ar)J_{n-1}(br)J_k(cr)rdr + \int_0^\infty J_0(ar)J_{n+1}(br)J_k(cr)rdr\right] \\ &= \frac{b}{2n}\left[\begin{pmatrix} 0 & n-1 & k \\ a & b & c \end{pmatrix}_J + \begin{pmatrix} 0 & n+1 & k \\ a & b & c \end{pmatrix}_J\right] \\ &= \frac{b}{2n}\left[x_{n-1,k}+x_{n+1,k}\right], \end{aligned} \tag{5.19}$$

and

$$\begin{aligned} g(a,b,c,m=0,n,k) &= \int_0^\infty J_0(ar)J_n(br)J_k(cr)dr \\ &= \int_0^\infty \frac{cr}{2w}J_0(ar)J_n(br)[J_{k-1}(cr)+J_{k+1}(cr)]dr \\ &= \frac{c}{2k}\left[\int_0^\infty J_0(ar)J_n(br)J_{k-1}(cr)rdr + \int_0^\infty J_0(ar)J_n(br)J_{k+1}(cr)rdr\right] \\ &= \frac{c}{2k}\left[\begin{pmatrix} 0 & n & k-1 \\ a & b & c \end{pmatrix}_J + \begin{pmatrix} 0 & n & k+1 \\ a & b & c \end{pmatrix}\right]_J \\ &= \frac{c}{2k}\left[x_{n,k-1}+x_{n,k+1}\right]. \end{aligned} \tag{5.20}$$

The term $J_0(ar)$ can't be split this way because $\frac{ar}{2m}$ diverges for $m = 0$. Integration by parts can be performed (fixing $m = 0$) to obtain another expression as

$$\begin{aligned}
g(a,b,c,m=0,n,k) &= \int_0^\infty J_0(ar)J_n(br)J_k(cr)dr \\
&= J_0(ar)J_n(br)J_k(cr)r\Big|_0^\infty - \int_0^\infty \frac{\partial}{\partial r}[J_0(ar)J_n(br)J_k(cr)]rdr \\
&= -\frac{a}{2}\begin{pmatrix} -1 & n & k \\ a & b & c \end{pmatrix}_J + \frac{a}{2}\begin{pmatrix} 1 & n & k \\ a & b & c \end{pmatrix}_J \\
&- \frac{b}{2}\begin{pmatrix} 0 & n-1 & k \\ a & b & c \end{pmatrix}_J + \frac{b}{2}\begin{pmatrix} 0 & n+1 & k \\ a & b & c \end{pmatrix}_J \\
&- \frac{c}{2}\begin{pmatrix} 0 & n & k-1 \\ a & b & c \end{pmatrix}_J + \frac{c}{2}\begin{pmatrix} 0 & n & k+1 \\ a & b & c \end{pmatrix}_J \\
&= -\frac{1}{2}\left[-2a\begin{pmatrix} 1 & n & k \\ a & b & c \end{pmatrix}_J + bx_{n-1,k} - bx_{n+1,k} + cx_{n,k-1} - cx_{n,k+1}\right] \\
&= ay_{n,k} - \frac{b}{2}x_{n-1,k} + \frac{b}{2}x_{n+1,k} - \frac{c}{2}x_{n,k-1} + \frac{c}{2}x_{n,k+1}.
\end{aligned} \tag{5.21}$$

Equating this integration by parts result for $g(a,b,c,m=0,n,k)$ to each of the two splitting methods on $J_n(br)$ and $J_k(cr)$ for $g(a,b,c,u=0,n,k)$ separately gives the two equations

$$\frac{b}{2n}[x_{n-1,k} + x_{n+1,k}] = ay_{n,k} - \frac{b}{2}x_{n-1,k} + \frac{b}{2}x_{n+1,k} - \frac{c}{2}x_{n,k-1} + \frac{c}{2}x_{n,k+1}, \tag{5.22}$$

and

$$\frac{c}{2k}[x_{n,k-1}+x_{n,k+1}] = ay_{n,k} - \frac{b}{2}x_{n-1,k} + \frac{b}{2}x_{n+1,k} - \frac{c}{2}x_{n,k-1} + \frac{c}{2}x_{n,k+1}, \tag{5.23}$$

which can be rearranged in matrix form as

$$\begin{bmatrix} \frac{b}{2}-\frac{b}{2n} & \frac{c}{2} \\ \frac{b}{2} & \frac{c}{2}-\frac{c}{2k} \end{bmatrix} \begin{pmatrix} x_{n+1,k} \\ x_{n,k+1} \end{pmatrix} = \begin{bmatrix} -a & \frac{b}{2n}+\frac{b}{2} & \frac{c}{2} \\ -a & \frac{b}{2} & \frac{c}{2k}+\frac{c}{2} \end{bmatrix} \begin{pmatrix} y_{n,k} \\ x_{n-1,k} \\ x_{n,k-1} \end{pmatrix}. \tag{5.24}$$

It is clear from equation (5.24) that two planes are needed: one for $m=0$ and one for $m=1$. Therefore the same process is repeated by fixing $m=1$ as

$$\begin{aligned} g(a,b,c,m=1,n,k) &= \int_0^\infty J_1(ar)J_n(br)J_k(cr)dr \\ &= \int_0^\infty \frac{br}{2n}J_1(ar)[J_{n-1}(br)+J_{n+1}(br)]J_k(cr)dr \\ &= \frac{b}{2n}\left[\int_0^\infty J_1(ar)J_{n-1}(br)J_k(cr)rdr + \int_0^\infty J_1(ar)J_{n+1}(br)J_k(cr)rdr\right] \\ &= \frac{b}{2n}\left[\begin{pmatrix} 1 & n-1 & k \\ a & b & c \end{pmatrix}_J + \begin{pmatrix} 1 & n+1 & k \\ a & b & c \end{pmatrix}_J\right] \\ &= \frac{b}{2n}\left[y_{n-1,k}+y_{n+1,k}\right], \end{aligned}$$

and

$$
\begin{aligned}
g(a,b,c,m=1,n,k) &= \int_0^\infty J_1(ar)J_n(br)J_k(cr)dr \\
&= \int_0^\infty \frac{cr}{2k} J_1(ar)J_n(br)[J_{k-1}(cr)+J_{k+1}(cr)]dr \\
&= \frac{c}{2k}\left[\int_0^\infty J_1(ar)J_n(br)J_{k-1}(cr)rdr + \int_0^\infty J_1(ar)J_n(br)J_{k+1}(cr)rdr\right] \\
&= \frac{c}{2k}\left[\begin{pmatrix} 1 & n & k-1 \\ a & b & c \end{pmatrix}_J + \begin{pmatrix} 1 & n & k+1 \\ a & b & c \end{pmatrix}_J\right] \\
&= \frac{c}{2k}\left[y_{n,k-1}+y_{n,k+1}\right],
\end{aligned}
$$

and

$$
\begin{aligned}
g(a,b,c,m=1,n,k) &= \int_0^\infty J_1(ar)J_n(br)J_k(cr)dr \\
&= J_1(ar)J_n(br)J_k(cr)r\Big|_0^\infty - \int_0^\infty \frac{\partial}{\partial r}[J_1(ar)J_n(br)J_k(cr)]rdr \\
&= -\frac{a}{2}\begin{pmatrix} 0 & n & k \\ a & b & c \end{pmatrix}_J + \frac{a}{2}\begin{pmatrix} 2 & n & k \\ a & b & c \end{pmatrix}_J \\
&- \frac{b}{2}\begin{pmatrix} 1 & n-1 & k \\ a & b & c \end{pmatrix}_J + \frac{b}{2}\begin{pmatrix} 1 & n+1 & k \\ a & b & c \end{pmatrix}_J \\
&- \frac{c}{2}\begin{pmatrix} 1 & n & k-1 \\ a & b & c \end{pmatrix}_J + \frac{c}{2}\begin{pmatrix} 1 & n & k+1 \\ a & b & c \end{pmatrix}_J \\
&= -\frac{1}{2}\left[ax_{n,k} - az_{n,k} + by_{n-1,k} - by_{n+1,k} + cy_{n,k-1} - cy_{n,k+1}\right] \\
&= -\frac{a}{2}x_{n,k} + \frac{a}{2}z_{n,k} - \frac{b}{2}y_{n-1,k} + \frac{b}{2}y_{n+1,k} - \frac{c}{2}y_{n,k-1} + \frac{c}{2}y_{n,k+1},
\end{aligned}
$$

in order to generate the two equations

$$
g(a,b,c,1,n,k) = \frac{b}{2n}[y_{n-1,k}+y_{n+1,k}] = -\frac{a}{2}x_{n,k}+\frac{a}{2}z_{n,k}-\frac{b}{2}y_{n-1,k}+\frac{b}{2}y_{n+1,k}-\frac{c}{2}y_{n,k-1}+\frac{c}{2}y_{n,k+1}, \tag{5.25}
$$

and

$$
g(a,b,c,1,n,k) = \frac{c}{2k}[y_{n,k-1}+y_{n,k+1}] = -\frac{a}{2}x_{n,k}+\frac{a}{2}z_{n,k}-\frac{b}{2}y_{n-1,k}+\frac{b}{2}y_{n+1,k}-\frac{c}{2}y_{n,k-1}+\frac{c}{2}y_{n,k+1}. \tag{5.26}
$$

The current issue with this result is that $z_{n,k}$ needs to be eliminated in order to have an expression that is contained within the $m = 0$ and $m = 1$ planes. Equation (5.3) can be manipulated for $m = 1$ as

$$J_{m+1}(ar) = \frac{2J_m}{ar} - J_{m-1}(ar), \tag{5.27}$$

giving

$$\begin{aligned}
z_{n,k} &= \int_0^\infty J_2(ar)J_n(br)J_k(cr)rdr \\
&= \int_0^\infty [\frac{2J_1(ar)}{ar} - J_0(ar)]J_n(br)J_k(cr)rdr \\
&= \int_0^\infty \frac{2J_1(ar)}{ar}J_n(br)J_k(cr)rdr - \int_0^\infty J_0(ar)J_n(br)J_k(cr)rdr \\
&= \frac{2}{a}\int_0^\infty J_1(ar)J_n(br)J_k(cr)dr - x_{n,k} \\
&= \frac{2}{a}\int_0^\infty J_1(ar)\frac{br}{2n}[J_{n-1}(br) + J_{n+1}(br)]J_k(cr)dr - x_{n,k} \\
&= \frac{b}{an}\int_0^\infty [J_1(ar)J_{n-1}(br)J_k(cr)rdr] + \frac{b}{an}\int_0^\infty [J_1(ar)J_{n+1}(br)]J_k(cr)rdr] - x_{n,k} \\
&= \frac{b}{an}y_{n-1,k} + \frac{b}{an}y_{n+1,k} - x_{n,k}.
\end{aligned} \tag{5.28}$$

Inserting equation (5.28) into equations (5.25) and (5.26) gives

$$\begin{aligned}
g(a,b,c,1,n,k) &= \frac{b}{2n}[y_{n-1,k} + y_{n+1,k}] \\
&= -ax_{n,k} + \frac{b}{2n}y_{n-1,k} + \frac{b}{2n}y_{n+1,k} - \frac{b}{2}y_{n-1,k} + \frac{b}{2}y_{n+1,k} - \frac{c}{2}y_{n,k-1} + \frac{c}{2}y_{n,k+1},
\end{aligned} \tag{5.29}$$

and

$$\begin{aligned} g(a,b,c,1,n,k) &= \frac{c}{2k}[y_{n,k-1} + y_{n,k+1}] \\ &= -ax_{n,k} + \frac{b}{2n}y_{n-1,k} + \frac{b}{2n}y_{n+1,k} - \frac{b}{2}y_{n-1,k} + \frac{b}{2}y_{n+1,k} - \frac{c}{2}y_{n,k-1} + \frac{c}{2}y_{n,k+1}. \end{aligned} \tag{5.30}$$

Collecting terms that include +1 to one side, and everything else to the other side gives the matrix relation

$$\begin{bmatrix} \frac{b}{2} & \frac{c}{2} \\ \frac{b}{2n} + \frac{b}{2} & \frac{c}{2} - \frac{c}{2k} \end{bmatrix} \begin{pmatrix} y_{n+1,k} \\ y_{n,k+1} \end{pmatrix} = \begin{bmatrix} a & \frac{b}{2} & \frac{c}{2} \\ a & \frac{b}{2} - \frac{b}{2n} & \frac{c}{2k} + \frac{c}{2} \end{bmatrix} \begin{pmatrix} x_{n,k} \\ y_{n-1,k} \\ y_{n,k-1} \end{pmatrix}. \tag{5.31}$$

Combining equations (5.24) and (5.31) into one matrix equation gives the final planar recurrence equation for 3J integrals

$$M_{2D} \begin{pmatrix} x_{n+1,k} \\ x_{n,k+1} \\ y_{n+1,k} \\ y_{n,k+1} \end{pmatrix} = N_{2D} \begin{pmatrix} x_{n,k} \\ x_{n-1,k} \\ x_{n,k-1} \\ y_{n,k} \\ y_{n-1,k} \\ y_{n,k-1} \end{pmatrix}, \tag{5.32}$$

where

$$M_{2D} = \begin{bmatrix} \frac{b}{2} - \frac{b}{2n} & \frac{c}{2} & 0 & 0 \\ \frac{b}{2} & \frac{c}{2} - \frac{c}{2k} & 0 & 0 \\ 0 & 0 & \frac{b}{2} & \frac{c}{2} \\ 0 & 0 & \frac{b}{2n} + \frac{b}{2} & \frac{c}{2} - \frac{c}{2k} \end{bmatrix}, \tag{5.33}$$

and

$$N_{2D} = \begin{bmatrix} 0 & \frac{b}{2n} + \frac{b}{2} & \frac{c}{2} & -a & 0 & 0 \\ 0 & \frac{b}{2} & \frac{c}{2k} + \frac{c}{2} & -a & 0 & 0 \\ a & 0 & 0 & 0 & \frac{b}{2} & \frac{c}{2} \\ a & 0 & 0 & 0 & \frac{b}{2} - \frac{b}{2n} & \frac{c}{2k} + \frac{c}{2} \end{bmatrix}. \tag{5.34}$$

M is invertible, and thus a solutions exists when

$$\det M_{2D} = \frac{b^2c^2(n^2 + 2nk - n + k^2 - k)}{16n^2k^2} \neq 0.$$

Moreover, the conditions on n and k are

$$n^2 + 2nk - n + k^2 - k \neq 0.$$

After inspection, it seems that the matrix is not invertible when either $[n, k] = [0, 0]$, $[n, k] = [1, 0]$, or $[n, k] = [0, 1]$. These conditions (for either $m = 0$ or 1) are points that lie on the axes, and will not be indexed in the planar recurrence equations.

Explicitly, the nonzero components of $D_{2D} = M_{2D}^{-1}$ are given as

$$D_{11} = -\frac{2n(k-1)}{b(n+k-1)},$$

$$D_{12} = \frac{2nk}{b(n+k-1)},$$

$$D_{21} = \frac{2nk}{c(n+k-1)},$$

$$D_{22} = -\frac{2k(n-1)}{c(n+k-1)},$$

$$D_{33} = -\frac{2n(k-1)}{b(n+k)},$$

$$D_{34} = \frac{2nk}{b(n+k)},$$

$$D_{43} = \frac{2k(n+1)}{c(n+k)},$$

and

$$D_{44} = -\frac{2nk}{c(n+k)}.$$

The next section derives a 1D recurrence relation for 3J integrals

5.4 Axial Recurrence Relations for $3J$ Integrals

For the axial recurrence relations, a similar approach is taken. First, four variables are defined by fixing m and n as

$$h_k \doteq \begin{pmatrix} 0 & 0 & k \\ a & b & c \end{pmatrix}_J , \tag{5.35}$$

$$i_k \doteq \begin{pmatrix} 1 & 0 & k \\ a & b & c \end{pmatrix}_J , \tag{5.36}$$

$$j_k \doteq \begin{pmatrix} 0 & 1 & k \\ a & b & c \end{pmatrix}_J , \tag{5.37}$$

and

$$l_k \doteq \begin{pmatrix} 1 & 1 & k \\ a & b & c \end{pmatrix}_J . \tag{5.38}$$

Next, Four g-functions are defined like before as

$$g_h \doteq \int_0^\infty J_0(ar)J_0(br)J_k(cr)dr, \tag{5.39}$$

$$g_i \doteq \int_0^\infty J_1(ar)J_0(br)J_k(cr)dr, \tag{5.40}$$

$$g_j \doteq \int_0^\infty J_0(ar)J_1(br)J_k(cr)dr, \tag{5.41}$$

and

$$g_l \doteq \int_0^\infty J_1(ar)J_1(br)J_k(cr)dr, \tag{5.42}$$

which can be split as

$$\begin{aligned} g_h &= \int_0^\infty J_0(ar)J_0(br)J_k(cr)dr \\ &= J_0(ar)J_0(br)\frac{cr}{2k}[J_{k-1}(cr) + J_{k+1}(cr)]dr \\ &= \frac{c}{2k}h_{k-1} + \frac{c}{2k}h_{k+1}, \end{aligned} \tag{5.43}$$

$$\begin{aligned} g_i &= \int_0^\infty J_1(ar)J_0(br)J_k(cr)dr \\ &= J_1(ar)J_0(br)\frac{cr}{2k}[J_{k-1}(cr) + J_{k+1}(cr)]dr \\ &= \frac{c}{2k}i_{k-1} + \frac{c}{2k}i_{k+1}, \end{aligned} \tag{5.44}$$

$$\begin{aligned} g_j &= \int_0^\infty J_0(ar)J_1(br)J_k(cr)dr \\ &= J_0(ar)J_1(br)\frac{cr}{2k}[J_{k-1}(cr) + J_{k+1}(cr)]dr \\ &= \frac{c}{2k}j_{k-1} + \frac{c}{2k}j_{k+1}, \end{aligned} \tag{5.45}$$

and

$$\begin{aligned} g_l &= \int_0^\infty J_1(ar)J_1(br)J_k(cr)dr \\ &= J_1(ar)J_1(br)\frac{cr}{2k}[J_{k-1}(cr) + J_{k+1}(cr)]dr \\ &= \frac{c}{2k}l_{k-1} + \frac{c}{2k}l_{k+1}. \end{aligned} \tag{5.46}$$

Then, the four g-functions can be shoehorned into a sum of 3J integrals (either h_k, i_k, j_k, and/or l_k) using integration by parts as

$$\begin{aligned}
g_h &= \int_0^\infty J_0(ar)J_0(br)J_k(cr)dr \\
&= J_0(ar)J_0(br)J_k(cr)r\Big|_0^\infty - \int_0^\infty \frac{\partial}{\partial r}[J_0(ar)J_0(br)J_k(cr)]rdr \\
&= 0 - \int_0^\infty [aJ_0'(ar)J_0(br)J_k(cr) + bJ_0(ar)J_0'(br)J_k(cr) + cJ_0(ar)J_0(br)J_k'(cr)]rdr \\
&= -\int_0^\infty \{\frac{a}{2}[J_{-1}(ar) - J_1(ar)]J_0(br)J_k(cr) + \frac{b}{2}J_0(ar)[J_{-1}(br) - J_1(br)]J_k(cr)\cdots \\
&+ \frac{c}{2}J_0(ar)J_0(br)[J_{k-1}(cr) - J_{k+1}(cr)]\}rdr \\
&= ai_k + bj_k - \frac{c}{2}h_{k-1} + \frac{c}{2}h_{k+1},
\end{aligned} \tag{5.47}$$

$$\begin{aligned}
g_i &= \int_0^\infty J_1(ar)J_0(br)J_k(cr)dr \\
&= J_1(ar)J_0(br)J_k(cr)r\Big|_0^\infty - \int_0^\infty \frac{\partial}{\partial r}[J_1(ar)J_0(br)J_k(cr)]rdr \\
&= 0 - \int_0^\infty [aJ_1'(ar)J_0(br)J_k(cr) + bJ_1(ar)J_0'(br)J_k(cr) + cJ_1(ar)J_0(br)J_k'(cr)]rdr \\
&= -\int_0^\infty \{\frac{a}{2}[J_0(ar) - J_2(ar)]J_0(br)J_k(cr) + \frac{b}{2}J_1(ar)[J_{-1}(br) - J_1(br)]J_k(cr)\cdots \\
&= -\{\frac{a}{2}h_k - \int_0^\infty J_1(ar)J_0(br)J_k(cr)dr + \frac{a}{2}h_k - bl_k + \frac{c}{2}i_{k-1} - \frac{c}{2}i_{k+1}\} \\
&= -\{ah_k - \frac{c}{2k}i_{k-1} - \frac{c}{2k}i_{k+1} - bl_k + \frac{c}{2}i_{k-1} - \frac{c}{2}i_{k+1}\} \\
&= -ah_k + bl_k + (\frac{c}{2k} - \frac{c}{2})i_{k-1} + (\frac{c}{2} + \frac{c}{2k})i_{k+1},
\end{aligned} \tag{5.48}$$

$$
\begin{aligned}
g_j &= \int_0^\infty J_0(ar)J_1(br)J_k(cr)dr \\
&= J_0(ar)J_1(br)J_k(cr)r\Big|_0^\infty - \int_0^\infty \frac{\partial}{\partial r}[J_0(ar)J_1(br)J_k(cr)]rdr \\
&= 0 - \int_0^\infty [aJ_0'(ar)J_1(br)J_k(cr) + bJ_0(ar)J_1'(br)J_k(cr) + cJ_0(ar)J_1(br)J_k'(cr)]rdr \\
&= -\int_0^\infty \{\frac{a}{2}[J_{-1}(ar) - J_1(ar)]J_1(br)J_k(cr) + \frac{b}{2}J_0(ar)[J_0(br) - J_2(br)]J_k(cr)\cdots \\
&= -\{-al_k + \frac{b}{2}h_k - \int_0^\infty J_0(ar)J_1(br)J_k(cr)dr + \frac{b}{2}h_k + \frac{c}{2}j_{k-1} - \frac{c}{2}j_{k+1}\} \\
&= -\{-al_k + bh_k - \frac{c}{2k}j_{k-1} - \frac{c}{2k}j_{k+1} + \frac{c}{2}j_{k-1} - \frac{c}{2}j_{k+1}\} \\
&= al_k - bh_k + (\frac{c}{2k} - \frac{c}{2})j_{k-1} + (\frac{c}{2} + \frac{c}{2k})j_{k+1},
\end{aligned}
\tag{5.49}
$$

and

$$
\begin{aligned}
g_l &= \int_0^\infty J_1(ar)J_1(br)J_k(cr)dr \\
&= J_1(ar)J_1(br)J_k(cr)r\Big|_0^\infty - \int_0^\infty \frac{\partial}{\partial r}[J_1(ar)J_1(br)J_k(cr)]rdr \\
&= 0 - \int_0^\infty [aJ_1'(ar)J_1(br)J_k(cr) + bJ_1(ar)J_1'(br)J_k(cr) + cJ_1(ar)J_1(br)J_k'(cr)]rdr \\
&= -\int_0^\infty \{\frac{a}{2}[J_0(ar) - J_2(ar)]J_1(br)J_k(cr) + \frac{b}{2}J_1(ar)[J_0(br) - J_2(br)]J_k(cr)\cdots \\
&+ \frac{c}{2}J_1(ar)J_1(br)[J_{k-1}(cr) - J_{k+1}(cr)]\}rdr \\
&= -\{\frac{a}{2}j_k - \frac{a}{2}\int_0^\infty J_2(ar)J_1(br)J_k(cr)rdr + \frac{b}{2}i_k \\
&- \frac{b}{2}\int_0^\infty J_1(ar)J_2(br)J_k(cr)rdr + \frac{c}{2}k_{k-1} - \frac{c}{2}k_{k+1}\} \\
&= -\{\frac{a}{2}j_k - \frac{ar}{2}\int_0^\infty [\frac{2}{ar}J_1(ar) - J_0(ar)]J_1(br)J_k(cr)dr + \frac{b}{2}i_k \\
&- \frac{br}{2}\int_0^\infty J_1(ar)[\frac{2}{br}J_1(br) - J_0(br)]J_k(cr)dr\cdots \\
&+ \frac{c}{2}k_{k-1} - \frac{c}{2}k_{k+1}\} \\
&= -\{\frac{a}{2}j_k - \int_0^\infty J_1(ar)J_1(br)J_k(cr)dr + \frac{a}{2}j_k + \frac{b}{2}i_k \\
&- \int_0^\infty J_1(ar)J_1(br)J_k(cr)dr + \frac{b}{2}i_k + \frac{c}{2}l_{k-1} - \frac{c}{2}l_{k+1}\} \\
&= -\{aj_k + bi_k - \frac{c}{k}l_{k-1} + \frac{c}{2}l_{k-1} - \frac{c}{k}l_{k+1} - \frac{c}{2}l_{k+1}\} \\
&= -aj_k - bi_k + (\frac{c}{k} - \frac{c}{2})l_{k-1} + (\frac{c}{2} + \frac{c}{k})l_{k+1}.
\end{aligned}
\tag{5.50}
$$

Finally, the g-functions can be equated and collected as

$$g_h = \frac{c}{2k}h_{k-1} + \frac{c}{2k}h_{k+1} = ai_k + bj_k - \frac{c}{2}h_{k-1} + \frac{c}{2}h_{k+1}, \tag{5.51}$$

$$g_i = \frac{c}{2k}i_{k-1} + \frac{c}{2k}i_{k+1} = -ah_k + bl_k + (\frac{c}{2k} - \frac{c}{2})i_{k-1} + (\frac{c}{2} + \frac{c}{2k})i_{k+1}, \tag{5.52}$$

$$g_j = \frac{c}{2k}j_{k-1} + \frac{c}{2k}j_{k+1} = al_k - bh_k + (\frac{c}{2k} - \frac{c}{2})j_{k-1} + (\frac{c}{2} + \frac{c}{2k})j_{k+1}, \tag{5.53}$$

and

$$g_l = \frac{c}{2k}k_{k-1} + \frac{c}{2k}k_{k+1} = -aj_k - bi_k + (\frac{c}{k} - \frac{c}{2})l_{k-1} + (\frac{c}{2} + \frac{c}{k})l_{k+1}. \tag{5.54}$$

Similar to before, these four equations can be rearranged in matrix form as

$$M_{1D}\begin{pmatrix} h_{k+1} \\ i_{k+1} \\ j_{k+1} \\ l_{k+1} \end{pmatrix} = N_{1D}\begin{pmatrix} h_{k-1} \\ i_{k-1} \\ j_{k-1} \\ l_{k-1} \\ h_k \\ i_k \\ j_k \\ l_k \end{pmatrix}, \tag{5.55}$$

where

$$M_{1D} = \begin{bmatrix} \frac{c}{2k} - \frac{c}{2} & 0 & 0 & 0 \\ 0 & -\frac{c}{2} & 0 & 0 \\ 0 & 0 & -\frac{c}{2} & 0 \\ 0 & 0 & 0 & -\frac{c}{2k} - \frac{c}{2} \end{bmatrix}, \tag{5.56}$$

and

$$N_{1D} = \begin{bmatrix} -\frac{c}{2k} - \frac{c}{2} & 0 & 0 & 0 & 0 & a & b & 0 \\ 0 & -\frac{c}{2} & 0 & 0 & -a & 0 & 0 & b \\ 0 & 0 & -\frac{c}{2} & 0 & -b & 0 & 0 & a \\ 0 & 0 & 0 & \frac{c}{2k} - \frac{c}{2} & 0 & -b & -a & 0 \end{bmatrix}. \tag{5.57}$$

The 4×4 matrix M_{1D} is invertible when

$$det(M_{1D}) = \frac{c^4(k-1)(k+1)}{16k^2} \neq 0.$$

Explicitly, the nonzero components of $D_{1D} = M_{1D}^{-1} N_{1D}$ are given as

$$D_{11} = -\frac{2k}{c(k-1)},$$

$$D_{22} = -\frac{2}{c},$$

$$D_{33} = -\frac{2}{c},$$

and

$$D_{44} = -\frac{2k}{c(k+1)}.$$

Since the $3J$ integral is invariant under permutation of the three underlying Bessel functions, the n and m axes can be filled out by exchanging the corresponding values a, b, and c. The next section states the starting conditions for the axes, and suggests some approaches for obtaining analytic solutions.

5.5 Starting Conditions and Differential Techniques for $3J$ Integrals

The 1D recurrence relation for a given axis requires eight $3J$ integrals, and will yield four new ones. More specifically, the twelve $3J$ integrals

$$\begin{pmatrix} 0 & 0 & k \\ a & b & c \end{pmatrix}_J, \begin{pmatrix} 1 & 0 & k \\ a & b & c \end{pmatrix}_J, \begin{pmatrix} 0 & 1 & k \\ a & b & c \end{pmatrix}_J, \begin{pmatrix} 1 & 1 & k \\ a & b & c \end{pmatrix}_J,$$

for $k = 0, 1, 2$ are the starting terms, and skipping $k = 0, 1$ (singular D matrix) and moving to $k = 2$ will produce

$$\begin{pmatrix} 0 & 0 & 3 \\ a & b & c \end{pmatrix}_J, \begin{pmatrix} 1 & 0 & 3 \\ a & b & c \end{pmatrix}_J, \begin{pmatrix} 0 & 1 & 3 \\ a & b & c \end{pmatrix}_J, \begin{pmatrix} 1 & 1 & 3 \\ a & b & c \end{pmatrix}_J.$$

These four 3J integrals can be added to a buffer and recursion will generate

$$\begin{pmatrix} 0 & 0 & 4 \\ a & b & c \end{pmatrix}_J, \begin{pmatrix} 1 & 0 & 4 \\ a & b & c \end{pmatrix}_J, \begin{pmatrix} 0 & 1 & 4 \\ a & b & c \end{pmatrix}_J, \begin{pmatrix} 1 & 1 & 4 \\ a & b & c \end{pmatrix}_J,$$

and so on. Permutation will fill out the other two axes, and then the planes can be filled according to equation (5.32), followed by full recursion (equation (5.12)). When considering permutation, the set of starting integrals can be reduced down to seven

$$\begin{pmatrix} 0 & 0 & 0 \\ a & b & c \end{pmatrix}_J, \begin{pmatrix} 0 & 1 & 0 \\ a & b & c \end{pmatrix}_J, \begin{pmatrix} 0 & 1 & 1 \\ a & b & c \end{pmatrix}_J, \begin{pmatrix} 1 & 1 & 1 \\ a & b & c \end{pmatrix}_J,$$

$$\begin{pmatrix} 0 & 0 & 2 \\ a & b & c \end{pmatrix}_J, \begin{pmatrix} 0 & 1 & 2 \\ a & b & c \end{pmatrix}_J, \begin{pmatrix} 1 & 1 & 2 \\ a & b & c \end{pmatrix}_J.$$

The integral

$$f(a,b,c,\alpha) = \int_0^\infty J_\alpha(ar)J_\alpha(br)J_\alpha(cr)r^{1-\alpha}dr = \frac{[c^2-(a-b)^2]^{\alpha-1/2}[(a+b)^2-c^2]^{\alpha-1/2}}{2^{3\alpha-1}\sqrt{\pi}\Gamma(\alpha+1/2)(abc)^\alpha}, \tag{5.58}$$

for $|a-b| < c < a+b$ can be used in deriving analytical expressions for the starting conditions. Note that equation (5.58) is zero when the conditions on a, b, and c do not hold. By taking derivatives and dividing with respect to a, b, and/or c, one can achieve an integral of the form $\int_0^\infty J_m(ar)J_n(br)J_k(cr)rdr$. Setting $\alpha = 0$ gives one

of the 3J integrals as

$$\begin{aligned} f(a,b,c,0) &= \int_0^\infty J_0(ar)J_0(br)J_0(cr)rdr \\ &= \frac{[c^2-(a-b)^2]^{-1/2}[(a+b)^2-c^2]^{-1/2}}{2^{-1}\sqrt{\pi}\Gamma(1/2)} \\ &= \begin{pmatrix} 0 & 0 & 0 \\ a & b & c \end{pmatrix}_J . \end{aligned} \tag{5.59}$$

Equation (5.58) can be rewritten after premultiplying by $[abc]^\alpha$ as

$$\begin{aligned} A^\alpha_{0,0,0}(a,b,c) = [abc]^\alpha f(a,b,c,\alpha) &= \int_0^\infty a^\alpha J_\alpha(ar)b^\alpha J_\alpha(br)c^\alpha J_\alpha(cr)r^{1-\alpha}dr \\ &= \int_0^\infty [ar]^\alpha J_\alpha(ar)[br]^\alpha J_\alpha(br)[cr]^\alpha J_\alpha(cr)r^{1-4\alpha}dr. \end{aligned} \tag{5.60}$$

Now, consider the quantity

$$[ar]^\alpha J_\alpha(ar),$$

which when taking the derivative with respect to a and then dividing by a gives

$$\begin{aligned} \frac{1}{a}\frac{\partial}{\partial a}[ar]^\alpha J_\alpha(ar) &= \frac{1}{a}\{\alpha(ar)^{\alpha-1}rJ_\alpha(ar) + (ar)^\alpha J'_{\alpha-1}(ar)r\} \\ &= \frac{1}{a}\{\alpha(ar)^{\alpha-1}rJ_\alpha(ar) + \frac{(ar)^\alpha r}{2}\left[J_{\alpha-1}(ar) - J_{\alpha+1}(ar)\right]\} \\ &= \frac{1}{a}\{\alpha(ar)^{\alpha-1}r\frac{ar}{2\alpha}\left[J_{\alpha-1}(ar) + J_{\alpha+1}(ar)\right] + \frac{(ar)^\alpha r}{2}\left[J_{\alpha-1}(ar) - J_{\alpha+1}(ar)\right]\} \\ &= \frac{1}{a}\{ar(ar)^{\alpha-1}\frac{\alpha r}{2\alpha}\left[J_{\alpha-1}(ar) + J_{\alpha+1}(ar)\right] + \frac{(ar)^\alpha r}{2}\left[J_{\alpha-1}(ar) - J_{\alpha+1}(ar)\right]\} \\ &= a^{\alpha-1}r^{\alpha+1}J_{\alpha-1}(ar). \end{aligned} \tag{5.61}$$

for a function f, the operator $D[f(a)] = \frac{1}{a}\frac{\partial f(a)}{\partial a}$ will be some shorthand notation. Applying this operator twice looks like

$$D[D[f]] = \frac{1}{a}\frac{\partial\{\frac{1}{a}\frac{\partial f(a)}{\partial a}\}}{\partial a},$$

which leads to

$$D[D[(ar)^{\alpha}J_{\alpha}(ar)]] = a^{\alpha-2}r^{\alpha+2}J_{\alpha-2}(ar). \tag{5.62}$$

Similarly, we can compose $D_3[f] = D[D[D[f]]]$, or more generally apply the D operator α_1 times as

$$D_{\alpha_1}[(ar)^{\alpha}J_{\alpha}(ar)] = a^{\alpha-\alpha_1}r^{\alpha+\alpha_1}J_{\alpha-\alpha_1}(ar). \tag{5.63}$$

The D operator can be applied to the quantity $[br]^{\alpha}J_{\alpha}(br)$ with respect to b α_2 times, giving

$$D_{\alpha_2}[(br)^{\alpha}J_{\alpha}(br)] = b^{\alpha-\alpha_2}r^{\alpha+\alpha_2}J_{\alpha-\alpha_2}(br), \tag{5.64}$$

and similarly for the quantity $[cr]^{\alpha}J_{\alpha}(cr)$. We can now apply D α_1, α_2, and α_3 times with respect to a, b, and c to the function $A^{\alpha}_{0,0,0}$, giving

$$\begin{aligned} A^{\alpha}_{\alpha_1,\alpha_2,\alpha_3} &= D_{\alpha_1}[D_{\alpha_2}[D_{\alpha_3}[A^{\alpha}_{0,0,0}]]] \\ &= \int_0^{\infty} a^{\alpha-\alpha_1}b^{\alpha-\alpha_2}c^{\alpha-\alpha_3}r^{\alpha+\alpha_1+\alpha+\alpha_2+\alpha+\alpha_3+1-4\alpha}J_{\alpha-\alpha_1}(ar)J_{\alpha-\alpha_2}(br)J_{\alpha-\alpha_3}(cr)dr \\ &= a^m b^n c^k \begin{pmatrix} m & n & k \\ a & b & c \end{pmatrix}_J . \end{aligned} \tag{5.65}$$

Dividing $A^{\alpha}_{\alpha_1,\alpha_2,\alpha_3}$ by $a^m b^n c^k$ will give the 3J integral. The constraints are $m = \alpha - \alpha_1$, $n = \alpha - \alpha_2$, $k = \alpha - \alpha_3$ and $\alpha_1 + \alpha_2 + \alpha_3 = \alpha$. The value for α can be determined from m, n, and k as

$$\alpha = \frac{m+n+k}{2}.$$

The solution to the integral $A^{\alpha}_{0,0,0}$ is explicitly

$$A^{\alpha}_{0,0,0} = [abc]^{\alpha} \int_0^{\infty} J_{\alpha}(ar) J_{\alpha}(br) J_{\alpha}(cr) r^{1-\alpha} dr = \frac{[c^2 - (a-b)^2]^{\alpha-1/2}[(a+b)^2 - c^2]^{\alpha-1/2}}{2^{3\alpha-1}\sqrt{\pi}\Gamma(\alpha+1/2)}. \tag{5.66}$$

The denominator can be treated as a constant, whereas the numerator varies with respect to a, b, and c. There are cases where the α_i's are negative and/or fractional, which means this approach cannot be used for all 3J integrals: it is not clear if fractional calculus could be used here. The table below shows the α parameters for different values of m, n, and k.

m	n	k	α	α_1	α_2	α_3
0	0	1	0.5	0.5	0.5	-0.5
0	1	1	1	1	0	0
1	1	1	1.5	0.5	0.5	0.5
0	0	2	1	0	0	-1
0	1	2	1.5	1.5	0.5	-0.5
1	1	2	2	1	1	0

There are only two integrals from the seven starters that can be obtained with the aforementioned differential technique (non-negative/non-fractional α's). Obtaining

the remaining four

$$\begin{pmatrix} 0 & 1 & 0 \\ a & b & c \end{pmatrix}_J, \begin{pmatrix} 1 & 1 & 1 \\ a & b & c \end{pmatrix}_J, \begin{pmatrix} 0 & 0 & 2 \\ a & b & c \end{pmatrix}_J, \begin{pmatrix} 0 & 1 & 2 \\ a & b & c \end{pmatrix}_J,$$

analytically is left as a topic for future research.

5.6 Numeric Examples

This section illustrates how critical the accuracy of the starting conditions is for recursion. Consider setting $a = b = c = 1$ for the corresponding 3J integrals. Using Mathematica, the analytic solutions to the starting integrals does exist, and were mostly comprised of Meijer-G functions [21]. Figure 5.1 juxtaposes the resulting 3J integrals using the full recurrence relation (equation (5.12)) with numeric starting conditions (left) versus true analytic starting conditions (right). Figure 5.2 shows the corresponding error.

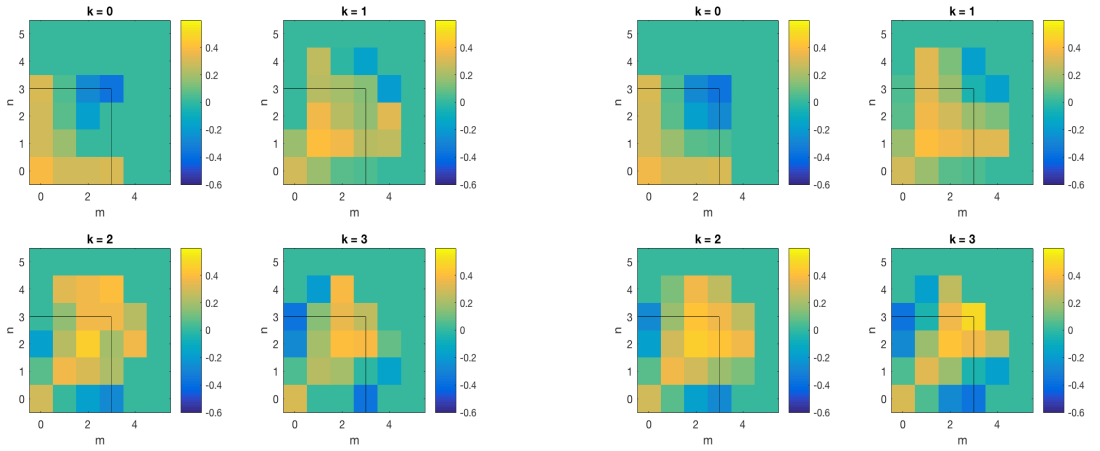

Numeric Starting Conditions Analytic Starting Conditions

Figure 5.1: Numerical Results for 3J Integrals

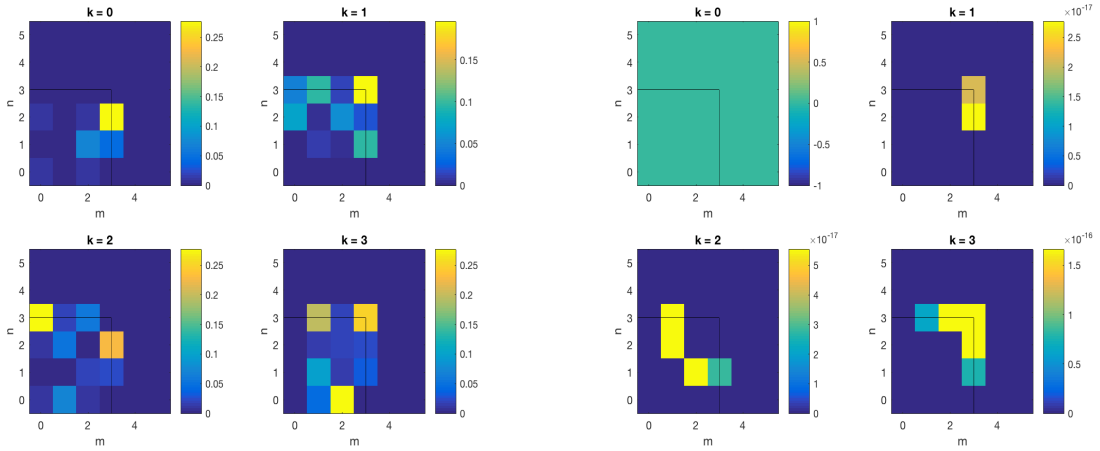

Numeric Starting Conditions Analytic Starting Conditions

Figure 5.2: 3J Integral Recurrence Relation Error

Figure 5.3 illustrates error for planar recursion with numeric versus analytic starting conditions, and Figure 5.4 shows an axial version of numeric results.

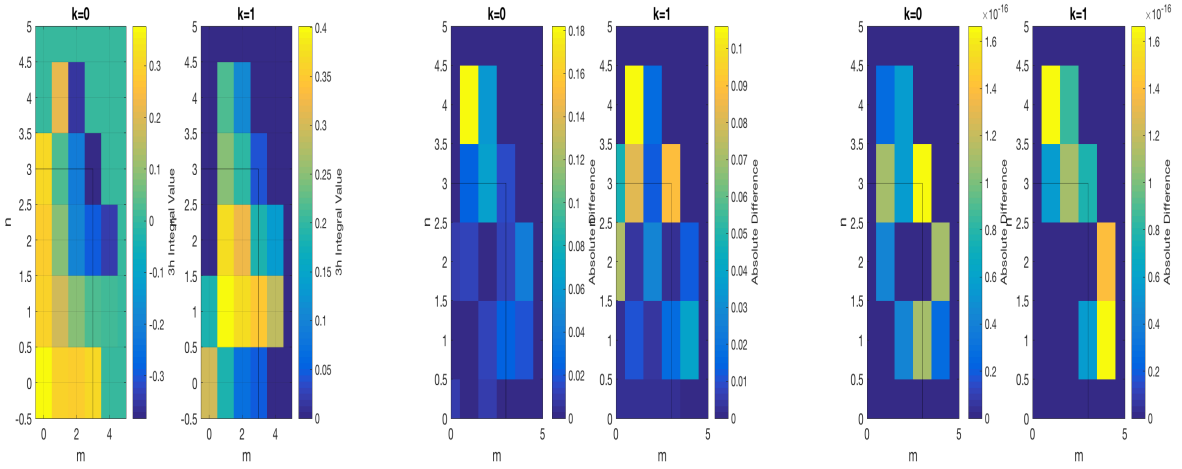

3J Values in mn Plane | Error with Numeric Starting Conditions | Error with True Starting Conditions

Figure 5.3: 3J Planar Recurrence Relation Error Plots

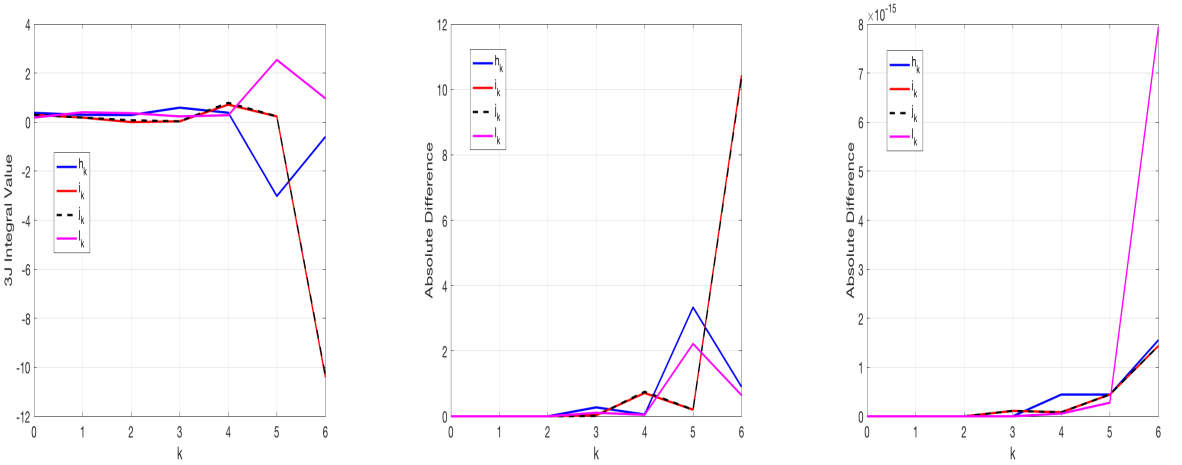

3J Values along k Axis | Error with Numeric Starting Conditions | Error with True Starting Conditions

Figure 5.4: 3J Axial Recurrence Relation Error Plots

5.7 Chapter Summary

This chapter completed the recurrence relations and stated the required $3J$ integrals needed to fill a lattice space. There is still the objective of finding the four starting integrals that could not be obtained analytically with the differential technique from Section 5.5. Once these four true starting conditions have been acquired, the $3J$ integrals can be computed for any scaling a, b, and c. As mentioned previously, the starting integrals for $a = b = c = 1$ do exist, so perhaps some scaling technique could be used to render results for any a,b, $c \in \mathbb{R}$.

Part III

Engineering Applications of Orthogonal Expansions

Chapter 6

Interconversion with Hermite Functions

6.1 Introduction

When working with functions in $\mathbb{R}^n$, there are various choices of coordinate systems available depending on the dimension. In 2D, one could use either Cartesian or polar coordinates, and there are situations where data is sampled in say polar coordinates [22, 23], but conventional displays are generally rectangular grids (Cartesian), where mathematical operations such distance metrics and convolution are more straight forward. In 3D, one could use either Cartesian or spherical coordinates. When functions are continuous, conversion between these coordinate parameterizations is clear, provided a relationship between the two coordinate systems has been

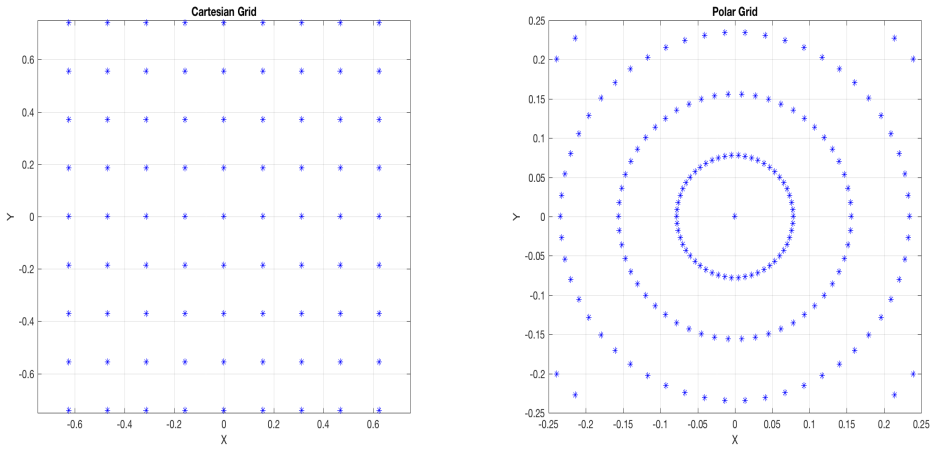

Cartesian Grid Polar Grid

Figure 6.1: Cartesian and Polar Grids

defined. However, given a discrete and finite grid of data for each coordinate system, the mapping between these grids in their respective coordinate systems is no longer bijective. This visualization is made clear with Fig. 6.1, where a grid in (x, y) coordinates is compared to a uniformly spaced grid in (ρ, ϕ) coordinates that has been mapped to (x, y) values through the well-known functions

$$x = \rho \cos \phi,$$

and

$$y = \rho \sin \phi.$$

This loss of information through the non-bijective grid mapping is also apparent in 3D coordinate conversion. This situation of handling two separate coordinate systems arises in tomography, where radial scans are collected to build a polar (or spherical)

grid and then conversion to a Cartesian grid follows [24]. One approximate way to solve this grid conversion problem is through an interpolation algorithm, something akin to either [23, 25, 26] . Moreover when invoking frequency based techniques (e.g. Fourier), there is not an exact conversion between a 2D Fourier series (Cartesian) and a Fourier-Bessel series (polar). There are of course alternate methods to interpolation. For example, a lossless method was showcased in [18] and [10] allowing interconversion between truncated Cartesian and polar expansions represented with Hermite functions and a Fourier-Laguerre basis respectively. This chapter builds upon the notion of interconversion using a Hermite basis, and properties thereof. Two frameworks are presented:

1. Cartesian-Polar Grid 2D Interconversion;

2. Cartesian-Spherical Grid 3D Interconversion;

These two frameworks of interconversion will heavily leverage rotational properties of Hermite expansions. The next section will describe how functions in Cartesian and polar coordinates can be approximated with expansions.

6.2 Hermite and Fourier-Laguerre Expansions

Consider an (x, y) grid for a function $f^c(x, y)$, with the superscript c denoting a Cartesian grid. This function can be expanded with a 2D Hermite series as

$$\tilde{f^c}(x, y) = \sum_{m=0}^{N} \sum_{n=0}^{N-m} \hat{f}_{m,n} h_m(x) h_n(y), \tag{6.1}$$

where

$$\hat{f}_{m,n} = \int_{-\infty}^{\infty} \int_{-\infty}^{\infty} f^c(x, y) h_m(x) h_n(y) dx dy, \tag{6.2}$$

are the 2D Hermite series coefficients. An (x, y, z) grid of data for a function $f^c(x, y, z)$ can be expanded similarly as

$$\tilde{f^c}(x, y, z) = \sum_{m=0}^{N} \sum_{n=0}^{N-m} \sum_{k=0}^{N-m-n} \hat{f}_{m,n,k} h_m(x) h_n(y) h_k(z), \tag{6.3}$$

where

$$\hat{f}_{m,n,k} = \int_{-\infty}^{\infty} \int_{-\infty}^{\infty} \int_{-\infty}^{\infty} f^c(x, y) h_m(x) h_n(y) h_k(z) dx dy dz. \tag{6.4}$$

Hermite coefficients of said expansions can be computed numerically (if an analytic solution does not exist) provided the function of interest is well-behaved, and decays to zero before the limits of integration. Now consider the same function f, only this time on a polar grid $f^p(\rho, \phi)$. This polar grid can be expanded with a Fourier-Laguerre

series as

$$\tilde{f}^p(\rho,\phi) = \sum_{m=0}^{N} \sum_{n=-m}^{m} \check{f}_{m,n} \chi^*_{m,n}(\rho,\phi), \tag{6.5}$$

where

$$\check{f}_{m,n} = \int_0^{2\pi} \int_0^{\infty} f^p(\rho,\phi) \chi_{m,n}(\rho,\phi) \rho d\rho d\phi, \tag{6.6}$$

are the Fourier-Laguerre series coefficients. The reader is referred to Chapter 2 for further background on the aforementioned basis functions, and properties thereof. Similarly, numerical integration can be done provided the underlying data is well-behaved. The next section will discuss interconversion between Cartesian and polar grids of data.

6.3 Interconversion Between Cartesian and Polar Data Grids

As mentioned earlier, interpolation provides an approximated way to convert between data represented with two distinct grids. This section presents two techniques of 2D interconversion between Cartesian and polar grids. The first technique converts coefficients of a Hermite series to coefficients of a Fourier-Lauguerre series and vice versa via a conversion matrix. This is in fact the method from [18] and [10]. The second technique converts between a Hermite series and an SH expansion (see Chapter 3). This technique is also lossless, and only requires computing coefficients once (in

either of the two data grids) and has similar accuracy to the first. The following two subsections articulate these two interconversion approaches.

6.3.1 Interconversion between Hermite and Fourier-Laguerre Expansions

Due to a localization property between Hermite and Laguerre functions, the expansions $\tilde{f}^c(x, y)$ and $\tilde{f}^p(\rho, \phi)$ as according to equations (6.1) and (6.5) are equivalent. Similar to how coefficients of a Hermite expansion can be mapped to coefficients of a rotated Hermite expansion, the following technique maps coefficients of a Hermite expansion to and from a Fourier-Laguerre series via the equations

$$\hat{f}_{k,m-k} = \sum_{n=-m}^{m} \check{f}_{m,n} Q_{k,n}^{m}, \tag{6.7}$$

and

$$\check{f}_{m,n} = \sum_{k=0}^{m} \hat{f}_{k,m-k} (Q_{k,n}^{m})^{*}, \tag{6.8}$$

where

$$Q_{k,n}^{m} = \int_{0}^{2\pi} \int_{0}^{\infty} \chi_{m,n}^{*}(\rho, \phi) h_k(\rho \cos\phi) h_{m-k}(\rho \sin\phi) \rho d\rho d\phi. \tag{6.9}$$

The conversion matrices Q^m have the following recurrence relations

$$\begin{pmatrix} Q^{m+1}_{k+1,n+1} \\ Q^{m+1}_{k,n+1} \end{pmatrix} = \frac{1}{2} \begin{pmatrix} \frac{1}{\sqrt{k+1}} & \frac{1}{\sqrt{k+1}} \\ -\frac{i}{\sqrt{m-k+1}} & \frac{i}{\sqrt{m-k+1}} \end{pmatrix} \begin{pmatrix} \sqrt{m-n} Q^m_{k,n+2} \\ \sqrt{m+n+2} Q^m_{k,n} \end{pmatrix}, \tag{6.10}$$

and

$$\begin{pmatrix} Q^{m+1}_{k,n+1} \\ Q^{m+1}_{k,n-1} \end{pmatrix} = \begin{pmatrix} \frac{1}{\sqrt{m+n+2}} & \frac{1}{\sqrt{m+n+2}} \\ -\frac{1}{\sqrt{m-n+2}} & \frac{1}{\sqrt{m-n+2}} \end{pmatrix} \begin{pmatrix} i\sqrt{m-k+1} Q^m_{k,n} \\ \sqrt{k} Q^m_{k-1,n} \end{pmatrix}. \tag{6.11}$$

Equation (6.10) originally had a $\frac{1}{2\sqrt{2}}$ instead of $\frac{1}{2}$, which the author believes was incorrect. The first three Q^m matrices are

$$Q^0 = 1,$$

$$Q^1 = \begin{pmatrix} -\frac{i\sqrt{2}}{2} & 0 & \frac{i\sqrt{2}}{2} \\ \frac{\sqrt{2}}{2} & 0 & \frac{\sqrt{2}}{2} \end{pmatrix},$$

and

$$Q^2 = \begin{pmatrix} -\frac{1}{2} & 0 & \frac{\sqrt{2}}{2} & 0 & -\frac{1}{2} \\ -\frac{i\sqrt{2}}{2} & 0 & 0 & 0 & \frac{i\sqrt{2}}{2} \\ -\frac{1}{2} & 0 & \frac{\sqrt{2}}{2} & 0 & -\frac{1}{2} \end{pmatrix}.$$

The recurrence equations will generate any higher order $Q^{m'}$, provided the corners are filled in after the completion of each pass (assuming $m > 2$) using the four equations

$$Q^{m'}_{0,-m'} = \frac{i}{m'-2} Q^{m'+1}_{2,-m'+2}, \tag{6.12}$$

$$Q^{m'}_{m',-m'} = (-1)^{m'-1}(-i)^{m'-2}Q^{m'}_{0,-m'}, \tag{6.13}$$

$$Q^{m'}_{0,m'} = (Q^{m'}_{0,-m'})^*, \tag{6.14}$$

and

$$Q^{m'}_{m',m'} = (Q^{m'}_{m',-m'})^*, \tag{6.15}$$

where * denotes the conjugate (no transposing).

6.3.2 Interconversion between Hermite and SH Expansions

When converting from Cartesian expansions to polar expansions, there is another method available where one can represent the new polar expansion in terms of steering coefficients and Hermite functions. Using the steering coefficients from Chapter 3, we can rewrite the expansion $\tilde{f}^c(x,y)$ as

$$\begin{aligned}
\tilde{f}^c(x,y) &= \sum_{m=0}^{N}\sum_{n=0}^{m} \hat{f}_{n,m-n} h_n(x) h_{m-n}(y) \\
&= \sum_{m=0}^{N}\sum_{n=0}^{m} \hat{f}_{n,m-n} h_n(\rho\cos\phi) h_{m-n}(\rho\sin\phi) \\
&= \sum_{m=0}^{N}\sum_{n=0}^{m} \hat{f}_{n,m-n} \sum_{q=0}^{m} S^m_{q,n}(-\phi) h_q(\rho) h_{m-q}(0) \\
&= \tilde{f}_{SH}(\rho,\phi).
\end{aligned} \tag{6.16}$$

This is the SH series, which was originally defined as equation (3.71). It is assumed that the corresponding Hermite series coefficients were computed from a Cartesian grid of data. Using a rectangular integration approach, the coefficients are

$$\begin{aligned}\hat{f}_{n,m-n} &= \int_{\mathbb{R}^2} f(x,y)h_n(x)h_{m-n}(y)dxdy \\ &= \int_{-\infty}^{\infty}\int_{-\infty}^{\infty} f(x,y)h_n(x)h_{m-n}(y)dxdy \\ &\approx \sum_{i=1}^{n_{samples}} f^c(x_i,y_i)h_n(x_i)h_{m-n}(y_i)\Delta x\Delta y.\end{aligned} \tag{6.17}$$

This SH series should not be confused with a rotated Hermite series, the latter of which uses one specific θ value. There is not actually any rotation being applied to the Hermite expansion at all, but rather a decomposition into separated angular and radial bases.

So far this coordinate conversion technique is strictly from Cartesian to polar. However, it is indeed possible for the Hermite series to be converted back to an expansion in Cartesian coordinates provided the coefficients $\hat{f}_{n,m-n}$ were somehow obtained from a polar grid. One way to compute the Hermite series coefficients $\hat{f}_{n,m-n}$ would be using numeric integration on a polar grid of data. This would be accomplished with

an integration scheme akin to

$$\begin{aligned}
\hat{f}_{n,m-n} &= \int_{\mathbb{R}^2} f(x,y)h_n(x)h_{m-n}(y)dxdy \\
&= \int_{-\infty}^{\infty}\int_{-\infty}^{\infty} f(x,y)h_n(x)h_{m-n}(y)dxdy \\
&= \int_{0}^{2\pi}\int_{0}^{\infty} f(\rho\cos\phi,\rho\sin\phi)h_n(\rho\cos\phi)h_{m-n}(\rho\sin\phi)\rho d\rho d\phi \\
&\approx \sum_{i=1}^{n_{samples}} f^p(\rho_i,\phi_i)h_n(\rho_i\cos\phi_i)h_{m-n}(\rho_i\sin\phi_i)\rho_i\Delta\rho\Delta\phi.
\end{aligned} \tag{6.18}$$

Alternatively, the coefficients could be obtained with a least-squares fitting technique. The discrete grid of data for points (ρ_i, ϕ_i) can be collected as

$$\bar{F}_i = \sum_{m=0}^{N}\sum_{n=0}^{m} \hat{f}_{n,m-n} \sum_{q=0}^{m} S_{q,n}^{m}(-\phi_i)h_q(\rho_i)h_{m-q}(0),$$

$$\bar{F}_i = \sum_{j=1}^{D} \hat{F}_j \sum_{k=1}^{m_j+1} A_{i,j}^{k},$$

$$\hat{F}_j = \hat{f}_{n_j,m_j-n_j},$$

$$A_{i,j}^{k} = S_{q_k,n_j}^{m_j}(-\phi_i)h_{q_k}(\rho_i)h_{m_j-q_k}(0),$$

$$A_{i,j} = \sum_{k} A_{i,j}^{k},$$

$$\bar{F} = A\hat{F},$$

to set up the least squares solution. The solution is given explicitly as

$$\hat{F} = (A^T A)^{-1} A^T \bar{F},$$

provided $A^T A$ is positive definite and hence invertible. Given the solution to $\hat{F}$, the solution for the corresponding Cartesian grid is according to $\tilde{f}^c(x, y)$ from equation (6.1).

This method of least squares could also be used to estimate Hermite series coefficients from a Cartesian grid of data, which could then be used for forming the corresponding SH series. Fitting an image to a Hermite series was illustrated originally in [18]. In fact, when dealing with images where the corresponding (x, y) coordinates are effectively arbitrary, least-squares is actually required since numeric integration does not make sense. Moreover, for functions that do not decay to zero at the boundaries, the least squares approach is preferable. This is due to the nonzero values at the edges of the integrated grid of data hindering the computation. Another thing to consider is that as the A matrices grow in size, the inevitable matrix inversion becomes expensive. One should be mindful of the SVD composition of A (specifically condition numbers), ensuring that the estimate has sufficient stability conditions.

Figures 6.2 and 6.3 showcase some results from interconverting between Cartesian

and polar grids of data. The function $f(\rho, \phi)$ was chosen to be a Gaussian in polar coordinates according to

$$f(\rho, \phi) = e^{-\frac{1}{2}\left[\frac{(\rho-\rho_0)^2}{\sigma_\rho^2} + \frac{(\phi-\phi_0)^2}{\sigma_\phi^2}\right]}.$$

The values parameterizing this function are $\rho_0 = 2.5$, $\phi_0 = 0.25$, $\sigma_\rho = \sqrt{0.25}$, and $\sigma_\phi = \sqrt{0.65}$. These are fixed parameters, so the corresponding function for a Cartesian grid follows

$$f(x, y) = e^{-\frac{1}{2}\left[\frac{\left(\sqrt{x^2+y^2}-\rho_0\right)^2}{\sigma_\rho^2} + \frac{\left(\tan^{-1}(\frac{y}{x})-\phi_0\right)^2}{\sigma_\phi^2}\right]}.$$

The Hermite series expansions were truncated at a bandlimit of $N = 50$. Since the distributions are concentrated, windows were applied to capture 99% of each distribution based off of the max value. Any errors outside of this confidence interval are negligible, and are thus discarded. Errors when converting to a polar grid are illustrated in Figure 6.2, and errors when converting to a Cartesian grid are shown in Figure 6.3. The method in [18] (interconversion to/from Fourier-Laguerre) as well as the SH expansion approach both have better performance than a bi-cubic interpolation method (see *interp*2( ) function in MATLAB) for the chosen band limit, which was $N = 50$. A sufficient band limit for the SH methods can be inferred from the error that the corresponding series expansion produces with respect to the original grid of data.

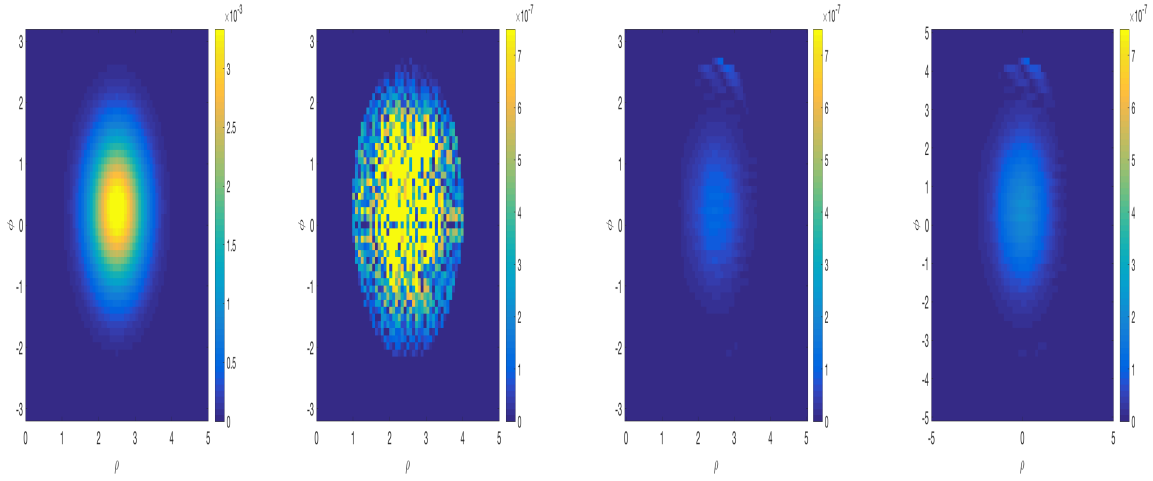

$f(\rho, \phi)$ | Interpolation Error | Fourier-Laguerre (from Hermite) Error | SH Series Error

Figure 6.2: Error in Conversion to Polar Grid

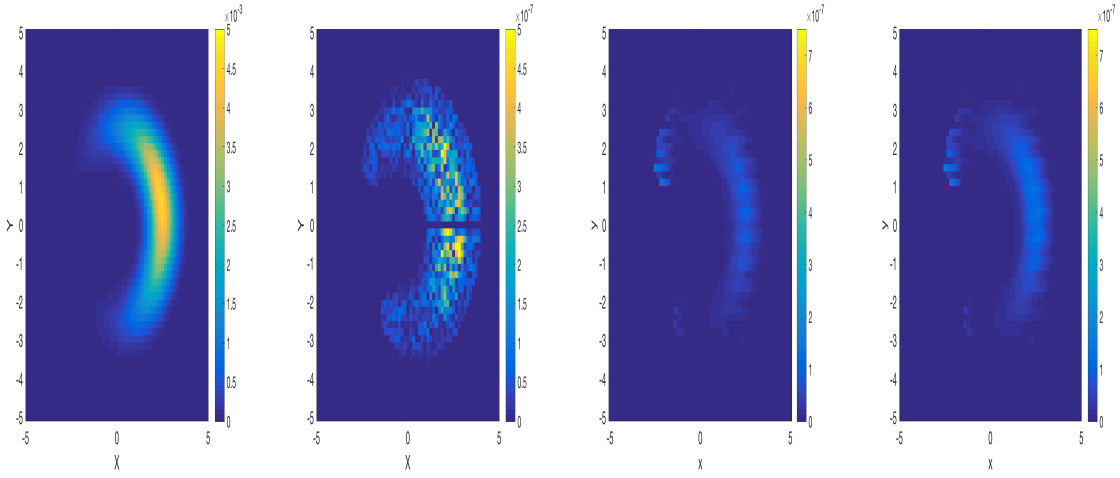

$f(x, y)$ | Interpolation Error | Hermite Series (from F-L) Error | Hermite Series (from SH) Error

Figure 6.3: Error in Conversion to Cartesian Grid

The two lossless interconversion techniques are preferable to 2D interpolation when converting between Cartesian and polar grids of data. The best method still appears to be the approach involvingQ^m matrices. However, the SH expansion approach is still

quite good, and has the added benefit of only having to compute coefficients in one coordinate system. This could prove to be much faster than having to perform matrix multiplication, which is an inevitable step in the coefficients conversion from [18]. Moreover, the SH expansion idea easily extends to 3D, and can be utilized as a means of converting between 3D cartesian and spherical grids of data. Since no conversion matrix approach has been derived yet in the 3D framework, The S^2H expansion is the exclusive topic of the next section.

6.4 Interconversion Between Cartesian and Spherical Data Grids

Like before, the notation $f^c(x, y, z)$ will denote a grid of Cartesian data and $f^p(r, \phi, \theta)$ will denote a grid of spherical data where

$$\begin{pmatrix} x \\ y \\ z \end{pmatrix} = \begin{pmatrix} r\sin\theta\cos\phi \\ r\sin\theta\sin\phi \\ r\cos\theta \end{pmatrix},$$

is the well-known conversion between Cartesian and spherical coordinates. Some convenient shorthand notation is $s\theta = \sin\theta$ and $c\theta = \cos\theta$. Consider the 3D Hermite

function expansion with the special band limits

$$\tilde{f}^c(x,y,z) = \sum_{v=0}^{N} \sum_{w=0}^{N-v} \sum_{m=0}^{N-v-w} \hat{f}_{v,w,m} h_v(x) h_w(y) h_m(z), \tag{6.19}$$

which after applying 3D rotation properties and a change of variables becomes

$$\begin{aligned}
\tilde{f}^c(rs\theta c\phi, rs\theta s\phi, rc\theta) &= \sum_{v=0}^{N} \sum_{w=0}^{N-v} \sum_{m=0}^{N-v-w} \hat{f}_{v,w,m} h_v(rs\theta c\phi) h_w(rs\theta s\phi) h_m(rc\theta) \\
&= \sum_{v=0}^{N} \sum_{w=0}^{N-v} \sum_{m=0}^{N-v-w} \hat{f}_{v,w,m} \sum_{d=0}^{v+w} S_{d,v}^{v+w}(-\phi) \sum_{t=0}^{m+d} S_{t,m}^{m+d}(-\theta) h_t(r) h_{m+d-t}(0) h_{v+w-d}(0) \\
&= \tilde{f}_{S^2H}(r,\phi,\theta).
\end{aligned} \tag{6.20}$$

Equations (6.19) and (6.20) are equivalent, the latter of which is the S^2H expansion.

6.4.1 Interconversion Between Hermite and S^2H Expansions

Given Hermite series coefficients $\hat{f}_{v,w,m}$ yielded from a Cartesian grid of data, one can obtain a corresponding spherical data grid using the S^2H series equation defined in (6.20). Similarly, if one had a spherical grid of data, one could compute the Hermite

coefficients as

$$\begin{aligned}\hat{f}_{v,w,m} &= \int_{-\infty}^{\infty}\int_{-\infty}^{\infty}\int_{-\infty}^{\infty} f(x,y,z)h_v(x)h_w(y)h_m(z)dxdydz \\ &= \int_0^{2\pi}\int_0^{\pi}\int_0^{\infty} f(r,\theta,\phi)h_v(rs\theta c\phi)h_w(rs\theta s\phi)h_m(rc\theta)rdrs\theta d\theta d\phi \\ &\approx \sum_{i=1}^{n_{samples}} f^p(r_i,\theta_i,\phi_i)h_v(rs\theta_i c\phi_i)h_w(rs\theta_i c\phi_i)h_m(r_i c\theta_i)r_i s\theta_i \Delta r\Delta\theta\Delta\phi,\end{aligned} \tag{6.21}$$

and then represent the Cartesian data with equation (6.19). Again, least squares techniques are available for these S^2H series computations.

Figures 6.4 and 6.5 show some results comparing the method of tri-cubic interpolation (see MATLAB's *interp*3( ) function) to the S^2H expansion method. The test function is

$$f(x,y,z) = e^{-\frac{1}{2}(x^2+y^2+z^2)} = e^{-\frac{r^2}{2}},$$

and was deliberately chosen to be spherically symmetric (more on why shortly). The band limit for the corresponding Hermite expansion is $N = 20$.

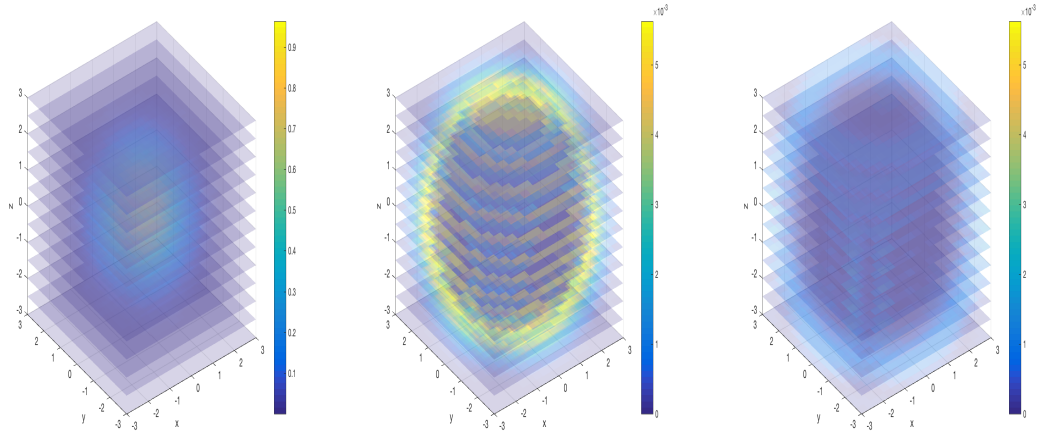

$f(x, y, z)$ Interpolation Error from S^2H Series Error

Figure 6.4: Error in Conversion to Cartesian Grid from Spherical Grid

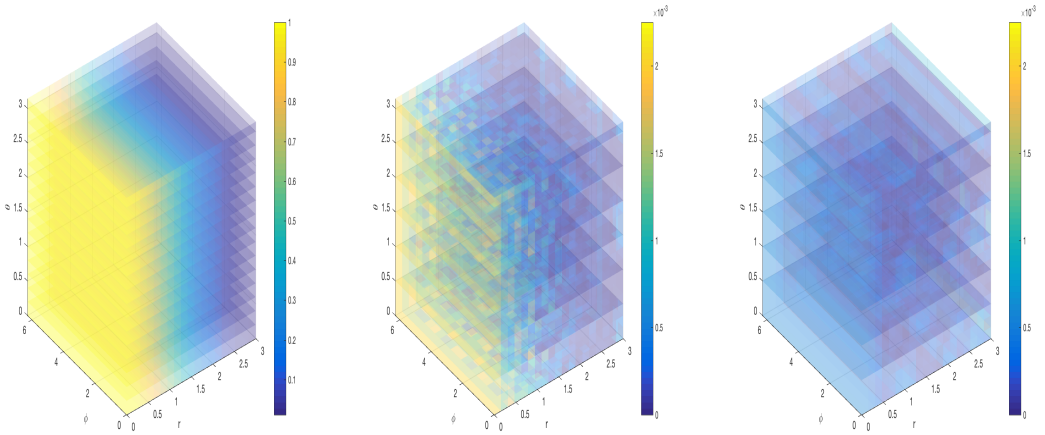

$f(r, \phi, \theta)$ Interpolation Error S^2H Series Error

Figure 6.5: Error in Conversion to Spherical Grid from Cartesian Grid

Clearly the S^2H expansions outperform tri-cubic interpolation. The purpose of this spherically symmetric example is to showcase another potential application of the SH and S^2H series expansions. More specifically, the S^2H series can be integrated

over azimuth and elevation to give a purely radial function

$$\begin{aligned} f(r) &= \frac{1}{4\pi}\int_0^{2\pi}\int_0^{\pi} f(r,\theta,\phi)s\theta d\theta d\phi \\ &= \frac{1}{4\pi}\sum_{v=0}^{N}\sum_{w=0}^{N-v}\sum_{m=0}^{N-v-w}\hat{f}_{v,w,m}\sum_{d=0}^{v+w}\int_0^{2\pi} S_{d,v}^{v+w}(-\phi)d\phi \\ &\sum_{t=0}^{m+d}\int_0^{\pi} S_{t,m}^{m+d}(-\theta)s\theta d\theta h_t(r)h_{m+d-t}(0)h_{v+w-d}(0) \\ &= \frac{1}{4\pi}\sum_{v=0}^{N}\sum_{w=0}^{N-v}\sum_{m=0}^{N-v-w}\hat{f}_{v,w,m}\sum_{d=0}^{v+w}\sigma_{d,v,v+w}^{\phi}\sum_{t=0}^{m+d}\sigma_{t,m,m+d}^{\theta}h_{m+d-t}(0)h_{v+w-d}(0)h_t(r). \end{aligned} \tag{6.22}$$

The coefficients $\sigma_{i,j,k}^{\phi}$ and $\sigma_{i,j,k}^{\theta}$ are called integrated steering coefficients (ISCs) for azimuth and elevation respectively. Figure 6.6 shows an example of the spherically symmetric function computed from a Cartesian grid using tri-cubic interpolation with numeric integration over azimuth and elevation (blue curve), vs. a spherically integrated S^2H series using ISCs (magenta curve). The ISCs for the integrated S^2H series can be computed in closed-form, by recursively computing the steering coefficients for symbolic representations of ϕ and θ, then using an integration package such as MATLAB to perform the integration. Alternatively, by starting with the equation for $S^m(\theta)$

$$S^m(\theta) = E\cdot\left(S^m(\frac{\pi}{4})\right)^T\cdot G(\theta)\cdot\left(S^m(\frac{\pi}{4})\right)\cdot E^*,$$

where

$$E = \mathrm{diag}\left(\begin{bmatrix} i^0 & i^1 & \dots & i^m \end{bmatrix}\right),$$

and

$$G(\theta) = \text{diag}\left(\left[e^{im\theta} \quad e^{i(m-2)\theta} \quad \dots \quad e^{-im\theta}\right]\right),$$

the diagonal matrix $G(\theta)$ can be integrated from 0 to 2π for azimuth ϕ or from 0 to π with multiplication by $\sin\theta$ for elevation. This gives ISCs according to

$$\sigma^{\phi}_{k,n,m} = \mathbf{e}_k^T \left[E \cdot \left(S^m(\frac{\pi}{4})\right)^T \cdot \Lambda_\phi \cdot \left(S^m(\frac{\pi}{4})\right) \cdot E^*\right] \mathbf{e}_n, \tag{6.23}$$

and

$$\sigma^{\theta}_{k,n,m} = \mathbf{e}_k^T \left[E \cdot \left(S^m(\frac{\pi}{4})\right)^T \cdot \Lambda_\theta \cdot \left(S^m(\frac{\pi}{4})\right) \cdot E^*\right] \mathbf{e}_n, \tag{6.24}$$

where

$$\Lambda_\phi = \int_0^{2\pi} \left[e^{im\alpha} \quad e^{i(m-2)\alpha} \quad \dots \quad e^{-im\alpha}\right] d\alpha, \tag{6.25}$$

and

$$\Lambda_\theta = \int_0^{\pi} \left[e^{im\alpha} \quad e^{i(m-2)\alpha} \quad \dots \quad e^{-im\alpha}\right] \sin\alpha d\alpha, \tag{6.26}$$

both of which have closed-form solutions. The vector $\mathbf{e}_k$ is the natural basis vector, and is used to pick off elements of the ISC matrices. Referring back to Figure 6.6, the method of ISCs outperforms a numeric interpolation/integration method. This makes sense intuitively since grid conversion via SH expansions is lossless and ISCs are analytic. Of course as the grid gets finer, the blue curve will approach the true solution (dashed black line). This finer grid can be accomplished with interpolation, but the approaches sought after here seek to avoid doing this by providing analytic

alternatives.

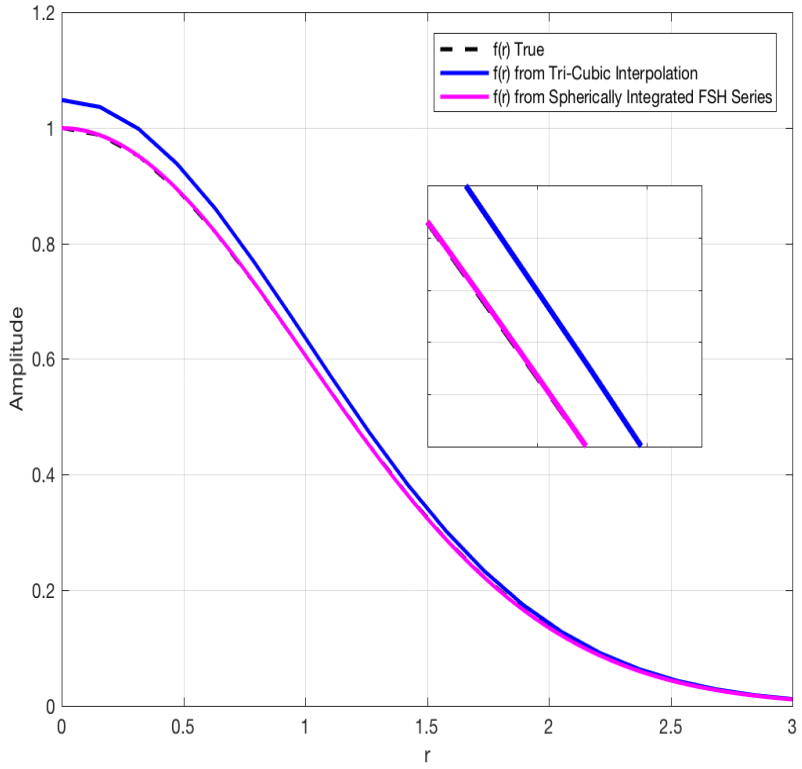

Figure 6.6: Spherically Integrated Grids

This angular integration concept can be applied to SH expansions as well for polar data. We will see the ISCs again in Chapter 9 because they play a key role in cryo-electron microscopy (cryo-EM) and Small Angle X-Ray Scattering (SAXS) data modality representations.

6.4.2 Towards Interconversion between 3D Hermite and Spherical-Gauss-Laguerre Expansions

From the Cartesian/polar interconversion part of this chapter, it was obvious that the conversion via the Q^m was the best. However, this approach has not been established as a means of converting between 3D Hermite and a a spherical basis (something akin to Fourier-Laguerre), hence why no spherical basis functions where utilized. In recent developments, this notion of some matrix that converts between 3D Hermite expansion coefficients and spherical-Gauss-Laguerre (SGL) coefficients has been considered. This is of course heavily dependent upon this 3D rendition having the same localization property, which allowed for the computation of Q^m matrices in 2D. The reader is referred to [27] for more on SGL basis functions, but on a high level, the idea would be linking the 3D Hermite expansion

$$\tilde{f}^c(x,y,z) = \sum_{m=0}^{N} \sum_{n=0}^{N-m} \sum_{k=0}^{N-m-n} \hat{f}_{m,n,k} h_m(x) h_n(y) h_k(z),$$

to an SGL expansion

$$\tilde{f}^p(r,\phi,\theta) = \sum_{m=1}^{B} \sum_{n=0}^{m-1} \sum_{l=-n}^{n} \check{f}_{m,n,l} H_{m,n,l}(r,\phi,\theta),$$

where

$$\check{f}_{m,n,l} =< f, H_{m,n,l} >,$$

as articulated in [27].

6.5 Chapter Summary

In summary, expressions involving Hermite and functions can help facilitate the interconversion between series expansions in different coordinate systems and/or bases. There are other reasons why basis conversion would be useful. In particular, Hermite functions posses some other useful properties with respect to convolution and projection. Therefore, given a grid of data (either polar or spherical), these discrete grids could be filtered with a series expansion, converted to a multi-dimensional Hermite series, and then these special properties of Hermite functions could be invoked. One extension of this research would be to consider Hermite expansions with scale factors as $h_m(ax)$, $h_n(bx)$, $h_n(cx)$. This would allow for a series fit with less basis functions.

Some other future research ideas include fitting a 3D Hermite series to a 3D Fourier series (and vice versa), in order to bootstrap FFTs for their speed. Another inquiry would be if this could be done in polar/spherical coordinates for an SH and S^2H expansions. Interconversion between 3D Hermite and Fourier Series expansions on SO(3) has some promise as well. It has been shown that the Fourier transform for

a Gaussian on SO(3) has a closed-form expression. Perhaps given these analytic expressions for Fourier coefficients, one could express Hermite series coefficients as a weighted sum of Fourier series coefficients. With this newly formed Hermite series, fusion and convolution become easily achievable.

Chapter 7

Data Fusion Methods with $3J$ Integrals

7.1 Introduction

This chapter presents some cases where integrals of the product of three Bessel functions (i.e. 3J integrals) can facilitate the representation and approximation of the product of two Bessel function expansions. Radial functions $f(r)$ and functions in polar coordinates $f(r, \phi)$ can use 3J integrals to implicitly fuse corresponding expansions thereof, and fusion of expansions on the Lie group SE(2) is a special case involving 3J integrals. Quite recently, data fusion and filtering on Lie groups for parametric distributions have had surges in development [28–35], where some focused on $SO(3)$ [36–38]. What is different about the $SE(2)$ formulation within this chapter

is that the resulting posterior distribution is general, and thus can also be used when the underlying functions are not just G-Gaussians (i.e. Gaussians on Lie groups). The notion of fusing Fourier expansions on $SO(3)$ was recently solved in [39], where the integral of three IUR matrices was expressed with Clebsch-Gordon (CG) coefficients [7]. The integral of three IURS for $SE(2)$ can be regarded as a scaled $3J$ integral (more on this later).

The outline of the remainder of this chapter is as follows. Section 7.2 reviews expansions with Bessel functions, describing numerical approximation techniques that can be used when analytic closed-form expressions are not available. Section 7.3 shows how radial expansions can be fused with $3J$ integrals. Section 7.4 articulates fusion of Fourier-Bessel expansions with the aid of $3J$ integrals. This section will also describe how a Fourier-Bessel expansion can be transformed from one polar grid (r', ϕ') to another (r, ϕ), making polar expansion fusion in multiple coordinate systems possible. Section 7.5 shows how fusion of Fourier series expansions on $SE(2)$ is an easy extension from fusion of polar expansions. Section 7.6 has some concluding remarks, and provides some possible future research avenues.

7.2 Expansions with Bessel Functions

Bessel functions have the orthogonality condition

$$\int_0^\infty J_m(ar)J_m(br)rdr = \frac{1}{a}\delta(a-b), \tag{7.1}$$

where $\delta(x)$ is the Dirac delta function and $a, b \in \mathbb{R}_{\geq 0}$. This makes possible the inversion formula

$$f(r) = \int_0^\infty \hat{f}_m(a)J_m(ar)ada, \tag{7.2}$$

where

$$\hat{f}_m(a) = \int_0^\infty f(r)J_m(ar)rdr. \tag{7.3}$$

The order m of the corresponding Bessel functions is arbitrary since it has no role in the orthogonality condition. The variable $a \in \mathbb{R}_{\geq 0}$ is a frequency parameter, and is (up to this point) a continuous variable. If the integral according to equation (7.2) does not have a closed form solution, then the inversion formula can be discretized. This discretized inverse Hankel transform will be defined as the series

$$\tilde{f}(r) = \sum_{i=0}^{N_a-1} \hat{f}(a_i)J_m(a_ir)a_i\Delta a, \tag{7.4}$$

where

$$\hat{f}_m(a_i) = \int_0^\infty f(r)J_m(a_ir)rdr, \tag{7.5}$$

are the coefficients. These coefficients can still have analytic solutions for frequency points a_i. The expansion $\tilde{f}(r)$ will be referred to as a Discrete Inverse Hankel Transform (DIHT). Also, The variable a has now been discretized into an array of length N_a with uniform spacing Δa. For a sufficient number of points N_a, and frequency resolution Δa, $\tilde{f}(r) \approx f(r)$. Data from polar grids $f(r, \phi)$ can be represented with the equation

$$f(r, \phi) = \sum_{n=-\infty}^{\infty} e^{in\phi} \int_0^{\infty} \hat{f}_n(a) J_n(ar) a da, \tag{7.6}$$

where

$$\hat{f}_n(a) = \frac{1}{2\pi} \int_0^{2\pi} \int_0^{\infty} f(r, \phi) e^{-in\phi} J_n(ar) r dr d\phi, \tag{7.7}$$

are the Fourier-Bessel series coefficients. The (r, ϕ) values are generated using the classic polar coordinate transformation equations

$$\phi = \mathrm{atan2}(y, x),$$

and

$$r = \sqrt{x^2 + y^2}.$$

This infinite series can be truncated at some bandlimit B as

$$f(r, \phi) \approx \sum_{n=-B}^{B} e^{in\phi} \int_0^{\infty} \hat{f}_n(a) J_n(ar) a da. \tag{7.8}$$

If the integral $\int_0^\infty \hat{f}_n(a) J_n(ar) a da$ does not have a closed-form solution, then the inversion formula (i.e. Fourier-Bessel series) can be discretized using the equation

$$\tilde{f}(r,\phi) = \sum_{n=-B}^{B} e^{in\phi} \sum_{l=0}^{N_a-1} \hat{f}_n(a_l) J_n(a_l r) a_l \Delta a, \tag{7.9}$$

which has coefficients

$$\hat{f}_n(a_l) = \frac{1}{2\pi} \int_0^{2\pi} \int_0^\infty f(r,\phi) e^{-in\phi} J_n(a_l r) r dr d\phi. \tag{7.10}$$

Similar to the radial expansion, parameters N_a, B (bandlimit), and Δa will ensure $\tilde{f}(r,\phi) \approx f(r,\phi)$. Lastly, the Fourier series for the Lie group $SE(2)$ is defined by the integral

$$f(g) = \int_0^\infty \text{trace}\left(\hat{f}(a) U(g,a)\right) a da, \tag{7.11}$$

where the variable

$$\hat{f}(a) = \int_{SE(2)} f(g) U(g^{-1}, a) dg, \tag{7.12}$$

holds the coefficients. At the limit, $\hat{f}(a)$ becomes an infinite-dimensional matrix. Rigid body transformation matrices $g \in SE(2)$ are of the form

$$g(x,y,\theta) = \begin{pmatrix} c\theta & -s\theta & x \\ s\theta & c\theta & y \\ 0 & 0 & 1 \end{pmatrix},$$

or equivalently

$$g(r,\phi,\theta) = \begin{pmatrix} c\theta & -s\theta & r\cos\theta \\ s\theta & c\theta & r\sin\theta \\ 0 & 0 & 1 \end{pmatrix},$$

and $U(g,a)$ are the IUR matrices for a frequency a and group element g. For more information regarding Fourier analysis on Lie groups, the reader is referred to Chapter 2. The Fourier series on $SE(2)$ can also be represented discretely as

$$\tilde{f}(g) = \sum_{l=0}^{N_a-1} \text{trace}\left(\hat{f}(a_l)U(g,a_l)\right) a_l \Delta a, \tag{7.13}$$

where

$$\hat{f}(a_l) = \int_{SE(2)} f(g)U(g^{-1},a_l)dg. \tag{7.14}$$

The trace of two N-dimensional matrices A and B can be equivalently represented with summations as

$$\begin{aligned} tr(AB) &= \sum_{j=1}^{N}(a_{1,j}b_{j,1} + a_{2,j}b_{j,2} + \cdots a_{N,j}b_{j,N} \\ &= \sum_{i=1}^{N}\sum_{j=1}^{N} a_{i,j}b_{j,i}. \end{aligned} \tag{7.15}$$

Inserting this equation into the definition of the truncated Fourier series on $SE(2)$ gives

$$\tilde{f}(g) = \sum_{l=0}^{N_a-1} \sum_{m,n=-l}^{l} \hat{f}_{m,n}(a_l)U_{n,m}(g,a_l)a_l\Delta a, \tag{7.16}$$

where

$$\hat{f}_{m,n}(a_l) = \int_{SE(2)} f(g) U_{m,n}(g^{-1}, a_l) dg. \tag{7.17}$$

Elements of $U(g, a_l)$ will be parameterized with Bessel functions

$$U_{m,n}(g(r,\phi,\theta), a_l) = i^{n-m} e^{-i[n\theta+(m-n)\phi]} J_{n-m}(a_l r), \tag{7.18}$$

and can be conjugated as

$$\begin{aligned} U_{m,n}(g^{-1}(r,\phi,\theta), a_l) &= U^{-1}_{m,n}(g(r,\phi,\theta), a_l) \\ &= \overline{U_{n,m}(g(r,\phi,\theta), a_l)} \\ &= i^{n-m} e^{+i[m\theta+(n-m)\phi]} J_{m-n}(a_l r). \end{aligned} \tag{7.19}$$

Using this parameterization, the discretized Fourier series on $SE(2)$, and its corresponding coefficients are

$$\begin{aligned} \tilde{f}(g) &= \sum_{l=0}^{N_a-1} \sum_{m,n=-l}^{l} \hat{f}_{m,n}(a_l) U_{n,m}(g, a_l) a_l \Delta a \\ &= \sum_{l=0}^{N_a-1} \sum_{m,n=-l}^{l} \hat{f}_{m,n}(a_l) i^{m-n} e^{-i[m\theta+(n-m)\phi]} J_{m-n}(a_l r) a_l \Delta a, \end{aligned} \tag{7.20}$$

and

$$\begin{aligned} \hat{f}_{m,n}(a_l) &= \int_{SE(2)} f(g) U_{m,n}(g^{-1}, a_l) dg \\ &= \int_0^{2\pi} \int_0^{2\pi} \int_0^{\infty} f(g(r,\phi,\theta)) i^{n-m} e^{+i[m\theta+(n-m)\phi]} J_{m-n}(a_l r) r dr d\phi d\theta, \end{aligned} \tag{7.21}$$

respectively. For a given index l the corresponding IUR $U(g, a_l)$ are of size $(2l+1) \times (2l+1)$.

Thus three expansions involving Bessel functions have been articulated. The next section will derive the fusion of radial expansions with 3J integrals, followed by fusing expansions on polar coordinates and then fusing expansions on $SE(2)$.

7.3 Fusing Radial Expansions with 3J Integrals

The 3J integral is defined as

$$\begin{pmatrix} m & n & l \\ a & b & c \end{pmatrix}_J \doteq \int_0^\infty J_m(ar) J_n(br) J_l(cr) r dr, \tag{7.22}$$

and has been investigated recently in [19, 20], and all the way back to several generations ago in [3]. There are certain situations where the 3J integral can be expressed in closed-form, but generally the solution is not so nice. On a related note, the integral of the product of four Bessel functions does have a closed-form solution [40]. Any computation of 3J integrals will be done so numerically when the analytic solution is not available. The functions $J_m(r)$ are Bessel functions of the first kind, not to be

confused with spherical Bessel functions, usually denoted as $j_m(r)$. The relationship between these two functions is given as

$$j_n(x) = \sqrt{\frac{\pi}{2x}} J_{n+\frac{1}{2}}(x).$$

Spherical Bessel functions have been used previously in $3j$ (i.e. the product of three spherical Bessel functions) integrals for representing the pair distance distribution function from SAXS data [41]. It will become clear soon how 3J integrals help facilitate the representation of functions involving radial expansions, having been fused together. Consider two radial expansions

$$\tilde{f}(r) = \sum_{i=0}^{N_a-1} \hat{f}_m(a_i) J_m(a_i r) a_i \Delta a, \tag{7.23}$$

and

$$\tilde{g}(r) = \sum_{j=0}^{N_b-1} \hat{g}_n(b_j) J_n(b_j r) b_j \Delta b, \tag{7.24}$$

as well as the product

$$h(r) = \tilde{f}(r)\tilde{g}(r) = \Delta a \Delta b \sum_{i=0}^{N_a-1} \sum_{j=0}^{N_b-1} \hat{f}_m(a_i)\hat{g}_n(b_j) a_i b_j J_m(a_i r) J_n(b_j r). \tag{7.25}$$

The l^{th} order Hankel transform of $h(r) = \tilde{f}(r)\tilde{g}(r)$ for a given frequency c can be represented with the double summation of 3J integrals as

$$\begin{aligned}
\hat{h}_l(c) &= \int_0^\infty h(r) J_l(cr) r dr \\
&= \int_0^\infty \tilde{f}(r)\tilde{g}(r) J_l(cr) r dr \\
&= \int_0^\infty \Delta a \Delta b \sum_{i=0}^{N_a-1} \sum_{j=0}^{N_b-1} \hat{f}_m(a_i)\hat{g}_n(b_j) a_i b_j J_m(a_i r) J_n(b_j r) \\
&= \Delta a \Delta b \sum_{i=0}^{N_a-1} \sum_{j=0}^{N_b-1} a_i b_j \hat{f}_m(a_i)\hat{g}_n(b_j) \int_0^\infty J_m(a_i r) J_n(b_j r) J_l(cr) r dr \\
&= \Delta a \Delta b \sum_{i=0}^{N_a-1} \sum_{j=0}^{N_b-1} a_i b_j \hat{f}_m(a_i)\hat{g}_n(b_j) \begin{pmatrix} m & n & l \\ a_i & b_j & c \end{pmatrix}_J .
\end{aligned} \tag{7.26}$$

An approximation of $h(r)$ can be represented with 3J integrals as

$$\begin{aligned}
h(r) \approx \tilde{h}(r) &= \sum_{k=0}^{N_c-1} J_l(c_k r) c_k \hat{h}_l(c_k) \Delta c \\
&= \Delta a \Delta b \Delta c \sum_{k=0}^{N_c-1} J_l(c_k r) c_k \sum_{i=0}^{N_a-1} \sum_{j=0}^{N_b-1} a_i b_j \hat{f}_m(a_i)\hat{g}_n(b_j) \begin{pmatrix} m & n & l \\ a_i & b_j & c_k \end{pmatrix}_J .
\end{aligned} \tag{7.27}$$

Alternatively, if all of the 3J integrals of interest have a closed-form solution, then the function $h(r)$ can be reconstructed exactly with the inversion formula

$$\begin{aligned} h(r) &= \int_0^\infty \hat{h}_l(c) J_l(cr) c dc \\ &= \int_0^\infty \Delta a \Delta b \sum_{i=0}^{N_a-1} \sum_{j=0}^{N_b-1} a_i b_j \hat{f}_m(a_i) \hat{g}_n(b_j) \begin{pmatrix} m & n & l \\ a_i & b_j & c \end{pmatrix}_J J_l(cr) c dc \\ &= \Delta a \Delta b \sum_{i=0}^{N_a-1} \sum_{j=0}^{N_b-1} a_i b_j \hat{f}_m(a_i) \hat{g}_n(b_j) \int_0^\infty \begin{pmatrix} m & n & l \\ a_i & b_j & c \end{pmatrix}_J J_l(cr) c dc. \end{aligned} \tag{7.28}$$

The caveat of equation (7.28) is that the integral

$$\int_0^\infty \begin{pmatrix} m & n & l \\ a_i & b_j & c \end{pmatrix}_J J_l(cr) c dc,$$

is available as a clear closed-form solution. For upcoming numerical examples $h(r)$ will be approximated as $\tilde{h}(r)$ according to equation (7.27). Figure 7.1 illustrates the fusion of two radial expansions that approximate the density function

$$\rho(r, r_0, s) = r e^{-s(r-r_0)^2}.$$

The radial functions $f(r)$ and $g(r)$ evaluate as $f(r) = \rho(r, 3.4, 1.5)$ and $g(r) = \rho(r, 3, 1.5)$. The relevant parameters are $\Delta a = 0.2$, $\Delta b = 0.2$, $\Delta c = 0.2$, and $N_a = 32$, $N_b = 32$, $N_c = 65$.

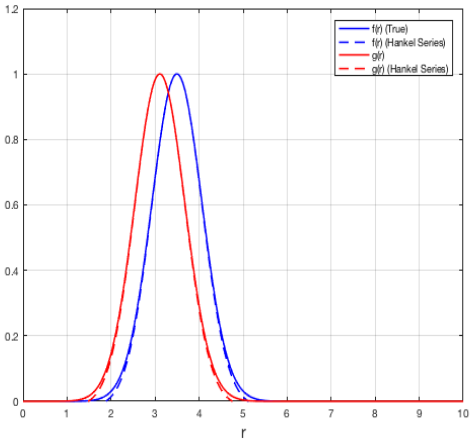

$f(r)/g(r)$ and $\tilde{f}(r)/\tilde{g}(r)$

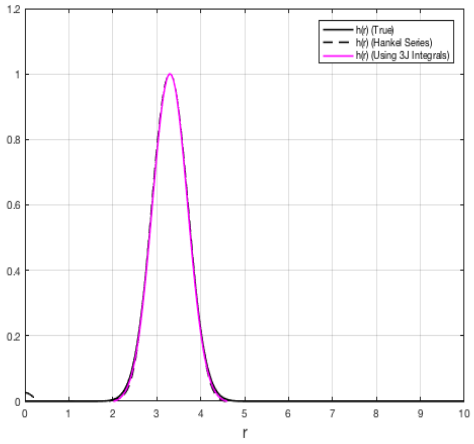

$h(r)$ and $\tilde{h}(r)$

Figure 7.1: Example for Fusion of Radial Expansions

The frequency parameters a, b and c have max values of 6.5, 6.5, and 13 respectively, and the Bessel function orders are $m = n = l = 0$. For these chosen orders, the 3J integrals have an analytic solution. The blue curves (solid and dashed) denote the functions $f(r)$ and $\tilde{f}(r)$ respectively, and the red curves show results for $g(r)$ and $\tilde{g}(r)$. These are illustrated with the left subplot. The right subplot shows three curves: 1. The product $f(r) \times g(r)$ (solid black curve), 2. a Hankel series approximation of $f(r) \times g(r)$ (dashed black curve), and 3. a reconstruction of $h(r)$ with 3J integrals according to equation (7.27) (magenta curve). The reconstruction of $h(r)$ with 3J integrals required a larger number of terms ($N = 65$) compared to the Hankel series approximation of the product $f(r) \times g(r)$ ($N = 32$). This is because the DIHT for the product $f(r) \times g(r)$ when represented with discrete data points has a fast convergence to zero, and so the frequency vector can be truncated much sooner.

However, for $\tilde{h}(r)$ according to equation (7.27), which is basically a sum of DIHT's for Bessel function products $J_m(ar)J_n(br)$, these Bessel products (i.e. 2J functions) decay much slower versus r, and therefore require more terms (with a higher max frequency) to reconstruct. This can be seen more clearly if each 2J function in the expansion

$$\tilde{f}(r) \times \tilde{g}(r) = \Delta a \Delta b \sum_i \sum_j \hat{f}_m(a_i)\hat{g}_n(b_j)a_i b_j J_m(a_i r)J_n(b_j r),$$

is stacked and plotted versus r. This stacked plotting is shown in Figure 7.2. The subfigure on the left showcases each Bessel product, where each row is an (i, j) pair. The middle subfigure reconstructs each 2J function with Hankel series parameters $N_c = 32$, $\Delta c = 0.2$ (poor reconstruction), and the subfigure on the right shows DIHTs for the 2J functions, only this time with sampling parameters $N_c = 65$ and $\Delta c = 0.2$ (better reconstruction). The variable along the y-axis for each subplot is the product of a and b, sorted from $\Delta a \Delta b$ to the max value (≈ 40).

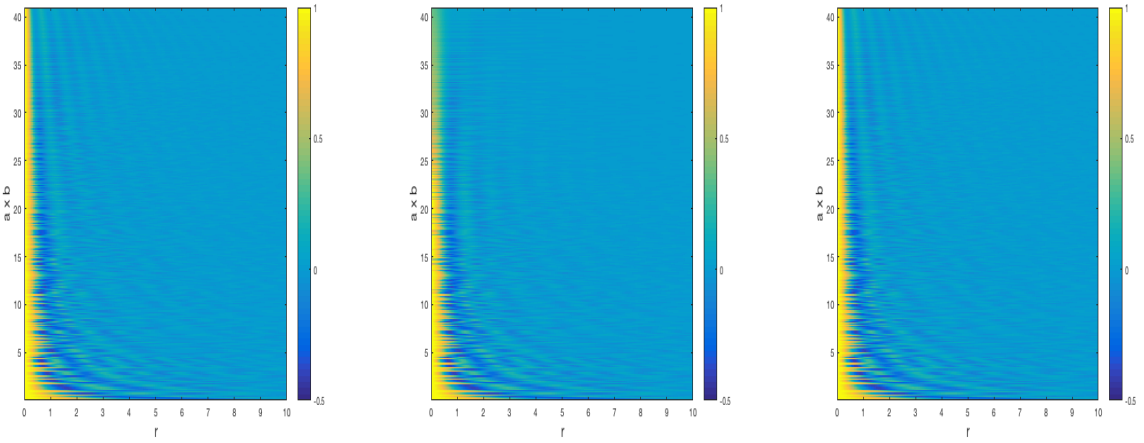

$J_0(ar)J_0(br)$ DIHTs $N = 32$, $\Delta c = 0.2$ DIHTs $N = 65$, $\Delta c = 0.2$

Figure 7.2: Reconstruction of $J_0(ar)J_0(br)$ Products

What is also helpful with inferring sufficient DHT/DIHT parameters for reconstructing these 2J functions is the 0^{th} order Hankel transform versus the frequency parameter c, illustrated below in Figure 7.3 for the product $f(r) \times g(r)$ (left) and each $J_0(ar)J_0(br)$ (right).

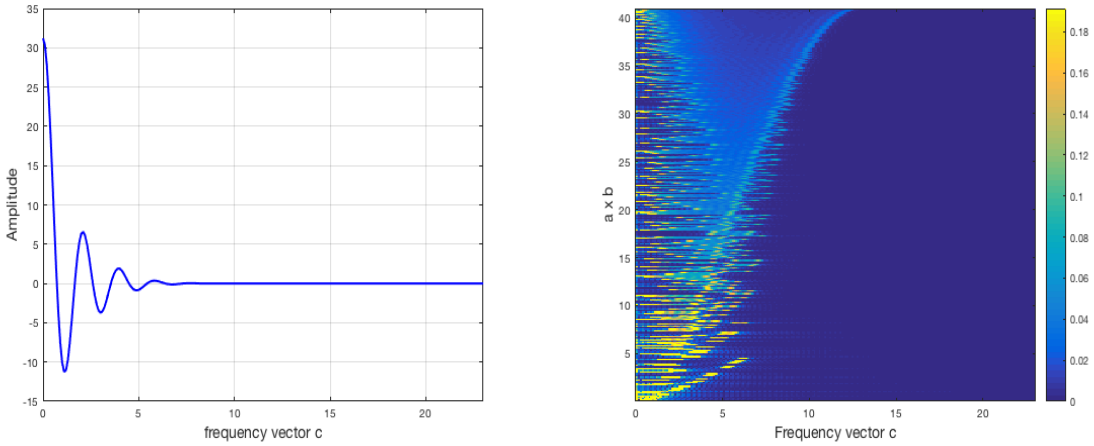

Hankel Transform of $f(r) \times g(r)$ Hankel Transforms of $J_0(ar)J_0(br)$

Figure 7.3: Hankel Transform Illustrations

These illustrations are for a particular choice of $m = n = l = 0$. Nonzero Bessel function orders will become relevant in the upcoming polar and $SE(2)$ series expansions. This figure shows that the discrete data representation of $f(r) \times g(r)$ can be captured with lower frequency values ($c < 6.5$) than all of the $J_0(ar)J_0(br)$ pairs ($c < 13$). It is clear from this above figure that for $h(r)$, a sufficient max frequency is $c \sim 6.5$, whereas for $J_0(ar)J_0(br)$ a max frequency of $c \sim 13$ is needed (an increase by a factor of two). It is not expected that this criteria is consistent for different Bessel function orders m, n, and l. Most likely, higher frequencies will be required for reconstructions involving 3J integrals with higher (m, n, k) order triplets. How these frequency conditions manifest is still unknown, and will be uncovered soon in the upcoming polar and SE(2) expansion sections.

Next it will be shown how 3J integrals can be used in facilitating/approximating the fusion of polar expansions.

7.4 Fusion of Polar Expansions with 3J Integrals

The fusion of two radial expansions using 3J integrals is extended to functions in polar coordinates, where the angular dependence utilizes an exponential basis. Given

two polar expansions $\tilde{f}(r,\phi)$ and $\tilde{g}(r,\phi)$

$$\tilde{f}(r,\phi) = \sum_{n_1=-B_1}^{B_1} e^{in_1\phi} \sum_{l_1=0}^{N_a-1} \hat{f}_{n_1}(a_{l_1}) J_{n_1}(a_{l_1} r) a_{l_1} \Delta a, \tag{7.29}$$

$$\tilde{g}(r,\phi) = \sum_{n_2=-B_2}^{B_2} e^{in_2\phi} \sum_{l_2=0}^{N_b-1} \hat{g}_{n_2}(b_{l_2}) J_{n_2}(b_{l_2} r) b_{l_2} \Delta b, \tag{7.30}$$

with the coefficients of $\tilde{g}(r,\phi)$ given by

$$\hat{g}_{n_2}(b_{l_2}) = \frac{1}{2\pi} \int_0^{2\pi} \int_0^{\infty} f(r,\phi) e^{-in_2\phi} J_{n_2}(b_{l_2} r) r dr d\phi, \tag{7.31}$$

the product $h(r,\phi) = \tilde{f}(r,\phi) \times \tilde{g}(r,\phi)$ is thus

$$h(r,\phi) = \Delta a \Delta b \sum_{n_1=-B_1}^{B_1} \sum_{n_2=-B_2}^{B_2} e^{i(n_1+n_2)\phi} \sum_{l_1=0}^{N_a-1} \sum_{l_2=0}^{N_b-1} a_{l_1} b_{l_2} \hat{f}_{n_1}(a_{l_1}) \hat{g}_{n_2}(b_{l_2}) J_{n_1}(a_{l_1} r) J_{n_2}(b_{l_2} r). \tag{7.32}$$

The Fourier-Bessel coefficients for this product of polar expansions are according to the integral

$$\begin{aligned} \hat{h}_{n_3}(c) &= \frac{1}{2\pi} \int_0^{2\pi} \int_0^{\infty} h(r,\phi) e^{-in_3\phi} J_{n_3}(cr) r dr d\phi \\ &= \Delta a \Delta b \frac{1}{2\pi} \sum_{n_1=-B_1}^{B_1} \sum_{n_2=-B_2}^{B_2} \sum_{l_1=0}^{N_a-1} \sum_{l_2=0}^{N_b-1} a_{l_1} b_{l_2} \hat{f}_{n_1}(a_{l_1}) \hat{g}_{n_2}(b_{l_2}) \\ &\int_0^{2\pi} e^{i(n_1+n_2-n_3)\phi} d\phi \int_0^{\infty} J_{n_1}(a_{l_1} r) J_{n_2}(b_{l_2} r) J_{n_3}(cr) r dr. \end{aligned} \tag{7.33}$$

Next, consider the well-known property

$$\int_0^L e^{\frac{2\pi i(u-v)\phi}{L}} d\phi = L\delta_{u,v},$$

where $\delta_{u,v}$ is the Kronecker Delta function. Choosing $u = n_1 + n_2$ and $v = n_3$, and $L = 2\pi$, the only nonzero terms are when $n_1 + n_2 = n_3$. Thus the coefficients $\hat{h}_{n_3}(c)$ become

$$\hat{h}_{n_3}(c) = \Delta a \Delta b \sum_{n_1=-B_1}^{B_1} \sum_{n_2=-B_2}^{B_2} \sum_{l_1=0}^{N_a-1} \sum_{l_2=0}^{N_b-1} a_{l_1} b_{l_2} \hat{f}_{n_1}(a_{l_1}) \hat{g}_{n_2}(b_{l_2}) \begin{pmatrix} n_1 & n_2 & n_3 \\ a_{l_1} & b_{l_2} & c \end{pmatrix}_J \delta_{n_1+n_2,n_3}. \tag{7.34}$$

truncating $h(r)$ at some bandlimit B_3 gives

$$\begin{aligned} h(r,\phi) &\approx \sum_{n_3=-B_3}^{B_3} e^{in_3\phi} \int_0^\infty \hat{h}_{n_3}(c) J_{n_3}(cr) c dc \\ &= \Delta a \Delta b \sum_{n_3=-B_3}^{B_3} e^{in_3\phi} \sum_{n_1=-B_1}^{B_1} \sum_{n_2=-B_2}^{B_2} \sum_{l_1=0}^{N_a-1} \sum_{l_2=0}^{N_b-1} a_{l_1} b_{l_2} \hat{f}_{n_1}(a_{l_1}) \hat{g}_{n_2}(b_{l_2}) \\ &\quad \delta_{n_1+n_2,n3} \int_0^\infty \begin{pmatrix} n_1 & n_2 & n_3 \\ a_{l_1} & b_{l_2} & c \end{pmatrix}_J J_{n_3}(cr) c dc \\ &= \Delta a \Delta b \sum_{n_1=-B_1}^{B_1} \sum_{n_2=-B_2}^{B_2} e^{i(n_1+n_2)\phi} \sum_{l_1=0}^{N_a-1} \sum_{l_2=0}^{N_b-1} a_{l_1} b_{l_2} \hat{f}_{n_1}(a_{l_1}) \hat{g}_{n_2}(b_{l_2}) \\ &\quad \int_0^\infty \begin{pmatrix} n_1 & n_2 & n_1+n_2 \\ a_{l_1} & b_{l_2} & c \end{pmatrix}_J J_{n_3}(cr) c dc. \end{aligned} \tag{7.35}$$

Notice that the Kronecker delta function eliminated the summation over n_3. When the integral

$$\int_0^\infty \begin{pmatrix} n_1 & n_2 & n_1+n_2 \\ a_{l_1} & b_{l_2} & c \end{pmatrix}_J J_{n_3}(cr)cdc,$$

is not available in closed-form, the inversion formula can be discretized as

$$\begin{aligned}\tilde{h}(r,\phi) = \Delta a \Delta b \Delta c \sum_{n_1=-B_1}^{B_1} \sum_{n_2=-B_2}^{B_2} e^{i(n_1+n_2)\phi} \sum_{l_1=0}^{N_a-1} \sum_{l_2=0}^{N_b-1} a_{l_1} b_{l_2} \hat{f}_{n_1}(a_{l_1}) \hat{g}_{n_2}(b_{l_2}) \\ \sum_{l_3=0}^{N_c-1} \begin{pmatrix} n_1 & n_2 & n_1+n_2 \\ a_{l_1} & b_{l_2} & c_{l_3} \end{pmatrix}_J J_{n_3}(c_{l_3} r) c_{l_3}.\end{aligned} \tag{7.36}$$

Figure 7.4 shows polar series approximations of the functions $f(r,\phi)$, $g(r,\phi)$, and the product $f(r,\phi) \times g(r,\phi)$. The series approximations have the bandlimit $B = 3$ and frequency vectors with a max value of 6.5 and resolution 0.2. The chosen densities are Gaussians of the form

$$\rho(r,\phi;r_0,\phi_0,\sigma_r,\sigma_\phi) = exp(-\frac{1}{2}\left[(r-r_0)^2/\sigma_r + (\phi-\phi_0)^2/\sigma_\phi\right]),$$

with values

$$f(r,\phi) = \rho(r,\phi;2,0.7854,1,1.25),$$

and

$$g(r,\phi) = \rho(r,\phi;2.4,20.6981,0.8333,0.75).$$

For an (x, y) grid, the function of interest is

$$\rho(x, y; r_0, \phi_0, \sigma_r, \sigma_\phi) = exp(-\frac{1}{2}\left[(\sqrt{x^2 + y^2} - r_0)^2/\sigma_r + (atan2(y, x) - \phi_0)^2/\sigma_\phi\right]).$$

Cartesian grids and corresponding Fourier-Bessel expansions are depicted in Figure 7.5

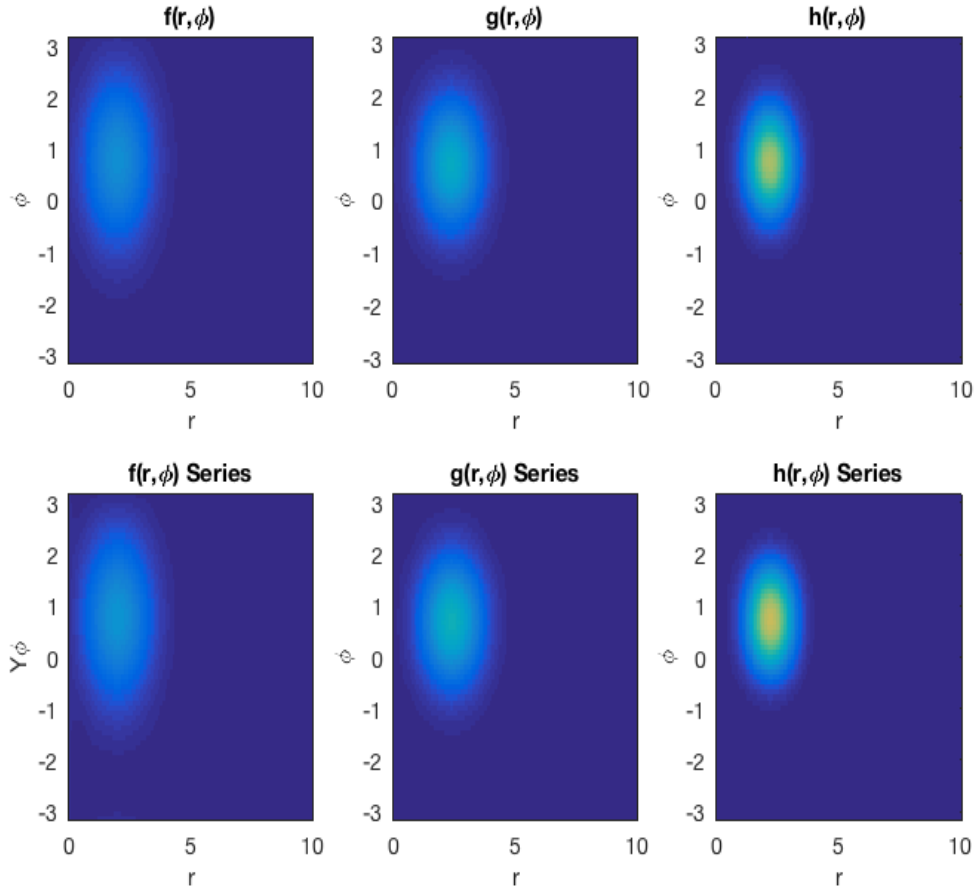

Figure 7.4: Fourier-Bessel Series Expansions for Gaussians (Polar Grids)

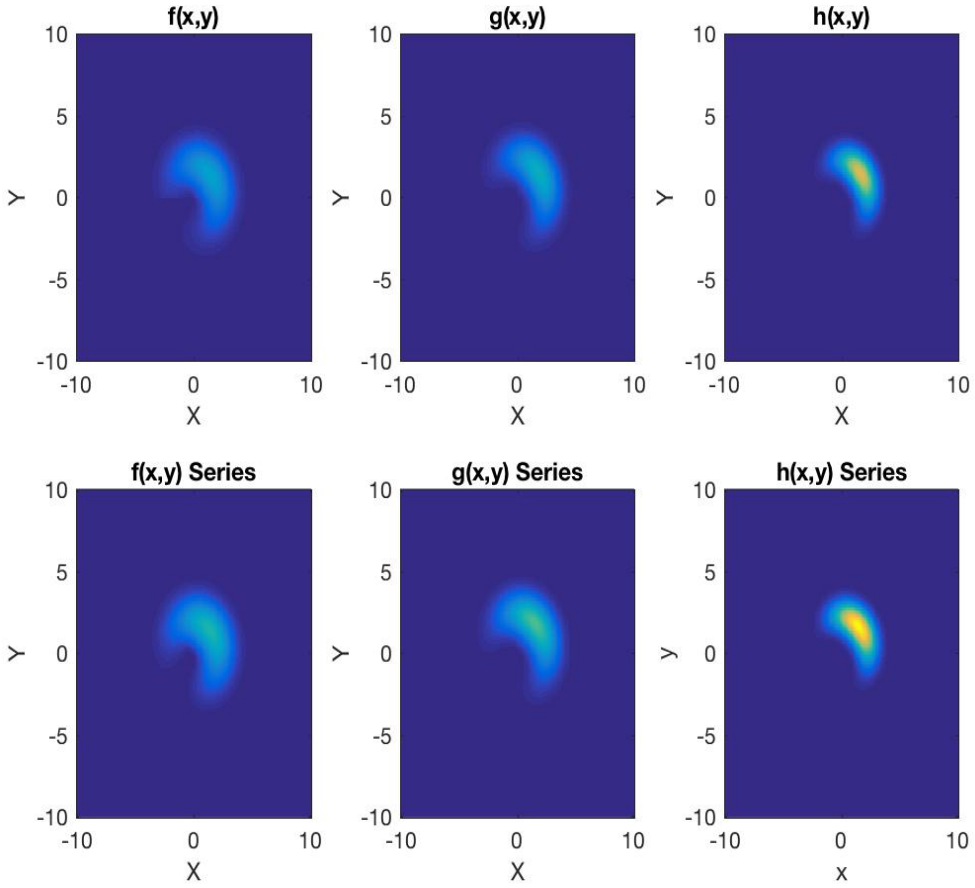

Figure 7.5: Fourier-Bessel Series Expansions for Gaussians (Cartesian Grids)

Equation (7.36), specifically the 3J integral part, has constraints on n_1 and n_2, which provides some insight into determining sufficient resolution parameters with respect to frequency c. Due to the Kronecker delta function killing the summation over n_3, 49 plots akin to Figure 7.3 would be needed to illustrate the required resolution. This is still quite vast, however since the three Bessel functions under the integral commute, and the frequency parameters a and b have been equated, some symmetries can be exploited to reduce this number of plots from 49 down to 6. Hankel transforms

of the relevant 2J functions are shown in Figure 7.6 for representative Bessel function orders. Only nonzero orders are considered since Bessel functions have the property

$$J_{-n}(x) = (-1)^n J_n(x),$$

for $n \geq 0$.

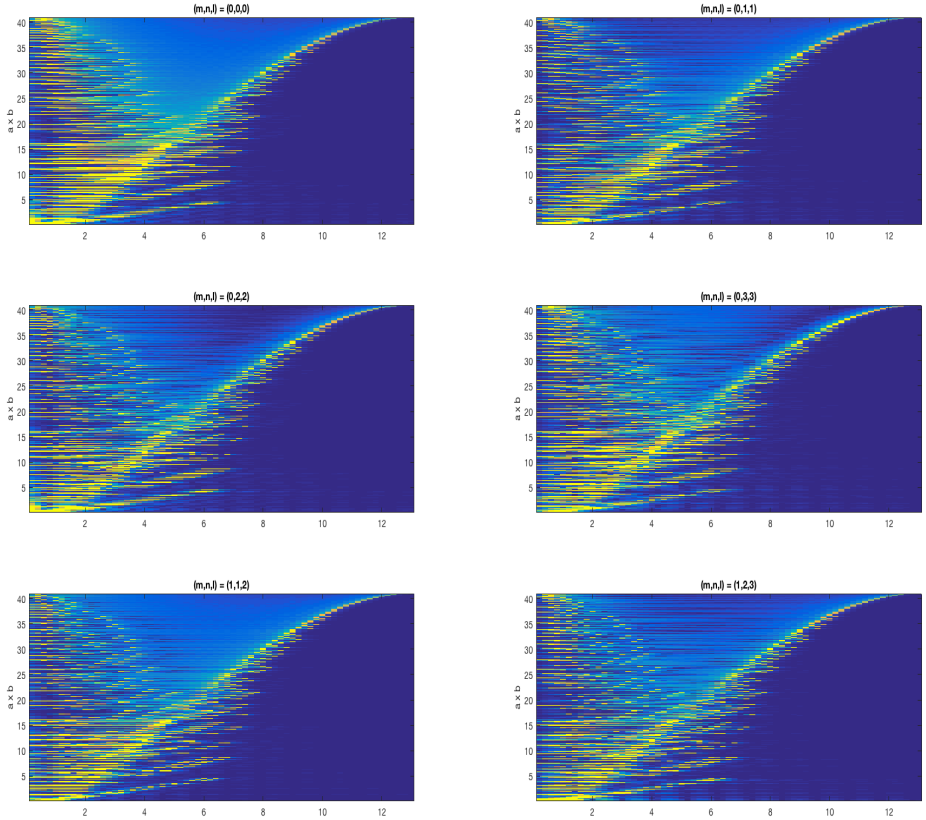

Figure 7.6: Hankel Transforms for Different Bessel Function Order Triplets

A max frequency value of $c = 13$ is still sufficient for this polar expansion example

and the resulting approximations leveraging 3J integrals. Figure 7.7 illustrates the 3J integrals being used to implicitly fuse the two polar expansions. The 3J integrals were computed numerically due to a lack of available analytic solutions. Notwithstanding, the reconstruction is approximately correct, but would be more accurate with exact results for the 3J integrals. Figure 7.8 shows the same fusion for an (x, y) grid.

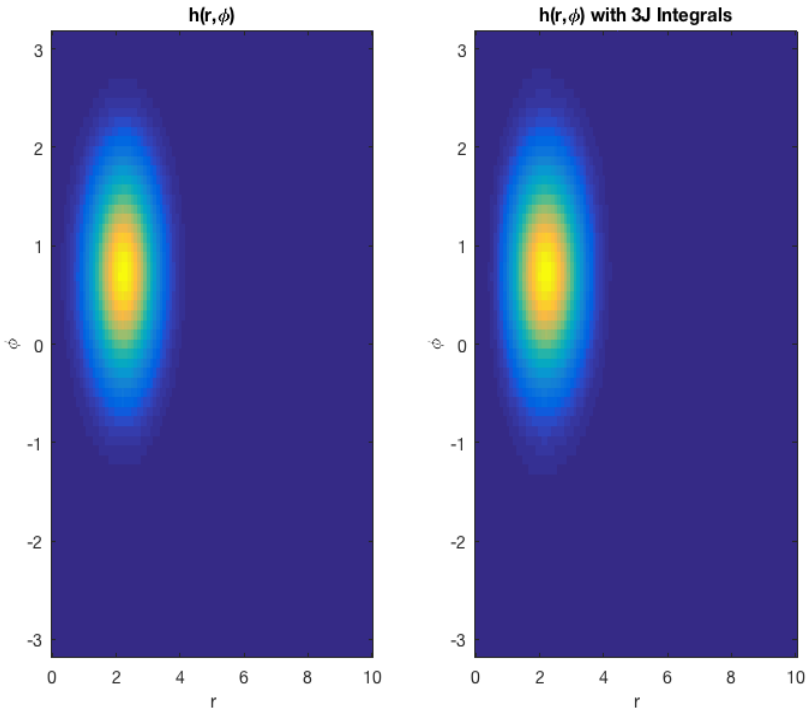

Figure 7.7: Fusion of Polar Expansions with 3J Integrals (Polar Grid)

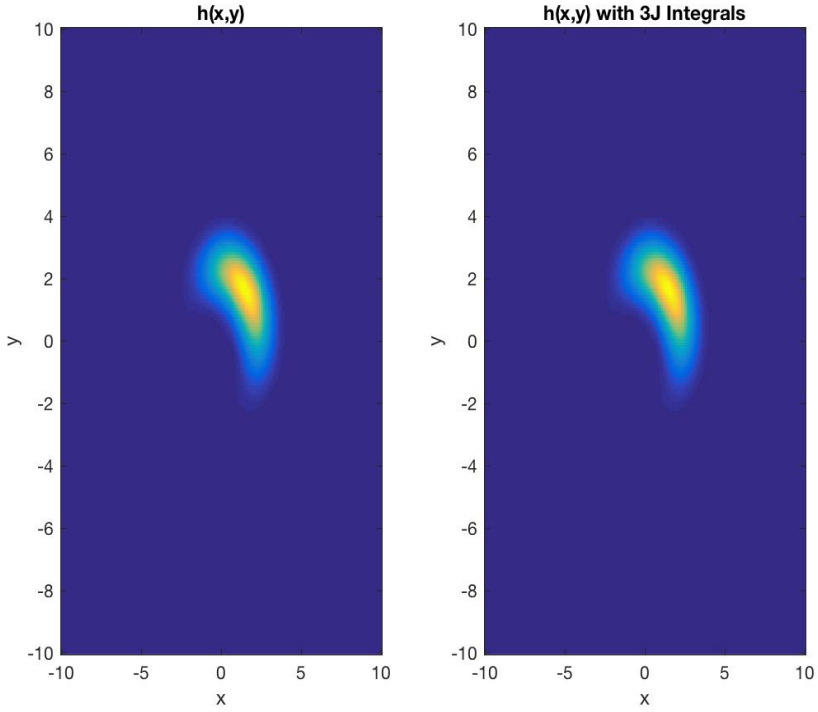

Figure 7.8: Fusion of Polar Expansions with 3J Integrals (Cartesian Grid)

7.4.1 Fusion of Polar Expansions with 3J Integrals: Two Coordinates Systems

This fusion idea was originally derived in [19] and extended above equations to consider the fusion of two functions $f(r, \phi)$ and $g(r', \phi')$ where $(r, \phi) \neq (r', \phi')$ are two unique polar coordinate systems. Consider (r, ϕ) as the global frame of reference viewed from say a sensor, which we will call robot 1. A second robot (i.e. robot 2) has the coordinate system $(r'\phi')$. Like before, the densities for each robot $f(r, \phi)$ and

$g(r', \phi')$ can be approximated with Fourier-Bessel expansions

$$\tilde{f}(r, \phi) = \sum_{n_1=-B_1}^{B_1} e^{in_1\phi} \sum_{l_1=0}^{N_a-1} \hat{f}_{n_1}(a_{l_1}) J_{n_1}(a_{l_1} r) a_{l_1} \Delta a,$$

and

$$\tilde{g}(r', \phi') = \sum_{n_2=-B_2}^{B_2} e^{in_2\phi'} \sum_{l_2=0}^{N_b-1} \hat{g}_{n_2}(b_{l_2}) J_{n_2}(b_{l_2} r') b_{l_2} \Delta b.$$

Using Watson's transformation [3]

$$e^{in\phi'} J_n(pr') \approx e^{in\phi} \sum_{m=-B_w}^{B_w} J_m(pr_0) J_{n+m}(pr) e^{im\phi}, \tag{7.37}$$

where $r_0 = |r - r'|$, the expansion for $g(r', \phi')$ can be represented in the coordinate system of robot 1 as

$$g(r, \phi) \approx \sum_{n_2=-B_2}^{B_2} e^{in_2\phi} \sum_{m=-B_w}^{B_w} J_m(pr_0) J_{n_2+m}(pr) e^{im\phi}. \tag{7.38}$$

The densities can now be combined as

$$\begin{aligned} h(r, \phi) &= f(r, \phi) g(r, \phi) \\ &= \Delta a \Delta b \sum_{n_1=-B_1}^{B_1} \sum_{n_2=-B_2}^{B_2} \sum_{m=-B_w}^{B_w} e^{i(n_1+n_2+m)\phi} \sum_{l_1=0}^{N_a-1} \sum_{l_2=0}^{N_b-1} a_{l_1} b_{l_2} \hat{f}_{n_1}(a_{l_1}) \hat{g}_{n_2}(b_{l_2}) \\ &\quad J_m(b_{l_2} r_0) J_{n_1}(a_{l_1} r) J_{n_2+m}(b_{l_2} r). \end{aligned} \tag{7.39}$$

Watson's Bessel function transformation assumes the angle that robot 1 makes with robot 2 is equal to zero (i.e. both sensors lie on the x-axis). Not that $J_m(b_{l_2}r_0)$ for each point b_{l_2} is a constant since r_0 is fixed. The Fourier-Bessel coefficients for this product of polar expansions are thus

$$\begin{aligned}
\hat{h}_{n_3}(c) &= \frac{1}{2\pi}\int_0^{2\pi}\int_0^{\infty} h(r,\phi)e^{-in_3\phi}J_{n_3}(c_{l_3}r)rdrd\phi \\
&= \Delta a\Delta b\frac{1}{2\pi}\sum_{n_1=-B_1}^{B_1}\sum_{n_2=-B_2}^{B_2}\sum_{m=-B_w}^{B_w}\sum_{l_1=0}^{N_a-1}\sum_{l_2=0}^{N_b-1} a_{l_1}b_{l_2}J_m(b_{l_2}r_0)\hat{f}_{n_1}(a_{l_1})\hat{g}_{n_2}(b_{l_2}) \\
&\int_0^{2\pi} e^{i(n_1+n_2+m-n_3)\phi}d\phi\int_0^{\infty} J_{n_1}(a_{l_1}r)J_{n_2+m}(b_{l_2}r)J_{n_3}(c_{l_3}r)rdr \\
&= \Delta a\Delta b\sum_{n_1=-B_1}^{B_1}\sum_{n_2=-B_2}^{B_2}\sum_{m=-B_w}^{B_w}\sum_{l_1=0}^{N_a-1}\sum_{l_2=0}^{N_b-1} a_{l_1}b_{l_2}J_m(b_{l_2}r_0)\hat{f}_{n_1}(a_{l_1})\hat{g}_{n_2}(b_{l_2}) \\
&\delta_{n_1+n_2+m,n_3}\int_0^{\infty} J_{n_1}(a_{l_1}r)J_{n_2+m}(b_{l_2}r)J_{n_3}(c_{l_3}r)rdr.
\end{aligned} \tag{7.40}$$

Truncating $h(r)$ at some bandlimit gives

$$\begin{aligned}
h(r,\phi) &\approx \sum_{n_3=-B_3}^{B_3} e^{in_3\phi} \int_0^\infty \hat{h}_{n_3}(c) J_{n_3}(cr) c dc \\
&= \sum_{n_3=-B_3}^{B_3} e^{in_3\phi} \Delta a \Delta b \sum_{n_1=-B_1}^{B_1} \sum_{n_2=-B_2}^{B_2} \sum_{m=-B_w}^{B_w} \sum_{l_1=0}^{N_a-1} \sum_{l_2=0}^{N_b-1} a_{l_1} b_{l_2} J_m(b_{l_2} r_0) \hat{f}_{n_1}(a_{l_1}) \hat{g}_{n_2}(b_{l_2}) \\
&\quad \delta_{n_1+n_2+m,n3} \int_0^\infty \begin{pmatrix} n_1 & n_2+m & n_3 \\ a_{l_1} & b_{l_2} & c \end{pmatrix}_J J_{n_3}(cr) c dc \\
&= \Delta a \Delta b \sum_{n_1=-B_1}^{B_1} \sum_{n_2=-B_2}^{B_2} \sum_{m=-B_w}^{B_w} e^{i(n_1+n_2+m)\phi} \sum_{l_1=0}^{N_a-1} \sum_{l_2=0}^{N_b-1} a_{l_1} b_{l_2} J_m(b_{l_2} r_0) \hat{f}_{n_1}(a_{l_1}) \hat{g}_{n_2}(b_{l_2}) \\
&\quad \int_0^\infty \begin{pmatrix} n_1 & n_2+m & n_1+n_2+m \\ a_{l_1} & b_{l_2} & c \end{pmatrix}_J J_{n_3}(cr) c dc.
\end{aligned} \tag{7.41}$$

Discretizing the inversion formula yields

$$\begin{aligned}
\tilde{h}(r,\phi) &= \Delta a \Delta b \Delta c \sum_{n_1=-B_1}^{B_1} \sum_{n_2=-B_2}^{B_2} \sum_{m=-B_w}^{B_w} e^{i(n_1+n_2+m)\phi} \sum_{l_1=0}^{N_a-1} \sum_{l_2=0}^{N_b-1} a_{l_1} b_{l_2} J_m(b_{l_2} r_0) \hat{f}_{n_1}(a_{l_1}) \hat{g}_{n_2}(b_{l_2}) \\
&\quad \sum_{l_3=0}^{N_c-1} \begin{pmatrix} n_1 & n_2+m & n_1+n_2+m \\ a_{l_1} & b_{l_2} & c_{l_3} \end{pmatrix}_J J_{n_3}(c_{l_3} r) c_{l_3}.
\end{aligned} \tag{7.42}$$

The following example will illustrate the effectiveness of fusion with 3J integrals, now for two coordinate systems. The choice will again be Gaussians, only this time each density is initially represented in its own coordinate system (either (r,ϕ) or (r',ϕ')). Fourier-Bessel expansions, and 3J integrals are utilized to stitch together

the coefficients of the fused distribution, according to equation (7.42). Each Gaussian distribution has standard deviations $\sigma_r = 0.4$, and $\sigma_\phi = 0.5$. The position of robot 1, 2, and the measured landmark are $\mathbf{x}_0 = [0, 0]$, $\mathbf{x}_1 = [2, 0]$, and $\mathbf{x}_2 = [1, 3]$ respectively. The red x denotes the true position of the landmark. Figure 7.9 shows the approximation of robot 1's density, and Figure 7.10 shows that for robot 2 (in both coordinate systems (r, ϕ) and (r', ϕ')).

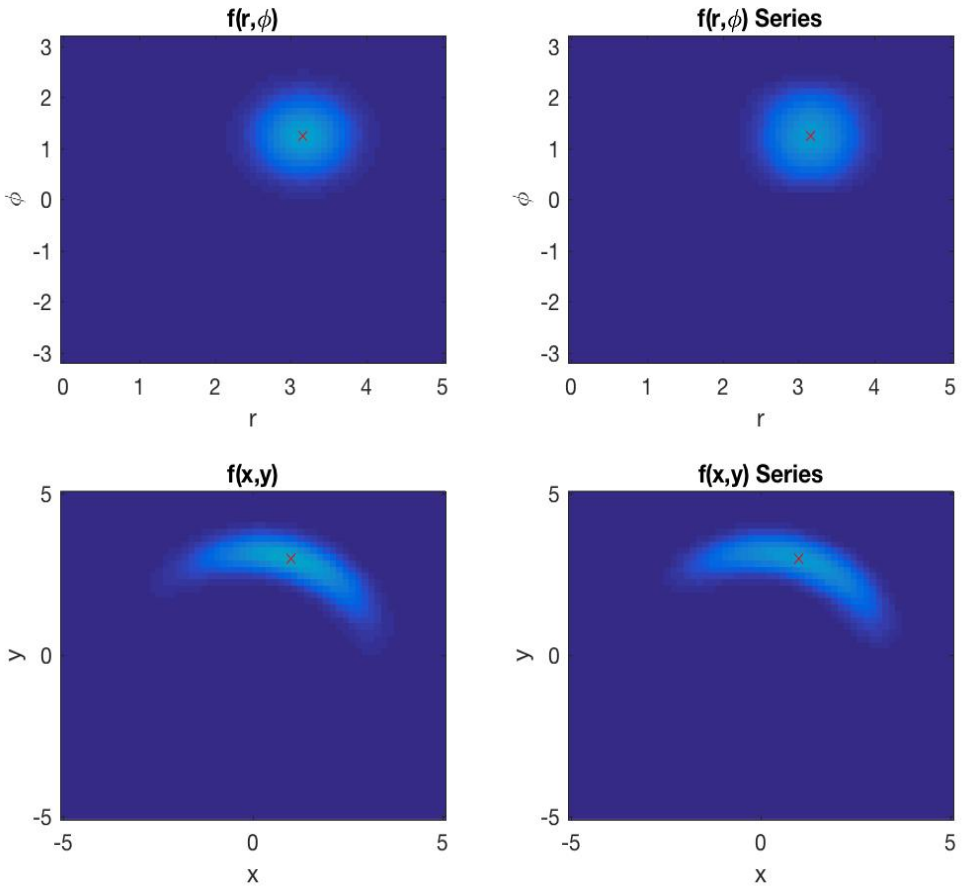

Figure 7.9: Fourier-Bessel Series Expansion for Robot 1

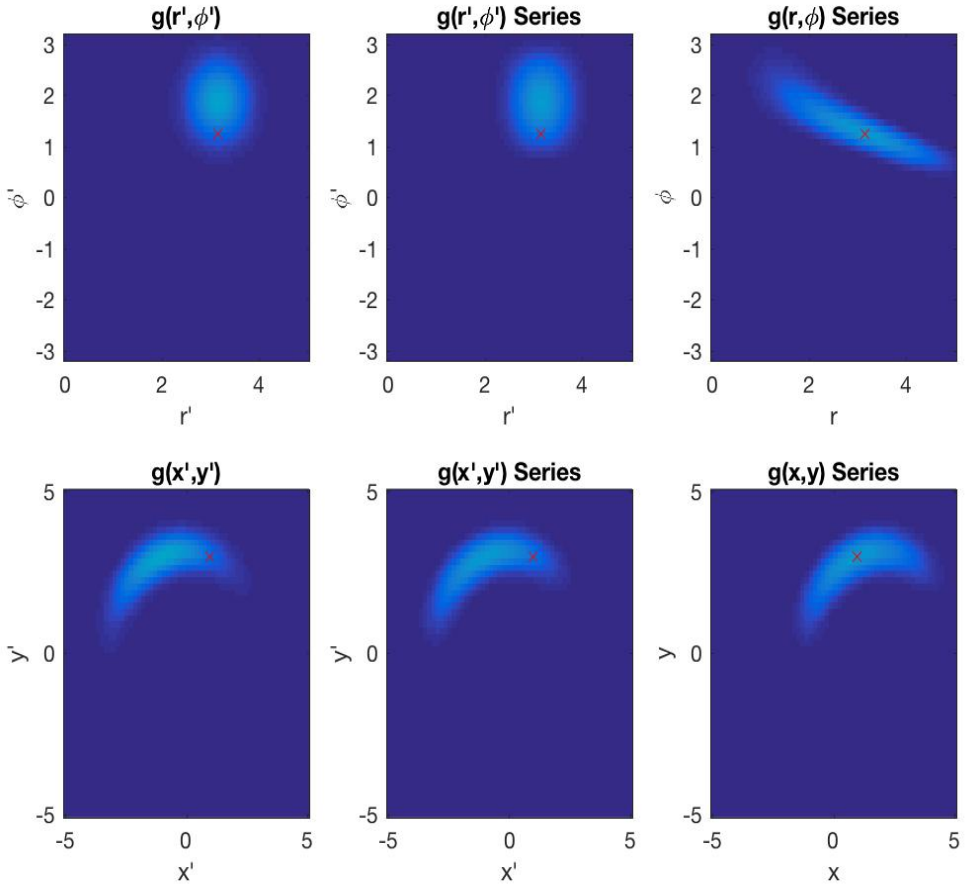

Figure 7.10: Fourier-Bessel Series Expansion for Robot 2

The fusion of both Fourier-Bessel expansions (in the same coordinate system) is depicted in Figure 7.11, and Figure 7.12 shows the fusion with the aid of 3J integrals

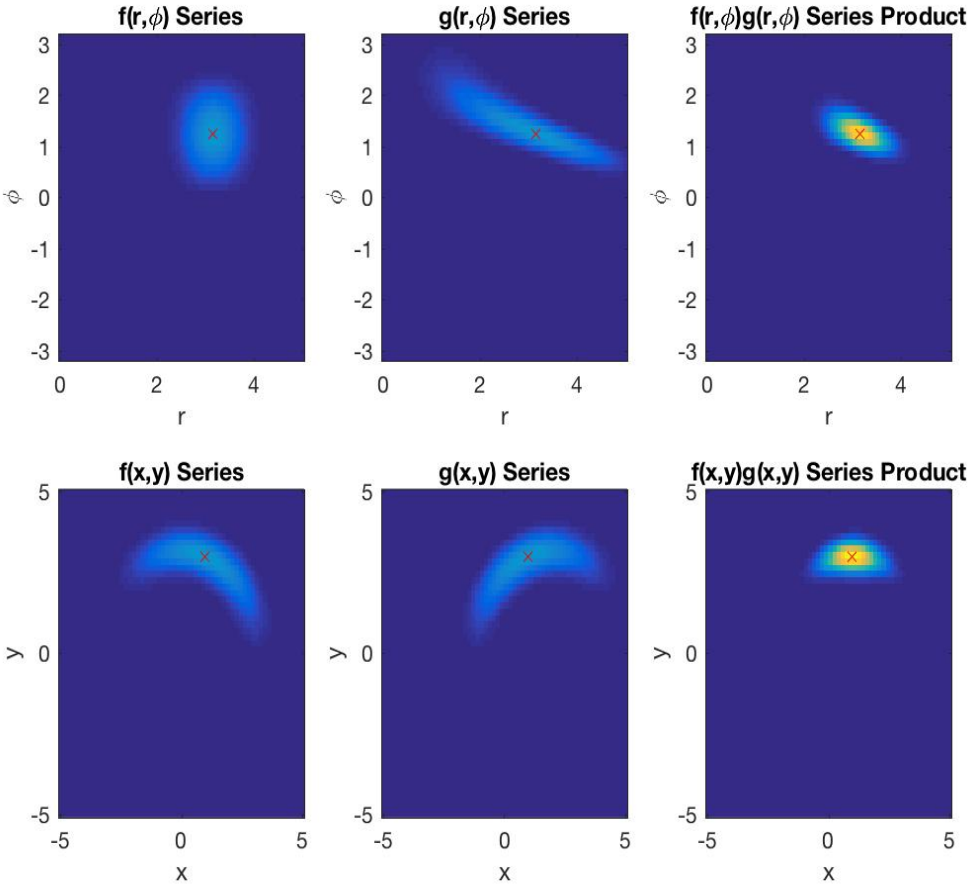

Figure 7.11: Fusion of f and g Expansions

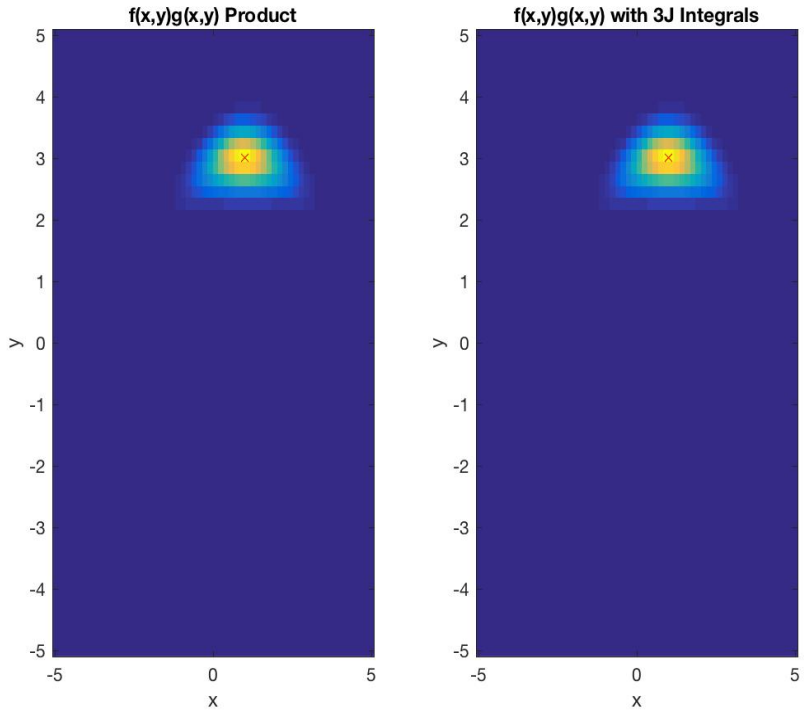

Figure 7.12: Fusion of Polar Expansions with 3J Integrals

The next section will solve the fusion problem for functions on the Lie group $SE(2)$.

7.5 Fusion of Fourier Expansions on $SE(2)$ with 3J Integrals

A similar derivation approach will be taken here, by first defining two Fourier series expansions on $SE(2)$ as

$$\tilde{f}_1(g) = \sum_{l_1=0}^{N_a-1} \sum_{m_1,n_1=-l_1}^{l_1} \hat{f}_{m_1,n_1}(a_{l_1}) U_{n_1,m_1}(g, a_{l_1}) a_{l_1} \Delta a, \tag{7.43}$$

and

$$\tilde{f}_2(g) = \sum_{l_2=0}^{N_b-1} \sum_{m_2,n_2=-l_2}^{l_2} \hat{f}_{m_2,n_2}(b_{l_2}) U_{n_2,m_2}(g, b_{l_2}) b_{l_2} \Delta b. \tag{7.44}$$

The product $h(r) = \tilde{f}_1(g)\tilde{f}_2(g)$ is

$$\begin{aligned} h(r) = \Delta a \Delta b \sum_{l_1=0}^{N_a-1} \sum_{l_2=0}^{N_b-1} \sum_{m_1,n_1=-l_1}^{l_1} \sum_{m_2,n_2=-l_2}^{l_2} \hat{f}_{m_1,n_1}(a_{l_1}) \hat{f}_{m_2,n_2}(b_{l_2}) a_{l_1} b_{l_2} \\ U_{n_1,m_1}(g, a_{l_1}) U_{n_2,m_2}(g, b_{l_2}). \end{aligned} \tag{7.45}$$

The Fourier transform of the product of $h(g)$ as defined by equation (7.45) for a given frequency c is

$$\begin{aligned} \hat{h}_{m_3,n_3}(c) = \Delta a \Delta b \sum_{l_1=0}^{N_{l_1}-1} \sum_{l_2=0}^{N_{l_2}-1} \sum_{m_1,n_1=-l_1}^{l_1} \sum_{m_2,n_2=-l_2}^{l_2} \hat{f}_{m_1,n_1}(a_{l_1}) \hat{f}_{m_2,n_2}(b_{l_2}) a_{l_1} b_{l_2} \\ \int_{SE(2)} U_{n_1,m_1}(g, a_{l_1}) U_{n_2,m_2}(g, b_{l_2}) \overline{U_{n_3,m_3}(g, c)} dg. \end{aligned} \tag{7.46}$$

If a group element $g \in SE(2)$ is parameterized as $g = g(r, \phi, \theta)$ then the integral of three IURs for $SE(2)$ is given by the equation

$$\begin{aligned}
&\int_{SE(2)} U_{n_1,m_1}(g, a_{l_1}) U_{n_2,m_2}(g, b_{l_2}) \overline{U_{n_3,m_3}(g, c)} dg \\
&= \int_0^{2\pi} \int_0^{2\pi} \int_0^{\infty} i^{m_1-n_1} e^{-i[m_1\theta+(n_1-m_1)\phi]} J_{m_1-n_1}(a_{l_1} r) \\
&i^{m_2-n_2} e^{-i[m_2\theta+(n_2-m_2)\phi]} J_{m_2-n_2}(b_{l_2} r) i^{n_3-m_3} e^{+i[m_3\theta+(n_3-m_3)\phi]} J_{m_3-n_3}(cr) r dr d\phi d\theta \\
&= i^{m_1+m_2-m_3-n_1-n_2+n_3} \int_0^{2\pi} e^{-i(m_1+m_2-m_3)\theta} d\theta \int_0^{2\pi} e^{-i[(n_1-m_1)+(n_2-m_2)-(n_3-m_3)]\phi} d\phi \\
&\begin{pmatrix} m_1 - n_1 & m_2 - n_2 & m_3 - n_3 \\ a_{l_1} & b_{l_2} & c \end{pmatrix}_J .
\end{aligned} \tag{7.47}$$

The integrals over θ and ϕ evaluate as

$$\int_0^{2\pi} e^{-i(m_1+m_2-m_3)\theta} d\theta = -i \frac{(1 - e^{-2\pi i(m_1+m_2-m_3)})}{m_1 + m_2 - m_3}, \tag{7.48}$$

and

$$\int_0^{2\pi} e^{-i[(n_1-m_1)+(n_2-m_2)-(n_3-m_3)]\phi} d\phi = -i \frac{(e^{2\pi i(m_1+m_2-m_3-n_1-n_2+n_3)} - 1)}{m_1 + m_2 - m_3 - n_1 - n_2 + n_3}. \tag{7.49}$$

The product of these integrals equals zero when either $m_1+m_2 = m_3$ or $m_1+m_2-n_1-n_2 = m_3 - n_3$. Therefore integral of three IURs over $SE(2)$ is simply a 3J integral scaled by a nonlinear function. The final form of this expression with coefficients

$\hat{h}_{m_3,n_3}(c)$ according to equation (7.46) is

$$\tilde{h}(g) = \sum_{l_3=0}^{N_c-1} \sum_{m_3,n_3=-l_3}^{l_3} \hat{h}_{m_3,n_3}(c_{l_3}) U_{n_3,m_3}(g, c_{l_3}) c_{l_3} \Delta c. \tag{7.50}$$

Consider a G-Gaussian (i.e. a Guassian for a Lie group) on SE(2), given by the equation

$$\rho(g; \mu, \Sigma) = exp\left([\log^{\vee}(\mu^{-1}g)]^T \Sigma^{-1} [\log^{\vee}(\mu^{-1}g)]\right),$$

where $log : G \to \mathcal{G}$ is the matrix logarithm, $^{\vee} : \mathcal{G} \to \mathbb{R}^d$ ($d = 3$ for SE(2)) is the vee operator, and $exp : \mathbb{R} \to \mathbb{R}$ is the exponential for scalars. Two G-Gaussians are used in this numeric example, namely $f_1(g) = \rho(g, \mu_1, \Sigma_1)$ and $f_2(g) = \rho(g, \mu_2, \Sigma_2)$, where

$$\mu_1 = \begin{bmatrix} 1 & 0 & 0.7 \\ 0 & 1 & 0.5 \\ 0 & 0 & 1 \end{bmatrix},$$

$$\mu_2 = \begin{bmatrix} 1 & 0 & 0.4 \\ 0 & 1 & 0.6 \\ 0 & 0 & 1 \end{bmatrix},$$

and

$$\Sigma_1 = \begin{bmatrix} 0.6 & 0 & 0 \\ 0 & 0.6 & 0 \\ 0 & 0 & 0.6 \end{bmatrix},$$

$$\Sigma_2 = \begin{bmatrix} 0.4 & 0 & 0 \\ 0 & 0.4 & 0 \\ 0 & 0 & 0.4 \end{bmatrix}.$$

These two functions, and the product $f(g) \times h(g)$ are illustrated in Figure 7.13.

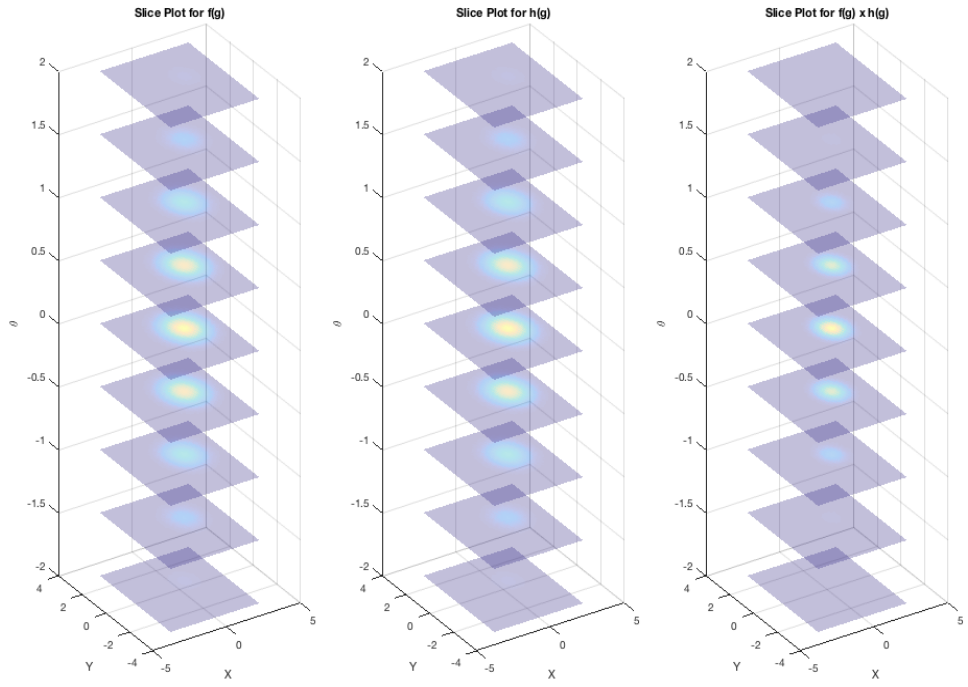

Figure 7.13: G-Gaussians for SE(2) Fusion Example

The SE(2)-series frequency parameters for $\tilde{f}_1(g)$, $\tilde{f}_2(g)$, and $\tilde{h}(g)$ are $\Delta a = 0.1552$,

$a_{max} = 4.5$, $\Delta b = 0.1552$, $b_{max} = 4.5$, and $\Delta c = 0.0776$, $c_{max} = 22$ respectively. The series approximations $\tilde{f}_1(g)$, $\tilde{f}_2(g)$, and a third for the product of $f_1(g)$ and $f_2(g)$ are shown in Figure 7.14.

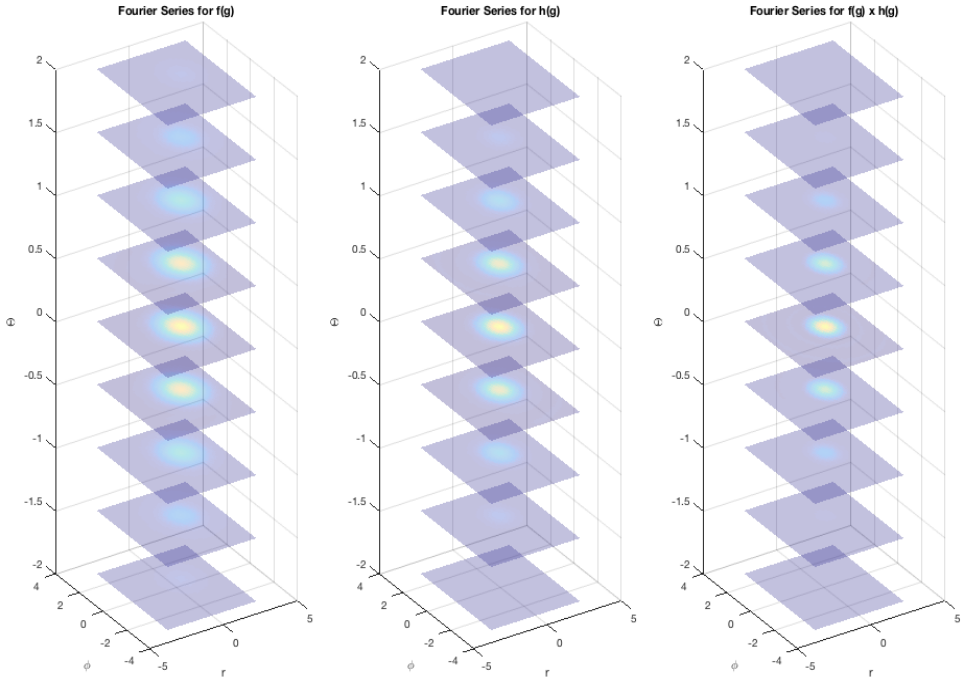

Figure 7.14: Fourier Series Approximations of G-Gaussians for SE(2)

The max Bessel function order used in all of these reconstructions is 60. Previous parameter studies with 3J integrals did not capture the essence of this higher order condition, and so a Hankel transform surface akin to Figures 7.3 and 7.6 will be generated. Figure 7.15 shows this surface, and that a frequency parameter s with the chosen max value of 22 captures all relevant frequency content.

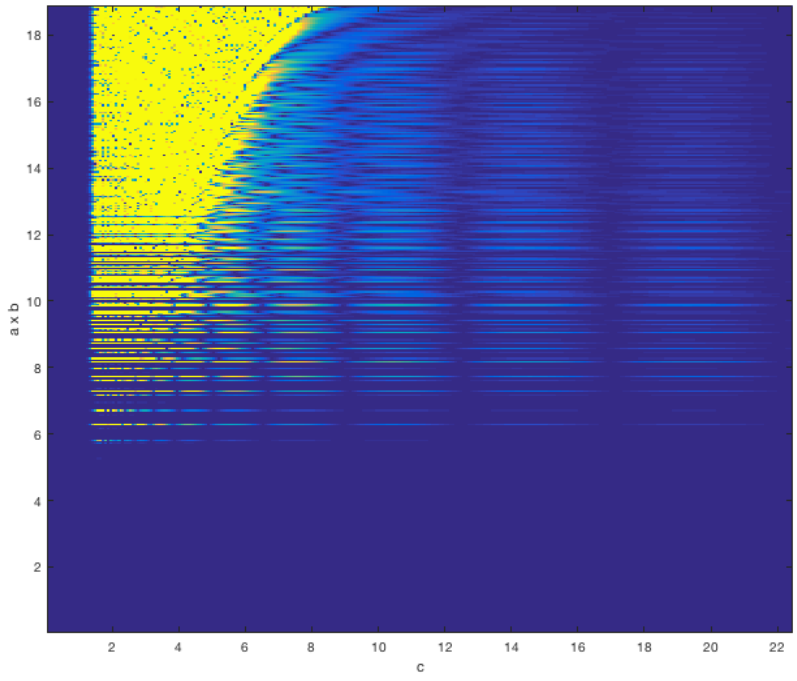

Figure 7.15: Hankel transforms of 2J functions for $m = n = l = 60$

Finally, Figure 7.16 juxtaposes the true fused result against one stitched together with 3J integrals.

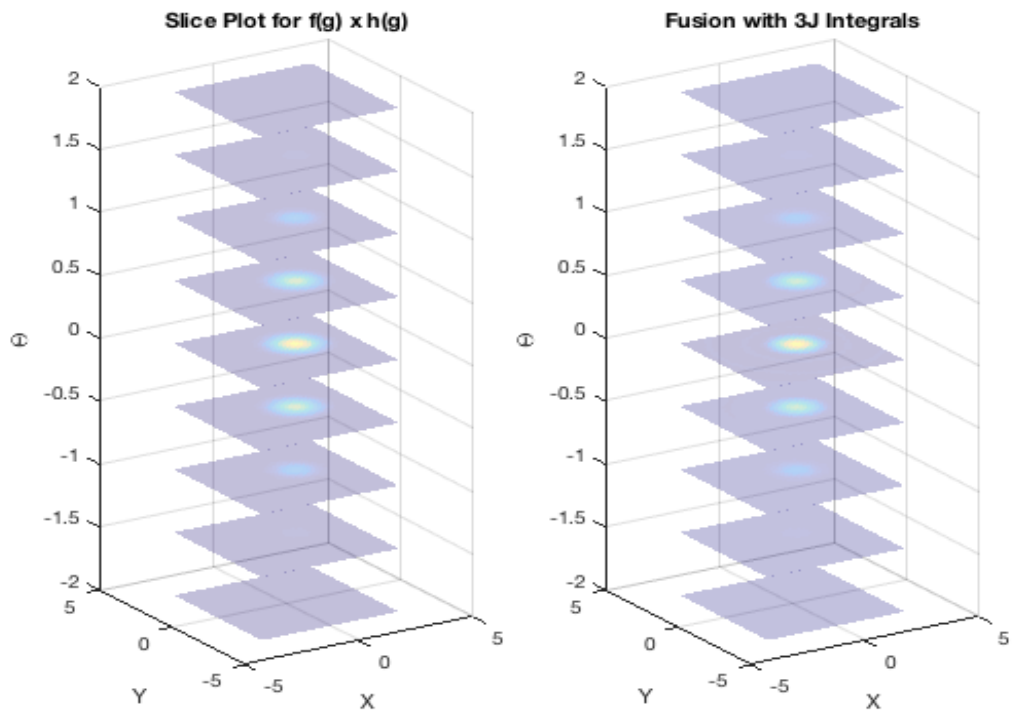

Figure 7.16: Example of SE(2) Fusion with 3J Integrals

7.6 Chapter Summary

This chapter comprehensively showed how 3J integrals facilitated the fusion of two Bessel function expansions, for radial, polar, and $SE(2)$ coordinate systems. Bessel functions are not the only radial basis: there is also Laguerre functions and spherical Bessel functions. The notion of $3X$ integrals, where X is the underlying basis function is general concept, and thus can be extended to solve fusion problems in spherical coordinates using say $3L$ (Laguerre) integrals or $3j$ integrals. These will be reserved for future research topics.

Chapter 8

Data Fusion with $3h$ Integrals

8.1 Introduction

This chapter will continue the analysis of fusing expansions using integrals of the product of three orthogonal functions, which are generally referred to as $3X$ integrals. Here the focus will be on $3h$ integrals, which are integrals of the product of three Hermite functions $h_n(x)$ over the real line. Unlike $3J$ integrals from the previous chapter, $3h$ integrals all have well-behaved closed-form solutions. Furthermore, they can be computed recursively given a finite set of analytic starting conditions. The reader is referred back to Chapter 4 for articulation on the starting conditions and statements of completeness.

Another elegant property of Hermite function expansions is that they are closed un-

der multiplication, meaning the product of two Hermite expansions is itself a Hermite expansion. Closure under multiplication in accordance with a lossless property under coordinate interconversion will be combined together to solve the following problems:

1. Fusion of Polar Expansions via 2D Interconversion and Multiplication;

2. Fusion of Spherical Expansions via 3D Interconversion and Multiplication;

For fusing polar expansions, there are two interconversion techniques available as articulated in Chapter 6, that being 1. interconversion between 2D Hermite and Fourier-Laguerre expansions via conversion matrices Q^m and 2. techniques of SH expansions. For fusing spherical expansions, the exclusive method is that of S^2H expansions.

The outline of the remainder of this chapter is as follows. Section 8.2 will redefine the $3h$ integral and showcase how it is used to represent the product of two Hermite expansions as another Hermite expansion. Section 8.3 will review the interconversion techniques. Section 8.4 will formulate the fusion of polar and spherical expansions via interconversion combined with the closure property of Hermite expansions under multiplication. Section 8.5 will showcase how two densities can be combined when they are in different coordinate frames, as long as one frame can be rotated into the other via some matrix $R \in SO(N)$. This will utilize a lossless rotation property of Hermite expansions that was derived in Chapter 3. Section 8.6 summarizes the

chapter and suggests algorithmic improvements that can be made in the future.

8.2 Hermite Expansions and the $3h$ Integral

Hermite functions are a complete orthonormal basis, allowing functions $f(x) \in \mathbb{R}$ to be approximated as

$$f(x) \approx \tilde{f}(x) = \sum_{m=0}^{M} \hat{f}_m h_m(ax),$$

for some large integer N. As derived in Chapter 3, the $3h$ integral

$$\begin{pmatrix} m & n & k \\ a & b & c \end{pmatrix}_h \doteq \int_{-\infty}^{\infty} h_m(ax) h_n(bx) h_k(cx) dx,$$

was used to show that $\tilde{f}(x)$ and another series $\tilde{g}(x)$ can be combined into one Hermite function expansion as

$$\begin{aligned} \tilde{q}(x) &= \tilde{f}(x)\tilde{g}(x) \\ &= \sqrt{a^2+b^2} \sum_{m=0}^{M} \sum_{n=0}^{N} \hat{f}_m \hat{g}_n \sum_{k=0}^{m+n} \eta_k \begin{pmatrix} m & n & k \\ a & b & \sqrt{a^2+b^2} \end{pmatrix}_h h_k(x\sqrt{a^2+b^2}), \end{aligned} \tag{8.1}$$

where $\eta_k = \frac{1}{c_k^2 2^k k! \sqrt{\pi}}$. This notion extends quite easily to 2D and 3D Hermite function expansions as

$$\begin{aligned}
\tilde{q}^c(x,y) &= \tilde{f}^c(x,y)\tilde{g}^c(x,y) \\
&= \sum_{m_1=0}^{M_1}\sum_{n_1=0}^{N_1} \hat{f}_{m_1,n_1} h_{m_1}(ax) h_{n_1}(ay) \sum_{m_2=0}^{M_2}\sum_{n_2=0}^{N_2} \hat{g}_{m_2,n_2} h_{m_2}(bx) h_{n_2}(by) \\
&= \sum_{m_1=0}^{M_1}\sum_{n_1=0}^{N_1}\sum_{m_2=0}^{M_2}\sum_{n_2=0}^{N_2} \hat{f}_{m_1,n_1}\hat{g}_{m_2,n_2} h_{m_1}(ax) h_{m_2}(bx) h_{n_1}(ay) h_{n_2}(by) \qquad (8.2) \\
&= \sum_{m_1=0}^{M_1}\sum_{n_1=0}^{N_1}\sum_{m_2=0}^{M_2}\sum_{n_2=0}^{N_2} \hat{f}_{m_1,n_1}\hat{g}_{m_2,n_2} \sum_{k_1=0}^{m_1+m_2} \alpha_{m_1,m_2}^{k_1} \sum_{k_2=0}^{n_1+n_2} \alpha_{n_1,n_2}^{k_2} \\
&\quad h_{k_1}(x\sqrt{a^2+b^2}) h_{k_2}(y\sqrt{a^2+b^2}),
\end{aligned}$$

and

$$\begin{aligned}
\tilde{q}^c(x,y,z) &= \tilde{f}^c(x,y,z)\tilde{g}^c(x,y,z) \\
&= \sum_{m_1=0}^{M_1}\sum_{n_1=0}^{N_1}\sum_{l_1=0}^{L_1} \hat{f}_{m_1,n_1,l_1} h_{m_1} h_{n_1} h_{l_1} \sum_{m_2=0}^{M_2}\sum_{n_2=0}^{N_2}\sum_{l_2=0}^{L_2} \hat{g}_{m_2,n_2,l_2} h_{m_2} h_{n_2} h_{l_2} \\
&= \sum_{m_1=0}^{M_1}\sum_{n_1=0}^{N_1}\sum_{l_1=0}^{L_1}\sum_{m_2=0}^{M_2}\sum_{n_2=0}^{N_2}\sum_{l_2=0}^{L_2} \hat{f}_{m_1,n_1,l_1}\hat{g}_{m_2,n_2,l_2} h_{m_1} h_{m_2} h_{n_1} h_{n_2} h_{l_1} h_{l_2} \\
&= \sum_{m_1=0}^{M_1}\sum_{n_1=0}^{N_1}\sum_{l_1=0}^{L_1}\sum_{m_2=0}^{M_2}\sum_{n_2=0}^{N_2}\sum_{l_2=0}^{L_2} \hat{f}_{m_1,n_1,l_1}\hat{g}_{m_2,n_2,l_2} \sum_{k_1=0}^{m_1+m_2} \alpha_{m_1,m_2}^{k_1} \sum_{k_2=0}^{n_1+n_2} \alpha_{n_1,n_2}^{k_2} \sum_{k_3=0}^{l_1+l_2} \alpha_{l_1,l_2}^{k_3} \\
&\quad h_{k_1}(x\sqrt{a^2+b^2}) h_{k_2}(y\sqrt{a^2+b^2}) h_{k_3}(z\sqrt{a^2+b^2}),
\end{aligned} \qquad (8.3)$$

where

$$\alpha_{i,j}^k = \eta_k \begin{pmatrix} i & j & k \\ a & b & \sqrt{a^2+b^2} \end{pmatrix}_h ,$$

is some convenient shorthand notation. Notice the superscript ^{c} to denote the two aforementioned expansions are for Cartesian grids of data. This is to distinguish a Cartesian expansion from a polar expansion, the latter of which will be defined in the proceeding section. The bandlimits are chosen to be $M_i = M_i$, $N_i = M_i - m_i$, and $L_i = M_i - m_i - n_i$, which allows for bandlimit invariance under rotation (more on this soon). Moreover, the scale factors will be set to $a = b = 1$. The next section will quickly state the interconversion techniques, leading into a description of how these techniques are to be combined with Hermite expansion multiplication.

8.3 Interconversion Techniques

Chapter 6 comprehensively covered interconversion techniques between Cartesian and polar/spherical coordinates. For Cartesian/polar interconversion in particular, there were two available interconversion techniques: 1. Interconversion between Hermite and Fourier-Laguerre expansions and 2. Interconversion between Hermite and SH expansions. Both showed superior performance over bi-cubic interpolation. Coefficients of a Fourier-Laguerre (F-L) series $\check{f}_{m,n}$ map to and from coefficients of a 2D Hermite function expansion $\hat{f}_{k,m-k}$ via

$$\hat{f}_{k,m-k} = \sum_{n=-m}^{m} \check{f}_{m,n} Q_{k,n}^{m}, \tag{8.4}$$

and

$$\check{f}_{m,n} = \sum_{k=0}^{m} \hat{f}_{k,m-k}(Q_{k,n}^{m})^{*}, \tag{8.5}$$

where

$$Q_{k,n}^{m} = \int_{0}^{2\pi} \int_{0}^{\infty} \chi_{m,n}^{*}(\rho,\phi) h_k(\rho\cos\phi) h_{m-k}(\rho\sin\phi)\rho d\rho d\phi. \tag{8.6}$$

The matrices Q^m have closed-form solutions and can be computed recursively. The F-L series once again is according to the equation

$$\tilde{f}^{p}(\rho,\phi) = \sum_{m=0}^{N} \sum_{n=-m}^{m} \check{f}_{m,n}\chi_{m,n}^{*}(\rho,\phi), \tag{8.7}$$

with

$$\check{f}_{m,n} = \int_{0}^{2\pi} \int_{0}^{\infty} f^{p}(\rho,\phi)\chi_{m,n}(\rho,\phi)\rho d\rho d\phi. \tag{8.8}$$

For more information on F-L series expansions, please see Chapter 2. To summarize the first technique, the conversion between a 2D Hermite and F-L expansion as

$$\tilde{f}^{c}(x,y) \leftrightarrow \tilde{f}^{p}(\rho,\phi),$$

uses equations (8.4) and (8.5) provided the coefficients of the starting expansion have been computed. The second 2D interconversion technique converts between a Hermite and an SH expansion as

$$\tilde{f}^{c}(x,y) \leftrightarrow \tilde{f}_{SH}(\rho,\phi),$$

where

$$\begin{aligned}
\tilde{f}^c(x,y) &= \sum_{m=0}^{N}\sum_{n=0}^{m} \hat{f}_{n,m-n} h_n(x) h_{m-n}(y) \\
&= \sum_{m=0}^{N}\sum_{n=0}^{m} \hat{f}_{n,m-n} h_n(\rho\cos\phi) h_{m-n}(\rho\sin\phi) \\
&= \sum_{m=0}^{N}\sum_{n=0}^{m} \hat{f}_{n,m-n} \sum_{q=0}^{m} S_{q,n}^{m}(-\phi) h_q(\rho) h_{m-q}(0) \\
&= \tilde{f}_{SH}(\rho,\phi).
\end{aligned} \tag{8.9}$$

Thus the difference between the two expansions is in how the coefficients are computed, which due to numerical methods will be slightly different. The coefficients of a 2D Hermite expansion integrate a Cartesian grid as

$$\begin{aligned}
\hat{f}_{n,m-n} &= \int_{\mathbb{R}^2} f(x,y) h_n(x) h_{m-n}(y) dxdy \\
&= \int_{-\infty}^{\infty}\int_{-\infty}^{\infty} f(x,y) h_n(x) h_{m-n}(y) dxdy \\
&\approx \sum_{i=1}^{n_{samples}} f^c(x_i,y_i) h_n(x_i) h_{m-n}(y_i) \Delta x \Delta y,
\end{aligned} \tag{8.10}$$

and coefficients of the SH expansion integrate a polar grid as

$$\begin{aligned}
\hat{f}_{n,m-n} &= \int_{\mathbb{R}^2} f(x,y) h_n(x) h_{m-n}(y) dxdy \\
&= \int_{-\infty}^{\infty}\int_{-\infty}^{\infty} f(x,y) h_n(x) h_{m-n}(y) dxdy \\
&= \int_{0}^{2\pi}\int_{0}^{\infty} f(\rho\cos\phi,\rho\sin\phi) h_n(\rho\cos\phi) h_{m-n}(\rho\sin\phi) \rho d\rho d\phi \\
&\approx \sum_{i=1}^{n_{samples}} f^p(\rho_i,\phi_i) h_n(\rho_i\cos\phi_i) h_{m-n}(\rho_i\sin\phi_i) \rho_i \Delta\rho \Delta\phi.
\end{aligned} \tag{8.11}$$

Therefore, given the coefficients from equation (8.10), an SH expansion can be evaluated as

$$\tilde{f}_{SH}(\rho,\phi) = \sum_{m=0}^{N}\sum_{n=0}^{m}\hat{f}_{n,m-n}\sum_{q=0}^{m}S_{q,n}^{m}(-\phi)h_q(\rho)h_{m-q}(0), \tag{8.12}$$

or given coefficients from equation (8.11) the SH expansion can be converted back to a 2D Hermite expansion. This second interconversion technique is nearly as good as the one with Q^m matrices, and does not require computing an additional set of coefficients, meaning it is faster computationally. Also this technique extends naturally to 3D interconversion, motivating the next topic. Converting between a Cartesian grid $f^c(x,y,z)$ and a spherical grid $f^p(r,\phi,\theta)$ follows

$$\tilde{f}^c(x,y,z) \leftrightarrow \tilde{f}_{S^2H}(r,\phi,\theta).$$

The difference is again in how the coefficients $\hat{f}_{u,v,w}$ are obtained numerically, either

$$\begin{aligned}\hat{f}_{v,w,m} &= \int_{-\infty}^{\infty}\int_{-\infty}^{\infty}\int_{-\infty}^{\infty} f(x,y,z)h_v(x)h_w(y)h_m(z)dxdydz \\ &\approx \sum_{i=1}^{n_{samples}} f^c(x_i,y_i,z_i)h_v(x_i)h_w(y_i)h_m(z_i)\Delta x\Delta y\Delta z,\end{aligned} \tag{8.13}$$

from a Cartesian grid or

$$\begin{aligned}\hat{f}_{v,w,m} &= \int_{-\infty}^{\infty}\int_{-\infty}^{\infty}\int_{-\infty}^{\infty} f(x,y,z)h_v(x)h_w(y)h_m(z)dxdydz \\ &= \int_{0}^{2\pi}\int_{0}^{\pi}\int_{0}^{\infty} f(r,\theta,\phi)h_v(rs\theta c\phi)h_w(rs\theta s\phi)h_m(rc\theta)rdrs\theta d\theta d\phi \\ &\approx \sum_{i=1}^{n_{samples}} f^p(r_i,\theta_i,\phi_i)h_v(rs\theta_i c\phi_i)h_w(rs\theta_i c\phi_i)h_m(r_i c\theta_i)r_i s\theta_i\Delta r\Delta\theta\Delta\phi,\end{aligned} \tag{8.14}$$

from a spherical grid. So given coefficients from a Cartesian grid, the S^2H expansion can be formed as

$$\tilde{f}_{S^2H}(r,\phi,\theta) = \sum_{v=0}^{N}\sum_{w=0}^{N-v}\sum_{m=0}^{N-v-w}\hat{f}_{v,w,m}\sum_{d=0}^{v+w}S_{d,v}^{v+w}(-\phi)\sum_{t=0}^{m+d}S_{t,m}^{m+d}(-\theta)h_t(r)h_{m+d-t}(0)h_{v+w-d}(0). \tag{8.15}$$

or given coefficients from a spherical grid, the 3D Hermite expansion can be constructed. Chapter 6 showed that this interconversion approach outperforms tri-cubic interpolation. The next section articulates how fusion of polar expansion can be done by stringing together interconversion and multiplication of Hermite expansions.

8.4 Polar and Spherical Expansion Fusion via Interconversion

Polar and spherical expansion fusion can be considered a two step process. For polar, the first step is to obtain coefficients from the polar grids $f^p(\rho,\phi)$ and $g^p(\rho,\phi)$ and then map them to corresponding Hermite expansions

$$\tilde{f}^c(x,y) = \sum_{m_1=0}^{M_1}\sum_{n_1=0}^{M_1-m_1}\hat{f}_{m_1,n_1}h_{m_1}(x)h_{n_1}(y),$$

and

$$\tilde{g}^c(x,y) = \sum_{m_2=0}^{M_2}\sum_{n_2=0}^{M_2-m_2}\hat{g}_{m_2,n_2}h_{m_2}(x)h_{n_2}(y),$$

and then multiply them together as

$$\begin{aligned}\tilde{q}^c(x,y) &= \tilde{f}^c(x,y)\tilde{g}^c(x,y) \\ &= \sum_{m_1=0}^{M_1}\sum_{n_1=0}^{M_1-m_1}\hat{f}_{m_1,n_1}h_{m_1}(x)h_{n_1}(ay)\sum_{m_2=0}^{M_2}\sum_{n_2=0}^{M_2-m_2}\hat{g}_{m_2,n_2}h_{m_2}(x)h_{n_2}(by) \\ &= \sum_{m_1,n_1,m_2,n_2}\hat{f}_{m_1,n_1}\hat{g}_{m_2,n_2}\sum_{k_1=0}^{m_1+m_2}\alpha_{m_1,m_2}^{k_1}\sum_{k_2=0}^{n_1+n_2}\alpha_{n_1,n_2}^{k_2}h_{k_1}(x\sqrt{2})h_{k_2}(y\sqrt{2}).\end{aligned} \tag{8.16}$$

Recall that the coefficients $\hat{f}_{m_1,n_1}$ are either from F-L coefficients $\check{f}_{m,n}$ or estimated using SH expansion techniques. In 3D, the coefficients would be from integration on a spherical grid, giving two Hermite expansions

$$\tilde{f}^c(x,y,z) = \sum_{m_1=0}^{M_1}\sum_{n_1=0}^{M_1-m_1}\sum_{l_1=0}^{M_1-m_1-n_1}\hat{f}_{m_1,n_1,l_1}h_{m_1}(x)h_{n_1}(y)h_{l_1}(z),$$

and

$$\tilde{g}^c(x,y,z) = \sum_{m_2=0}^{M_2}\sum_{n_2=0}^{M_2-m_2}\sum_{l_2=0}^{M_2-m_2-n_2}\hat{g}_{m_2,n_2,l_2}h_{m_2}(x)h_{n_2}(y)h_{l_2}(z),$$

which when multiplied together becomes

$$\begin{aligned}\tilde{q}^c(x,y,z) &= \tilde{f}^c(x,y,z)\tilde{g}^c(x,y,z) \\ &= \sum_{m_1,n_1,l_1} \hat{f}_{m_1,n_1,l_1} h_{m_1}(x)h_{n_1}(y)h_{l_1}(z) \sum_{m_2,n_2,l_2} \hat{g}_{m_2,n_2,l_2} h_{m_2}(x)h_{n_2}(y)h_{l_2}(z) \\ &= \sum_{m_1,n_1,l_1,m_2,n_2,l_2} \hat{f}_{m_1,n_1,l_1}\hat{g}_{m_2,n_2,l_2} \\ &\sum_{k_1=0}^{m_1+m_2} \alpha_{m_1,m_2}^{k_1} \sum_{k_2=0}^{n_1+n_2} \alpha_{n_1,n_2}^{k_2} \sum_{k_3=0}^{l_1+l_2} \alpha_{l_1,l_2}^{k_3} h_{k_1}(x\sqrt{2})h_{k_2}(y\sqrt{2})h_{k_3}(z\sqrt{2}).\end{aligned} \tag{8.17}$$

As an illustration of this approach, consider two functions f and g defined by the density

$$p(\rho,\phi) = e^{-\frac{1}{2}\left[\frac{(\rho-\rho_0)^2}{\sigma_\rho^2}+\frac{(\phi-\phi_0)^2}{\sigma_\phi^2}\right]}.$$

The values parameterizing this function for f are $\rho_0 = 2.5$, $\phi_0 = 0.25$, $\sigma_\rho = \sqrt{0.25}$, and $\sigma_\phi = \sqrt{0.65}$, and the values for g are $\rho_0 = 2.2$, $\phi_0 = 0.4$, $\sigma_\rho = \sqrt{0.35}$, and $\sigma_\phi = \sqrt{0.75}$. The corresponding function for a Cartesian grid follows

$$p(x,y) = e^{-\frac{1}{2}\left[\frac{\left(\sqrt{x^2+y^2}-\rho_0\right)^2}{\sigma_\rho^2}+\frac{\left(\tan^{-1}(\frac{y}{x})-\phi_0\right)^2}{\sigma_\phi^2}\right]}.$$

The band limit was $M_1 = M_2 = N = 50$, where N is used in the corresponding F-L series approximations. Figure 8.1 compares the fusion technique with F-L expansions to that with SH expansions. A third approach, namely interpolation and direct multiplication is compared to the two interconversion methods next to the true analytic

solution. Both again outperform bi-cubic interpolation.

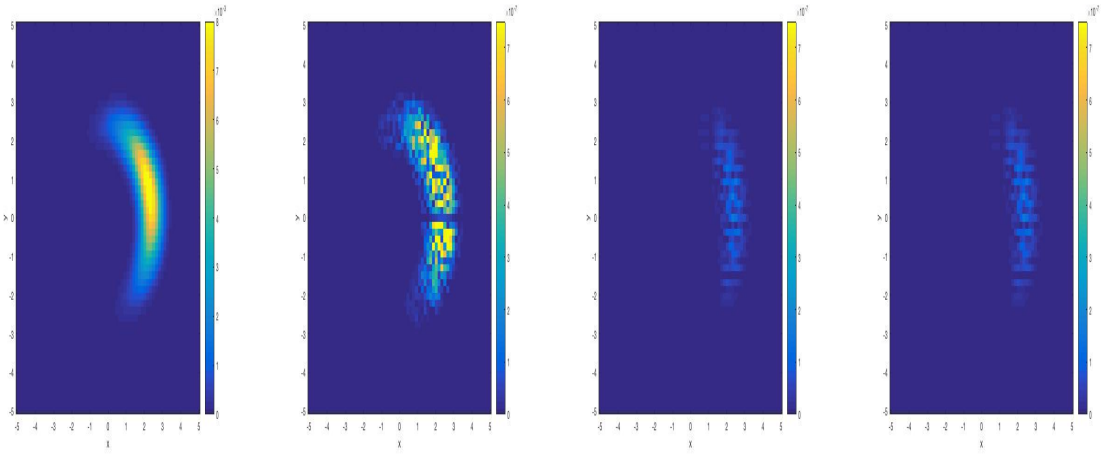

$f^c(x,y)g^c(x,y)$ | Interpolation Error | Interconversion via Q^m Error | Interconversion via SH Error

Figure 8.1: Error in Fusion after Conversion from Polar Grids

Now consider a second illustration in spherical coordinates. Figure 8.2 shows the fusion of two functions f and g both of which are Gaussians

$$p(r,\phi,\theta;\mu_r,\mu_\phi,\mu_\theta,\sigma_r,\sigma_\phi,\sigma_\theta) = e^{-\frac{1}{2}[(r+\mu_r)^2/\sigma_r^2+(\phi+\mu_\phi)^2/\sigma_\phi^2+(\theta+\mu_\theta)^2/\sigma_\theta^2]},$$

where $\mu_r = 1.7321$, $\mu_\phi = 0.6155$, $\mu_\theta = 0.7854$, $\sigma_r = 0.25$, $\sigma_\phi = 0.25$ and $\sigma_\theta = 0.15$.

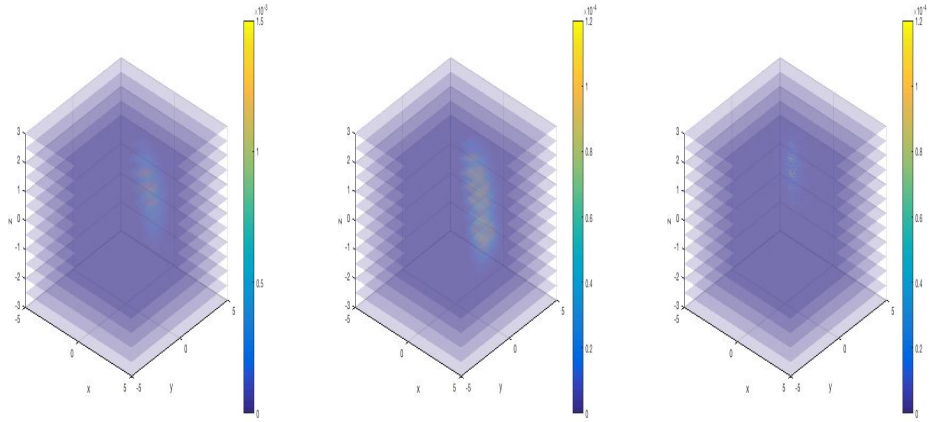

$f^c(x,y,z)g^c(x,y,z)$ | Interpolation Error | Interconversion via S^2H Error

Figure 8.2: Error in Fusion after Conversion from Spherical Grids

The following section extends the techniques by considering how two polar grids $(\rho,\phi)/(\rho',\phi')$ or two spherical grids $(r,\phi,\theta)/(r',\phi',\theta')$ can be combined if the frames can be mapped between each other by some fixed rotation R.

8.5 Fusing Expansions in Rotated Coordinate Frames

Consider a grid of data $(x,y) = (\rho\cos\phi, \rho\sin\phi)$ and a second grid of data $(x',y') = (\rho'\cos\phi', \rho'\sin\phi')$ that is related by some rotation angle α as

$$\begin{pmatrix} x' \\ y' \end{pmatrix} = R(\alpha) \begin{pmatrix} x \\ y \end{pmatrix},$$

where

$$R(\alpha) = \begin{pmatrix} \cos\alpha & -\sin\alpha \\ \sin\alpha & \cos\alpha \end{pmatrix},$$

is a 2D rotation that belongs to the Lie group $SO(2)$. Alternatively, if just considering the polar coordinates, (ρ, ϕ) and (ρ', ϕ') have the relationship

$$(\rho', \phi') = (\rho, \phi + \alpha).$$

This can be verified with trigonometric identities. Now suppose each grid has the corresponding functions $f^p(\rho, \phi)$ and $g^p(\rho', \phi')$, that have been converted into two separate Hermite function expansions as

$$\tilde{f}^c(x, y) = \sum_{m_1=0}^{M_1} \sum_{n_1=0}^{M_1 - m_1} \hat{f}_{m_1, n_1} h_{m_1}(x) h_{n_1}(y),$$

and

$$\tilde{g}^c(x', y') = \sum_{m_2=0}^{M_2} \sum_{n_2=0}^{M_2 - m_2} \hat{g'}_{m_2, n_2} h_{m_2}(x') h_{n_2}(y').$$

The Hermite expansion $\tilde{g}(x', y')$ can be recast using a property derived in [park2009rotation], which states

$$\begin{aligned}\tilde{g}(x', y') &= \sum_{m_2=0}^{M_2} \sum_{n_2=0}^{M_2-m_2} \hat{g'}_{m_2,n_2} h_{m_2}(x') h_{n_2}(y') \\ &= \sum_{m_2=0}^{M_2} \sum_{n_2=0}^{M_2-m_2} \hat{g}^{\alpha}_{m_2,n_2} h_{m_2}(x) h_{n_2}(y) \\ &= \sum_{m_2=0}^{M_2} \sum_{n_2=0}^{m_2} \hat{g}^{\alpha}_{n_2,m_2-n_2} h_{n_2}(x) h_{m_2-n_2}(y).\end{aligned} \tag{8.18}$$

Given the coefficients $\hat{g'}_{m_2,n_2} = \hat{g}^{\alpha}_{m_2,n_2}$ from the rotated grid, and using the property

$$\hat{g}^{\theta}_{q,m-q} = \sum_{n=0}^{m} S^m_{q,n}(\theta) \hat{g}_{n,m-n}.$$

the expansion $\tilde{g}(x', y')$ can be moved into the frame of the first density by applying

$$\hat{g}_{q,m-q} = \sum_{n=0}^{m} S^m_{q,n}(-\theta) \hat{g}^{\theta}_{n,m-n}.$$

This results in the expansion

$$\tilde{g}^c(x, y) = \sum_{m_2=0}^{M_2} \sum_{n_2=0}^{M_2-m_2} \hat{g}_{m_2,n_2} h_{m_2}(x) h_{n_2}(y),$$

which, like before, $\tilde{g}^c(x, y)$ can now be combined with $\tilde{f}^c(x, y)$ using the technique involving 3h integrals. As an illustration, consider again the Gaussian in polar coordinates

$$p(\rho, \phi) = e^{-\frac{1}{2}\left[\frac{(\rho-\rho_0)^2}{\sigma^2_\rho} + \frac{(\phi-\phi_0)^2}{\sigma^2_\phi}\right]},$$

with values for f being $\rho_0 = 2.5$, $\phi_0 = 0.25$, $\sigma_\rho = \sqrt{0.25}$, and $\sigma_\phi = \sqrt{0.65}$. This is the same parameterization of f from the unrotated example. Now let the second function $g(\rho, \phi) = f(\rho, \phi - \alpha)$, where $\alpha = 0.25$. Performing bi-cubic interpolation and multiplying the discrete grids will give the subplot on the far left of Figure 8.3. The middle subplot is the result from interconverting, rotating, and fusing f and g together, and the subplot on the far right is truth. Corresponding errors for the two approaches are shown in Figure 8.4.

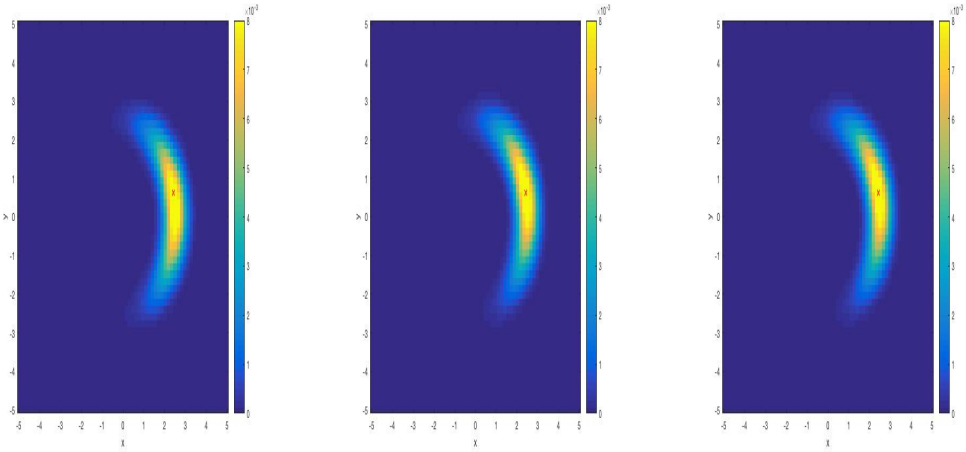

Misaligned Fusion from Interpolation | Fusion from Interconversion/Rotation | $f^c(x,y)g^c(x,y)$ (Truth)

Figure 8.3: Fusion of 2D Grids (Multiple Frames)

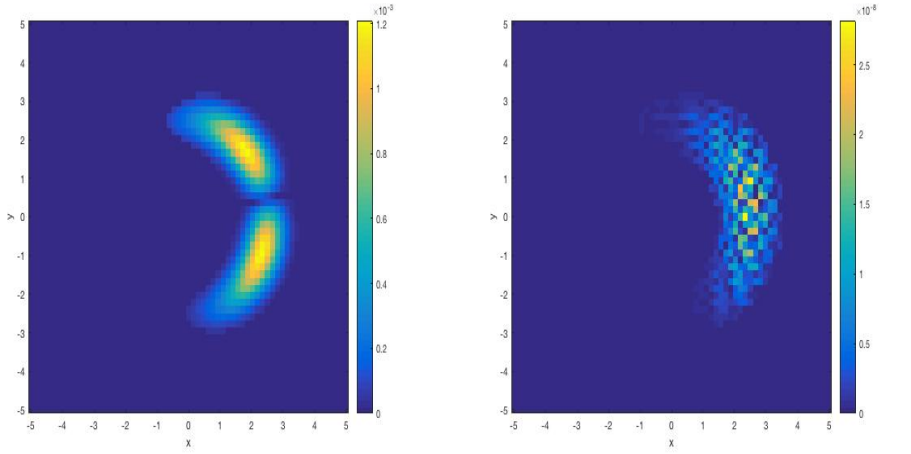

Error from Interpolation/Misaligned Fusion

Error from Interconversion/Rotation/Fusion

Figure 8.4: Error in Fusion of 2D Grids (Multiple Frames)

Recent developments have extended this rotation property to 3D (see Chapter 3). Therefore if the coefficients of the rotated frame are $\hat{g}^{\alpha,\beta,\gamma}_{m,n,k}$ for a ZXZ Euler angle parameterization of the corresponding rotation matrix $R(\alpha,\beta,\gamma)$, then the coefficients in the unrotated frame fit into the sequence.

$$\hat{g}_{m,n,k} \to \hat{g}^{\gamma}_{m,n,k} \to \hat{g}^{\beta,\gamma}_{m,n,k} \to \hat{g}^{\alpha,\beta,\gamma}_{m,n,k}.$$

For rotations about z, the coefficient transformation is

$$\hat{g}^{\alpha}_{d,m-d,k} = \sum_{n=0}^{m} S^{m}_{d,n}(\alpha)\hat{g}_{n,m-n,k}.$$

and

$$\hat{g}^{\gamma}_{d,m-d,k} = \sum_{n=0}^{m} S^{m}_{d,n}(\gamma)\hat{g}_{n,m-n,k},$$

for the second Euler angle about z. For rotations about x, the coefficient transformation is

$$\hat{g}^{\beta}_{m,d,n-d} = \sum_{k=0}^{n} S^{n}_{d,k}(\beta)\hat{g}_{m,k,n-k}.$$

Starting with an unrotated frame, a transformation for γ is applied, then β, and finally α. To transform the coefficients from the rotated frame back to the unrotated one, apply $S^m(-\alpha)$, then $S^m(-\beta)$ and then $S^m(-\gamma)$. Now similar to before, given the realigned coefficients $\hat{g}_{m,n,k}$, fusion of two 3D Hermite expansions can be invoked. It is easy enough to see that this alignment would also work in 3D. Chapter 3 shows the effectiveness of the lossless rotation approach.

8.6 Chapter Summary

This chapter put together a solution to fusing expansions in polar and spherical coordinates by solving an equivalent problem in Cartesian coordinates with the help of Hermite function expansions, and their properties under coordinate conversion, rotation, and multiplication. What has not been mentioned until now is that convolution of polar and spherical expansions could also be done by solving the equivalent problem in Cartesian coordinates. Recall from Chapter 3 that the convolution of

two Hermite expansions is itself another Hermite expansion. This property together with interconversion and/or rotation will render accurate convolution results (for polar/spherical data).

Chapter 9

Applications of Hermite Expansions to Cryo-EM and SAXS

9.1 Introduction

This chapter articulates the case for using multi-dimensional Hermite functions as a basis for cross-modal validation in biomolecular structure determination. Cryo Electron Microscopy (cryo-EM) [42] and Small-Angle X-Ray Scattering (SAXS) [43–45] are two commonly used experimental methods for extracting information about biomolecular structures. In cryo-EM, 3D reconstructions can be obtained via noisy projections from directions in the the body-fixed frame that are a priori unknown. In SAXS, the pair-distribution function is obtained, which contains spherically averaged information about the self-convolution of the shape of the biomolecular structure.

Hermite functions (and expansions) have several useful properties that are ideal for handling both of these data sets:

1. These bandlimited three-dimensional Hermite function expansions transform nicely under rotation and projection;

2. When converting Cartesian to spherical coordinates

$$(x, y, z) \longrightarrow (r \sin\theta \cos\phi, r \sin\theta \sin\phi, r \cos\theta),$$

   they transform easily as

$$f(x, y, z) \longrightarrow \tilde{f}(r, \phi, \theta) \sim \sum_{m,n,k} c_{m,n,k}(\phi, \theta) h_m(r);$$

3. Hermite functions are eigenfunctions of the Fourier transform, and hence are useful for

   self-convolutions/autocorrelations of the form $f(x, y, z) * f(-x, -y, -z)$;

4. They behave well under the Abel transform, which relates spherical averaged data in 3D to circularly averaged data in 2D.

The above properties of Hermite functions make them ideally suited for cross-modal data analysis involving validation of information from cryo-EM and SAXS.

CHAPTER 9. APPLICATIONS OF HERMITE EXPANSIONS TO CRYO-EM AND SAXS

In [46, 47], it was shown that EM and SAXS data can be linked via the Abel transform. This relationship provides a means to validate the compatibility between these two sensing modalities. Moreover, by establishing this relationship between EM and SAXS data, one can potentially fuse these two sources of information providing a more accurate estimation of the structural complex of interest.

The outline of the remainder of this chapter is as follows. Section 9.2 will model the EM and SAXS data as circularly symmetric and spherically symmetric functions respectively. Section 9.3 will show how EM and SAXS data can be represented as bandlimited Hermite expansions by invoking properties defined in Chapter 3. Section 9.4 will show how the Hermite function behaves under the Abel transform, and a recurrence relation for the Abel transform of Hermite functions will be derived. Section 9.5 will show how the Abel transform of Hermite functions can be used to cross-validate EM and SAXS data when both modalities are represented as Hermite expansions. Expectation over $SO(3)$ for non-uniform distributions is explored in Section 9.6, and Section 9.7 concludes the chapter.

9.2 Cryo-EM and SAXS Data

Consider some closed body B, and its corresponding characteristic function $\chi(\mathbf{x}) = \chi(x, y, z)$ [41] such that

$$\chi(\mathbf{x}) = \begin{cases} 1, & \mathbf{x} \in B \\ 0, & \mathbf{x} \notin B. \end{cases} \tag{9.1}$$

The characteristic function $\chi(\mathbf{x})$ is considered here to be a uniform density map for a corresponding biomolecular structure. This function can be projected onto the plane by integrating over the z-axis as

$$(\chi(\mathbf{x}))^p = \chi^p(x, y) = \int_{-\infty}^{\infty} \chi(x, y, z) dz. \tag{9.2}$$

In an experiment for EM, copies of $\chi(\mathbf{x})$ are randomly oriented and translated, and then projected to yield a set of images. Therefore the EM data for a given rotation translation pair $g = (R, \mathbf{t})$ is of the form

$$(\chi_g(\mathbf{x}))^p = \chi_g^p(x, y) = \chi^p(R^T(\mathbf{x} - \mathbf{t})) = \int_{-\infty}^{\infty} \chi(R^T(\mathbf{x} - \mathbf{t})) dz. \tag{9.3}$$

Note that $g^{-1} = (R^T, -R^T\mathbf{t})$ and that the action of a rigid-body transformation on a point is $g \cdot \mathbf{x} = R\mathbf{x} + \mathbf{t}$. Hence

$$g^{-1} \cdot \mathbf{x} \; = \; R^T(\mathbf{x} - \mathbf{t}),$$

which is what appears under the function when that function is moved by $g = (R, \mathbf{t})$. Figure 9.1 shows an an illustration of the EM projection process for a large number of randomly rotated copies (left) as well as the 3D reconstruction from the 2D projections (right). A comprehensive mathematical and physical analysis of EM data is articulated in [42]. Here, some of the techniques are simplified for analytical convenience.

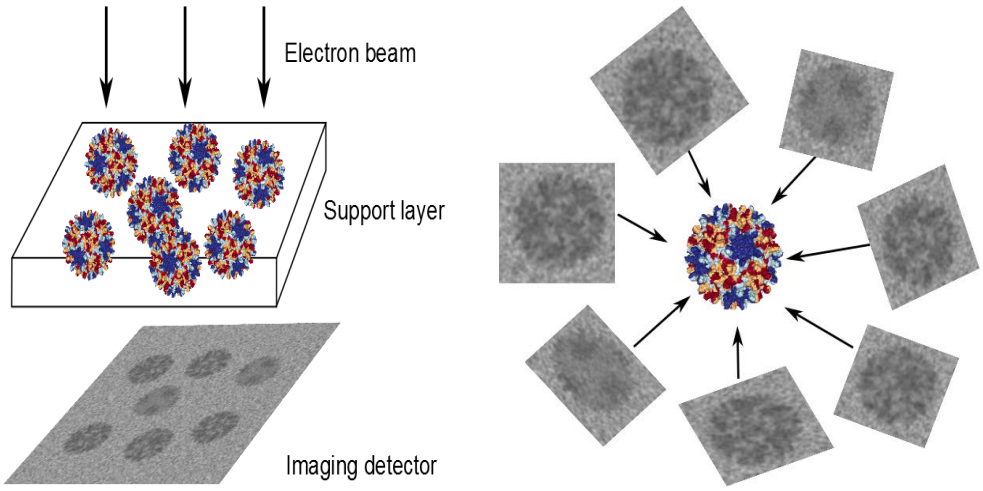

Cryo-EM Images Reconstruction from Cryo-EM Images

Figure 9.1: Cryo-EM Experiment Illustration

Consider the self-convolution operation (also known as the Patterson function [45]) given by

$$\begin{aligned} C_\chi(\mathbf{x}) &= \chi(\mathbf{x}) * \chi(-\mathbf{x}) \\ &= \chi(x,y,z) * \chi(-x,-y,-z) \\ &= \int_{-\infty}^{\infty}\int_{-\infty}^{\infty}\int_{-\infty}^{\infty} \chi(\sigma,\tau,\zeta)\chi(\sigma-x,\tau-y,\zeta-z)d\sigma d\tau d\zeta, \end{aligned} \tag{9.4}$$

which is invariant to translational shifts. Similarly, 2D self-convolution of noisy images $\chi_g^P(x,y)$ for arbitrary rotation/translation pairs $g = (R, \mathbf{t})$ is also translationally invariant, and can represented by the equation

$$\begin{aligned} C_{\chi_g^p}(x,y) = C_{\chi_R^p}(x,y) &= \chi_R^p(x,y) * \chi_R^p(-x,-y) \\ &= \int_{-\infty}^{\infty}\int_{-\infty}^{\infty} \chi_R^p(\sigma,\tau)\chi_R^p(\sigma - x, \tau - y)d\sigma d\tau. \end{aligned} \tag{9.5}$$

The process of self-convolution on EM images $\chi_R^P(x,y)$ is then followed by averaging the 2D self-convolution function $C_{\chi_R^p}(x,y)$ over orientation. This will render the circularly symmetric quantity $\gamma_{\chi^p}(\rho) = E_R\left[C_{\chi_R^p}(x,y)\right]$, where $\rho = \sqrt{x^2+y^2}$ is the planar radius. The operation $E_R[\ ]$ denotes expected value over a distribution of rotations $R \in SO(3)$. More concretely

$$E_R[g(R^T\mathbf{x})] = \int_{SO(3)} g(R^T\mathbf{x})dR, \tag{9.6}$$

for some function $g(\mathbf{x})$. Since expectation and projection commute [47], it is also true that

$$\gamma_{\chi^p}(\rho) = E_R\left[C_{\chi_R^p}(x,y)\right] = (E_R\left[C_{\chi_R}(\mathbf{x})\right])^p. \tag{9.7}$$

It is assumed that this distribution over $SO(3)$ is uniform. This is a relaxed assumption, since it is known that complexes have preferred orientations (see chapter 3 of [42]), which is not the focus. This caveat is discussed towards the end of this chapter and is withheld for future research. To summarize, below depicts the processing string for

EM starting with a set of images $\{\chi_g^p(x,y)\}_i$

$$\{\chi_g^p(x,y)\}_i \to \{C_{\chi_g^p}(x,y)\}_i = \{C_{\chi_R^p}(x,y)\}_i \to E_R\left[C_{\chi_R^p}(x,y)\right] = \gamma_{\chi^p}(\rho).$$

The data acquisition from SAXS can be understood with the visualization in Figure 9.2. The reader is referred to [48] for more information on the experimental procedure for SAXS.

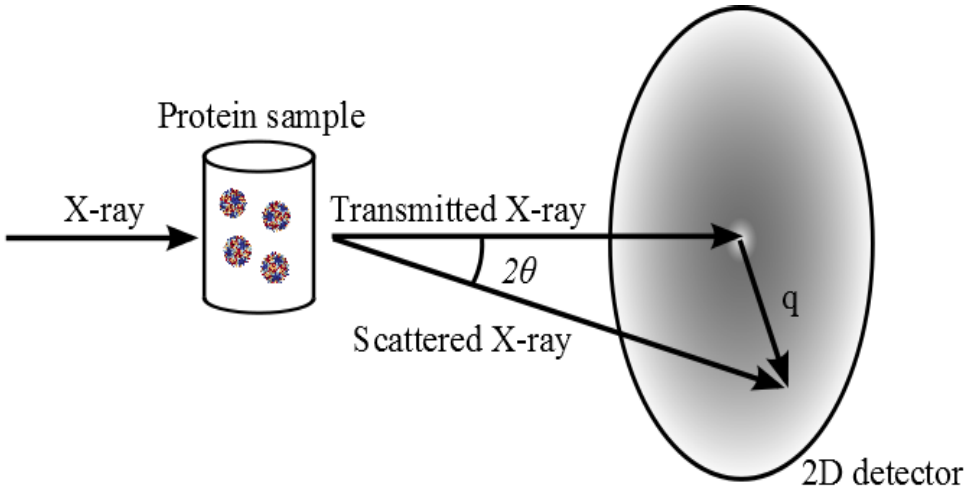

Figure 9.2: SAXS Illustration

A spherical average of the 3D self-convolution function gives

$$\gamma_\chi(r) = \int_{\mathbf{u}\in\mathbb{S}^2} C_\chi(r\mathbf{u})d\mathbf{u}, \tag{9.8}$$

where $||\mathbf{u}||_2 = 1$ and $d\mathbf{u}$ is the natural measure for integrating on the 2-sphere, $\mathbb{S}^2$.

When using the coordinates

$$\mathbf{u}(\phi,\theta) = \begin{pmatrix} \sin\theta\cos\phi \\ \sin\theta\sin\phi \\ \cos\theta \end{pmatrix}, \tag{9.9}$$

the above integral over $\mathbb{S}^2$ becomes

$$\gamma_\chi(r) = \frac{1}{4\pi}\int_0^\pi \int_0^{2\pi} C_\chi(r\mathbf{u}(\phi,\theta))\sin\theta d\phi d\theta. \tag{9.10}$$

So starting with a complex $\chi(\mathbf{x})$, the SAXS data follows the string

$$\chi(x,y,z) \to C_\chi(x,y,z) \to \frac{1}{4\pi}\int_0^\pi \int_0^{2\pi} C_\chi(r\mathbf{u}(\phi,\theta))\sin\theta d\phi d\theta = \gamma_\chi(r).$$

The Abel Transform, which is defined by the equation [49]

$$\mathcal{A}[f](\rho) \doteq 2\int_\rho^\infty f(r)\frac{r}{\sqrt{r^2-\rho^2}}dr, \tag{9.11}$$

is the last piece needed to relate Cryo-EM data $\gamma_{\chi^P}(\rho)$ to SAXS data $\gamma_\chi(r)$ via

$$\gamma_{\chi^P}(\rho) = \mathcal{A}[\gamma_\chi](\rho). \tag{9.12}$$

This equation holds up to scale since the two experiments will have different corre-

sponding amplitudes and dynamic ranges. Therefore some notion of normalization is required. Next, it will be shown how cryo-EM and SAXS data can be represented with Hermite function expansions assuming the original complex $\chi(\mathbf{x})$ is available for manipulating in both formulations.

9.3 Representing Cryo-EM and SAXS Data with Hermite Expansions

Recall that EM data follows the processing string

$$\{\chi_R^p(x,y)\}_i \rightarrow \{C_{\chi_R^p}(x,y)\}_i \rightarrow E_{R\in SO(3)}[C_{\chi_R^p}](\rho) = \gamma_{\chi^p}(\rho),$$

where again $C_\chi(\mathbf{x}) = \chi(\mathbf{x}) * \chi(-\mathbf{x})$ is 3D self-convolution. A 3D Hermite-function expansion (endowed with special bandlimits) can be used to approximate $\chi(\mathbf{x})$ as

$$\chi(\mathbf{x}) \approx \tilde{\chi}(\mathbf{x}) = \sum_{m=0}^{N} \sum_{n=0}^{N-m} \sum_{k=0}^{N-m-n} \hat{\chi}_{m,n,k} h_m(x) h_n(y) h_k(z). \tag{9.13}$$

The first step in the chain is to perform self-convolution. From Chapter 3, the self-convolution of a 1D Hermite expansion $\tilde{f}(x)$ was derived, and is restated here as

$$C_{\tilde{f}}(x) = \tilde{f}(x) * \tilde{f}(-x) = \sum_{m=0}^{N}\sum_{n=0}^{N} \hat{f}_m \hat{f}_n (-i)^{m+n}(-1)^n \sum_{k=0}^{m+n} i^k \eta_k \begin{pmatrix} m & n & k \\ 1 & 1 & \sqrt{2} \end{pmatrix}_h h_k(x/\sqrt{2}), \tag{9.14}$$

for $h_m(ax) = h_m(bx) = h_m(x)$. The 1D self-convolution of $\tilde{f}(x)$ can be rewritten as

$$\tilde{f}(x) * \tilde{f}(-x) = \sum_{l=0}^{2N} \hat{q}_l h_l(x/\sqrt{2}), \tag{9.15}$$

where

$$\hat{q}_l = i^l \eta_l \sum_{m=0}^{N}\sum_{n=0}^{N} \hat{f}_m \hat{f}_n (-i)^{m+n}(-1)^n \alpha_{m,n}^l \delta_{m,n}^l, \tag{9.16}$$

with

$$\alpha_{m,n}^l = \begin{pmatrix} m & n & l \\ 1 & 1 & \sqrt{2} \end{pmatrix}_h,$$

and

$$\delta_{m,n}^l = \begin{cases} 1, \ m+n \geq l \\ 0, \text{otherwise} \end{cases}.$$

The self-convolution of $\tilde{\chi}(\mathbf{x})$ follows

$$\begin{aligned}
C_{\tilde{\chi}}(\mathbf{x}) &= \tilde{\chi}(\mathbf{x}) * \tilde{\chi}(-\mathbf{x}) \\
&= \sum_{m,n,k} \sum_{m',n',k'} \hat{\chi}_{m,n,k} \hat{\chi}_{m',n',k'} \left(h_m(x) * h_{m'}(-x)\right) \left(h_n(y) * h_{n'}(-y)\right) \left(h_k(z) * h_{k'}(-z)\right) \\
&= \sum_{m,n,k} \sum_{m',n',k'} \hat{\chi}_{m,n,k} \hat{\chi}_{m',n',k'} (-i)^{m+m'+n+n'+k+k'} (-1)^{m'+n'+k'} \\
&\sum_{l=0}^{m+m'} \sum_{l'=0}^{n+n'} \sum_{l''=0}^{k+k'} i^{l+l'+l''} \eta_l \eta_{l'} \eta_{l''} \alpha^{l}_{m,m'} \alpha^{l'}_{n,n'} \alpha^{l''}_{k,k'} h_l(x/\sqrt{2}) h_{l'}(y/\sqrt{2}) h_{l''}(z/\sqrt{2}) \\
&= \sum_{u=0}^{2N} \sum_{v=0}^{N-u} \sum_{w=0}^{N-u-v} (\widehat{C_{\tilde{\chi}}})_{u,v,w} h_u(x/\sqrt{2}) h_v(y/\sqrt{2}) h_w(z/\sqrt{2}),
\end{aligned} \tag{9.17}$$

where

$$\begin{aligned}
(\widehat{C_{\tilde{\chi}}})_{u,v,w} = i^{u+v+w} \eta_u \eta_v \eta_w \sum_{m,m',n,n',k,k'} & \hat{f}_{m,n,k} \hat{f}_{m',n',k'} (-i)^{m+m'+n+n'+k+k'} \\
& (-1)^{m'+n'+k'} \alpha^{u}_{m,m'} \alpha^{v}_{n,n'} \alpha^{w}_{k,k'} \delta^{u}_{m,m'} \delta^{v}_{n,n'} \delta^{w}_{k,k'}.
\end{aligned} \tag{9.18}$$

Computing the expected value over $SO(3)$ for a 3D Hermite function expansion is quite simple. We will use $\tilde{f}(x,y,z)$ in place of $C_{\tilde{\chi}}(\mathbf{x})$ for this part of the derivation to avoid subscript and superscript overloading. Recall that an expansion $\tilde{f}(x,y,z)$ can be rotated by any $R = R_{ZXZ}(\alpha,\beta,\gamma)$ by transforming the corresponding Hermite series coefficients as

$$\hat{f}_{m,n,k} \rightarrow \hat{f}^{\gamma}_{m,n,k} \rightarrow \hat{f}^{\beta,\gamma}_{m,n,k} \rightarrow \hat{f}^{\alpha,\beta,\gamma}_{m,n,k},$$

using equations (3.58) and (3.63) from Chapter 3. Now integrating $\tilde{f}(x,y,z)$ over $SO(3)$ looks like

$$\begin{aligned} E_R[\tilde{f}](x,y,z) &= \frac{1}{8\pi^2}\int_{SO(3)} \sum_{m,n,k} \hat{f}_{m,n,k} h_m(x'/\sqrt{2}) h_n(y'/\sqrt{2}) h_k(z'/\sqrt{2}) dR \\ &= \frac{1}{8\pi^2} \sum_{m,n,k} \int_0^{2\pi}\int_0^{\pi}\int_0^{2\pi} \hat{f}^{\alpha,\beta,\gamma}_{m,n,k} h_m(x/\sqrt{2}) h_n(y/\sqrt{2}) h_k(z/\sqrt{2}) \sin\beta d\alpha d\beta d\gamma. \end{aligned} \tag{9.19}$$

Since the coefficients are are the only part of the summation that contain the Euler angles, the expectation operation can be wrapped into equations (3.57) and (3.62) as

$$\begin{aligned} \hat{f}^{\bar{\gamma}}_{d,m-d,k} &= \int_0^{2\pi} \sum_{n=0}^{m} S^m_{d,n}(\gamma) \hat{f}_{n,m-n,k} d\gamma \\ &= \sum_{n=0}^{m} \left(\int_0^{2\pi} S^m_{d,n}(\gamma) d\gamma \right) \hat{f}_{n,m-n,k} \\ &= \sum_{n=0}^{m} \sigma^{\gamma}_{d,n,m} \hat{f}_{n,m-n,k}, \end{aligned} \tag{9.20}$$

$$\begin{aligned} \hat{f}^{\bar{\beta},\bar{\gamma}}_{m,d,n-d} &= \int_0^{\pi} \sum_{k=0}^{n} S^n_{d,k}(\beta) \hat{f}^{\bar{\gamma}}_{m,k,n-k} \sin\beta d\beta \\ &= \sum_{k=0}^{n} \left(\int_0^{\pi} S^n_{d,k}(\beta) \sin\beta d\beta \right) \hat{f}^{\bar{\gamma}}_{m,k,n-k} \\ &= \sum_{k=0}^{n} \sigma^{\beta}_{d,k,n} \hat{f}^{\bar{\gamma}}_{m,k,n-k}, \end{aligned} \tag{9.21}$$

and

$$\hat{f}^{\bar{\alpha},\bar{\beta},\bar{\gamma}}_{d,m-d,k} = \sum_{n=0}^{m} \sigma^{\alpha}_{d,n,m} \hat{f}^{\bar{\beta},\bar{\gamma}}_{n,m-n,k}. \tag{9.22}$$

The expectation over $SO(3)$ for $\tilde{f}$ is now

$$E_R[\tilde{f}](x,y,z) = \frac{1}{8\pi^2}\sum_{m=0}^{2N}\sum_{n=0}^{N-m}\sum_{k=0}^{N-m-n} \hat{f}^{\bar{\alpha},\bar{\beta},\bar{\gamma}}_{m,n,k} h_m(x/\sqrt{2})h_n(y/\sqrt{2})h_k(z/\sqrt{2}). \quad (9.23)$$

Therefore applying expectation (over $SO(3)$) to a 3D Hermite expansion is effectively the same (in terms of mathematical operation) as applying a Euler-angle parameterized rotation. This again assumes a uniform distribution over $SO(3)$, but it is easy to see that a probability distribution could be imposed on equations $(9.20) - (9.22)$. Since expectation over $SO(3)$ and projection commute, the next step in the processing chain invokes the Hermite projection coefficients ν_k (see Chapter 3) as

$$\{E_R[\tilde{f}]\}^p(x,y) = \frac{1}{8\pi^2}\sum_{m=0}^{2N}\sum_{n=0}^{N-m}\sum_{k=0}^{N-m-n} \hat{f}^{\bar{\alpha},\bar{\beta},\bar{\gamma}}_{m,n,k} h_m(x/\sqrt{2})h_n(y/\sqrt{2})\nu_k(1/\sqrt{2}). \quad (9.24)$$

The final step in representing EM data with a Hermite expansion is to circularly average this quantity, which using Integrated Steering Coefficients (ISCs) for angles ϕ around the circle gives the final representation of Cryo-EM data as a Hermite

expansion

$$\begin{aligned}\gamma_{\tilde{f}^p}(\rho) &= \frac{1}{2\pi}\int_0^{2\pi}\{E_R[\tilde{f}]\}^p(\rho\cos\phi/\sqrt{2},\rho\sin\phi/\sqrt{2})d\phi \\ &= \frac{1}{16\pi^3}\sum_{m=0}^{2N}\sum_{n=0}^{N-m}\sum_{k=0}^{N-m-n}\hat{f}^{\bar{\alpha},\bar{\beta},\bar{\gamma}}_{m,n,k}\nu_k(1/\sqrt{2})\int_0^{2\pi}h_m(\rho\cos\phi/\sqrt{2})h_n(\rho\cos\phi/\sqrt{2})d\phi \\ &= \frac{1}{16\pi^3}\sum_{m=0}^{2N}\sum_{n=0}^{N-m}\sum_{k=0}^{N-m-n}\hat{f}^{\bar{\alpha},\bar{\beta},\bar{\gamma}}_{m,n,k}\nu_k(1/\sqrt{2})\sum_{q=0}^{m+n}\left(\int_0^{2\pi}S^{m+n}_{q,m}(-\phi)d\phi\right)h_q(\rho/\sqrt{2})h_{m+n-q}(0) \\ &= \frac{1}{16\pi^3}\sum_{m=0}^{2N}\sum_{n=0}^{N-m}\sum_{k=0}^{N-m-n}\hat{f}^{\bar{\alpha},\bar{\beta},\bar{\gamma}}_{m,n,k}\nu_k(1/\sqrt{2})\sum_{q=0}^{m+n}\sigma^{\phi}_{q,m,m+n}h_q(\rho/\sqrt{2})h_{m+n-q}(0).\end{aligned} \tag{9.25}$$

If the Hermite expansion adequately approximates the density map, then $\tilde{\chi}(\mathbf{x}) \approx \chi(\mathbf{x}) \implies \gamma_{\tilde{f}^p}(\rho) \approx \gamma_{f^p}(\rho)$. The data from SAXS can also be represented by a Hermite function expansion. Consider again the self-convolution $\tilde{f}(\mathbf{x})$, which can be converted to an S^2H series expansion as

$$\begin{aligned}\tilde{f}(x,y,z) &= \tilde{f}(rs\theta c\phi, rs\theta s\phi, rc\theta) \\ &= \sum_{v=0}^{N}\sum_{w=0}^{N-v}\sum_{m=0}^{N-v-w}\hat{f}_{v,w,m}h_v(rs\theta c\phi/\sqrt{2})h_w(rs\theta s\phi/\sqrt{2})h_m(rc\theta/\sqrt{2}) \\ &= \sum_{v=0}^{N}\sum_{w=0}^{N-v}\sum_{m=0}^{N-v-w}\hat{f}_{v,w,m}\sum_{d=0}^{v+w}S^{v+w}_{d,v}(-\phi)\sum_{t=0}^{m+d}S^{m+d}_{t,m}(-\theta)h_t(r/\sqrt{2})h_{m+d-t}(0)h_{v+w-d}(0).\end{aligned} \tag{9.26}$$

Integrating this expansion over $\mathbb{S}^2$ gives the radial expansion

$$\begin{aligned}\gamma_{\tilde{f}}(r) &= \frac{1}{4\pi^2}\int_0^{2\pi}\int_0^{\pi}\tilde{f}(rs\theta c\phi, rs\theta s\phi, rc\theta)s\theta d\theta d\phi \\ &= \frac{1}{4\pi^2}\sum_{v=0}^{2N}\sum_{w=0}^{N-v}\sum_{m=0}^{N-v-w}\hat{f}_{v,w,m}h_v(rs\theta c\phi/\sqrt{2})h_w(rs\theta s\phi/\sqrt{2})h_m(rc\theta/\sqrt{2})s\theta d\theta d\phi \\ &= \frac{1}{4\pi^2}\sum_{v=0}^{2N}\sum_{w=0}^{N-v}\sum_{m=0}^{N-v-w}\hat{f}_{v,w,m}\sum_{d=0}^{v+w}\int_0^{2\pi}S_{d,v}^{v+w}(-\phi)d\phi\sum_{t=0}^{m+d}\int_0^{\pi}S_{t,m}^{m+d}(-\theta)\sin\theta d\theta \\ &\quad h_t(r/\sqrt{2})h_{m+d-t}(0)h_{v+w-d}(0) \\ &= \frac{1}{4\pi^2}\sum_{v=0}^{2N}\sum_{w=0}^{N-v}\sum_{m=0}^{N-v-w}\hat{f}_{v,w,m}\sum_{d=0}^{v+w}\sigma_{d,v,v+w}^{\phi}\sum_{t=0}^{m+d}\sigma_{t,m,m+d}^{\theta}h_t(r/\sqrt{2})h_{m+d-t}(0)h_{v+w-d}(0),\end{aligned} \tag{9.27}$$

which is in fact a representation of SAXS data. Similarly, $\tilde{\chi}(\mathbf{x}) \approx \chi(\mathbf{x}) \implies \gamma_{\tilde{f}}(r) \approx \gamma_f(r)$. Figure 9.3 shows computed SAXS data for a toy function $f(\mathbf{x})$ that is the sum of three multi-variate Gaussian distributions (with zero-mean) that have the covariance matrices $S = diag(\frac{1}{2}, 2, \frac{3}{2})$,

$$S_2 = R_1 S R_1^T,$$

and

$$S_3 = R_2 S R_2^T,$$

where $R_1 = e^{\widehat{[1;2;3]}}$, and $R_2 = e^{\widehat{[4;5;6]}}$. This test function has SAXS data that has been computed two ways: 1. numerical integration and interpolation and 2. with a Hermite expansion according to equation (9.27). Figure 9.4 shows the corresponding EM data computed with equation (9.24) and is also compared to numerical integration

and interpolation.

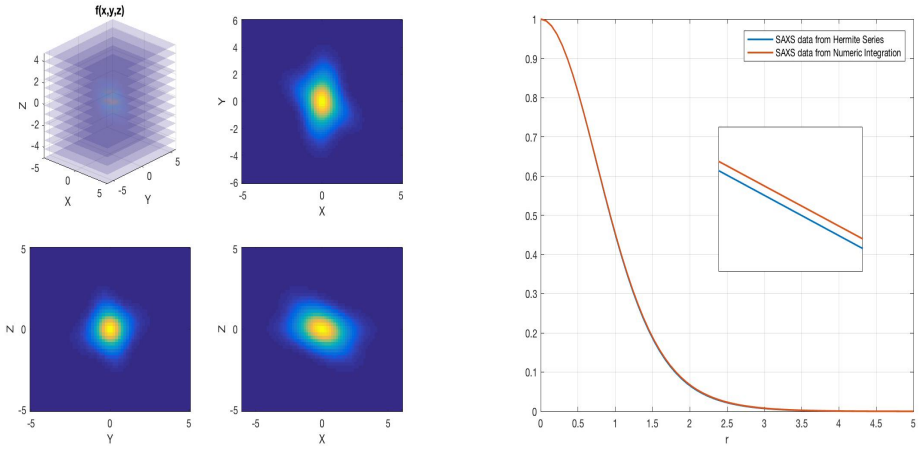

Self-Convolution Function $f(\mathbf{x})$ SAXS Data

Figure 9.3: Representing SAXS Data as Hermite Expansion

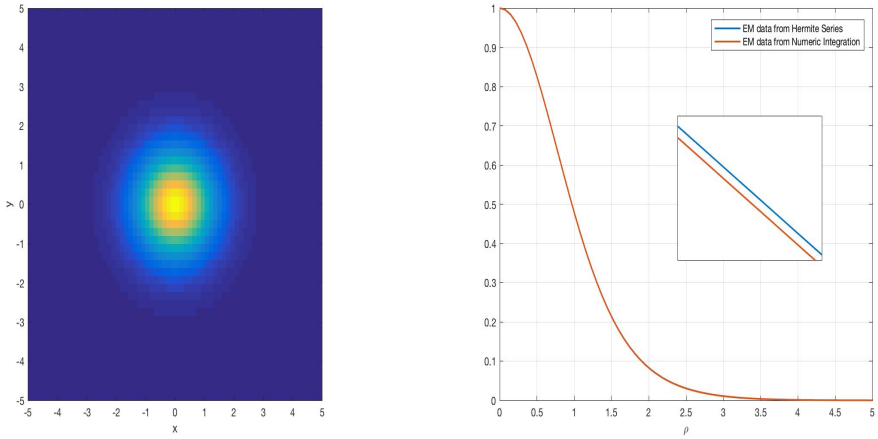

$\{E_R[f]\}^p(x,y)$ cryo-EM Data

Figure 9.4: Representing Cryo-EM Data as Hermite Expansion

The next section discusses the Abel transform of Hermite functions.

9.4 The Abel Transform of Hermite Functions

For spherically symmetric functions $f(r)$, with radius $r = \sqrt{x^2+y^2+z^2}$, the Abel transform is again

$$\mathcal{A}[f](\rho) = 2\int_{\rho}^{\infty} \frac{f(r)rdr}{\sqrt{r^2-\rho^2}}, \tag{9.28}$$

where $\rho = \sqrt{x^2+y^2}$ is the planar radius. Using the change of variables $z = \sqrt{r^2-\rho^2}$, $dz = \frac{rdr}{\sqrt{r^2-\rho^2}}$, the Abel transform can be equivalently represented as

$$\mathcal{A}[f](\rho) = \int_{-\infty}^{\infty} f(\sqrt{\rho^2+z^2})dz. \tag{9.29}$$

This formulation is attractive since it suppresses the singularity at $\rho = r$. Conventionally, there are two ways to handle the singularity: 1. change of variables (like what is shown here), which requires knowing the integrand at infinite accuracy or 2. ignoring the singularity. When considering in particular the Abel transform of a Hermite function, we do indeed know the integrand at infinite accuracy. Therefore if a radial function is approximated as a bandlimited Hermite expansion, then the Abel transform of this function is approximately a sum of Abel transforms of Hermite functions. This motivates a recurrence relation for the Abel transform of a Hermite function, which is derived next.

First, consider the Abel transform integral for a Hermite function of order n

$$\int_{\rho}^{\infty} \frac{h_n(r)r}{\sqrt{r^2-\rho^2}}dr, \tag{9.30}$$

and the two recurrence relation equations for Hermite functions

$$h_n(r) = \frac{\sqrt{n}}{\sqrt{2}}h_{n-1}(r) + \frac{\sqrt{n+1}}{\sqrt{2}}h_{n+1}(r),$$

and

$$h_n'(r) = \frac{\partial h_n(r)}{\partial r} = \frac{\sqrt{n}}{\sqrt{2}}h_{n-1}(r) - \frac{\sqrt{n+1}}{\sqrt{2}}h_{n+1}(r).$$

Using integration by parts, the Abel transform can be rewritten as

$$\begin{aligned}\int_{\rho}^{\infty} \frac{h_n(r)r}{\sqrt{r^2-\rho^2}}dr &= \frac{h_n(r)}{\sqrt{r^2-\rho^2}}\frac{r^2}{2}\Big|_{r=\rho}^{\infty} - \int_{\rho}^{\infty}\frac{r^2}{2}\left(\frac{h_n(r)}{\sqrt{r^2-\rho^2}}\right)'dr \\ &= 0 - \int_{\rho}^{\infty}\frac{r^2}{2}\left(\frac{h_n'(r)}{\sqrt{r^2-\rho^2}} - \frac{h_n(r)r}{(r^2-\rho^2)^{3/2}}\right)dr \\ &= -\int_{\rho}^{\infty}\frac{h_n'(r)r^2}{2\sqrt{r^2-\rho^2}}dr + \int_{\rho}^{\infty}\frac{h_n(r)r^3}{2(r^2-\rho^2)^{3/2}}dr.\end{aligned} \tag{9.31}$$

The integral

$$\int_{\rho}^{\infty} \frac{h_n'(r)r^2}{2\sqrt{r^2-\rho^2}}dr,$$

after inserting the two recurrence relation equations becomes

$$\begin{aligned}\int_\rho^\infty \frac{h_n'(r)r^2}{2\sqrt{r^2-\rho^2}}dr &= \frac{1}{2}\frac{\sqrt{n(n-1)}}{2}\mathcal{A}[h_{n-2}](\rho) - \frac{1}{4}\mathcal{A}[h_n](\rho) - \frac{1}{2}\frac{\sqrt{(n+1)(n+2)}}{2}\mathcal{A}[h_{n+2}](\rho) \\ &= \frac{1}{2}\eta_{n-2}\mathcal{A}[h_{n-2}](\rho) + \frac{1}{2}\eta_n\mathcal{A}[h_n](\rho) + \frac{1}{2}\eta_{n+2}\mathcal{A}[h_{n+2}](\rho).\end{aligned} \tag{9.32}$$

The second integral

$$\int_\rho^\infty \frac{h_n(r)r^3}{2(r^2-\rho^2)^{3/2}}dr,$$

can be reshaped using integration by parts as

$$\begin{aligned}\int_\rho^\infty \frac{h_n(r)r^3}{2(r^2-\rho^2)^{3/2}}dr &= -\frac{h_n(r)r^4}{2\rho^2\sqrt{r^2-\rho^2}}\Big|_{r=\rho}^\infty + \int_\rho^\infty \frac{r}{2\rho^2\sqrt{r^2-\rho^2}}(h_n(r)r^3)'dr \\ &= \int_\rho^\infty \frac{r}{2\rho^2\sqrt{r^2-\rho^2}}(h_n'(r)r^3 + 3h_n(r)r^2)dr \\ &= \int_\rho^\infty \frac{3h_n(r)r^3}{2\rho^2\sqrt{r^2-\rho^2}}dr + \int_\rho^\infty \frac{h_n'(r)r^4}{2\rho^2\sqrt{r^2-\rho^2}}dr.\end{aligned} \tag{9.33}$$

Finally, we will take these two sub-integrals and apply the two recurrence relation equations repeatedly until the only function in the numerator is $h_n(r)r$, albeit scaling. This follows

$$\begin{aligned}\int_\rho^\infty \frac{3h_n(r)r^3}{2\rho^2\sqrt{r^2-\rho^2}}dr &= \frac{3\sqrt{n(n-1)}}{4\rho^2}\mathcal{A}[h_{n-2}](\rho) + \frac{3(2n+1)}{4\rho^2}\mathcal{A}[h_n](\rho) \\ &\quad + \frac{3\sqrt{(n+1)(n+2)}}{4\rho^2}\mathcal{A}[h_{n+2}](\rho) \\ &\quad \frac{3}{2\rho^2}\gamma_{n-2}\mathcal{A}[h_{n-2}](\rho) + \frac{3}{2\rho^2}\gamma_n\mathcal{A}[h_n](\rho) + \frac{3}{2\rho^2}\gamma_{n+2}\mathcal{A}[h_{n+2}](\rho),\end{aligned} \tag{9.34}$$

and

$$\begin{aligned} h_n'(r)r^4 &= (h_n'(r)r^2)r^2 \\ &= (\eta_{n-2}h_{n-2}r + \eta_n h_n r + \eta_{n+2}h_{n+2}r)r^2 \\ &= (\alpha_{n-3}h_{n-3}r + \alpha_{n-1}h_{n-1}r + \alpha_{n+1}h_{n+1}r + \alpha_{n+3}h_{n+3}r)r \\ &= \beta_{n-4}h_{n-4}r + \beta_{n-2}h_{n-2}r + \beta_n h_n r + \beta_{n+2}h_{n+2}r + \beta_{n+4}h_{n+4}r, \end{aligned} \tag{9.35}$$

which leads to

$$\begin{aligned} \int_\rho^\infty \frac{h_n'(r)r^4}{2\rho^2\sqrt{r^2-\rho^2}}dr &= \frac{1}{2\rho^2}\beta_{n-4}\mathcal{A}[h_{n-4}](\rho) + \frac{1}{2\rho^2}\beta_{n-2}\mathcal{A}[h_{n-2}](\rho) \\ &\quad + \frac{1}{2\rho^2}\beta_n\mathcal{A}[h_n](\rho) + \frac{1}{2\rho^2}\beta_{n+2}\mathcal{A}[h_{n+2}](\rho) + \frac{1}{2\rho^2}\beta_{n+4}\mathcal{A}[h_{n+4}](\rho), \end{aligned} \tag{9.36}$$

where

$$\beta_{n-4} = \frac{\alpha_{n-3}\sqrt{n-3}}{\sqrt{2}},$$

$$\beta_{n-2} = \alpha_{n-3}\frac{\sqrt{n-2}}{\sqrt{2}} + \alpha_{n-1}\frac{\sqrt{n-1}}{\sqrt{2}},$$

$$\beta_n = \alpha_{n-1}\frac{\sqrt{n}}{\sqrt{2}} + \alpha_{n+1}\frac{\sqrt{n+1}}{\sqrt{2}},$$

$$\beta_{n+2} = \alpha_{n+1}\frac{\sqrt{n+2}}{\sqrt{2}} + \alpha_{n+3}\frac{\sqrt{n+3}}{\sqrt{2}},$$

$$\beta_{n+4} = \alpha_{n+3}\frac{\sqrt{n+4}}{\sqrt{2}},$$

and

$$\alpha_{n-3} = \eta_{n-2}\frac{\sqrt{n-2}}{\sqrt{2}},$$

$$\alpha_{n-1} = \eta_{n-2}\frac{\sqrt{n-1}}{\sqrt{2}} + \eta_n\frac{\sqrt{n}}{\sqrt{2}},$$

$$\alpha_{n+1} = \eta_n\frac{\sqrt{n+1}}{\sqrt{2}} + \eta_{n+2}\frac{\sqrt{n+2}}{\sqrt{2}},$$

$$\alpha_{n+3} = \eta_{n+2}\frac{\sqrt{n+3}}{\sqrt{2}}.$$

By setting (9.30) = −(9.32) + (9.34) + (9.36)

$$\begin{aligned}\mathcal{A}[h_n](\rho) = &-\frac{1}{2}\eta_{n-2}\mathcal{A}[h_{n-2}](\rho) - \frac{1}{2}\eta_n\mathcal{A}[h_n](\rho) - \frac{1}{2}\eta_{n+2}\mathcal{A}[h_{n+2}](\rho) + +\frac{3}{2\rho^2}\gamma_{n-2}\mathcal{A}[h_{n-2}](\rho)\\ &+ \frac{3}{2\rho^2}\gamma_n\mathcal{A}[h_n](\rho) + \frac{3}{2\rho^2}\gamma_{n+2}\mathcal{A}[h_{n+2}](\rho) + \frac{1}{2\rho^2}\beta_{n-4}\mathcal{A}[h_{n-4}](\rho)\\ &+ \frac{1}{2\rho^2}\beta_{n-2}\mathcal{A}[h_{n-2}](\rho) + \frac{1}{2\rho^2}\beta_n\mathcal{A}[h_n](\rho) + \frac{1}{2\rho^2}\beta_{n+2}\mathcal{A}[h_{n+2}](\rho) + \frac{1}{2\rho^2}\beta_{n+4}\mathcal{A}[h_{n+4}](\rho),\end{aligned} \tag{9.37}$$

and rearranging, we get

$$\begin{aligned}\mathcal{A}[h_{n+4}](\rho) = -\frac{1}{\sigma_{n+4}}&[\sigma_{n-4}\mathcal{A}[h_{n-4}](\rho) + \sigma_{n-2}(\rho)\mathcal{A}[h_{n-2}](\rho)\\ &+ \sigma_n(\rho)\mathcal{A}[h_n](\rho) + \sigma_{n+2}(\rho)\mathcal{A}[h_{n+2}](\rho)],\end{aligned} \tag{9.38}$$

where

$$\sigma_{n-4} = \beta_{n-4},$$

$$\sigma_{n-2}(\rho) = \left(3\gamma_{n-2} + \beta_{n-2} - \rho^2\eta_{n-2}\right),$$

$$\sigma_n(\rho) = \left(3\gamma_n + \beta_n - \rho^2\eta_n - 2\rho^2\right),$$

$$\sigma_{n+2}(\rho) = \left(3\gamma_{n+2} + \beta_{n+2} - \rho^2\eta_{n+2}\right),$$

and

$$\sigma_{n+4} = \beta_{n+4}.$$

The starting conditions for this Abel transform recurrence relation are

$$\mathcal{A}[h_0](\rho) = c_0\sqrt{2\pi}e^{-\rho^2/2} = \sqrt{2\pi}h_0(\rho),$$

$$\mathcal{A}[h_1](\rho) = \begin{cases} 4c_1e^{-\rho^2/2}\sqrt{\pi}\sqrt{\frac{1}{\rho^2}}\sqrt{\rho^2}U(-\frac{1}{2},0,\frac{\rho^2}{2}), & \rho > 0 \\ 4c_1, \ \rho = 0, \end{cases}$$

$$\mathcal{A}[h_2](\rho) = 2c_2\sqrt{2\pi}e^{-\rho^2/2}(2\rho^2+1),$$

$$\mathcal{A}[h_3](\rho) = \begin{cases} 2c_3e^{-\rho^2/4}\sqrt{\frac{1}{\rho^2}}(\rho^2)^{3/2}[(2\rho^2-3)K(0,\frac{\rho^2}{4}) + (1+2\rho^2)K(1,\frac{\rho^2}{4})], & \rho > 0, \\ 8c_3, \ \rho = 0. \end{cases}$$

$$\mathcal{A}[h_4](\rho) = 4c_4\sqrt{2\pi}e^{-\rho^2/2}(3-4\rho^2+4\rho^4),$$

$$\mathcal{A}[h_5](\rho) = \begin{cases} 4c_5e^{-\rho^2/4}\sqrt{\frac{1}{\rho^2}}(\rho^2)^{3/2}[(15-16\rho^2+4\rho^4)K(0,\frac{\rho^2}{4})\cdots \\ +(7-8\rho^2+4\rho^4)K(1,\frac{\rho^2}{4})], & \rho > 0, \\ 112c_5, \ \rho = 0. \end{cases}$$

$$\mathcal{A}[h_6](\rho) = 8c_6\sqrt{2\pi}e^{-\rho^2/2}(15+42\rho^2-36\rho^4+8\rho^6),$$

$$\mathcal{A}[h_7](\rho) = \begin{cases} 8c_7e^{-\rho^2/4}\sqrt{\frac{1}{\rho^2}}(\rho^2)^{3/2}[(-105+174\rho^2-68\rho^4+8\rho^6)K(0,\frac{\rho^2}{4})\cdots \\ +(27+86\rho^2-52\rho^4+8\rho^6)K(1,\frac{\rho^2}{4})], & \rho > 0, \\ 864c_7, \ \rho = 0. \end{cases}$$

The function $U(a, b, z)$ is the confluent hypergeometric function of the second kind, which can be represented as the solution to the integral

$$U(a, b, z) = \frac{1}{\Gamma(a)} \int_0^\infty e^{-zt} t^{a-1} (1+t)^{b-a-1} dt, \tag{9.39}$$

and $K(n, z)$ is the modified Bessel function of the second kind. Figure 9.5 shows a comparison of the Abel transforms for various Hermite functions using numeric integration (left) versus recursion (right). Figure 9.6 shows the NLSE between the two.

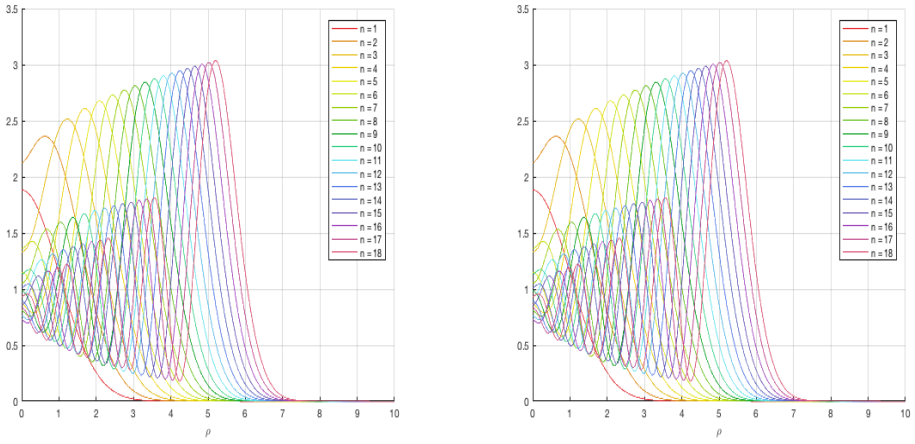

Numeric Recursion

Figure 9.5: Abel Transform of Hermite Functions

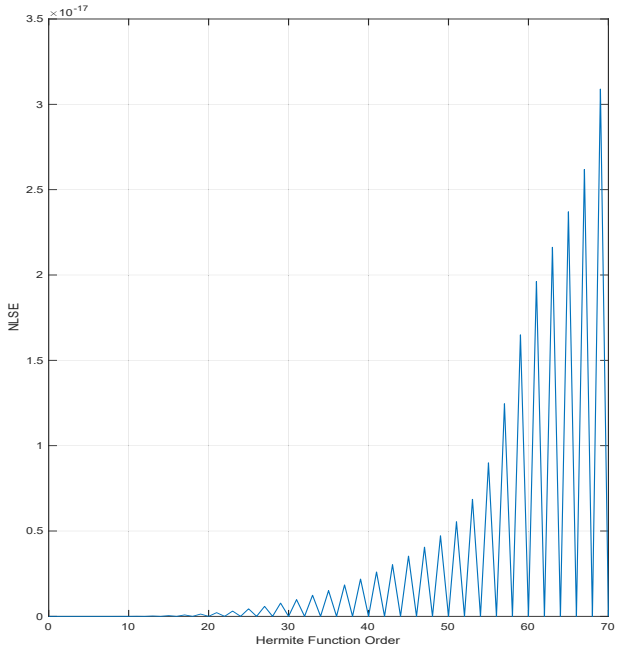

Figure 9.6: Abel Transform Error

This recurrence relation for the Abel transform of a Hermite function can be used to approximate the Abel transform of a Hermite expansion. There is a well-known relationship between the Abel transform, the zeroth order Hankel transform, and the Fourier transform, which states

$$\mathcal{F}\mathcal{A} = \mathcal{H}_0.$$

This means that the Abel transform followed by a one-dimensional Fourier transform applied to a radial function is equivalent to applying the Hankel transform of order zero to that same function. Since the Fourier transform is linear, it can be carried through the Abel transform recurrence relation from equation (9.38) to provide a

recurrence relation for the zeroth order Hankel transform of a Hermite function. The Hankel transform of a Hermite function is a special case of Weber's integral [3], and so this can help set up the starting conditions for this recurrence relation. This will be tested in future research.

The next section will show how the Abel transform of Hermite functions fits into cross-validating EM/SAXS data.

9.5 Cross-Modal Validation with Hermite Expansions

Recall the representation of EM and SAXS data as Hermite expansions according to equations (9.25) and (9.27) respectively. Taking the Abel transform of SAXS data Hermite expansion according to (9.27) gives

$$\mathcal{A}[\gamma_{\tilde{f}}](\rho) = \frac{1}{4\pi^2} \sum_{v=0}^{N} \sum_{w=0}^{N-v} \sum_{m=0}^{N-v-w} \hat{f}_{v,w,m} \sum_{d=0}^{v+w} \sigma^{\phi}_{d,v,v+w} \sum_{t=0}^{m+d} \sigma^{\theta}_{t,m,m+d} h_{m+d-t}(0) h_{v+w-d}(0) \mathcal{A}[h_t](\rho). \tag{9.40}$$

Cross-validation then implies

$$\mathcal{A}[\gamma_{\tilde{f}}](\rho) = \gamma_{\tilde{f}^p}(\rho), \tag{9.41}$$

where

$$\gamma_{\tilde{f}^p}(\rho) = \frac{1}{16\pi^3} \sum_{m=0}^{N} \sum_{n=0}^{N-m} \sum_{k=0}^{N-m-n} \hat{f}^{\bar{\alpha},\bar{\beta},\bar{\gamma}}_{m,n,k} \nu_k(1/\sqrt{2}) \sum_{q=0}^{m+n} \sigma^{\phi}_{q,m,m+n} h_q(\rho/\sqrt{2}) h_{m+n-q}(0),$$

is equation (9.25) restated.

Figure 9.7 shows an example two-ellipsoid model with a corresponding characteristic function $\chi(\mathbf{x})$. This characteristic function $\chi(\mathbf{x})$ is approximated as a Hermite series $\tilde{\chi}(\mathbf{x})$, and is then converted into EM and SAXS data according to equations (9.25) and (9.27) respectively. In Figure 9.8, the EM data is depicted with the blue curve, and SAXS data is represented by the black curve. The Abel transform of SAXS data (equation (9.40)) follows the magenta curve.

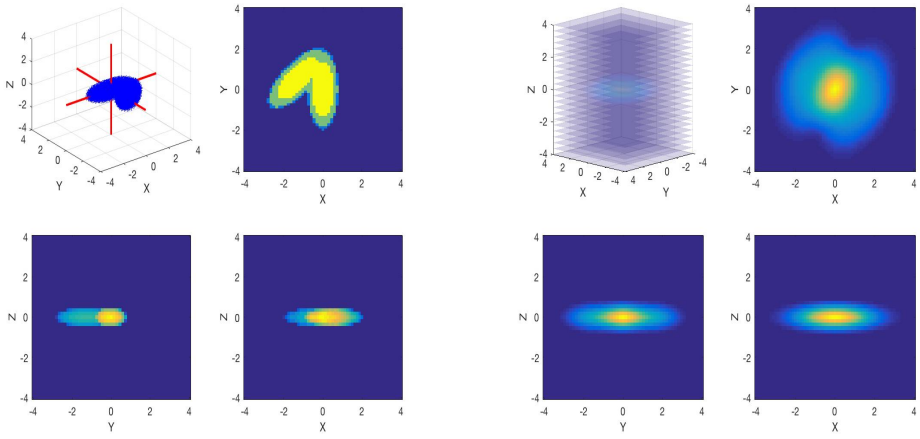

$\chi(\mathbf{x})$ $C_\chi(\mathbf{x})$

Figure 9.7: Two-Ellipsoid Model for Cryo-EM/SAXS

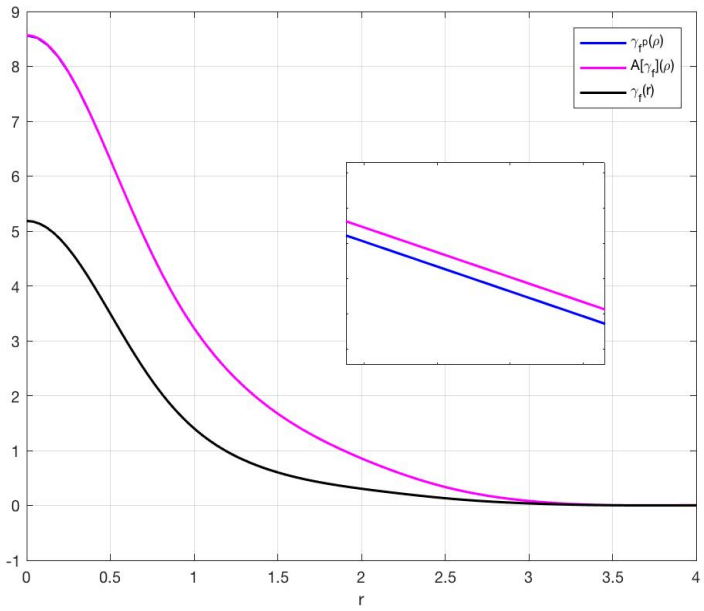

Figure 9.8: Cross-Validation of Two-Ellipsoid Model with Hermite Expansions

9.6 Towards Representing Expectations over $SO(3)$ for Non-Uniform Distributions with Hermite Expansions

Recall from the introduction section that the uniformity assumption for distributions over $SO(3)$ was caveated when expectation was defined. In recent literature, the distance between EM and SAXS profiles was studies versus various cases that constrained the distributions over $SO(3)$ [46]. Preferred orientations were investigated a decade earlier in [50]. Now suppose one wanted to impose some distribution

$\rho(R)$, and wrap this function into the expectation definition. This will modify the expectation integral as

$$E_{R;\rho(R)}[f](\mathbf{x}) = \int_{SO(3)} f(R^T\mathbf{x})\rho(R)dR. \tag{9.42}$$

for a Hermite series approximation of f, the integral becomes

$$\begin{aligned} E_{R;\rho(R)}[\tilde{f}](\mathbf{x}) &= \frac{1}{8\pi^2}\int_{SO(3)} \sum_{m,n,k} \hat{f}_{m,n,k} h_m(x'/\sqrt{2})h_n(y'/\sqrt{2})h_k(z'/\sqrt{2})\rho(R)dR \\ &= \frac{1}{8\pi^2}\sum_{m,n,k}\int_0^{2\pi}\int_0^{\pi}\int_0^{2\pi} \hat{f}^{\alpha,\beta,\gamma}_{m,n,k} h_m(x/\sqrt{2})h_n(y/\sqrt{2})h_k(z/\sqrt{2})\rho(\alpha,\beta,\gamma)\sin\beta d\alpha d\beta d\gamma. \end{aligned} \tag{9.43}$$

If the density separated as $\rho(\alpha,\beta,\gamma) = \rho_1(\alpha)\rho_2(\beta)\rho_3(\gamma)$, then the ISCs can be modified to account for this distribution. This modifies the matrix-vector equations as

$$\begin{aligned} \hat{f}^{\grave{\gamma}}_{d,m-d,k} &= \int_0^{2\pi}\sum_{n=0}^{m} S^m_{d,n}(\gamma)\rho_3(\gamma)\hat{f}_{n,m-n,k}d\gamma \\ &= \sum_{n=0}^{m}\left(\int_0^{2\pi} S^m_{d,n}(\gamma)\rho_3(\gamma)d\gamma\right)\hat{f}_{n,m-n,k} \\ &= \sum_{n=0}^{m} \grave{\sigma}^{\gamma}_{d,n,m}\hat{f}_{n,m-n,k}, \end{aligned} \tag{9.44}$$

$$\begin{aligned} \hat{f}^{\grave{\beta},\grave{\gamma}}_{m,d,n-d} &= \int_0^{\pi}\sum_{k=0}^{n} S^n_{d,k}(\beta)\rho_2(\beta)\hat{f}^{\grave{\gamma}}_{m,k,n-k}\sin\beta d\beta \\ &= \sum_{k=0}^{n}\left(\int_0^{\pi} S^n_{d,k}(\beta)\sin\beta\rho_2(\beta)d\beta\right)\hat{f}^{\grave{\gamma}}_{m,k,n-k} \\ &= \sum_{k=0}^{n} \grave{\sigma}^{\beta}_{d,k,n}\hat{f}^{\grave{\gamma}}_{m,k,n-k}, \end{aligned} \tag{9.45}$$

and

$$\begin{aligned}\hat{f}^{\grave{\alpha},\grave{\beta},\grave{\gamma}}_{d,m-d,k} &= \int_0^{2\pi} \sum_{n=0}^{m} S^m_{d,n}(\alpha)\rho_1(\alpha)\hat{f}^{\grave{\beta},\grave{\gamma}}_{n,m-n,k} d\gamma \\ &= \sum_{n=0}^{m} \left(\int_0^{2\pi} S^m_{d,n}(\alpha)\rho_1(\alpha) d\alpha \right) \hat{f}^{\grave{\beta},\grave{\gamma}}_{n,m-n,k} \\ &= \sum_{n=0}^{m} \grave{\sigma}^{\alpha}_{d,n,m} \hat{f}^{\grave{\beta},\grave{\gamma}}_{n,m-n,k},\end{aligned} \tag{9.46}$$

The expectation over $SO(3)$ for $\tilde{f}$ with the distribution $\rho(\alpha, \beta, \gamma)$ is now

$$E_{R;\rho(R)}[\tilde{f}](x,y,z) = \frac{1}{8\pi^2} \sum_{m=0}^{2N} \sum_{n=0}^{N-m} \sum_{k=0}^{N-m-n} \hat{f}^{\grave{\alpha},\grave{\beta},\grave{\gamma}}_{m,n,k} h_m(x/\sqrt{2}) h_n(y/\sqrt{2}) h_k(z/\sqrt{2}). \tag{9.47}$$

Projection and averaging over the circle will then give a Hermite expansion like equation (9.25), only now with an induced orientational distribution. Computing the induced ISCs

$$\grave{\sigma}^{\alpha}_{d,n,m} = \left(\int_0^{2\pi} S^m_{d,n}(\alpha)\rho_1(\alpha) d\alpha \right),$$

$$\grave{\sigma}^{\beta}_{d,k,n} = \left(\int_0^{\pi} S^n_{d,k}(\beta) \sin\beta \rho_2(\beta) d\beta \right)$$

and

$$\grave{\sigma}^{\gamma}_{d,n,m} = \left(\int_0^{2\pi} S^m_{d,n}(\gamma)\rho_3(\gamma) d\gamma \right),$$

can be done for a distribution $\rho(\alpha,\beta,\gamma) = \rho_1(\alpha)\rho_2(\beta)\rho_3(\gamma)$ if it is expanded with the $SO(3)$-Fourier series

$$\begin{aligned}\rho(R(\alpha,\beta,\gamma)) &\approx \tilde{\rho}(\alpha,\beta,\gamma) \\ &= \sum_{l=0}^{B}(2l+1)\sum_{m,n=-l}^{l}\hat{\rho}^l_{m,n}U^l_{n,m}(\alpha,\beta,\gamma) \\ &= \sum_{l=0}^{B}(2l+1)\sum_{m,n=-l}^{l}\hat{\rho}^l_{m,n}e^{-in\alpha}d^l_{n,m}(\cos\beta)e^{-im\gamma},\end{aligned} \tag{9.48}$$

where $\rho_1(\alpha)$, $\rho_2(\beta)$, and $\rho_3(\gamma)$ can be assigned to

$$\rho_1(\alpha) = \sum_{l=0}(2l+1)\sum_{m,n=-l}^{l}\hat{\rho}^l_{m,n}e^{-in\alpha}, \tag{9.49}$$

$$\rho_2(\beta) = \sum_{l=0}(2l+1)\sum_{m,n=-l}^{l}\hat{\rho}^l_{m,n}d^l_{n,m}(\cos\beta), \tag{9.50}$$

and

$$\rho_3(\gamma) = \sum_{l=0}(2l+1)\sum_{m,n=-l}^{l}\hat{\rho}^l_{m,n}e^{-im\gamma}. \tag{9.51}$$

9.7 Chapter Summary

Hermite functions fit right into the representation of EM and SAXS data, and can be used for cross-validating the two modalities. From properties under rotation, the effect of preferred orientations could be explored in the future since it is easy to wrap these densities into the ISCs. This could provide some useful insight into how

sensitive the cross-validation result is to the uniformity assumption.

Another related application would be if these cross-validation ideas could be used to solve tomographic reconstruction of 3D densities when the projection angles are a priori unknown, an idea that was entertained in [9] chapter 6 for reconstructing 2D images.

Chapter 10

Deconvolution and Normal Mode Analysis with Hermite Expansions

10.1 Introduction

This chapter describes two more applications that utilize properties of Hermite expansions, namely deconvolution (translational and rotational) and normal mode analysis.

10.2 Deconvolution with Hermite Expansions

There are two popular ways to perform translational deconvolution on discrete data. The first method represents the convolution of two vectors f, g as

$$\gamma = f * g = Fg = Gf,$$

where F, G are Toeplitz matrices [51]. The solution to f from g and γ is in the least-squares sense

$$f = G^{+}\gamma,$$

pending adequate condition numbers on G. The second method is a Fourier approach, where convolution in the frequency domain is simply multiplication. The Discrete Fourier transforms of f, g and γ describe convolution as

$$\hat{\gamma}(\omega) = \hat{f}(\omega)\hat{g}(\omega) = \hat{g}(\omega)\hat{f}(\omega), \tag{10.1}$$

and f can be recovered using

$$\hat{f}(\omega) = \frac{\hat{\gamma}(\omega)\overline{\hat{g}(\omega)}}{\epsilon + |\hat{g}(\omega)|^2}. \tag{10.2}$$

The parameter ϵ regularizes the solution. These two concepts generalize to $2D$ and $3D$ translational deconvolution.

Translational deconvolution using Hermite expansions was derived in [park2008thesis],[parkpaper] as a means to de-blur images where the blurring function was a Gaussian. The approach involved sampling Hermite functions in the frequency domain and performing a matrix inversion.

Rotational deconvolution is classically formulated by setting up the integral as one of two functions expanded on a circle via the Fourier series. The solution to coefficients of the deconvolved Fourier series is akin to equation (10.2). For angular Gaussian blurring, the rotational deconvolution problem was solved using properties of Hermite and Fourier-Laguerre expansions under coordinate conversion (see [park2007interconv]). The next two subsections seek to generalize the aformentioned methods involving Hermite functions to not only Gaussians, but all square-integrable functions.

10.2.1 Translational Deconvolution

With the help of $3h$ integrals

$$\alpha_{m,n}^{k} = \begin{pmatrix} m & n & k \\ 1 & 1 & \sqrt{2} \end{pmatrix},$$

the convolution of two band-limited Hermite expansions can be represented with the equation

$$\begin{aligned} \tilde{\gamma}(x) = (\tilde{f} * \tilde{g})(x) &= \sum_{m=0}^{M} \sum_{n=0}^{N} \hat{f}_m \hat{g}_n (-i)^{m+n} \sum_{k=0}^{m+n} i^k \eta_k \alpha_{m,n}^{k} h_k(x\sqrt{2}) \\ &= \sum_{l=0}^{M+N} \hat{\gamma}_l h_l(x\sqrt{2}), \end{aligned} \tag{10.3}$$

where

$$\hat{\gamma}_l = i^l \eta_l \sum_{m=0}^{M} \sum_{n=0}^{N} \hat{f}_m \hat{g}_n (-i)^{m+n} \alpha_{m,n}^{l} \delta_{m,n}^{l}. \tag{10.4}$$

By setting up equation (10.4) in matrix-vector form

$$\hat{\Gamma} = \mathcal{G}\hat{F},$$

and given $\tilde{g}$ and $\tilde{\gamma}$, one can obtain $\tilde{f}$ by solving for the coefficients $\hat{f}_m$ as

$$\hat{F} = \mathcal{G}^{+}\hat{\Gamma}.$$

This technique extends naturally to $2D$ as

$$\begin{aligned}\tilde{\gamma}(x,y) = (\tilde{f} * \tilde{g})(x,y) &= \sum_{m=0}^{M}\sum_{n=0}^{M-m}\sum_{m'=0}^{M'}\sum_{n'=0}^{M'-m'} \hat{f}_{m,n}\hat{g}_{m',n'}\left(h_m * h_{m'}(x)\right)\left(h_n * h_{n'}(y)\right) \\ &= \sum_{m=0}^{M}\sum_{n=0}^{M-m}\sum_{m'=0}^{M'}\sum_{n'=0}^{M'-m'} \hat{f}_{m,n}\hat{g}_{m',n'}(-i)^{m+m'+n+n'} \\ &\sum_{k=0}^{m+m'} i^k \alpha_{m,m'}^{k}\eta_k h_k(x) \sum_{k'=0}^{n+n'} i^{k'}\eta_{k'}\alpha_{n,n'}^{k'}h_{k'}(y) \\ &= \sum_{m''=0}^{M+M'}\sum_{n''=0}^{M+M'-m''} \hat{\gamma}_{m'',n''}h_{m''}(x)h_{n''}(y),\end{aligned} \tag{10.5}$$

where

$$\hat{\gamma}_{m'',n''} = i^{m''+n''}\eta_{m''}\eta_{n''}\sum_{m,m',n,n'} \hat{f}_{m,n}\hat{g}_{m',n'}(-i)^{m+m'+n+n'}\alpha_{m,m'}^{m''}\delta_{m,m'}^{m''}\alpha_{n,n'}^{n''}\delta_{n,n'}^{n''}. \tag{10.6}$$

We can put the above equation into matrix-vector form

$$\hat{\Gamma} = \mathcal{G}\hat{F},$$

and solve for the coefficients $\hat{f}_{m,n}$ using least-squares. The attractive part of these translational deconvolution techniques is no further sampling of γ and g is required after coefficients $\hat{\gamma}$ and $\hat{g}$ have been obtained. This approach is quite similar to the Toeplitz matrix method, but the Toeplitz matrix G compared to could be quite large, whereas the size of $\mathcal{G}$ can be adjusted according to bandlimits. The next subsection will showcase how rotational deconvolution is solved with Hermite and

Fourier-Laguerre expansions.

10.2.2 Rotational Deconvolution

Given F-L expansions $\tilde{f}$ and $\tilde{\gamma}$, and assuming Gaussian blurring with variance σ, the coefficients of the three expansions make up the equation [52]

$$\check{\gamma}_{m,n} = \check{f}_{m,n} e^{-n^2\sigma}, \tag{10.7}$$

and inversion follows

$$\check{f}_{m,n} = \frac{\check{\gamma}_{m,n}}{e^{-n^2\sigma} + \epsilon}. \tag{10.8}$$

We now seek to generalize (10.8). Consider the rotational deconvolution integral

$$\tilde{\gamma}(r,\phi) = \int_0^{2\pi} \tilde{f}(r,\phi-\theta) g(\theta) d\theta. \tag{10.9}$$

The function $g(\theta)$ can be approximated with a 1D Hermite expansion as

$$\tilde{g}(x) = \sum_{k=0}^{B} \hat{g}_k h_k(x), \tag{10.10}$$

where

$$\hat{g}_k = s\int_{-\infty}^{\infty} g(x)h_k(x)dx = s\int_{-\pi/s}^{\pi/s} g(x)dx = \int_{-\pi}^{\pi} h_k(\theta/s)d\theta. \tag{10.11}$$

The left-hand side of (10.9) can be written as

$$\tilde{\gamma}(r,\phi) = \sum_{m,n} \check{\gamma}_{m,n} \chi^*_{m,n}(r,\phi), \tag{10.12}$$

and the right-hand side is

$$\begin{aligned} \int_0^{2\pi} \tilde{f}(r,\phi-\theta) g(\theta) d\theta &= \int_0^{2\pi} \sum_{m,n} \check{f}_{m,n} \chi^*_{m,n}(r,\phi-\theta) g(\theta) d\theta \\ &= \sum_{m,n} \check{f}_{m,n} \chi^*_{m,n}(r,\phi) \int_0^{2\pi} e^{in\theta} g(\theta) d\theta. \end{aligned} \tag{10.13}$$

The integral

$$\int_0^{2\pi} e^{in\theta} g(\theta) d\theta,$$

is approximately

$$\begin{aligned} \int_0^{2\pi} e^{in\theta} g(\theta) d\theta &\approx \int_0^{2\pi} e^{in\theta} \tilde{g}(\theta) d\theta \\ &= \int_{-\pi}^{\pi} e^{in\theta} \tilde{g}(\theta) d\theta \\ &= \sum_{k=0}^{N} \hat{g}_k \int_{-\pi}^{\pi} e^{in\theta} h_k(\theta/s) d\theta \\ &= \sum_{k=0}^{N} \hat{g}_k \sqrt{2\pi} i^k s h_k(ns) \\ &= \sum_{k=0}^{N} \hat{g}_k \alpha_k^n. \end{aligned} \tag{10.14}$$

Locally this implies

$$\check{\gamma}_{m,n} = \check{f}_{m,n} \sum_{k=0}^{N} \hat{g}_k \alpha_k^n, \tag{10.15}$$

or inversely

$$\check{f}_{m,n} = \frac{\check{\gamma}_{m,n}}{\sum_{k=0}^{N} \hat{g}_k \alpha_k^n + \epsilon}. \tag{10.16}$$

Another method is available that works directly with Hermite expansions instead of F-L expansions with a need to interconvert. The quantity

$$\mathcal{R}^m = \int_0^{2\pi} S^m(\theta) g(\theta) d\theta,$$

will be used in the following rotational deconvolution method. Consider rewriting the steering coefficient matrices as

$$S^m(\theta) = E \cdot \left(S^m(\frac{\pi}{4})\right)^T \cdot G(\theta) \cdot \left(S^m(\frac{\pi}{4})\right) \cdot E^*, \tag{10.17}$$

where

$$E = \text{diag}\left(\begin{bmatrix} i^0 & i^1 & \dots & i^m \end{bmatrix}\right), \tag{10.18}$$

and

$$G(\theta) = \text{diag}\left(\begin{bmatrix} e^{im\theta} & e^{i(m-2)\theta} & \dots & e^{-im\theta} \end{bmatrix}\right). \tag{10.19}$$

Now given the distribution

$$g(\theta) \approx \tilde{g}(\theta) = \sum_{k=0}^{N} \hat{g}_k h_k(\theta/s),$$

we can approximate $g(\theta)$ with a 1D Hermite series (like before), and then multiply by an element of $G(\theta)$ to get

$$q(\theta) = e^{im'\theta}\tilde{g}(\theta) = e^{im'\theta}\sum_{k=0}^{N} \hat{g}_k h_k(\theta/s).$$

Integrating $q(\theta)$ over the circle gives

$$d_{m'} = \int_{-\pi}^{\pi} q(\theta)d\theta \approx \sum_{k=0}^{N} \hat{g}_k \int_{-\pi}^{\pi} e^{im'\theta} h_k(\theta/s)d\theta = \sum_{k=0}^{N} \hat{g}_k \alpha_k^{m'},$$

where

$$\alpha_k^{m'} = \sqrt{2\pi} i^k s h_k(m's).$$

If

$$D^m = \text{diag}\left(\begin{bmatrix} d_m & d_{m-2} & \cdots & d_{-m} \end{bmatrix}\right), \tag{10.20}$$

Then

$$\begin{aligned} \mathcal{R}^m &= \int_{-\pi}^{\pi} S^m(\theta) g(\theta) d\theta \\ &= E \cdot \left(S^m(\frac{\pi}{4})\right)^T \cdot \left(\int_{-\pi}^{\pi} G(\theta) g(\theta) d\theta\right) \cdot \left(S^m(\frac{\pi}{4})\right) \cdot E^* \\ &= E \cdot \left(S^m(\frac{\pi}{4})\right)^T \cdot D^m \cdot \left(S^m(\frac{\pi}{4})\right) \cdot E^*. \end{aligned} \tag{10.21}$$

In this form, rotation convolution and deconvolution act like image rotation in that the coefficients of the original image $\hat{f}_{m,n}$ map to the rotationally convolved ones $\hat{\gamma}_{m,n}$ as

$$\hat{\gamma}_{q,m-q} = \sum_{n=0}^{m} \mathcal{R}^m_{q,n} \hat{f}_{n,m-n}. \tag{10.22}$$

Obtaining the coefficients $\hat{f}_{m,n}$ from the rotationally convolved ones $\hat{\gamma}_{m,n}$ depends on $\mathcal{R}^m$ in terms of least-squares. From this point, it is easy to image that translational and rotational deconvolution can be combined into general $SE(2)$-deconvolution ideas. This is left as a topic for future research. The next section shows how $3h$ integrals can be used to obtain normal modes of a closed body.

10.3 Continuum Normal Mode Analysis with $3h$ Integrals

This section presents a new approach for obtaining normal mode equations of motion. Usually, normal mode equations are modeled for specific points within a body. Instead, a new method is formulated where a body is defined by its boundary via a characteristic equation (i.e. a uniform density map) that is then approximated with a Hermite expansion. Following this, a deformation function is represented with another Hermite expansion together with a temporal basis. This allows for kinetic and potential energy (integrated over the body) to be represented as two separate

series expansions. These energy expansions (integrated over the body) contain 3h integrals, which are the product of three Hermite functions. Relating kinetic and potential energy (when represented with 3h integrals) to the general form of energy for a mass-spring system provides a new way to do normal mode decomposition. The novelty here is that normal mode decomposition is made possible without having to specify interior points within the body.

As an intermediate example, consider a 1D system of n identical point masses connected by $n-1$ identical springs, where the whole system is free to move without constraint. The total kinetic energy for this system can be modeled as the summation

$$T(t) = \frac{1}{2} m \sum_{i=1}^{n} \dot{u}(x_i, t)^2, \tag{10.23}$$

and a total potential energy

$$V(t) = \frac{1}{2} k \sum_{i=1}^{n-1} \left(u(x_i, t) - u(x_{i+1}, t) \right)^2, \tag{10.24}$$

with $u(x_i, t)$ describing the deformation at a point x_i and time t. Moreover,

$$x_i(t) = x_i(0) + u(x_i, t),$$

where $x_i(0)$ is the equilibrium position of $x_i(t)$ for the i^{th} point mass. The deformations can be collected in a vector as

$$\mathbf{U}(t) = \begin{bmatrix} u(x_1,t) \\ u(x_2,t) \\ \vdots \\ u(x_n,t) \end{bmatrix}. \tag{10.25}$$

Applying the Euler-Lagrange equation

$$\frac{d}{dt}\frac{\partial L}{\partial \dot{\mathbf{U}}} - \frac{\partial L}{\partial \mathbf{U}} = \mathbf{0}, \tag{10.26}$$

to $L = T - V$ gives

$$M\ddot{\mathbf{U}} + K\mathbf{U} = \mathbf{0}, \tag{10.27}$$

where

$$M = \begin{bmatrix} m & 0 & \cdots & 0 \\ 0 & m & \cdots & 0 \\ \vdots & \vdots & \ddots & 0 \\ 0 & 0 & 0 & m \end{bmatrix}, \tag{10.28}$$

and

$$K = \begin{bmatrix} k & -k & 0 & \cdots & 0 \\ -k & 2k & -k & \cdots & 0 \\ 0 & -k & 2k & \cdots & 0 \\ \vdots & \vdots & \vdots & \ddots & -k \\ 0 & 0 & 0 & -k & k \end{bmatrix}. \tag{10.29}$$

The matrices M and K are symmetric positive definite and symmetric positive semidefinite respectively. If the above system was attached to walls at the ends, then K would become symmetric positive definite. This system of n point masses connected by identical springs has the assumed solution of a simple harmonic oscillator

$$\mathbf{U}(t) = \mathbf{c}\cos(\omega t), \tag{10.30}$$

where $\mathbf{U}(t), \mathbf{c} \in \mathbb{R}^n$. Taking two derivatives with respect to time gives

$$\ddot{\mathbf{U}}(t) = -\omega^2 \mathbf{c}\cos(\omega t). \tag{10.31}$$

Inserting these two equations into equation (10.27) gives

$$\left(-\omega^2 M + K\right)\mathbf{c} = \mathbf{0}, \tag{10.32}$$

This is an eigenvalue-eigenvector formulation. Since the matrix $(-\omega^2 M + K)$ is symmetric, it can always be diagonalized. Equation (10.32) can be rewritten as

$$A\mathbf{c} = \lambda\mathbf{c}, \tag{10.33}$$

where $A = M^{-1}K$ and $\lambda = \omega^2$. The eigenvectors $\mathbf{c} \in Null(A(\omega))$.

As $n \to \infty$, the 1D system becomes continuous, and the corresponding kinetic and potential energy equations take different forms. In 1D, the kinetic energy at a point x and time t (both in $\mathbb{R}$) is

$$T(x,t) = \frac{1}{2}\rho(x)\left(\frac{\partial u(x,t)}{\partial t}\right)^2, \tag{10.34}$$

and potential energy is given by the equation

$$V(x,t) = \frac{1}{2}\chi(x)k(x)\left(\frac{\partial u(x,t)}{\partial x}\right)^2. \tag{10.35}$$

The function $\chi(x)$ is a characteristic function, giving a 1 for points within the 1D body and a 0 otherwise. For uniform density, $\rho(x) = \rho_0\chi(x)$. The function $k(x) = EA(x)$, where E is Young's modulus and $A(x)$ is the cross sectional area of the body, which is constant if all of the springs in the corresponding discrete model are constant. The

total kinetic and potential energies for a 1D body after integration are

$$T(t) = \frac{1}{2}\rho_0 \int_{\mathbb{R}} \chi(x) \left(\frac{\partial u(x,t)}{\partial t} \right)^2 dx, \tag{10.36}$$

$$V(t) = \frac{1}{2} EA \int_{\mathbb{R}} \chi(x) \left(\frac{\partial u(x,t)}{\partial x} \right)^2 dx. \tag{10.37}$$

The characteristic function $\chi(x)$ and the deformation function $u(x,t)$ can both be approximated with 1D Hermite function expansions as

$$\chi(x) \approx \tilde{\chi}(x) = \sum_{i=0}^{N_i} \hat{\chi} h_i(x), \tag{10.38}$$

and

$$u(x,t) \approx \tilde{u}(x,t) = \sum_{j=0}^{N_j} q_j(t) h_j(x). \tag{10.39}$$

$$\begin{aligned} T(t) &= \frac{1}{2}\rho_0 \int_{\mathbb{R}} \chi(x) \left(\frac{\partial u(x,t)}{\partial t} \right)^2 dx \\ &\approx \frac{1}{2}\rho_0 \int_{\mathbb{R}} \tilde{\chi}(x) \left(\frac{\partial \tilde{u}(x,t)}{\partial t} \right)^2 dx \\ &= \frac{1}{2}\rho_0 \int_{\mathbb{R}} \sum_{i=0}^{N_i} \sum_{j=0}^{N_j} \sum_{k=0}^{N_k} \hat{\chi}_i \dot{q}_j(t) \dot{q}_k(t) h_i(x) h_j(x) h_k(x) dx \\ &= \frac{1}{2}\rho_0 \sum_{i=0}^{N_i} \sum_{j=0}^{N_j} \sum_{k=0}^{N_k} \hat{\chi}_i \dot{q}_j(t) \cdot \dot{q}_k(t) \begin{pmatrix} i & j & k \\ & & \\ 1 & 1 & 1 \end{pmatrix}_h . \end{aligned} \tag{10.40}$$

We can use the differential recurrence relation for Hermite functions together with integrating over the real line to approximate the total potential energy as

$$V(t) \approx \frac{1}{2} EA \sum_{i=0}^{N_i} \sum_{j=0}^{N_j} \sum_{k=0}^{N_k} \hat{\chi}_i q_j(t) q_k(t) \{ \frac{\sqrt{jk}}{2} \begin{pmatrix} i & j-1 & k-1 \end{pmatrix}_h - \frac{\sqrt{k(j+1)}}{2} \begin{pmatrix} i & j+1 & k-1 \end{pmatrix}_h - \frac{\sqrt{j(k+1)}}{2} \begin{pmatrix} i & j-1 & k+1 \end{pmatrix}_h + \frac{\sqrt{(j+1)(k+1)}}{2} \begin{pmatrix} i & j+1 & k+1 \end{pmatrix}_h \}. \tag{10.41}$$

Recall the kinetic energy over a 1D body, and the potential energy over a 1D body. If one were to solve a system akin to

$$T = \frac{1}{2} \sum_{j=0}^{B} \sum_{k-0}^{B} M_{j,k} \dot{u}(x_j, t) \dot{u}(x_k, t),$$

and

$$V = \frac{1}{2} \mathbf{U}^T K \mathbf{U} = \frac{1}{2} \sum_{j=0}^{B} \sum_{k=0}^{B} K_{j,k} u(x_j, t) u(x_k, t),$$

for $N_j = N_k = B$ and $N_i = N$, Then elements of the mass matrix would be

$$\mathcal{M}_{j,k} = \rho_0 \sum_{i=0}^{N} \hat{\chi}_i \begin{pmatrix} i & j & k \end{pmatrix}_h, \tag{10.42}$$

and elements of the spring constant matrix would be

$$\mathcal{K}_{j,k} = EA \sum_{i=0}^{N} \hat{\chi}_i \{ \frac{\sqrt{jk}}{2} \begin{pmatrix} i & j-1 & k-1 \end{pmatrix}_h - \frac{\sqrt{k(j+1)}}{2} \begin{pmatrix} i & j+1 & k-1 \end{pmatrix}_h - \frac{\sqrt{j(k+1)}}{2} \begin{pmatrix} i & j-1 & k+1 \end{pmatrix}_h + \frac{\sqrt{(j+1)(k+1)}}{2} \begin{pmatrix} i & j+1 & k+1 \end{pmatrix}_h \}. \tag{10.43}$$

Thus

$$\mathcal{M} \ddot{\mathbf{q}} + \mathcal{K} \mathbf{q} = \mathbf{0},$$

for

$$\mathbf{q} = \begin{bmatrix} q_0(t) \\ q_2(t) \\ \vdots \\ q_B(t) \end{bmatrix}.$$

From inspection, these matrices appear to be symmetric. It is assumed that each $q_j(t)$ has the general solution

$$q_j(t) = c_j \cos(\omega t).$$

After an eigenvalue/eigenvector decomposition, B solution pairs $(\omega, \mathbf{c})$ result, with the k^{th} mode given as

$$u(x,t)_{mode,k} = \sum_{j=0}^{B} c_j^{(k)} \cos(\omega_k t) h_j(x).$$

Parameters: $L = 4$. Bandwidth for $\chi(x)$ approximation $N = 95$. $B = 95$. $n = 80$ points and $n - 1 = 79$ springs. $\rho_0 = \frac{m \cdot 40}{L} = 8$. $EA = k\Delta x = 0.1282$.

$$\chi(x) = \begin{cases} 1, & -L/2 \leq x \leq L/2 \\ 0, & \text{Otherwise} \end{cases}.$$

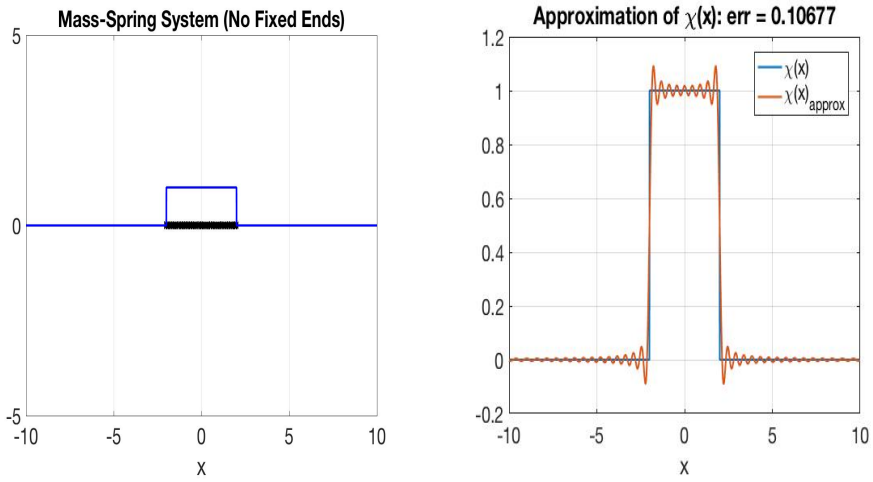

1 2

Figure 10.1: 1D Example Geometry

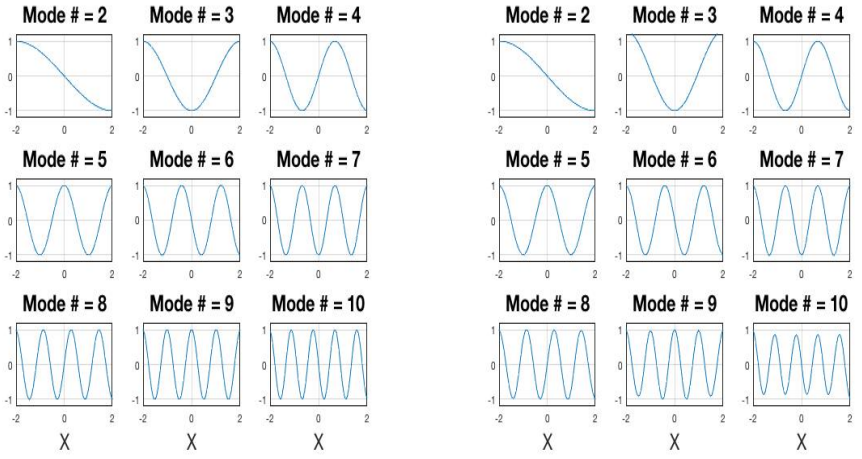

Discrete Model with 3h Integrals

Figure 10.2: Comparison of Modes

10.4 Chapter Summary

This chapter presented two new applications that utilize Hermite expansions and $3h$ integrals. For deconvolution, the limitations are in the form of condition numbers on the underlying matrices formulated in the approach. Translational deconvolution

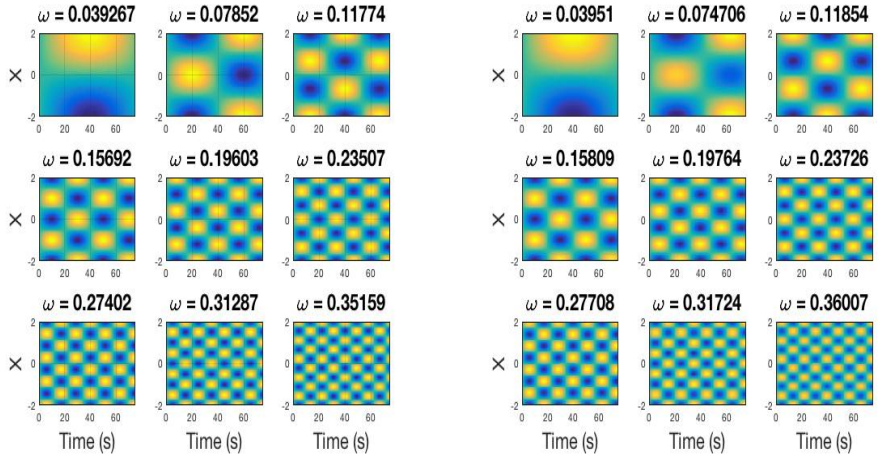

Figure 10.3: Comparison of Modes versus Time

can be extended to 3D, and perhaps deconvolution using techniques of image rotation could be carried over to $SO(3)$. Then given the newly formulated pose change group [see Sipu 2018], it is possible that deconvolution on $SE(3)$ can be entertained.

Chapter 11

Conclusions and Future Work

This thesis showcased the versatility of orthogonal expansions and their roles in a wide variety of engineering applications. It was shown that Hermite function expansions have a lot of useful properties under multiplication, convolution, rotation, projection, and coordinate conversion. The $3h$ integrals were applied to data fusion, deconvolution, EM and SAXS data representation, and continuum normal mode analysis.

The $3J$ integrals were also used in data fusion, and recurrence relations for $3h$ and $3J$ were derived. One loose end for $3J$ integrals was the lack of general solutions for the required axial starting conditions. It was proposed that perhaps with some scaling (since a solution does exist when the scale factors a, b, and c all equal 1), a general solution could arise. Notwithstanding, the accuracy of the recurrence relation did

appear stable for this particular case when $a = b = c = 1$ given analytic starting conditions. Coordinate interconversion was accomplished in $3D$ using S^2H expansions, but perhaps using SGL series, matrices similar to the Q^m matrices when converting between Hermite and F-L expansions could be derived.

Even though this thesis comprehensively covered a fair number of topics, there are still a lot of ideas for future work. In particular, the concept of reconstruction from random a priori unknown view angles was proposed in [park2008thesis], and some of the limitations were for objects with k=fold symmetry. One thought would be to utilize the steering coefficient matrices, more specifically that the coefficients of the bandlimited approximation of an image (with say 3-fold symmetry) are invariant to rotations that are multiples of $\frac{2\pi}{3}$. Wrapping these constraints into a gradient descent approach for rendering the coefficients of the original image (from projections) seems promising.

The continuum normal mode analysis with $3h$ integrals was only accomplished for $1D$ systems, which in and of itself is not terribly interesting. However, for $2D$ and $3D$ versions, if this method holds true in these dimensions, then one could also utilize Hermite expansions under coordinate conversion. By doing this, the normal modes for a 2D (or 3D) system could be displayed in multiple coordinate systems, a notion that is not possible for a discrete lattice.

Bibliography

[1] W. W. Bell, *Special functions for scientists and engineers.* Courier Corporation, 2004.

[2] S. Thangavelu, *Lectures on Hermite and Laguerre expansions.* Princeton University Press, 1993, vol. 42.

[3] G. Watson, *A Treatise on the Theory of Bessel Functions.* Cambridge University Press, 1995.

[4] G. S. Chirikjian and A. B. Kyatkin, *Engineering applications of noncommutative harmonic analysis: with emphasis on rotation and motion groups.* CRC press, 2000.

[5] G. S. Chirikjian, *Stochastic Models, Information Theory and Lie Groups.* Birkhäuser, 2012, vol. 2.

[6] J. Wendel, "Haar measure and the semigroup of measures on a compact group,"

Proceedings of the American Mathematical Society, vol. 5, no. 6, pp. 923–929, 1954.

[7] D. A. Varshalovich, A. N. Moskalev, and V. K. Khersonskii, *Quantum Theory of Angular Momentum*. World Science Publishing, 1988.

[8] A. Averbuch, I. Sedelnikov, and Y. Shkolnisky, "Ct reconstruction from parallel and fan-beam projections by a 2-d discrete radon transform," *IEEE Transactions on Image Processing*, vol. 21, no. 2, pp. 733–741, 2012.

[9] W. Park, *Inverse problems in structural biology and flexible needle steering*. The Johns Hopkins University, 2008.

[10] W. Park and G. S. Chirikjian, "Tomographic reconstruction of band-limited hermite expansions," in *Medical Imaging 2008: Physics of Medical Imaging*, vol. 6913. International Society for Optics and Photonics, 2008, p. 691330.

[11] A. W. Paeth, "A fast algorithm for general raster rotation," in *Graphics Interface*, vol. 86, no. 5, 1986.

[12] C. B. Owen and F. Makedon, "High quality alias free image rotation," in *Signals, Systems and Computers, 1996. Conference Record of the Thirtieth Asilomar Conference on*, vol. 1. IEEE, 1996, pp. 115–119.

[13] M. Unser, P. Thevenaz, and L. Yaroslavsky, "Convolution-based interpolation for

fast, high-quality rotation of images," *IEEE Transactions on image processing*, vol. 4, no. 10, pp. 1371–1381, 1995.

[14] B. Chen and A. Kaufman, "3d volume rotation using shear transformations," *Graphical Models*, vol. 62, no. 4, pp. 308–322, 2000.

[15] R. W. Cox and R. Tong, "Two-and three-dimensional image rotation using the fft," *IEEE Transactions on Image Processing*, vol. 8, no. 9, pp. 1297–1299, 1999.

[16] T. Toffoli and J. Quick, "Three-dimensional rotations by three shears," *Graphical Models and Image Processing*, vol. 59, no. 2, pp. 89–95, 1997.

[17] W. Park, G. Leibon, D. N. Rockmore, and G. S. Chirikjian, "Accurate image rotation using hermite expansions," *IEEE transactions on image processing: a publication of the IEEE Signal Processing Society*, vol. 18, no. 9, p. 1988, 2009.

[18] W. Park and G. Chirikjian, "Interconversion between truncated cartesian and polar expansions of images," *IEEE Transactions on Image Processing*, vol. 16, no. 8, pp. 1946–1955, 2007.

[19] D. Hui and G. Chirikjian, "Information fusion in polar coordinates," in *ASME 2016 International Design Engineering Technical Conferences and Computers and Information in Engineering Conference*. American Society of Mechanical Engineers, 2016, pp. V01AT02A006–V01AT02A006.

[20] S. Auluck, "On the integral of the product of three Bessel functions over an

infinite domain Fourier-space representation of nonlinear dynamics of continuous media in cylindrical geometry," *Mathematical Journal*, vol. 14, pp. 1–39, 2012.

[21] R. Beals and J. Szmigielski, "Meijer g-functions: a gentle introduction," *Notices of the AMS*, vol. 60, no. 7, pp. 866–872, 2013.

[22] D.-C. Chang, W.-R. Wu, and J.-H. Jeng, "An efficient architecture of ultrasonic scan conversion for implementing the cubic convolution interpolation," in *Nuclear Science Symposium, 1997. IEEE*, vol. 2. IEEE, 1997, pp. 1546–1550.

[23] S. J. Julier and J. K. Uhlmann, "Consistent debiased method for converting between polar and cartesian coordinate systems," in *Acquisition, Tracking, and Pointing XI*, vol. 3086. International Society for Optics and Photonics, 1997, pp. 110–122.

[24] Z. Chen and R. Ning, "Filling the radon domain in computed tomography by local convex combination," *Applied optics*, vol. 42, no. 35, pp. 7043–7051, 2003.

[25] C. Basoglu, Y. Kim, and V. Chalana, "A real-time scan conversion algorithm on commercially available microprocessors," *Ultrasonic Imaging*, vol. 18, no. 4, pp. 241–260, 1996.

[26] A. Berkhoff, H. Huisman, J. Thijssen, E. Jacobs, and R. Homan, "Fast scan conversion algorithms for displaying ultrasound sector images," *Ultrasonic Imaging*, vol. 16, no. 2, pp. 87–108, 1994.

[27] J. Prestin and C. Wülker, "Fast fourier transforms for spherical gauss-laguerre basis functions," in *Frames and Other Bases in Abstract and Function Spaces*. Springer, 2017, pp. 237–263.

[28] G. Chirikjian and M. Kobilarov, "Gaussian approximation of non-linear measurement models on lie groups," in *Decision and Control (CDC), 2014 IEEE 53rd Annual Conference on*. IEEE, 2014, pp. 6401–6406.

[29] K. C. Wolfe and M. Mashner, "Bayesian fusion on lie groups," *Journal of Algebraic Statistics*, vol. 2, no. 1, 2011.

[30] M. Brossard, S. Bonnabel, and J.-P. Condomines, "Unscented kalman filtering on lie groups," in *Intelligent Robots and Systems (IROS), 2017 IEEE/RSJ International Conference on*. IEEE, 2017, pp. 2485–2491.

[31] G. Bourmaud, R. Mégret, A. Giremus, and Y. Berthoumieu, "Discrete extended kalman filter on lie groups," in *Signal Processing Conference (EUSIPCO), 2013 Proceedings of the 21st European*. IEEE, 2013, pp. 1–5.

[32] K. C. Wolfe and G. S. Chirikjian, "Signal detection on euclidean groups: applications to dna bends, robot localization, and optical communication," *IEEE Journal of Selected Topics in Signal Processing*, vol. 7, no. 4, pp. 708–719, 2013.

[33] S. Bonnable, P. Martin, and E. Salaün, "Invariant extended kalman filter: theory and application to a velocity-aided attitude estimation problem," in *Decision*

and Control, 2009 held jointly with the 2009 28th Chinese Control Conference. CDC/CCC 2009. Proceedings of the 48th IEEE Conference on. IEEE, 2009, pp. 1297–1304.

[34] S. Bonnabel, "Left-invariant extended kalman filter and attitude estimation," in *Decision and Control, 2007 46th IEEE Conference on.* IEEE, 2007, pp. 1027–1032.

[35] S. Bonnabel, P. Martin, and P. Rouchon, "Non-linear symmetry-preserving observers on lie groups," *IEEE Transactions on Automatic Control*, vol. 54, no. 7, pp. 1709–1713, 2009.

[36] T. Hamel and R. Mahony, "Attitude estimation on so [3] based on direct inertial measurements," in *Robotics and Automation, 2006. ICRA 2006. Proceedings 2006 IEEE International Conference on.* IEEE, 2006, pp. 2170–2175.

[37] A. Barrau and S. Bonnabel, "Intrinsic filtering on so (3) with discrete-time observations," in *Decision and Control (CDC), 2013 IEEE 52nd Annual Conference on.* IEEE, 2013, pp. 3255–3260.

[38] P. Batista, C. Silvestre, and P. Oliveira, "Attitude and earth velocity estimation-part ii: Observer on the special orthogonal group," in *Decision and Control (CDC), 2014 IEEE 53rd Annual Conference on.* IEEE, 2014, pp. 127–132.

[39] J. S. Kim and G. S. Chirikjian, "Bayesian filtering for orientational distributions:

A fourier approach," in *Information Fusion (Fusion), 2015 18th International Conference on*. IEEE, 2015, pp. 748–753.

[40] M. Cohen, "On jacobi functions and multiplication theorems for integrals of bessel functions," *Journal of Mathematical Analysis and Applications*, vol. 57, no. 2, pp. 469–475, 1977.

[41] H. Dong, J. S. Kim, and G. S. Chirikjian, "Computational analysis of saxs data acquisition," *Journal of Computational Biology*, vol. 22, no. 9, pp. 787–805, 2015.

[42] J. Frank, *Three-dimensional electron microscopy of macromolecular assemblies: visualization of biological molecules in their native state*. Oxford University Press, 2006.

[43] D. I. Svergun and M. H. Koch, "Small-angle scattering studies of biological macromolecules in solution," *Reports on Progress in Physics*, vol. 66, no. 10, p. 1735, 2003.

[44] L. Feigin, D. Svergun, and G. W. Taylor, "Structure analysis by small-angle x-ray and neutron scattering 1987."

[45] D. I. Svergun, M. H. Koch, P. A. Timmins, and R. P. May, *Small angle X-ray and neutron scattering from solutions of biological macromolecules*. Oxford University Press, 2013, vol. 19.

[46] J. S. Kim, B. Afsari, and G. S. Chirikjian, "Cross-validation of data compatibility

between small angle x-ray scattering and cryo-electron microscopy," *Journal of Computational Biology*, vol. 24, no. 1, pp. 13–30, 2017.

[47] B. Afsari, J. S. Kim, and G. S. Chirikjian, "Cross-validation of data in saxs and cryo-em," in *Bioinformatics and Biomedicine (BIBM), 2015 IEEE International Conference on*. IEEE, 2015, pp. 1224–1230.

[48] L. Feigin and D. Svergun, "General principles of small-angle diffraction."

[49] R. Bracewell, *Fourier analysis and imaging*. Springer Science & Business Media, 2004.

[50] R. van Antwerpen, "Preferred orientations of ldl in vitreous ice indicate a discoid shape of the lipoprotein particle," *Archives of biochemistry and biophysics*, vol. 432, no. 1, pp. 122–127, 2004.

[51] R. M. Gray *et al.*, "Toeplitz and circulant matrices: A review," *Foundations and Trends® in Communications and Information Theory*, vol. 2, no. 3, pp. 155–239, 2006.

[52] W. Park, D. R. Madden, D. N. Rockmore, and G. S. Chirikjian, "Deblurring of class-averaged images in single-particle electron microscopy," *Inverse problems*, vol. 26, no. 3, p. 035002, 2010.

[53] N. J. Vilenkin, "Klimyk, representation of lie groups and special functions vol. 1," 1991.

[54] E. Wigner, *Group theory: and its application to the quantum mechanics of atomic spectra*. Elsevier, 2012, vol. 5.

Vita

Kristopher Lewis Reynolds was born on November 25, 1988 and raised in Cooperstown, NY. He received his Bachelor of Mechanical Engineering (Summa Cum Laude) from the Catholic University of America (CUA) in 2011 and a Masters of Science in Mechanical Engineering in 2012 (also from CUA). His honors from CUA include the Anthony Scullen award for excellent academic performance in engineering and the C.C. Chang award in recognition of further outstanding academic achievement in mechanical engineering, and potential contribution to the field. In 2015, Kris received a Masters of Science in Engineering degree in Robotics from The Johns Hopkins University (JHU). From 2012-2017, Kris was also working full time at the Naval Research Lab (NRL) in the physical acoustics branch, designing algorithms for underwater sensing applications. In 2018, he transferred jobs, and is now working at the Johns Hopkins Unversity Applied Physics Lab (APL) in the Force Projection Sector (FPS) designing algorithms for underwater array sensing systems. His current

research interests at APL include time-frequency analysis and machine learning.